2019

Toward Macromolecular Shape And Size Control: Novel Enantioselective Nitrations And Iterative Exponential Growth Methods For Polymer Synthesis

Joseph Patrick Campbell
University of Vermont

TOWARD MACROMOLECULAR SHAPE AND SIZE CONTROL: NOVEL ENANTIOSELECTIVE NITRATIONS AND ITERATIVE EXPONENTIAL GROWTH METHODS FOR POLYMER SYNTHESIS

A Dissertation Presented

by

Joseph Patrick Campbell

to

The Faculty of the Graduate College

of

The University of Vermont

In Partial Fulfillment of the Requirements
for the Degree of Doctor of Philosophy
Specializing in Chemistry

August, 2019

Defense Date: May 10, 2019
Dissertation Examination Committee:

Severin T. Schneebeli, Ph. D., Advisor
Adrian Del Maestro, Ph. D., Chairperson
Adam C. Whalley, Ph. D.
Matthew D. Liptak, Ph. D.
Cynthia J. Forehand, Ph. D., Dean of the Graduate College

ABSTRACT

Chirality is a key principle in organic chemistry. All chiral compounds are non-superimposable mirror images of each other and therefore lack an improper axis of rotation (S_n). These mirror images often have identical properties in an achiral environment, however when two chiral molecules interact, they produce different shapes and properties. Nature, to this extent takes advantage of this aspect through unique formation of shape defined biological macromolecules that are tailored to carry out various life processes. This level of shape control is only made possible because of natural chiral monomers such as amino acids or glycosides that make up such macromolecules. Under new methods such as Chirality Assisted Synthesis (CAS), shape and size-controlled polymers and macromolecules can be realized through the use of chiral monomers to make well defined macromolecules. Because chirality dictates shape, and shape defines function in reference to macromolecules, controlling the chirality of monomers, while concurrently dictating shape and size can lead to the potential of biomimetic methodologies and cage like structures.

Accessing shape defined monomers can be difficult especially when in reference to chiral compounds. The unique structure of enantiopure tribenzotriquinacenes show promise in the formation of well-defined cage like structures through utilization of CAS methodology. Synthesis of functionalized tribenzotriquinacenes along with development of an enantioselective electrophilic aromatic nitration method was attempted. Further exploration into the effectiveness of through-space enantioselective nitrations found a dependence on solvent temperature, and the auxiliary that is used. Synthetic difficulties, results, modifications and processes toward a generalized method are presented herein.

In addition, controlling the size of polymers has always been a difficult synthetic challenge. Overall selectivity toward one product over another is determined via a variety of chemical properties. However, the formation of sequence and size defined polymers are a prominent aspect of natural polymers. The size selective synthesis, of unique ABAB sequenced polymers was attempted using an iterative exponential growth method. The ability to scale up these processes and create monodisperse oligoethers is also presented and described herein.

CITATIONS

Material from this dissertation has been published in the following form:

Campbell, J. P.; Rajappan, S. C.; Jaynes, T. J.; Sharafi, M.; Ma, Y.-T.; Li, J.; Schneebeli, S. T..(**2019),**Enantioselective Electrophilic Aromatic Nitration: A Chiral Auxiliary Approach. *Angew. Chem., Int. Ed.***,** *58* (4), 1035-1040.

AND

Material from this dissertation has been submitted for publication in Supramolecular Chemistry on (March 8th, 2019) in the following form:

Campbell, J.P, Sharafi, M. Murphy, K.E, Schneebeli,S.T.. Precise Molecular Shape Control of Linear and Branched Strips with Chirality-Assisted Synthesis. Journal of Supramolecular Chemistry.

DEDICATION

I dedicate this work to my parents Linda and David Kezar. Thank you for your constant love, understanding, and support.

And in remembrance of those family members that were inspirational and supportive in this endeavor as I saw it through. You are loved and missed dearly:

Bernadette Campbell, and Karen Maguire,

ACKNOWLEDGMENTS

There are numerous people that were integral parts to me successfully obtaining my Ph.D. First and foremost, I would like to thank the members of my committee, Drs. Adam Whalley, Matthew Liptak, and Adrian Del Maestro. Each of you has expressed support guidance and genuine interest in my progress throughout my time here. The guidance, insight, advice and encouragement you all have provided were greatly appreciated. I also want to express my deepest gratitude to my advisor Dr. Severin Schneebeli. Your mentorship, guidance, and outlook on research have helped me grow as a researcher and chemist in a way that I never thought was possible. Thank you for taking a chance with me as one of the first members of your group when I felt lost my first year here. I am very grateful for the opportunity you gave me and the mentorship you have provided. Your trust in allowing me to work autonomously while providing encouragement and direction when I've needed it has allowed me to learn how to be an independent researcher.

My Fellow graduate students, during my time here have, you all have proven to be a group of been truly amazing people. Thank you all for the friendship and support you all have provided. Unfortunately, I don't have to space necessary to mention everyone but there are several people would like to thank specifically. I will be forever grateful for the friendships I have formed; Drs Ramya Srinivasan, Jonathan Holland and Nick Dodge for advice, helpful discussions, and "life talks". To Lindsay LeBlanc, Brandon Ackley, Emma Ste. Marie, Jessica Bocanegra, Dillon McCarthy, Mona Sharafi, Mike Cibuzar Michelle DiPinto, Kourtney Penatzar, Kyle Murphy, thank you all for your friendships and support.

Thank you to previous and current members of the Schneebeli group. Working in lab with you all was often a fun experience even when science was hard to work through. To Sinu Rajappan, I would like to thank you for the numerous times you helped me, both in and out of lab throughout our time in the group together, for teaching me how to be a productive graduate student, and for being a great friend and coworker. Thank you to Kyle Murphy and Mona Sharafi , for helpful insights and discussions and for making our half of the lab enjoyable and friendly environment, from Lab dances to drawing cartoons on the white board hoods, it was always good to be in lab.

Of course, I would not have been able to accomplish anything without the love and support of my family. Meghan and Evan both of you were always there to talk even when I felt like no one was around or too busy. Kristin, Kate, Kevin, and John all of you are constants for me, when people come and go in life, each one of you were always there for me. Finally, my Grammy (Bernadette Campbell), ever since I was a toddler you told me I would make it really far in school and that someday I would be a Doctor. You were right, and a lot of this is due to your love and support of me, my endeavors, and forever will be apart of me. You are loved and missed, and I hope I can continue to make you proud.

Linda and Dave (Mom and Dad) words cannot describe the gratitude I have for both of you. You both have been nothing but supportive of this endeavor since I took it on when I graduated from Wheaton college. Both of you have been a constant source of support throughout all of this and I am forever appreciative. I rely on you both for so much and hope that my success can in some small way repay you both for the sacrifices you have made to always provide for us.

TABLE OF CONTENTS

LIST OF TABLES

Table **Page**

LIST OF FIGURES

Figure **Page**

LIST OF SCHEMES

Scheme **Page**

CHAPTER 1: CHIRALITY ASSISTED SYNTHESIS: BACKGROUND

1.1 CAS Overview

Nature can control the sequences and shapes of large macromolecules precisely in 3D[1, 2].This exquisite level of natural shape-control is made possible by the chiral building blocks (e.g. amino acids or glycosides) employed as the monomers. The well-defined shapes adopted by most chiral biological macromolecules are key to enabling highly selective recognition events, complex self-assembly, and efficient catalysis that are crucial for life.[3-7] Nevertheless, most biological macromolecules only adopt well-defined shapes under specific conditions (e.g. in a certain solvent, at a certain pH, at a certain temperature, at a certain ionic strength, etc.). For this reason, learning how to generalize macromolecular shape control, so that it becomes more predictable and less-dependent on the environmental conditions has been a long-sought-after endeavor of biomimetic and supramolecular synthetic chemists. One of the ultimate goals of this biomimetic research is to create synthetic, shape-defined polymers which consistently form singular structures, regardless of the solvent, the temperature, the pH, or the ionic strength employed.

Chirality-assisted synthesis (CAS) developed in 2015[8] is a relatively new chemical method to control macromolecular shape in a programmable manner. Inspired by nature, which makes extensive use of chiral monomers to control macromolecular shape, CAS

employs chiral building blocks to assemble 3D molecular strips with predictable geometries shown as a concept in Figure 1.1

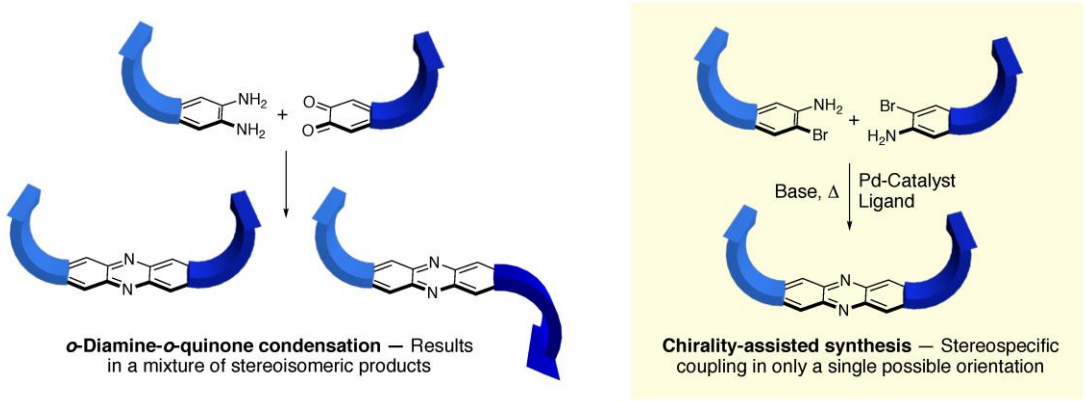

Figure 1.1: Systematic concept of chirality-assisted synthesis and the advantage it has for unilaterlly forming a singular shape.

In its prototypical version, CAS couples[8] chiral monomers with *o*-bromo-aniline functionalities together in a stereospecific manner. A Pd-catalyst with SPhos or RuPhos as the ligand[9] is generally employed for these double amination reactions, to form phenazines, which not only proceed stereo specifically but functionally, have shown promise in applications such as therapeutics[10-13] photoredox catalysts[14-18]and organic electronics[19]. The CAS approach to form phenazines offers the distinct advantage of predictable molecular shape control over alternative phenazine-formation protocols. For example, coupling (Figure 1.1 left) two molecular strips together with *o*-dianiline/*o*-quinone condensations leads[20-23] to nearly equimolar amounts of both the *syn* and the *anti*-isomers. On the other hand, an analogous CAS-based coupling of two identical strips (Figure 1.1 right) leads to the *syn*-isomer only in a fully stereospecific and thus predictable manner.

The predictability of such couplings in essence is the most powerful aspect of the CAS concept. Because the *syn*-stereospecificity can, in principle, be readily converted to *anti*, by simply changing the chirality of one of the coupling partners[8]. CAS encompasses an intrinsic ability to program a wide-variety of molecular shapes in a deterministic fashion by simply adjusting the chiralities of the building blocks. This unique programmability aspect is really what sets CAS apart from other well-known methods (e.g. alternating *exo*/*endo* selective Diels Alder reactions[24] that are also used to control the shapes of molecular strips.

Recently, the CAS concept has been adopted and extended by several research groups to form enantiomerically pure molecular strips[25-35] helices, shape-defined molecular claws and large hydrogen-bonded capsules.[36-43] Furthermore, efficient synthetic methodology including enantioselective syntheses[44-48]to access the enantiomerically pure monomers required for CAS has recently become available and will be discussed further in chapter 2.

1.2 CAS with Linear Structures

C-shaped molecular strips[9, 49-51] and belts[25-35] have found extensive use as molecular tweezers e.g. to bind[52-55] to carbon nanotubes of different sizes selectively, or different theraputics[10-13]. However, creating C-shaped molecular strips with large internal cavities efficiently has proven challenging, since mixtures of *syn*- and *anti*-stereoisomers are obtained (Figure 1.1 left) with traditional coupling methods like *o*-dianiline/*o*-quionone condensations[9, 56-58]. CAS overcomes this fundamental synthetic challenge, which allowed

the Schneebeli group to synthesize [59]some of the largest C-shaped molecular strips created to date as shown in Scheme 1.1.

This early CAS work showed that if concave, enantiopure, monomeric, building

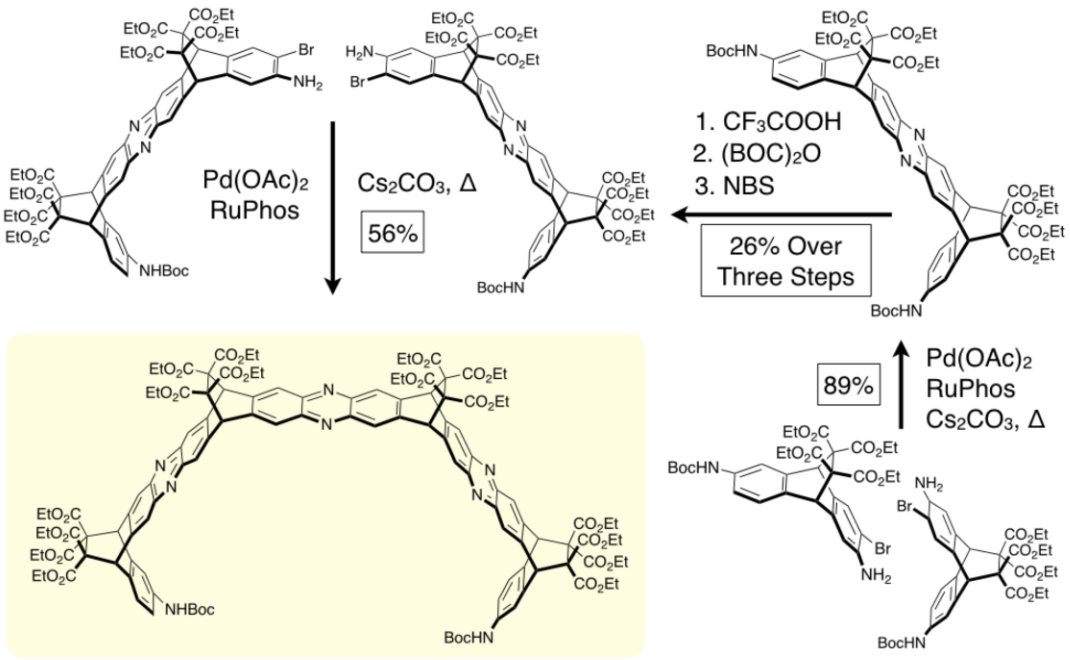

Scheme 1.1: Synthesis of novel belts as a direct result of the use of shape-defined chiral monomers and CAS.

blocks can be formed, then the desired curvature and chirality of the overall C-shaped strip macrocycle is fully defined by the chirality of the monomers. For the CAS growth, *o*-bromoaniline-containing monomers were synthesized, the enantiomers were resolved, and finally coupled (Scheme 1.1) in an iterative exponential growth[60, 61] fashion with double Buchwald-Hartwig[23] aminations. Ultimately, the power of this method is the singular reason that macro structures like this have the potential to be formed. In addition, it should be noted that, because the individual monomers in these systems that utilize CAS, not only are maintaining their shape, but because the monomers themselves are chiral many of the

resulting macrostructures maintain the same chirality of their chiral precursors and therefore their optical properties.

1.2.1 Applications of CAS with linear structures

The C-shaped strips formed with CAS not only contains a prominent chiral cavity but are also able to achieve[59] supramolecular shape recognition. Based on NMR evidence and all-atom molecular dynamics (MD) simulations, the CAS-based strips were found to encircle (Figure 1.2) pillar[5]arene macrocycles. In this type of interaction, the CAS-based strips

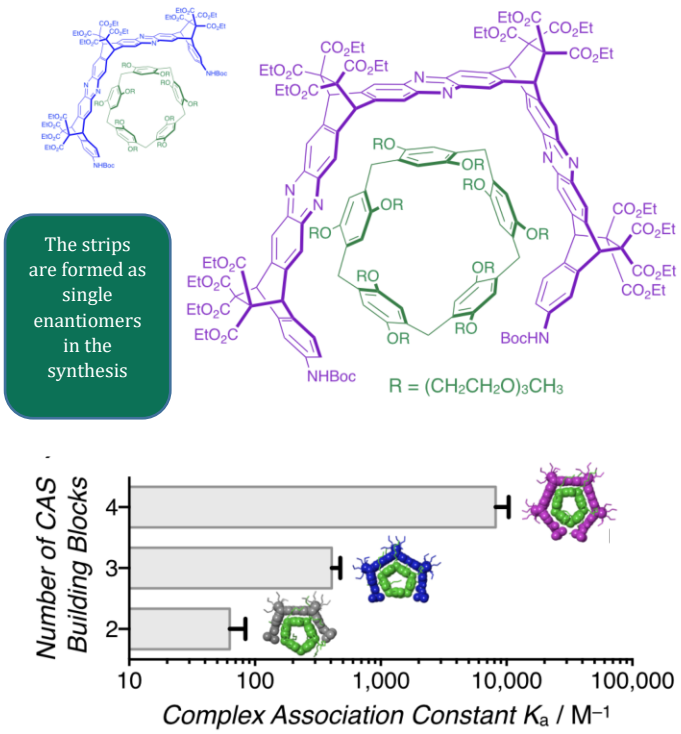

Figure 1.2: Cooperative binding exhibited in molecular belt complexes observed by Schneebeli and co-workers.

behave like wrenches, which tightly surround the five-sided pillar [5]arene "nut".

Consistent with this wrench-like binding mode, the association constants for the pillar[5]arene@C-shaped-strip complexes increase consistently with increasing lengths of the molecular strips. Furthermore, the affinity of a third guest (e.g. viologen) for the central cavity of the pillar[5]arene ring increases, when a C-shaped strip is bound to the outside of the pillar[5]arene. This observed cooperative binding interaction between the C-shaped strips, the pillararene, and the viologen is likely caused by preorganization of the pillar[5]arene's cavity for viologen binding, when a C-shaped strip binds tightly to the outside of the pillar[5]arene[8]

Another example of cooperative binding inside CAS-based C-shaped strips was reported in 2016 by Sharafi *et al.* Specifically, the C-shaped molecular strip was shown to selectively bind to stacked perylene-diimide dyes inside of the chiral cavity [62-64] Perylene-based dyes have found extensive applications as light-responsive, semiconducting organic materials for solar cells, detergents, and light-emitting diodes[65]. The stacking of aromatic dyes has a profound impact on the potophysical properties of the resulting materials and CAS-based strips are now emerging as a viable method to selectively identify stacks of certain sizes and chiralities to further tune the properties of these materials. Furthermore, computer aided MD-simulations were again able to identify suitable guest molecules as candidates for supramolecular recognition, even if multiple guests bind to a single host. Since the cavities of the CAS-created molecular strips are chiral, a bound perylenediimide-stack[59], should preferentially form with one chirality inside of the strips, *i.e*. in either mostly its left- or right-handed form. These simulations not only revealed that the complexes are stable at room temperature, but also that the binding with the guests showed

unique π-π-stacking interactions, which were further enhanced[8] by π-π-stacking of the hosts with the phenazine rings of the chiral molecular strips. The MD-based predictions were verified experimentally with the help of NMR titrations and diffusion ordered NMR spectroscopy (DOSY). The overall promise shown with the CAS made linear analogs allowed for a more generalized approach to larger branched structures.

1.3 CAS with Branched Structures

In this generalization of chirality-assisted synthesis, concave chiral monomers with rotational symmetry such as the C_3 symmetrical tribenzoquinacene (TBTQ) derivative in

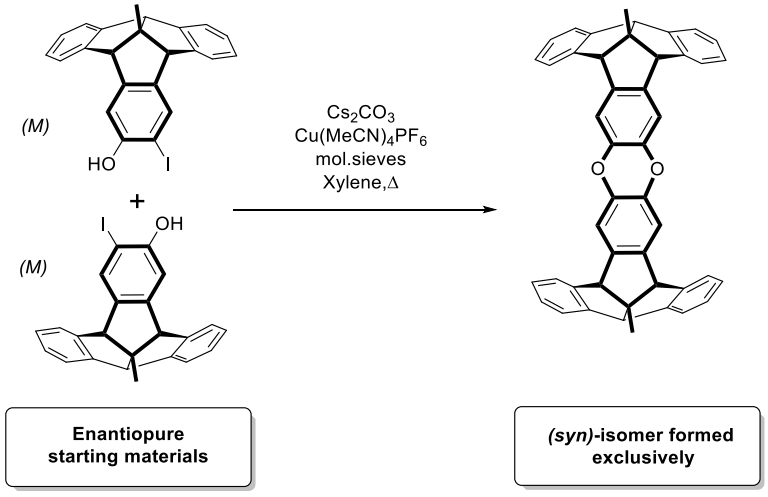

Scheme 1.2: Ullman cross couplings utilizing enantiopure TBTQ systems to make CAS enhanced curved molecular surfaces by Kuck and co-workers.

Scheme1.2 are linked together to afford curved molecular surfaces. Analogous to the linear version of CAS, the shapes of the surfaces formed are precisely defined by the monomer

sequences and chiralities. In the special case where all the monomers are the same, unique chiral molecular cages and capsules[57] are formed.

CAS helps to meet the fundamental challenge of creating the more robust molecular cages and large supramolecular capsules with closed shells[36-43] (akin to virus capsids) which are difficult to synthesize with other methods. Compared to traditional dynamic/supramolecular synthesis of cages and capsules, which has been used [66-70] widely to create rings, cages, and capsules, chirality assisted synthesis offers the advantage that it specifies, with high confidence, the curvature and orientation of structural extensions. Thus, by exploiting different chiral molecular building blocks — devised to form linkages with a minimum number of possible geometrical orientations — CAS is able to overcome unfavorable entropic effects, which often hinder the efficient formation of *de novo* designed large cages and closed-shell capsules.

At the core of this challenge lies the often unpredictable directionality of noncovalent interactions when used without CAS, which leads[24, 71-78] to complex mixtures and lattice frameworks rather than to the desired cages or close-shell capsules. Thus, by applying the CAS concept to chiral, C_3-symmetric TBTQ monomers, Mastalerz and coworkers discovered a way to form molecular capsules with an inner volume of approximately 2,300 Å (Figure1.3) [6]. The CAS-base capsule-formation employed the rigid structure of the TBTQ core, functionalized with cyclic-amides. Following resolution, self-assembly of these monomers into chiral capsules occurred, primarily driven by N-H···O hydrogen bonds between the amide functionalities. The directionality induced by the chiral monomers allow for 72 cooperative noncovalent hydrogen bonds to form making this

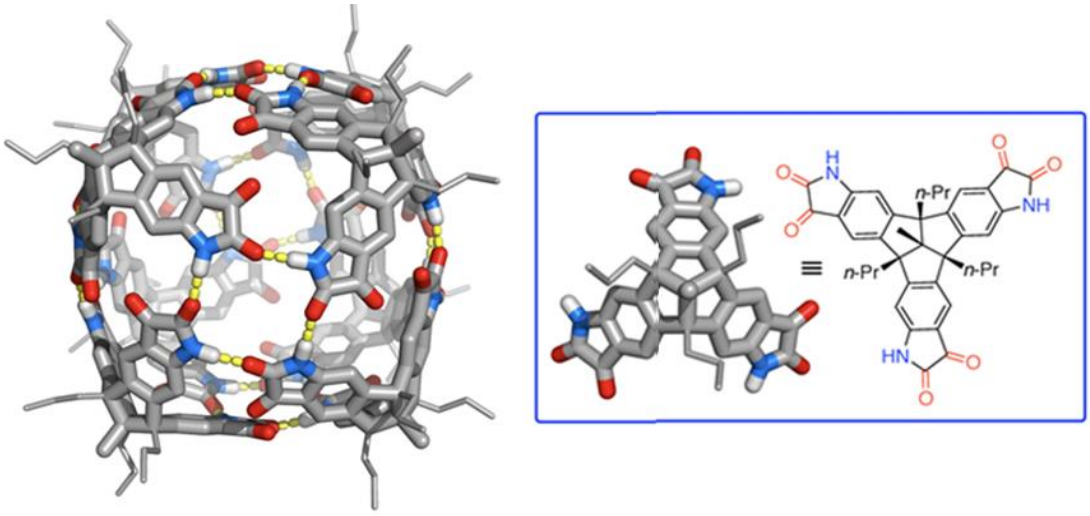

Figure 1.3: Mastelerez's hydrogen bonded capsules formed through use of enantiopure TBTQ and its respective monomer shown in 3D and 2D

chemical engineering feat possible. Semi empirical computer modeling at the PM6[79]level of theory clearly showed that these hydrogen bonding interactions between the amide units dictate the formation of the targeted capsules. Such structures paved the way toward the formation of static capsules and covalent dimers using the TBTQ systems.

Kuck and coworkers were able to further expand[57] the concept of branched CAS with TBTQ monomers to the synthesis of covalent TBTQ dimers. Enantiopure TBTQ derivatives with *o*-phenol functionalities were coupled (Scheme1.2) in a double Ullman reaction. While the double-Ullman reaction only led to the product in about 10% under the reaction conditions employed, the concave *syn*- product was formed exclusively. Starting with racemic starting material on the other hand, the *anti*-product was formed with a 7:3 preference over the *syn*-isomer. The result of this control reaction highlights again the importance of the CAS concept in being able to access the *syn*-dimer selectively, even

though formation of the *anti*-dimer is favored for steric reasons. Further evaluation of chirality assisted synthesis reveals that the individual monomers play a key role in the overall success of the method and therefore adequate, scalable, selective methods are needed in the synthesis of the chiral monomers addressed in chapters 2 and 3.

1.4 Chiral Monomers and Selectivity

Being able to access the chiral monomers needed for CAS efficiently in enantiopure[46, 80-83] form is crucial for practical applications of CAS. Recently, several advances in regio- and stereoselective synthetic methodology — geared specifically toward stereoselective access to CAS monomers — have been described. Due to the fundamental importance of these inventions for the field of CAS, methods to obtain these monomers selectively is to the overall shape control that CAS offers.

Liu *et al.* discovered that diastereoselective gelation, brought about by simply mixing a warm acetonitrile solution of the chiral diamine with dibenzoyl-*D*-tartaric acid, represents an effective means to isolate a chiral diamine in over 98% e.e. on a multi-gram scale. Surprisingly, this chiral resolution method seems to be fairly general for chiral aromatic polyamines; for instance, Mastalerz and coworkers were able to apply a similar procedure with dibenzoyl-*D*-tartaric acid to resolve the enantiomers of chiral TBTQ derivatives[46]. As another resolution-based method to access chiral CAS monomers, Kuck et al. also discovered [45] a highly selective, enzyme-based kinetic resolution methodology

for TBTQ derivatives. TBTQ systems have been notoriously difficult to make enantiopure as will be discussed in chapter 2.

While all of these resolution-based approaches are scalable, at least 50% of the material (the undesired enantiomer) is generally wasted during resolution. Therefore, it is preferable to pursue enantioselective syntheses of the monomers required for CAS instead, as much higher yields of the desired enantiomers are obtainable, in principle, with fully regio- and stereoselective methodology. The regio- and stereo-determining steps in the synthesis of many CAS monomers generally involve substitution reactions on aromatic rings — either with classical electrophilic aromatic nitration reactions, or with transition-metal-catalyzed C-H activations. Consequently, it is these types of reactions that have primarily been targeted as candidates for regio- and stereoselective syntheses of CAS monomers.

Mastalerz and coworkers recently reported[48] an elegant approach to selectively form the C_3-symmetric regioisomer of the TBTQ derivative with three consecutive, Ir-catalyzed C-H activation reactions (scheme 1.3). The three Bpin functional groups introduced can subsequently be converted to boronic acids, amines, aryl halides, methoxyl groups, and alcohols. The origin of the observed regioselectivity stems[48]primarily from steric repulsion between the three Bpin groups introduced into the product; and in the C_3-symmetric product, the three Bpin groups are furthest apart from each other. Up to this report by the Mastalerz group, functionalization of TBTQ systems (e.g. with conventional electrophilic aromatic nitration[48] had always resulted in the undesired C_1 symmetric tri-

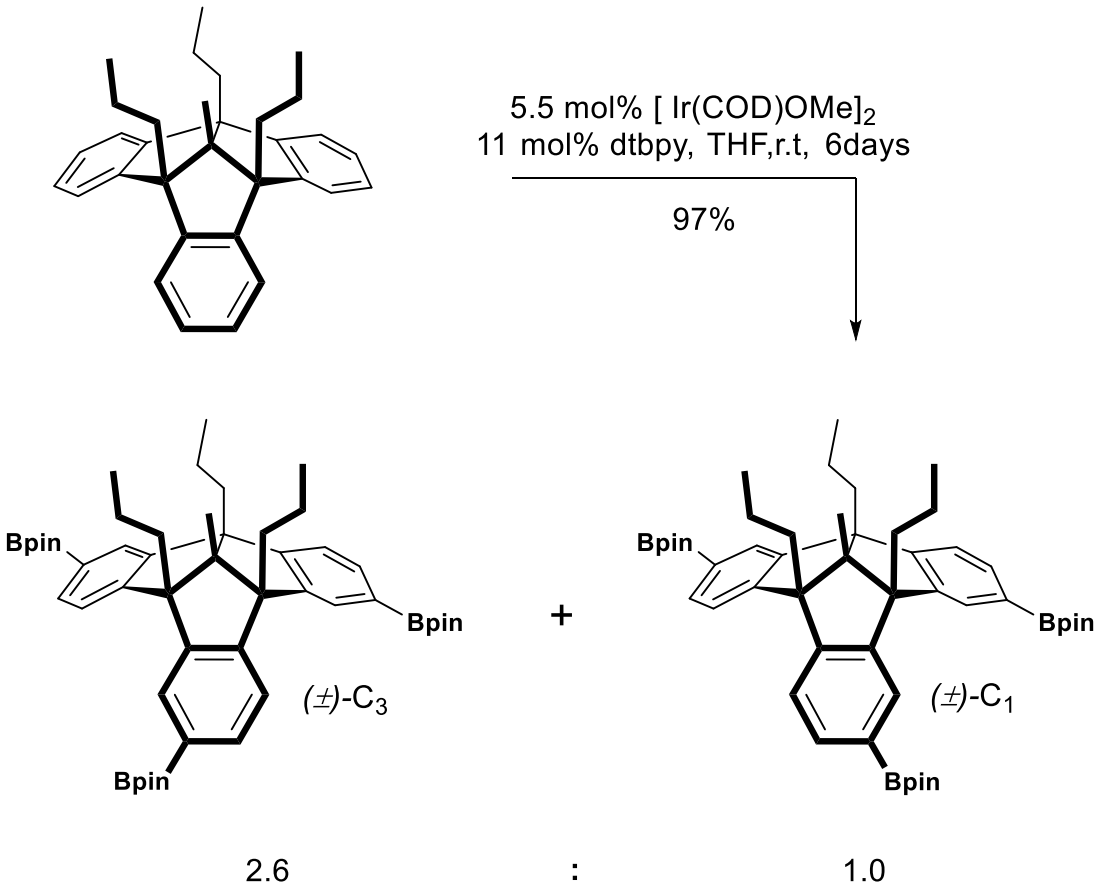

Scheme 1.3: Regio selectivity observed to steric effects of iridium complex during three-fold borylation. A lead advancement in selectivity of TBTQ moieties by Mastalerz and co-workers

functionalized product being favored by at least a 3:1 ratio. In contrast, the report by Mastalerz and coworkers — where the C_3 symmetric product was formed as the major product in a 2.6:1 ratio — now provides a practical synthetic avenue to previously difficult to access *C*$_3$-symmetric TBTQ derivatives for CAS.

Nevertheless, the (±)-C_3 product obtained with this regioselective borylation protocol are still racemic and must be resolved[48] Thus, to access key substrates for linear and branched CAS in a resolution free manner, the Schneebeli group has recently introduced diastereo-[47] and enantioselective[44] aromatic nitration protocols. These new synthetic strategies control both the regio- and the stereochemistry of nitrations through space[47] with chiral diester auxiliaries positioned precisely above the aromatic rings of the

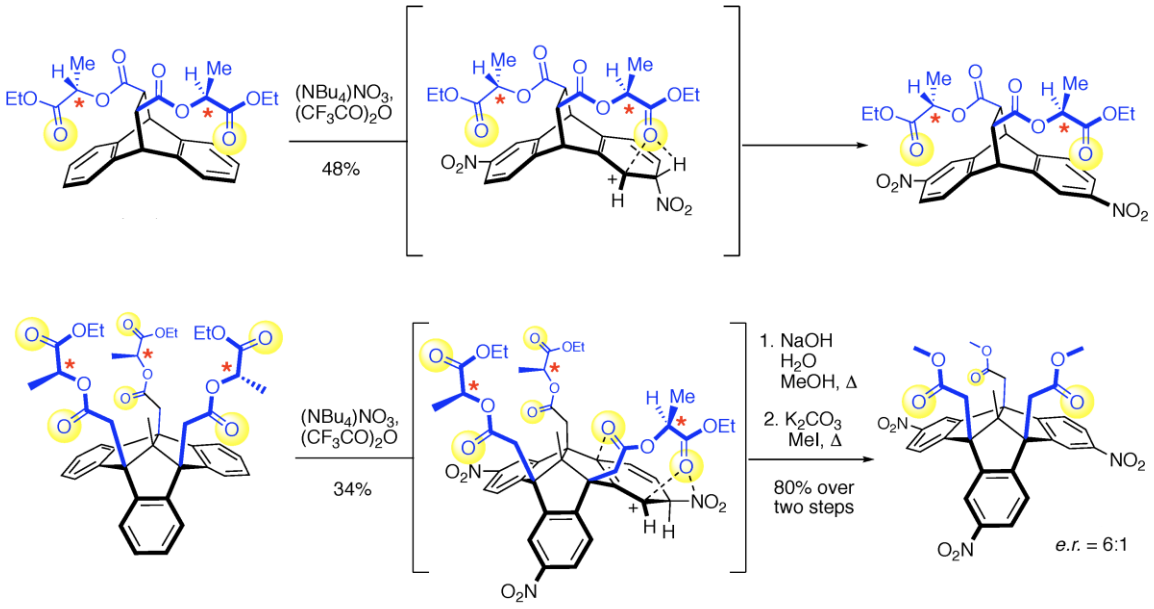

Scheme 1.4: Diastereo-and enantioselective nitrations methodologies coming out of the Schneebeli lab toward well-defined chiral monomers for macrostructures.

substrates (Scheme 1.4). The regio- and stereo control enacted by this through-space-directed methodology is fundamentally distinct from the approach by Wagner *et al*[48]. In particular, the through space tactic makes extensive use of carbonyl groups, positioned precisely above the aromatic rings of the substrates, to stabilize specific, delocalized

carbocation intermediates underneath with oxygen-lone-pair-to-carbocation electron donation. These new developments in stereoselective organic methodology helped clear the path toward the enantioselective nitrations that will be discussed herein. Specifically, on TBTQ systems functionalized with chiral auxiliaries on the benzylic bridgehead positions.

1.4.1 Enantiopure TBTQ Systems

TBTQ systems in regards to CAS are attractive systems to build well defined molecular super structures including fullerene receptors, cryptophanes and covalent organic cages[84-89]. The racemic mixtures of such have been used for a variety of applications. However, enantiopure forms have been showing promise in the development and formation of chiral nanomaterials. In this regard, enantiopure TBTQ compounds are exceedingly rare[90]. And of those that have been reported, are resolved using chiral preparative high-performance liquid chromatography HPLC, cumbersome resolution techniques or through enzyme catalyzed kinetic resolutions. Ultimately enantiopure TBTQ is significantly hindered since these methods are costly and, in most cases, impractical on larger scales that would be needed to pursue the formation of chiral nano materials. These difficulties can ultimately be attributed to the axial chirality that some TBTQ derivatives exhibit.

Axial chirality is a unique example of chirality where a molecule does not possess a stereogenic center, which is the most common case with respect to organic molecules. Instead it possesses an axis of chirality where the substituents are in such an orientation that it is not superimposable on its mirror image. Functionalized TBTQ systems observe this type of chirality. Designations are labeled accordingly in reference to the "front" vs "back" designations similar to helicity. *P* designation is indicative of the right-handed

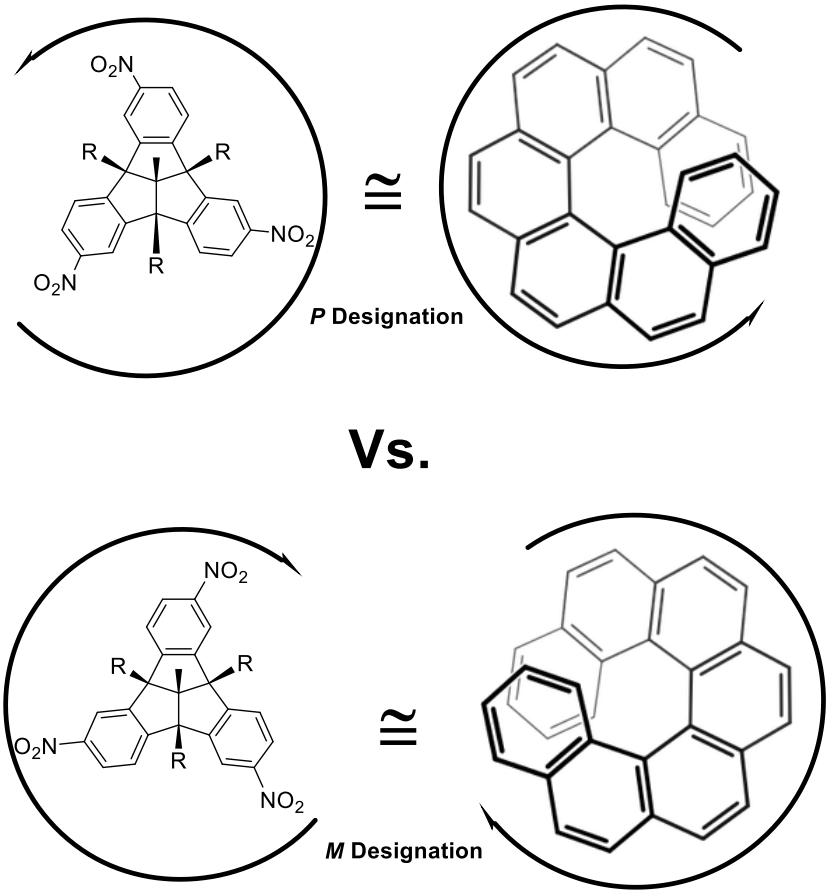

Figure 1.4: Axial chiral designations in reference to helicity.

helicity and the *M* designation is indicative of the lefthanded helicity and can be described as such as demonstrated in Figure 1. 4. Ultimately molecules that observe a chiral axis are

hard to resolve [91-93] and many have turned to enantioselective synthetic approaches. A few groups have however, managed to produce methods in which enantiopure TBTQ can be resolved with moderate success using recrystallization or enzymatic techniques [90]

Kuck and Co-workers in tangent with Mastalerz and coworkers have shown successfully, that it is possible to resolve both a TBTQ system with a single functionalized wing as well as the 3-fold versions[90, 94, 95]. Enzymatic resolution is a powerful tool when working with these TBTQ systems. Enzymatic hydrolysis of a racemic 2-hydroxy-TBTQ acetate employed by kuck allows for high selectivity in moderate yields of an enantio-pure product. In this study a variety of different active enzymes were screened; lipases CAL-B and CAL-A as an immobilized form, gave the *M*-TBTQ with 33% yield and 99% e.e as summarized in Scheme 1.5 scheme below.

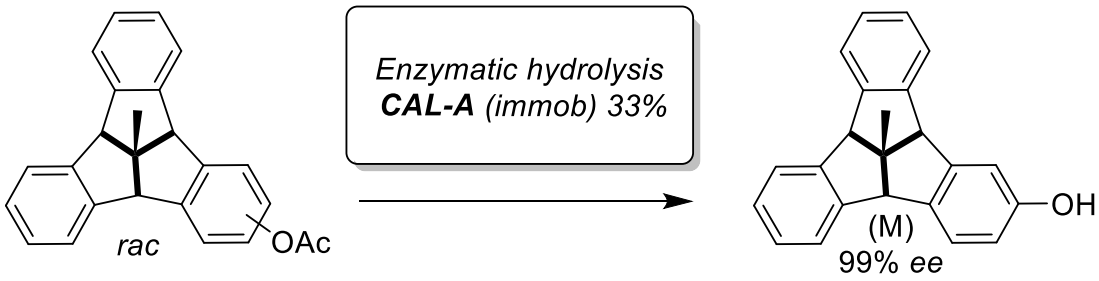

Scheme 1.5 : Kuck's Enzymatic hydrolysis scheme leading to the formation of axially chiral TBTQ systems in high enantiomeric excess

In contrast to their mono-functionalized forms, enantiopure TBTQs that are functionalized in three positions are of particular interest especially in regard to CAS coupling methods. These moieties show promise in the formation of well-defined molecular covalently bound cubes. Enantiopure forms of the C_3, three-fold moieties, can

be further functionalized in the remaining peripheral positions for stereo specific reactions. However, these enantiopure TBTQs are not practical to synthesize on a large scale for two reasons. 1) The regioselectivity of the formations of the C_3 to C_1 regioisomers is 1 to 3 respectively. 2) The resolution based method developed by Mastalerz [94] and co-workers gives relatively low yields of the enantiopure products. Furthermore, repeated processing results in a cumbersome and time-consuming process that gives diminishing yields as demonstrated in Scheme 1.6. Ultimately an enantioselective process that provides direct

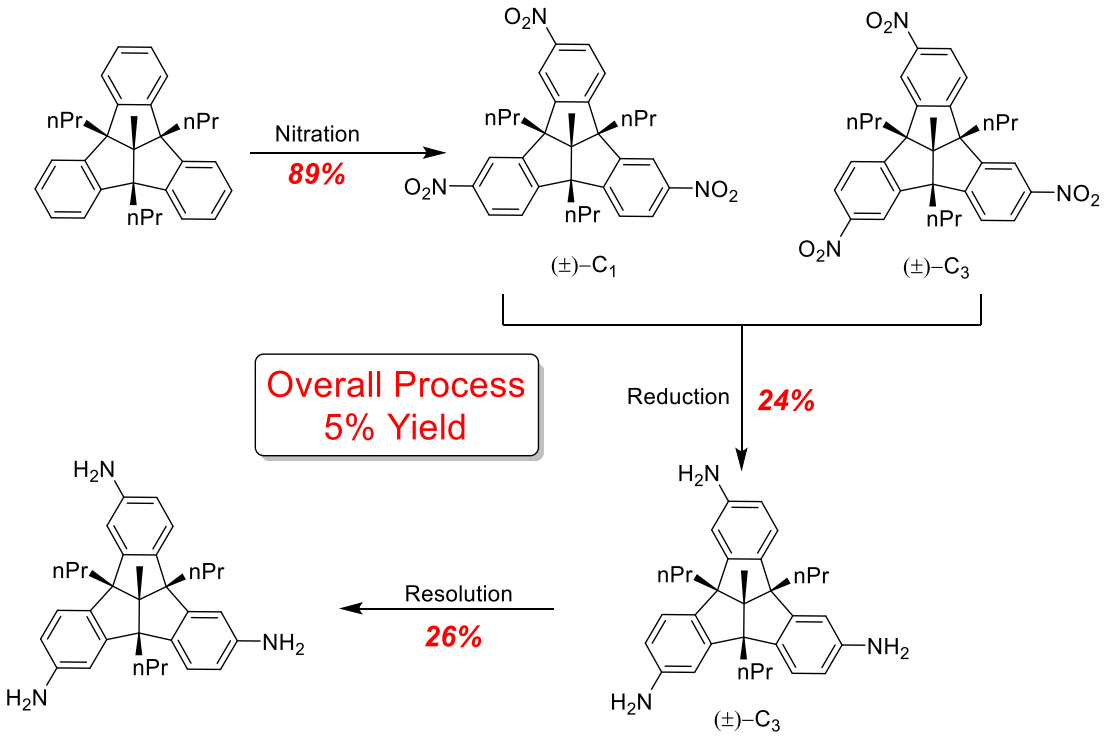

Scheme 1.6: Synthetic process and chiral resolutions using benzoyl-tartaric acid on three-fold chiral TBTQ systems.

access to axially chiral TBTQ derivatives would provide access to well defined monomers to be used with CAS.

1.4.2 Enantioselective processes

Axially chiral compounds have been becoming more and more prevalent over the past decade. They occur in numerous natural products and have been investigated extensively, as such enantioselective electrophilic aromatic substitutions (S_EAr) are often key to induce such an axis in these syntheses. However, control outside of the conventional *ortho, meta, para*, directing has been difficult when looking at many of the multi-dimensional monomers used for molecular strips and branched structures.

SEAr nitrations, highly sought after for the use in TBTQ systems, have had no exploration in regard to enantioselective, aromatic, nitrations to control or induce a chiral axis. The idea of through-space directed functionalization utilized by Letcka and coworkers[80, 96-98] has given way to a more pronounced manner of control of such complex systems. Installation of polarized fluorine atoms above aromatic systems, in the proximity

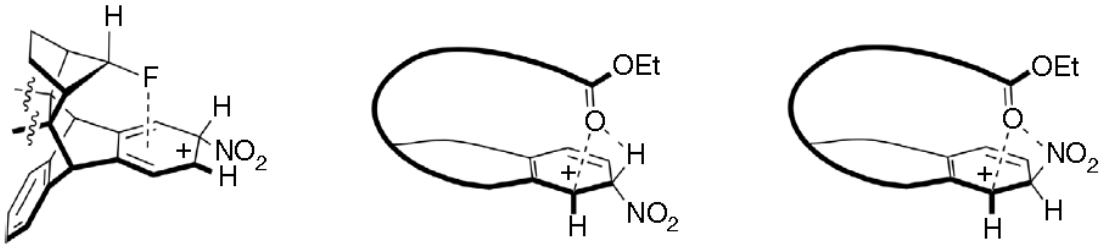

Figure 1.5: Directing SEAr reactions from above and below aromatic rings to control stereo and regio isomers

of a delocalized ring, allows activation of two symmetrically equivalent positions on the ring for SEAr reactions as demonstrated in Figure 1.5.

Under typical SEAr nitration conditions there is no bias toward the formation of stereoisomers that formed after a singular nitration, and after subsequent nitrations there is an added complexity in the regioselectivity that was exhibited in the final monomers. Further expansion in *Murphy et al* demonstrated[99] that carbonyl groups located directly above two atoms of an aromatic ring (Figure 1.5,) can precisely direct the substitution to one specific location. Careful dictation and placement of stabilizing interactions of ester moieties can influence not only the stereochemical outcome of the mononitrations but the regioselective outcome of the dinitration of subsequent SEAr reactions. The primary influence of this control is attributed to interactions both above and below the aromatic rings of interest. Stabilization of a specific wheland intermediate, therefore occurs via tailored carbonyls from partially flexible ester moieties, utilizes non-classical hydrogen bonding which in turn allows for moderate selectivity. This concept has shown excellent promise in extending control to induce such chiral axes and represents the core of the work presented herein.

1.5 Conclusions and Introductory Remarks

Due to the specific nuances in control that chirality assisted synthesis offers toward making highly coveted macromolecules as demonstrated in the past half-decade, the

development of enantioselective methods – especially in regard to electrophilic aromatic nitrations – has seen a significant growth in the field. The CAS method critically depends on the formation and use of enantiopure starting materials to fully maintain the founded shape control as described in chapter 1. The second aspect that leads to the described shape control lies in the selection of the curved monomers, rigid backbones and a defined 3-dimensional shape. For this reason, two core materials have been targeted and utilized in the Schneebeli group. The first, used primarily for c-shape strips and molecular belts, is a curved anthracene-based structure. The second, to be used in the formation of large well defined cubic organic cages, is a functionalized and enantiopure tribenzotriquinacenes system which is the primary focus of the main body of this work presented.

Described in the following chapters is prior work as well as research performed in our laboratory to (i) synthesize and optimize the core structure of TBTQ, (ii) access a targeted bromoaniline derivative to be used as a monomer of a cubic cage, and (iii) develop an enantioselective electrophilic aromatic nitration to induce a chiral axis in a C_3 symmetric tribenzotriquinacene system. Additionally, ongoing work aimed at expanding the reaction scope of through-space directed enantioselective electrophilic aromatic nitration reactions for enantioselective synthesis is presented. Finally, a brief exploration of size control in polymer synthesis with a novel unique iterative exponential growth (IEG) methodology, which operates with nucleophilic aromatic substitution chemistry, is described. The following chapters will include discussion of synthetic challenges, outcomes, characterization, future works, and outlooks.

References

1. Oliver, K.; Seddon, A.; Trask, R. S., Morphing in nature and beyond: a review of natural and synthetic shape-changing materials and mechanisms. *J. Mater. Sci.* **2016,** *51* (24), 10663.
2. Skubi, K. L.; Yoon, T. P., Organic chemistry Shape control in reactions with light. *Nature* **2014,** *515* (7525), 45.
3. Northrup, J. D.; Mancini, G.; Purcell, C. R.; Schafmeister, C. E., Development of spiroligomer-peptoid hybrids. *J. Org. Chem.* **2017,** *82* (24), 13020.
4. Pfeiffer, C. T.; Northrup, J. D.; Cheong, J. E.; Pham, M. A.; Parker, M. F. L.; Schafmeister, C. E., Utilization of the p-nitrobenzyloxycarbonyl (pNZ) amine protecting group and pentafluorophenyl (Pfp) esters for the solid phase synthesis of spiroligomers. *Tetrahedron Lett.* **2018,** *59* (30), 2884.
5. Schafmeister, C. E.; Po, J.; Verdine, G. L., An All-Hydrocarbon Cross-Linking System for Enhancing the Helicity and Metabolic Stability of Peptides. *J. Am. Chem. Soc.* **2000,** *122* (24), 5891.
6. Sinclair, J. K. L.; Walker, A. S.; Doerner, A. E.; Schepartz, A., Mechanism of Allosteric Coupling into and through the Plasma Membrane by EGFR. *Cell Chem. Biol.* **2018,** *25* (7), 857.
7. Tjin, C. C.; Wissner, R. F.; Jamali, H.; Schepartz, A.; Ellman, J. A., Synthesis and Biological Evaluation of an Indazole-Based Selective Protein Arginine Deiminase 4 (PAD4) Inhibitor. *ACS Med. Chem. Lett.* **2018,** *9* (10), 1013.
8. Liu, X.; Weinert, Z. J.; Sharafi, M.; Liao, C.; Li, J.; Schneebeli, S. T., Regulating Molecular Recognition with C-Shaped Strips Attained by Chirality-Assisted Synthesis. *Angew. Chem., Int. Ed.* **2015,** *54* (43), 12772.
9. Winkler, J. D.; Twenter, B. M.; Gendrineau, T., Synthesis of substituted phenazines via palladium-catalyzed aryl ligation. *Heterocycles* **2012,** *84* (2), 1345.
10. Gao, X.; Lu, Y.; Xing, Y.; Ma, Y.; Lu, J.; Bao, W.; Wang, Y.; Xi, T., A novel anticancer and antifungus phenazine derivative from a marine actinomycete BM-17. *Microbiol Res* **2012,** *167* (10), 616.
11. Hassan, S. S. u.; Anjum, K.; Abbas, S. Q.; Akhter, N.; Shagufta, B. I.; Shah, S. A. A.; Tasneem, U., Emerging biopharmaceuticals from marine actinobacteria. *Environ. Toxicol. Pharmacol.* **2017,** *49*, 34.
12. Trabelsi, I.; Oves, D.; Magan, B. G.; Manteca, A.; Genilloud, O.; Nour, M., Isolation, characterization and antimicrobial activities of actinomycetes isolated from a Tunisian Saline Wetland. *J. Microb. Biochem. Technol.* **2016,** *8* (6), 465.
13. Yadav, D.; Shukla, G.; Ansari, M. A.; Srivastava, A.; Singh, M. S., Chemoselective one-pot access to benzo[e]indole-4,5-diones and naphtho[2,1-b]thiophene-4,5-diones via copper-catalyzed oxidative [3 + 2] annulation of α-oxoketene N,S-acetals/β-ketothioamides with α-/β-naphthols. *Tetrahedron* **2018,** *74* (40), 5920.
14. Aoki, Y.; O'Brien, H. M.; Kawasaki, H.; Takaya, H.; Nakamura, M., Ligand-Free Iron-Catalyzed C-F Amination of Diarylamines: A One-Pot Regioselective Synthesis of Diaryl Dihydrophenazines. *Org. Lett.* **2019,** *21* (2), 461.

15. Jia, T.; Huang, S.; Bohra, H.; Wang, M., Examining derivatives of quinacridone, diketopyrrolopyrrole and indigo as the visible-light organic photocatalysts for metal-free atom transfer radical polymerization. *Dyes Pigm.* **2019,** *165*, 223.
16. Lim, C.-H.; Ryan, M. D.; McCarthy, B. G.; Theriot, J. C.; Sartor, S. M.; Damrauer, N. H.; Musgrave, C. B.; Miyake, G. M., Intramolecular Charge Transfer and Ion Pairing in N,N-Diaryl Dihydrophenazine Photoredox Catalysts for Efficient Organocatalyzed Atom Transfer Radical Polymerization. *J. Am. Chem. Soc.* **2017,** *139* (1), 348.
17. Miyake, G. In *Organocatalyzed atom transfer radical polymerization driven by visible light*, American Chemical Society: 2017; pp ORGN.
18. Zhang, N.-N.; Sa, R.-J.; Sun, S.-S.; Li, M.-D.; Wang, M.-S.; Guo, G.-C., Photoresponsive triazole-based donor-acceptor molecules: color change and heat/air-stable diradicals. *J. Mater. Chem. C* **2019**, Ahead of Print.
19. Shaikh, A. M.; Sharma, B. K.; Chacko, S.; Kamble, R. M., Novel electroluminescent donor–acceptors based on dibenzo[a,c]phenazine as hole-transporting materials for organic electronics. *New J. Chem.* **2017,** *41* (2), 628.
20. Bolibrukh, K.; Khoumeri, O.; Polovkovych, S.; Novikov, V.; Terme, T.; Vanelle, P., Novel Synthesis of 5-Substituted 5H-Benzo[b]carbazole-6,11-diones via Double Buchwald-Hartwig Reaction. *Synlett* **2014,** *25* (19), 2765.
21. Hahn, S.; Koser, S.; Hodecker, M.; Seete, P.; Rominger, F.; Miljanic, O. S.; Dreuw, A.; Bunz, U. H. F., Phenylene Bridged Cyclic Azaacenes: Dimers and Trimers. *Chem. - Eur. J.* **2018,** *24* (27), 6968.
22. Ohlendorf, L.; Velandia, J. E. D.; Konya, K.; Ehlers, P.; Villinger, A.; Langer, P., Synthesis and properties of 5,7-disubstituted 5,7-dihydropyrido[2,3-b:6,5-b']diindoles. *Adv. Synth. Catal.* **2017,** *359* (10), 1758.
23. Winkler, J. D.; Twenter, B.; Gendrineau, T., Aryl ligation: A new approach to the synthesis of unnatural products. *Heterocycles* **2011,** *84*, 1345.
24. Ashton, P. R.; Brown, G. R.; Isaacs, N. S.; Giuffrida, D.; Kohnke, F. H.; Mathias, J. P.; Slawin, A. M. Z.; Smith, D. R.; Stoddart, J. F.; Williams, D. J., Molecular LEGO. 1. Substrate-directed synthesis via stereoregular Diels-Alder oligomerizations. *J. Am. Chem. Soc.* **1992,** *114* (16), 6330.
25. Cao, J.; Zhu, X.-Z.; Chen, C.-F., Synthesis, Structure, and Binding Property of Pentiptycene-Based Rigid Tweezer-like Molecules. *J. Org. Chem.* **2010,** *75* (21), 7420.
26. Chen, Z.; Swager, T. M., Synthesis and Characterization of Poly(2,6-triptycene). *Macromolecules (Washington, DC, U. S.)* **2008,** *41* (19), 6880.
27. Chong, J. H.; MacLachlan, M. J., Iptycenes in supramolecular and materials chemistry. *Chem. Soc. Rev.* **2009,** *38* (12), 3301.
28. Crane, A. K.; Wong, E. Y. L.; MacLachlan, M. J., Metal-organic frameworks from novel flexible triptycene- and pentiptycene-based ligands. *CrystEngComm* **2013,** *15* (45), 9811.
29. Hilton, C. L.; Jamison, C. R.; Zane, H. K.; King, B. T., A Triphenylene-Based Triptycene with Large Free Volume Synthesized by Zirconium-Mediated Biphenylation. *J. Org. Chem.* **2009,** *74* (1), 405.
30. Jiang, Y.; Chen, C.-F., Synthesis and structures of 1,10-phenanthroline-based extended triptycene derivatives. *Synlett* **2010,** (11), 1679.

31. Liang, Q.; Chong, J. H.; White, N. G.; Zhao, Z.; MacLachlan, M. J., Towards a self-assembled honeycomb structure via diaminotriptycene metal complexes. *Dalton Trans.* **2013,** *42* (47), 16474.
32. Lou, K.; Prior, A. M.; Wiredu, B.; Desper, J.; Hua, D. H., Synthesis of Cyclododeciptycene Quinones. *J. Am. Chem. Soc.* **2010,** *132* (49), 17635.
33. Mastalerz, M., Single-Handed Towards Nanosized Organic Molecules. *Angew. Chem., Int. Ed.* **2016,** *55* (1), 45.
34. White, N. G.; MacLachlan, M. J., Soluble Tetraaminotriptycene Precursors. *J. Org. Chem.* **2015,** *80* (16), 8390.
35. Zhao, L.; Li, Z.; Wirth, T., Triptycene derivatives: synthesis and applications. *Chem. Lett.* **2010,** *39* (7), 658.
36. Beaudoin, D.; Rominger, F.; Mastalerz, M., Chirality-Assisted Synthesis of a Very Large Octameric Hydrogen-Bonded Capsule. *Angew. Chem., Int. Ed.* **2016,** *55* (50), 15599.
37. Bernstein, J.; Davis, R. E.; Shimoni, L.; Chang, N.-L., Patterns in hydrogen bonding: functionality and graph set analysis in crystals. *Angew. Chem., Int. Ed. Engl.* **1995,** *34* (15), 1555.
38. MacGillivray, L. R.; Atwood, J. L., A chiral spherical molecular assembly held together by 60 hydrogen bonds. *Nature* **1997,** *389* (6650), 469.
39. Maehara, T.; Sekiya, R.; Harada, K.; Haino, T., Tunable enforced cavities inside self-assembled capsules. *Org. Chem. Front.* **2019**, Ahead of Print.
40. Martin, T.; Obst, U.; Rebek, J., Jr., Molecular assembly and encapsulation directed by hydrogen-bonding preferences and the filling of space. *Science* **1998,** *281* (5384), 1842.
41. Rahman, F.-U.; Feng, H.-N.; Yu, Y., A new water-soluble cavitand with deeper guest binding properties. *Org. Chem. Front.* **2019**, Ahead of Print.
42. Young, M. C.; Djernes, K. E.; Payton, J. L.; Liu, D.; Hooley, R. J., Resorcin[4]arenes: A Convenient Scaffold To Study Supramolecular Self-Assembly and Host:Guest Interactions for the Undergraduate Curriculum. *J. Chem. Educ.* **2019**, Ahead of Print.
43. Zhang, G.; Mastalerz, M., Organic cage compounds - from shape-persistency to function. *Chem. Soc. Rev.* **2014,** *43* (6), 1934.
44. Campbell, J. P.; Rajappan, S. C.; Jaynes, T. J.; Sharafi, M.; Ma, Y.-T.; Li, J.; Schneebeli, S. T., Enantioselective Electrophilic Aromatic Nitration: A Chiral Auxiliary Approach. *Angew. Chem., Int. Ed.* **2019,** *58* (4), 1035.
45. Greschner, W.; Neumann, B.; Stammler, H.-G.; Groeger, H.; Kuck, D., Enantiomerically Pure Tribenzotriquinacenes through Stereoselective Synthesis. *Angew. Chem., Int. Ed.* **2015,** *54* (46), 13764.
46. Mastalerz, M.; Rominger, F.; Beaudoin, D., Synthesis and Chiral Resolution of C3-symmetric Tribenzotriquinacenes. *Eur. J. Org. Chem.* **2016,** *2016* (26), 4470.
47. Murphy, K. E.; Bocanegra, J. L.; Liu, X.; Chau, H. K.; Lee, P. C.; Li, J.; Schneebeli, S. T., Precise through-space control of an abiotic electrophilic aromatic substitution reaction. *Nature Commun.* **2017,** *8*, 14840.
48. Wagner, P.; Rominger, F.; Mastalerz, M., Switching the Statistical C3 /C1 Ratio in the Threefold Aromatic Substitution of Tribenzotriquinacenes towards the C3 Isomer. *Angew. Chem. Int. Ed.* **2018,** *57* (35), 11321.

49. Chong, J. H.; MacLachlan, M. J., Synthesis and Structural Investigation of New Triptycene-Based Ligands: En Route to Shape-Persistent Dendrimers and Macrocycles with Large Free Volume. *J. Org. Chem.* **2007,** *72* (23), 8683.
50. Dietrich-Buchecker, C. O.; Sauvage, J. P.; Kern, J. M., Templated synthesis of interlocked macrocyclic ligands: the catenands. *J. Am. Chem. Soc.* **1984,** *106* (10), 3043.
51. Quernheim, M.; Golling, F. E.; Zhang, W.; Wagner, M.; Raeder, H.-J.; Nishiuchi, T.; Muellen, K., The Precise Synthesis of Phenylene-Extended Cyclic Hexa-peri-hexabenzocoronenes from Polyarylated [n]Cycloparaphenylenes by the Scholl Reaction. *Angew. Chem., Int. Ed.* **2015,** *54* (35), 10341.
52. Harmata, M., Chiral Molecular Tweezers. *Acc. Chem. Res.* **2004,** *37* (11), 862.
53. Ma, D.; Glassenberg, R.; Ghosh, S.; Zavalij, P. Y.; Isaacs, L., Acyclic cucurbituril congener binds to local anaesthetics. *Supramol. Chem.* **2012,** *24* (5), 325.
54. Sheikh, A. H.; Khalid, A.; Khan, F.; Begum, A., Fluorescent Gadolinium(III)-Oligopeptide Complexes and Carbon Nanotube Composite as Dual Modality Anticancer Agents. *ChemistrySelect* **2019,** *4* (1), 228.
55. Sumerin, V.; Schulz, F.; Atsumi, M.; Wang, C.; Nieger, M.; Leskelae, M.; Repo, T.; Pyykkoe, P.; Rieger, B., Molecular Tweezers for Hydrogen: Synthesis, Characterization, and Reactivity. *J. Am. Chem. Soc.* **2008,** *130* (43), 14117.
56. Gong, X.; Wu, J.; Meng, Y.; Zhang, Y.; Ye, L.-W.; Zhu, C., Ligand-free palladium catalyzed Ullmann biaryl synthesis: 'household' reagents and mild reaction conditions. *Green Chem.* **2019**, Ahead of Print.
57. Rommelmann, P.; Greschner, W.; Ihrig, S.; Neumann, B.; Stammler, H.-G.; Gröger, H.; Kuck, D., Combining Stereoselective Enzyme Catalysis with Chirality-Assisted Synthesis in Tribenzotriquinacene Chemistry. *Eur. J. Org. Chem.* **2018,** *2018* (29), 3891.
58. Vasconcelos, S. N. S.; Reis, J. S.; de Oliveira, I. M.; Balfour, M. N.; Stefani, H. A., Synthesis of symmetrical biaryl compounds by homocoupling reaction. *Tetrahedron* **2019**, Ahead of Print.
59. Schneebeli, S.; Li, J.; Sharafi, M.; Weinert, Z.; Cohen, I.; Liao, C.; Ivancic, M., Controlled Self-Assembly inside C-Shaped Polyaromatic Strips. *Synlett* **2016,** *27* (14), 2145.
60. Barnes, J. C.; Ehrlich, D. J. C.; Gao, A. X.; Leibfarth, F. A.; Jiang, Y.; Zhou, E.; Jamison, T. F.; Johnson, J. A., Iterative exponential growth of stereo- and sequence-controlled polymers. *Nat. Chem.* **2015,** *7* (10), 810.
61. Hawker, C. J.; Malmstroem, E. E.; Frank, C. W.; Kampf, J. P., Exact Linear Analogs of Dendritic Polyether Macromolecules: Design, Synthesis, and Unique Properties. *J. Am. Chem. Soc.* **1997,** *119* (41), 9903.
62. Estrella, L. L.; Balanay, M. P.; Kim, D. H., Theoretical Insights into D-D-π-A Sensitizers Employing N-Annulated Perylene for Dye-Sensitized Solar Cells. *J. Phys. Chem. A* **2018,** *122* (30), 6328.
63. Hestand, N. J.; Spano, F. C., Molecular Aggregate Photophysics beyond the Kasha Model: Novel Design Principles for Organic Materials. *Acc. Chem. Res.* **2017,** *50* (2), 341.
64. Kim, J. Y.; Hwang, T. G.; Kim, S. H.; Namgoong, J. W.; Kim, J. E.; Sakong, C.; Choi, J.; Lee, W.; Kim, J. P., Synthesis of high-soluble and non-fluorescent perylene

derivatives and their effect on the contrast ratio of LCD color filters. *Dyes Pigm.* **2017,** *136*, 836.
65. Gu, P. Y.; Zhao, Y.; He, J. H.; Zhang, J.; Wang, C.; Xu, Q. F.; Lu, J. M.; Sun, X. W.; Zhang, Q., Synthesis, physical properties, and light-emitting diode performance of phenazine-based derivatives with three, five, and nine fused six-membered rings. *J. Org. Chem.* **2015,** *80* (6), 3030.
66. Asadi, A.; Ajami, D.; Rebek, J., Covalent capsules: reversible binding in a chiral space. *Chem. Sci.* **2013,** *4* (3), 1212.
67. Elbert, S. M.; Rominger, F.; Mastalerz, M., Synthesis of a rigid C3v -symmetric tris-salicylaldehyde as a precursor for a highly porous molecular cube. *Chem. Eur. J.* **2014,** *20* (50), 16707.
68. Galan, A.; Escudero-Adan, E. C.; Ballester, P., Template-directed self-assembly of dynamic covalent capsules with polar interiors. *Chem. Sci.* **2017,** *8* (11), 7746.
69. Rowan, S. J.; Cantrill, S. J.; Cousins, G. R. L.; Sanders, J. K. M.; Stoddart, J. F., Dynamic covalent chemistry. *Angew. Chem., Int. Ed.* **2002,** *41* (6), 899.
70. Xu, X.-N.; Wang, L.; Wang, G.-T.; Lin, J.-B.; Li, G.-Y.; Jiang, X.-K.; Li, Z.-T., Hydrogen-Bonding-Mediated Dynamic Covalent Synthesis of Macrocycles and Capsules: New Receptors for Aliphatic Ammonium Ions and the Formation of Pseudo[3]rotaxanes. *Chem. - Eur. J.* **2009,** *15* (23), 5763.
71. Ashwell, G. J.; Hamilton, R.; Wood, B. J.; Gentle, I. R.; Zhou, D., Molecular Lego non-centrosymmetric alignment within interdigitating layers. *J. Mater. Chem.* **2001,** *11* (12), 2966.
72. Lu, Y.; Huang, F.; Wang, J.; Xia, J., Affinity-Guided Covalent Conjugation Reactions Based on PDZ-Peptide and SH3-Peptide Interactions. *Bioconjugate Chem.* **2014,** *25* (5), 989.
73. Mano, N.; Kuhn, A., Molecular lego for the assembly of biosensing layers. *Talanta* **2005,** *66* (1), 21.
74. Mathias, J. P.; Stoddart, J. F., Constructing a molecular LEGO set. *Chem. Soc. Rev.* **1992,** *21* (4), 215.
75. Muto, Y.; Yokoyama, S., Structural insight into RNA recognition motifs: versatile molecular Lego building blocks for biological systems. *Wiley Interdiscip. Rev.: RNA* **2012,** *3* (2), 229.
76. Sadeghi, S. J.; Meharenna, Y. T.; Fantuzzi, A.; Valetti, F.; Gilardi, G., Engineering artificial redox chains by molecular 'Lego'. *Faraday Discuss.* **2000,** *116* (Bioelectrochemistry), 135.
77. Takaba, H.; Omachi, H.; Yamamoto, Y.; Bouffard, J.; Itami, K., Selective Synthesis of [12]Cycloparaphenylene. *Angew. Chem., Int. Ed.* **2009,** *48* (33), 6112.
78. Villalonga-Barber, C.; Micha-Screttas, M.; Steele, B. R.; Georgopoulos, A.; Demetzos, C., Dendrimers as biopharmaceuticals: synthesis and properties. *Curr. Top. Med. Chem.* **2008,** *8* (14), 1294.
79. Stewart, J. J., Optimization of parameters for semiempirical methods V: modification of NDDO approximations and application to 70 elements. *J Mol Model* **2007,** *13* (12), 1173.

80. Holl, M. G.; Struble, M. D.; Singal, P.; Siegler, M. A.; Lectka, T., Positioning a Carbon-Fluorine Bond over the pi Cloud of an Aromatic Ring: A Different Type of Arene Activation. *Angew. Chem. Int. Ed.* **2016,** *55* (29), 8266.
81. Rommelmann, P.; Nachtigall, B.; Guntelmann, T.; Groeger, H.; Kuck, D., Stereoselective synthesis of enantiomerically pure bowl-shaped hydroxytribenzotriquinacenes. *Org. Biomol. Chem.* **2018,** *16* (31), 5635.
82. Sakata, Y.; Yamamoto, R.; Saito, D.; Tamura, Y.; Maruyama, K.; Ogoshi, T.; Akine, S., Metallonanobelt: A Kinetically Stable Shape-Persistent Molecular Belt Prepared by Reversible Self-Assembly Processes. *Inorg. Chem.* **2018,** *57* (24), 15500.
83. Wong, W.-S.; Tse, H.-W.; Cheung, E.; Kuck, D.; Chow, H.-F., Enantiopure Aromatic Saddles Bearing the Fenestrindane Core. *J. Org. Chem.* **2019,** *84* (2), 869.
84. Klotzbach, S.; Beuerle, F., Shape-Controlled Synthesis and Self-Sorting of Covalent Organic Cage Compounds. *Angew. Chem., Int. Ed.* **2015,** *54* (35), 10356.
85. Kuck, D.; Lindenthal, T.; Schuster, A., Benzanellated centropolyquinanes. 11. Synthesis of tribenzotriquinacene and some centro-substituted derivatives. *Chem. Ber.* **1992,** *125* (6), 1449.
86. Kuck, D.; Schuster, A.; Krause, R. A.; Tellenbroker, J.; Exner, C. P.; Penk, M.; Bogge, H.; Muller, A., Multiply bridgehead- and periphery-substituted tribenzotriquinacenes - highly versatile rigid molecular building blocks with C3v or C3 symmetry. *Tetrahedron* **2001,** *57* (17), 3587.
87. Linke, J.; Bader, N.; Tellenbroeker, J.; Kuck, D., Sixfold Peripheral Halogenation of Tribenzotriquinacenes: An Alternative Access to Useful TBTQ Building Blocks. *Synthesis* **2018,** *50* (1), 175.
88. Narita, A.; Wang, X.-Y.; Feng, X.; Muellen, K., New advances in nanographene chemistry. *Chem. Soc. Rev.* **2015,** *44* (18), 6616.
89. Wang, T.; Zhang, Y.-F.; Hou, Q.-Q.; Xu, W.-R.; Cao, X.-P.; Chow, H.-F.; Kuck, D., C3-Symmetrical Tribenzotriquinacene Derivatives: Optical Resolution through Cryptophane Synthesis and Supramolecular Self-Assembly into Nanotubes. *J. Org. Chem.* **2013,** *78* (3), 1062.
90. Niu, W. X.; Wang, T.; Hou, Q. Q.; Li, Z. Y.; Cao, X. P.; Kuck, D., Synthesis and optical resolution of inherently chiral difunctionalized tribenzotriquinacenes. *J. Org. Chem.* **2010,** *75* (19), 6704.
91. Mino, T.; Yamaguchi, D.; Masuda, C.; Youda, J.; Ebisawa, T.; Yoshida, Y.; Sakamoto, M., Synthesis and application of P,olefin type axially chiral ligands with sec-alkyl groups. *Org. Biomol. Chem.* **2019,** *17* (6), 1455.
92. Vergura, S.; Scafato, P.; Belviso, S.; Superchi, S., Absolute Configuration Assignment from Optical Rotation Data by Means of Biphenyl Chiroptical Probes. *Chem. - Eur. J.* **2019**, Ahead of Print.
93. Wang, J.; Shi, X. In *Novel design and preparation of an triazole-based axial chiral P,N-ligand*, American Chemical Society: 2019; pp ORGN.
94. Beaudoin, D.; Rominger, F.; Mastalerz, M., Synthesis and Chiral Resolution ofC3-Symmetric Tribenzotriquinacenes. *Eur. J. Org. Chem.* **2016,** *2016* (26), 4470.
95. Xu, W.-R.; Wang, X.-R.; Chow, H.-F.; Kuck, D., Synthesis and Characterization of Enantiopure Tribenzotriquinacene Dimers Bearing a Platinum-Diacetylene Unit. *Synthesis* **2019**.

96. Bume, D. D.; Pitts, C. R.; Ghorbani, F.; Harry, S. A.; Capilato, J. N.; Siegler, M. A.; Lectka, T., Ketones as directing groups in photocatalytic sp(3) C-H fluorination. *Chem Sci* **2017,** *8* (10), 6918.
97. Guan, L.; Holl, M. G.; Pitts, C. R.; Struble, M. D.; Siegler, M. A.; Lectka, T., Through-Space Activation Can Override Substituent Effects in Electrophilic Aromatic Substitution. *J. Am. Chem. Soc.* **2017,** *139* (42), 14913.
98. Holl, M. G.; Pitts, C. R.; Lectka, T., Fluorine in a C-F Bond as the Key to Cage Formation. *Angew. Chem. Int. Ed.* **2018,** *57* (11), 2758.
99. Murphy, K. E.; Bocanegra, J. L.; Liu, X.; Chau, H. Y. K.; Lee, P. C.; Li, J.; Schneebeli, S. T., Precise through-space control of an abiotic electrophilic aromatic substitution reaction. *Nature communications* **2017,** *8*, 14840.

CHAPTER 2: THROUGH SPACE SELECTIVITY: ENANTIOSELECTIVE ELECTROPHILIC AROMATIC NITRATIONS TOWARD WELL DEFINED MACROSTRUCTURES

2.1 Introduction: Tribenzotriquinacene

Tribenzotriquinacene is a structurally interesting aralipahatic hydrocarbon. It is comprised of a fused core of three separate indan units to form a cup or bowl like structure similar to corannulene and extended with three benzo units. In this instance an even more pronounced curvature is present where the indan units are directly annulated [1] and the

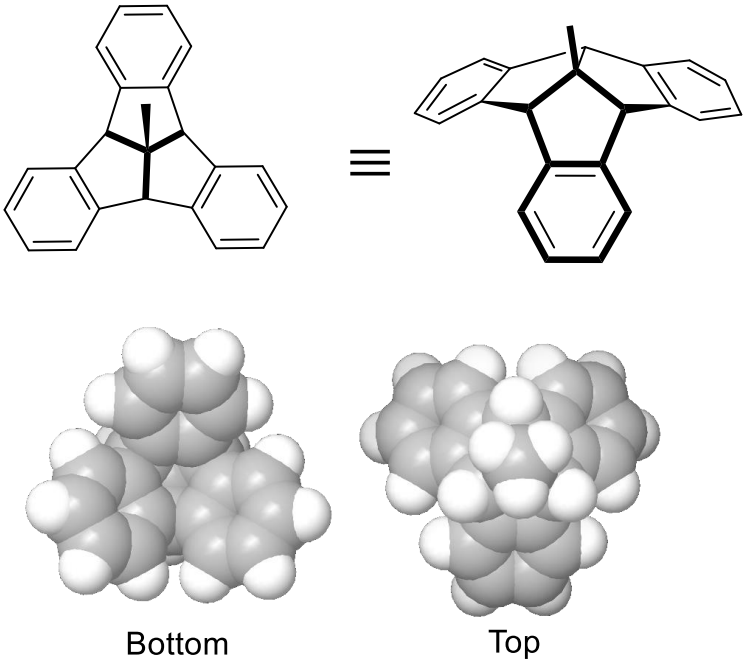

Figure 2.1: Chem draw (flat and 3 dimensional) and space filling molecular model of core TBTQ structure.

substituents of the inner four carbon atoms are arranged in an all cis fashion. This extension not only gives considerable stabilization when compared to the triquinacene core, but it offers enhanced reactivity and opportunity for post synthetic modification offered at the multiple positions[1] of the core structure shown in figure 2.1.

2.1.1 TBTQ Core: Synthesis and Characteristics

The most important aspect of the TBTQ systems resides in the unique structure of the core. The core is comprised of the three orthogonally annulated wings as previously discussed. This provides a rigid C_{3v}-symmetric structure. The carbon atoms in those respective indane wings are in a single plane, and the three axes formed from the vertex point carbon to the center of the surrounding phenylenes is approximately 87.2° [2]. This aspect, is unique in regard to how close it is to a right angle and the implications it has when comparing TBTQs to other organic building blocks[1]. When compared to conventional arrangements of bonds around a carbon atom (tetrahedral, triangular, and linear) they are 109.5°, 120°, and 180° for sp^3, sp^2 and sp hybridizations respectively. The overall perpendicular orientation of this molecule and the defined shape is what makes TBTQ molecules ideal building block candidates in CAS method.

Synthesis of the core TBTQ structure was first done in 1984 by Kuck and coworkers and modified again in 1992 [2, 3]. The synthetic strategy begins with the formation of and an indandione by reacting a dialkyl phthalate **1** and a ketone. The corresponding

indandione is reacted with PTSA and diphenyl methanol **4**, to give the substituted indane-1,3-diones **5** which is reduced to the diol **6** using lithium aluminum hydride (LAH). Two-fold dehydrocyclization leads to the corresponding TBTQ **7** as summarized in Scheme 2.1

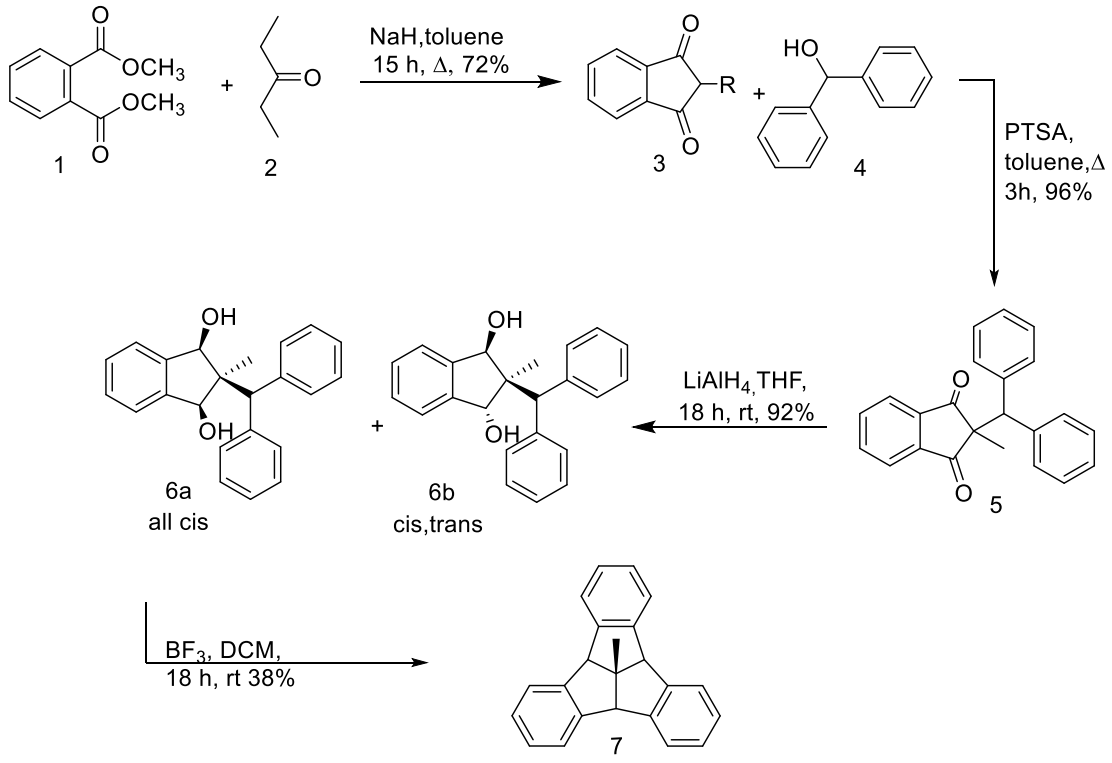

Scheme 2.1: General synthesis to the core methyltribenzotriquinacene.

It is important to note that the first opportunity for functionalization of the vertex point can be done through modification of the ketone used to form the indandione[3]. Preliminary work involving tribenzotriquinacene involved both synthesizing and modest optimizations to the C_{3v}- symmetric analog with a methyl group at the vertex point.

Whereas many of the reactions in the original scheme boast yields of greater than 70%, the cyclodehydration to afford the methyltribenzotriquinacene has been reported to give only about 30% yields in the literature[2]. Initial attempts to optimize this reaction include the use of polyphosphoric acid to contain the reaction to a single interface which in turn allowed for the minimization of unwanted polymerization of cationic intermediates. Trials into this optimization found that there was an increase of about 8% to the overall yield of this reaction. The challenges in the formation of Methyltribenzotriquinacene are due to two main factors, the first being the cleavage of ***C-C*** bonds in the beta position of the incipient carbenium ion. The second can be attributed to the prochirality of the benzhydryl group. This inherently leads to two different stereoisomers upon mono cyclization shown in Figure 2.2. Of these two intermediates, the less favored endo

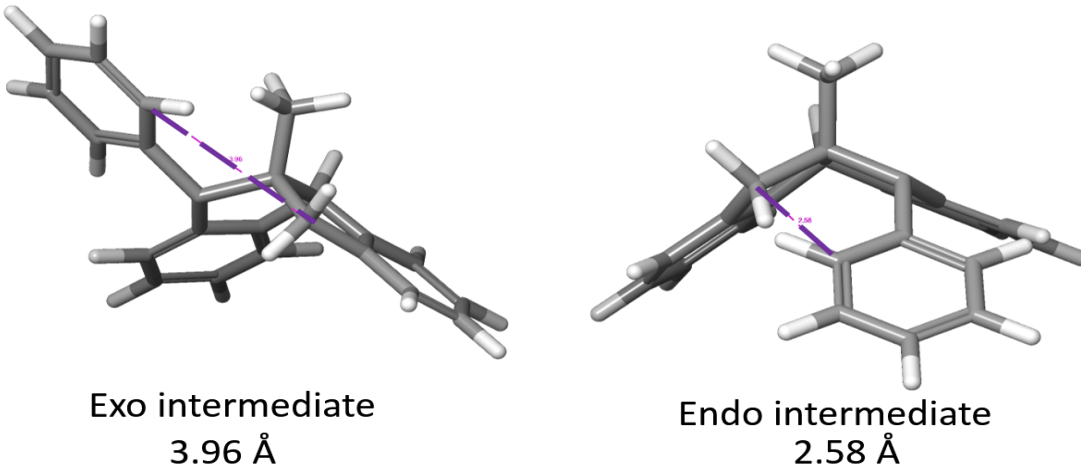

Figure 2.2: Stereoisomers of monocyclized intermediate. Relative distances between of cyclization sites is shown in purple.

intermediate will then go on to fully cyclize to the desired product[2]. The difficulty with the second cyclization in the more favored exo intermediate, is due to the fact that the recipient

aromatic ring is too far away to undergo a nucleophilic attack to complete the desired cyclization. Instead there are various eliminations and fragmentations that occur further hindering the yield.

In order to remedy the latter of these difficulties, introduction of a Lewis acid (LA) shows a 10% increase in yields. The idea behind this method is to potentially use the LA to loosely coordinate the mono cyclized intermediate to maybe favor the *endo* formation. Optimization efforts found that, with a larger excess of LA used with longer run time gave more unwanted side products. By keeping the molar equivalents of the LA to a minimum and diluting the reaction solution, under optimal conditions this reaction can proceed with yields ranging from 40-60%. These yields can ultimately be attributed to a variety of external variables such as humidity and are the reason for the range in yields. With generally acceptable yields for the formation of the core structure, synthetic ventures turned toward making the functionalized chiral monomer that showed promise in the formation of a well-defined cubic cage.

2.2 Functionalizing TBTQ

Following the report of the formation of TBTQ the process to investigate all of its unique properties and by extension derivatizing every potential position has been extensively studied[4]. For each of the sites shown (Figure 2.3). There has been substantial

headway toward the functionality introduced to the vertex point, the bridgehead, the ortho, and the peripheral positions And will also be referred to such from here on out.

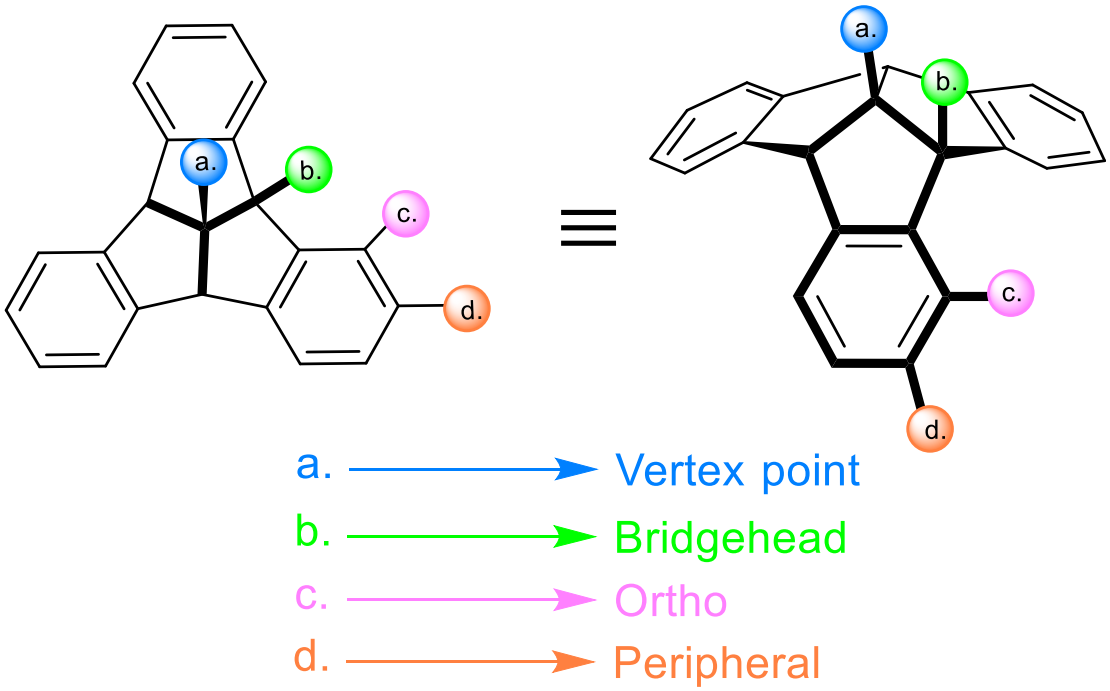

Figure 2.3: Post synthetic functionalization positions on a conventional TBTQ structure.

Both the vertex point and the bridgehead positions on the molecule offer handles to control solubility[5-7], surface attachment for self-assembly[8], or more specifically for the use of auxiliary moieties to be discussed later in chapter 2. The peripheral positions can generate unique building blocks toward the formation of supramolecular structures, especially in methods such as chirality-assisted synthesis [9, 10 4, 8, 11, 12]. In addition, extension of the aromatic framework from the benzo moieties can provide for suitable sites for novel host-guest chemistry[13, 14]. Finally, when the *ortho* positions are functionalized and followed

by a ring closure they could result in large polycyclic aromatic hydrocarbons (PAHs) used toward nanographene structures.

Of the most commonly researched post modifications that are done to TBTQ moieties, functionalization to the bridge head positions is of key importance. Introducing three bromine groups to the reactive benzylic positions is often a key intermediate which is easily obtained through use of elemental bromine and carbon tetrachloride[15]. Further optimization gave bromo bridgeheads under more benign conditions using *N*-

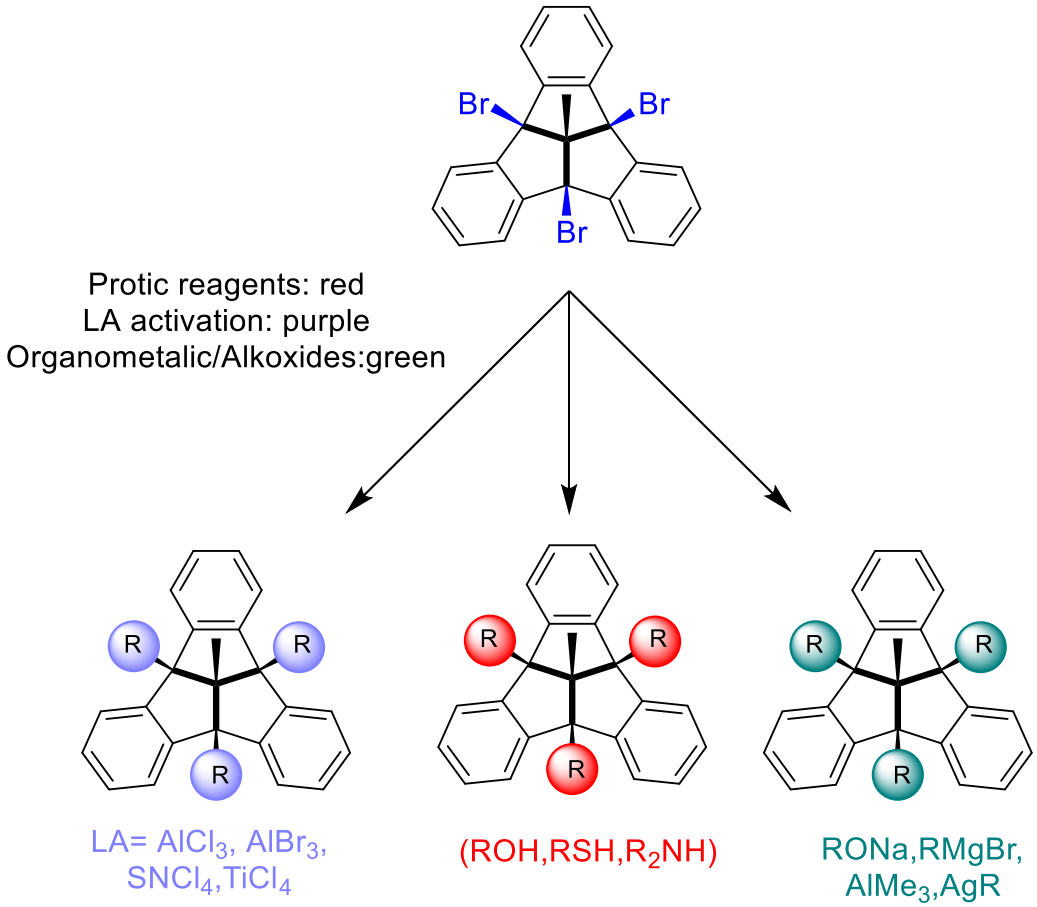

Figure 2.4: Functionalization scope of the bridgehead positions on conventional TBTQ moieties.

bromosuccinimide (NBS). This synthetic handle allows for a variety of different S_N1 type reactions to install a variety of bridge-head-functionalized TBTQ derivatives via carbon or carbon-heteroatom bond formation as shown in Figure 2.4. Mechanistically many of these reactants are introduced as acids at high temperatures, lewis activated compounds, alkoxides, and in some cases organometallic species[15]. Whereas the unique core shape of TBTQ is a primary reason for the use of these systems, it's important to note that none of these reactions have an effect on the concave shape of the TBTQ. This is largely because functionalization takes place on the convex side of the molecule. The introduction of many of these functionalities do however increase the solubility as referenced in literature and further verified in practice.

Concurrently the functionalization of the peripheral positions is powerful in the fact that it extends the valuable orthogonal framework exhibited in the TBTQ core. These unique new frameworks have been used in a variety of different host guest interactions with C_{60} and C_{70}[16] and has a dramatic impact on the binding affinities of said molecules based on the extended frameworks that are attached to the outer rim of the TBTQ. In addition, and most related to chirality assisted synthesis, derivatizing the peripheral sites introduce new reactive sites that can be further utilized as directional arrangements for a myriad of applications. Metallospheres, supramolecular structures covalently bound cages and microporous materials[12, 15, 17-20] have all peaked the interest in synthetic materials groups researching these unique compounds.

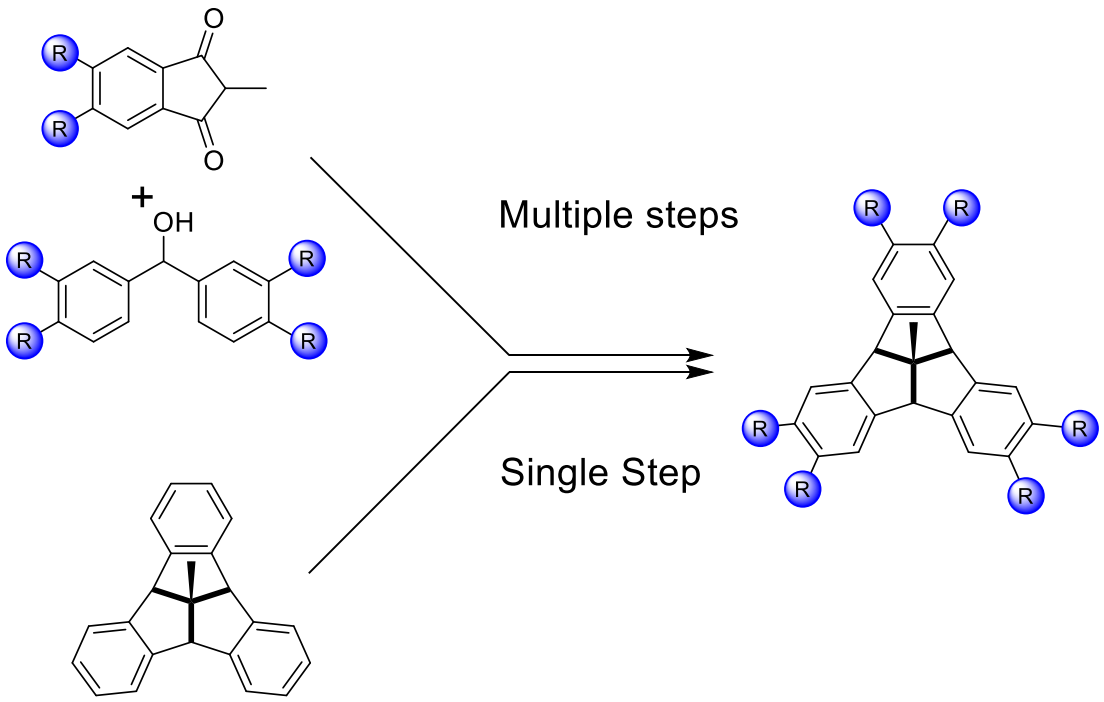

Scheme 2.2: Post-modification of peripheral positions (bottom) vs pre-modification prior to ring closure and indan core formation (top).

Synthetically, the functionalization of the peripheral positions is done in two different ways as summarized in Scheme 2.2. *i*) The peripheral positions are introduced prior to the dehydrocyclization reactions to give the functional units in the outer rim of the structure or *ii*) The peripheral functionalities are introduced via post synthetic modification usually via electrophilic aromatic substitution (SEAr) reactions. Unfortunately, the route of functionalizing prior to the formation of the core requires functional groups to be unreactive and unhampering to the remaining steps in forming the TBTQ core. This requirement restricts the types of substituents that can be placed in the peripheral positions of the TBTQ structure and the reason that post synthetic strategies are preferred to functionalize the various bridgehead positions.

2.2.1 Chiral TBTQ Monomer Towards Shape Defined CAS

The curved nature of the TBTQ backbone in conjunction with peripheral functionalization provides the unique structure necessary to be used in the monomeric form of the corner of a novel covalent cage structure. Similar to how Schneebeli and co-workers were able to form[21] molecular belts with CAS, the functionalization and transformation of the unique TBTQ shaped monomers to enantiopure bromoaniline moieties will lead to

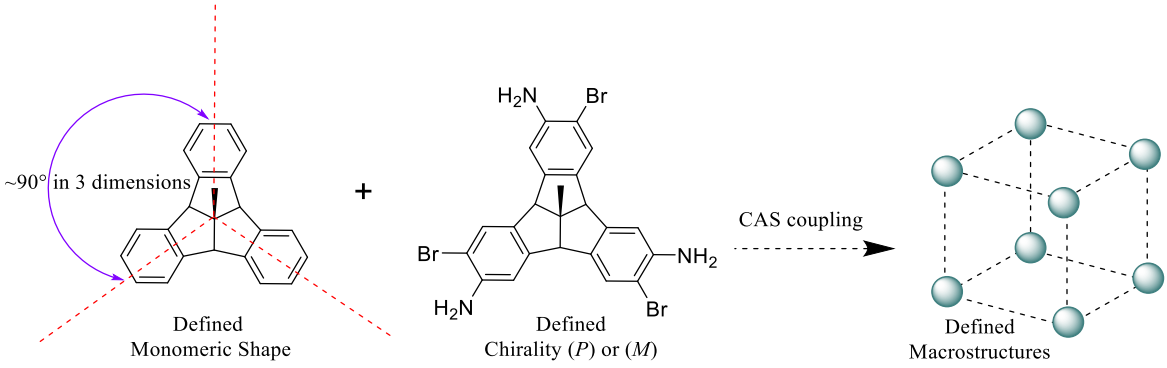

Figure 2.5: Conceptualized integration of core structure and enantiopurity toward macrostructures.

cubic structures as depicted in Figure 2.5. following the formation of the TBTQ core the designated peripheral positions are installed via SEAr reactions in an effort to synthesize a novel tri-bromoaniline moiety.

Synthetic endeavors consisted of the nitration, subsequent reduction and bromination of the TBTQ system to reach the target molecule depicted in the center of figure 2.5. Three-fold nitration of the methyltribenzotriquinacene was initially carried out

following a modified procedure by Kuck and co-workers. Whereas the six fold nitration is well established in literature following Kucks procedure, the threefold nitration can be done by simply decreasing the reaction time[10]. This reaction gave a mixture of isomers in a 1:3 ratio respectively in nearly quantitative yields. Upon scaling up this reaction, both the work up and purification were found to be impractical and hazardous due to TFA being used as the solvent[22], which lead to the development of a similar reaction from a modified procedure, utilizing trifluoroacetic anhydride and anhydrous THF as the solvent. This not only remedied the hazardous workup, but, stopped at the trinitrated form of the desired form of the TBTQ and the crude product was pure enough to move on to the reduction phase.

Reduction of the nitro groups to the corresponding aniline moieties was carried out using Raney nickel and hydrazine monohydrate to afford the racemic mixture of both of

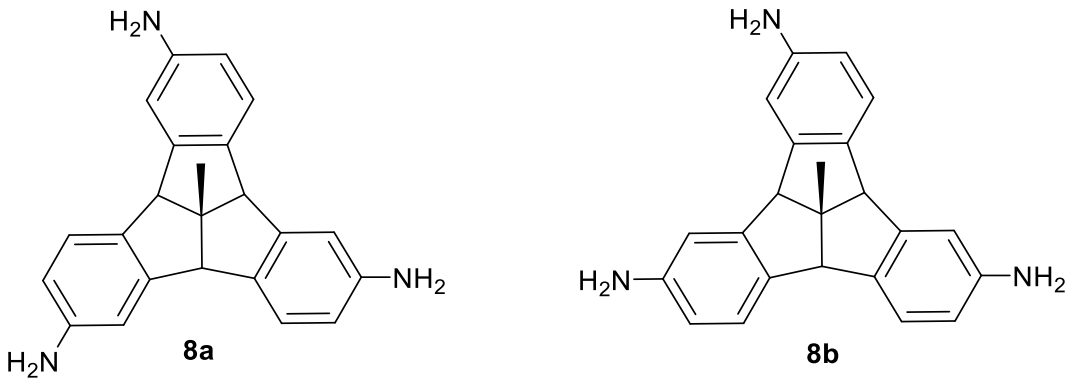

Figure 2.6: Regioisomers of tri-amine building blocks. Isomers can be separated via column chromatography.

the regioisomers **8** shown in Figure 2.6 in good yields. Column chromatography was used to separate the regioisomers, and efforts to resolve the enantiomers effectively began to take place. A variety of different resolution attempts were carried out including various

solvents and resolving agents. In our experience, and in line with what was experienced in literature[23] resolutions were extensive, time consuming, cumbersome difficult to scale and the process resulted in overall poor yields. It was the hope that by synthesizing the bromoanilines that chiral resolutions would be more practical then what has succeeded in literature.

Bromination of the TBTQ systems was carried out to functionalize the remaining peripheral positions. To this extent, three-fold SEAr brominations proved to be much more

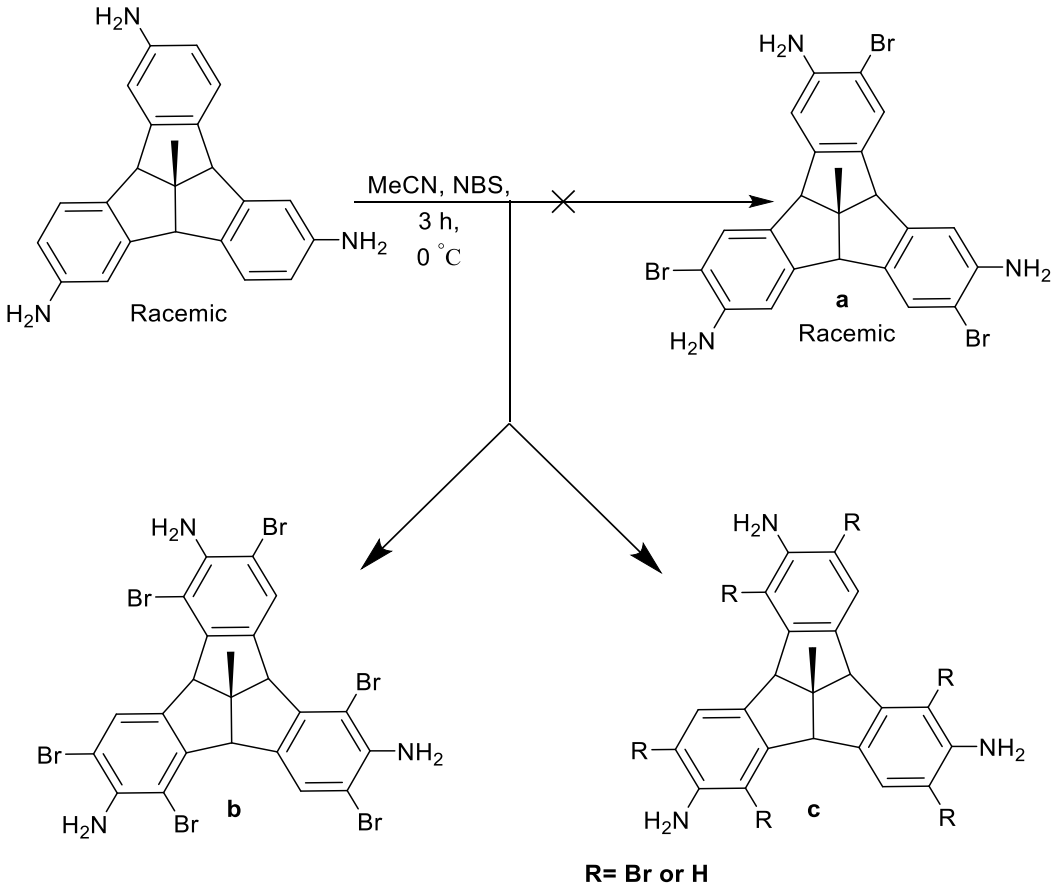

Scheme 2.3: Synthetic attempts at selective bromination. (a): Desired product unable to be isolated. (b): Isolated product following the addition of excess NBS. (c): Potential combinations of formed products after bromination.

difficult to control on the TBTQ systems[18] than the nitrations. Initial trials used acetonitrile and *N*-bromosuccinimide (NBS) in attempts to form the desired bromoanilines. After countless trials and a variety of different reaction conditions it was hypothesized that the amine on each of the aromatic systems activated the ring enough that the second bromination on any given ring could occur prior to the initial bromination of a subsequent aromatic ring. The addition of excess NBS proceeded to the six-fold bromination and slow addition a solution of NBS gave an array of products depending on the amount of NBS or the time that this reaction was allowed to proceed. Scheme 2.3 shows the summary of this process.

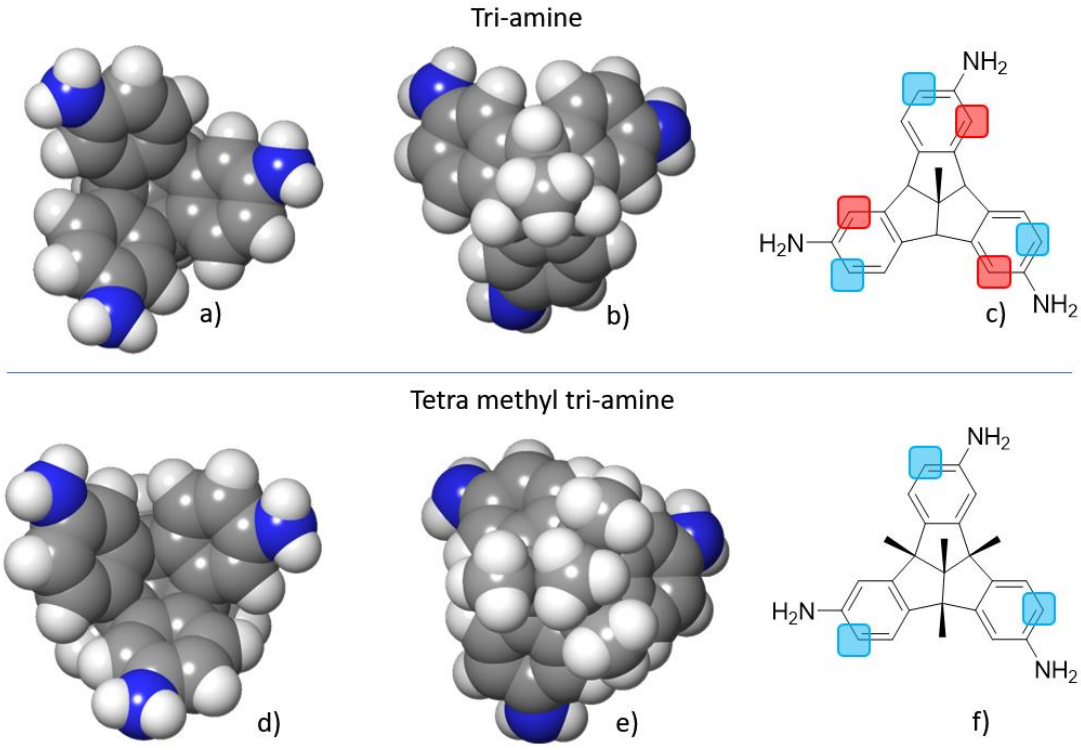

Figure 2.7: Unblocked ortho positions (top) and the desired and undesired potential bromination positions. Blocked undesired positions (bottom) of methylated bridgeheads.

because of the curved nature of TBTQ, it was hypothesized that the attack from the brominating agent comes from the top face of the TBTQ system because there is a considerable amount of steric hinderence on the bottom face of the tri-amine (Figure 2.7a). This, in contrast to the amount of steric bulk from the top face, comparatively showed much less around the ortho positions of interest (Figure 2.7b). Whereas the reactivity in this compound could be difficult to control, the installation of alkyl groups prior to the installation of the amine moieties proved to serve two functions. *i*) The functionalization of **8a** in a way that introduced steric bulk (Figure 2.7d and e) to hinder the bromination of the undesired positions (Figure 2.7c red) would lead to bromination of the desired positions (Figure 2.7f blue) *ii*) synthesis with the bridgehead moieties lead to changes in solubility making handling the compound easier. Therefore, functionalizing the bridgehead moieties as a post-synthetic method was pursued before further modification on the peripheral positions as originally planned. In order to install the desired alkyl substituents on to the bridgehead radical bromination using NBS and light as an iniator, proceeded to the threefold brominated bridgehead **9**. Subsequent alkylation using trimethyl aluminum lead exclusively to the methylated product **10** on the bridgehead positions as shown in Scheme 2.4.

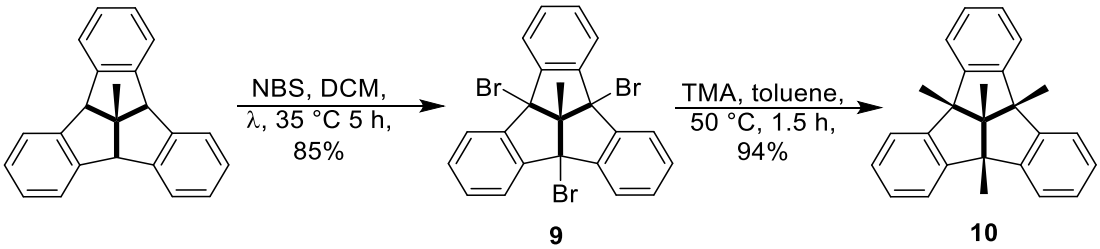

Scheme 2.4: Synthetic modifications to the bridgeheads needed to induce steric bulk.

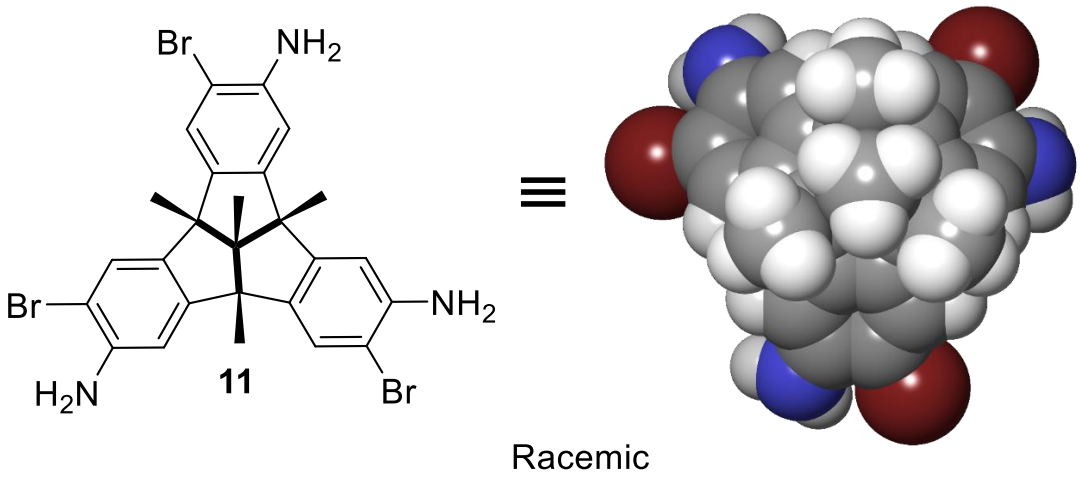

Figure 2.8: desired ortho-bromoanaline monomer target in the formation of well-defined cubic covalent cages. Resolution to its enantiopure form is the last synthetic challenge prior to CAS coupling.

Ultimately after the added steric interactions to the TBTQ derivative from the methyl groups were installed on the bridgehead, the nitration and reduction proceeded as they had previously and the bromination proceeded to the desired synthetic target **11** (Figure 2.8.) Through SEAr bromination using NBS and acetonitrile. It is important to note that the core shape as exhibited by the unfunctionalized TBTQ moiety is maintained throughout the synthetic steps and at this stage, resolution is the only thing standing in the way of applying CAS to make well defined cubic cages. Unfortunately, resolutions and recrystallization techniques were still equally as cumbersome and impractical on larger scales which prompted the exploration of an enantioselective electrophilic aromatic nitration method.

2.3 Enantioselective Electrophilic aromatic Nitration: A Chiral Auxiliary Approach

Classical electrophilic aromatic nitration reactions are among the best known and most frequently employed aromatic transformations[24-27]. They readily proceed [28, 29] with un-activated aromatic substrates and provide exquisite control over the number of NO_2 groups introduced, unlike for instance most Friedel–Crafts alkylations and aromatic brominations.[24, 26, 30, 31] Nevertheless, resolution-free, enantioselective electrophilic aromatic nitration processes (even with chiral auxiliaries) have yet to be reported. While enantioselective Friedel–Crafts type reactions[32-40] and enantioselective aromatic brominations[41-45] have been studied extensively, only the enantioselective nitration of crotylsilanes,[46] but not of aromatic substrates, has been described.

To advance the growing field of chirality-assisted synthesis[21, 47-49] (CAS), an enantioselective nitration strategy which makes use of chiral diester auxiliaries with remote stereocenters to induce axial chirality upon trifold-nitration is described herein. chiral auxiliaries are employed to achieve the first enantioselective synthesis of a C_3-symmetric (TBTQ)[50-52] derivative, which is not based on either a kinetic[53, 54] crystallization-based,[55, 56] or chromatographic[57] resolution. Directing arms with remote stereocenters are positioned at equal distances from the favored and disfavored sites of reactivity to provide for an enantioselective nitration methodology after removal (Figure 2.9 b) of the through-space directing groups. The success of our strategy stems from 1) chelation (Figure 2.9 b) of two

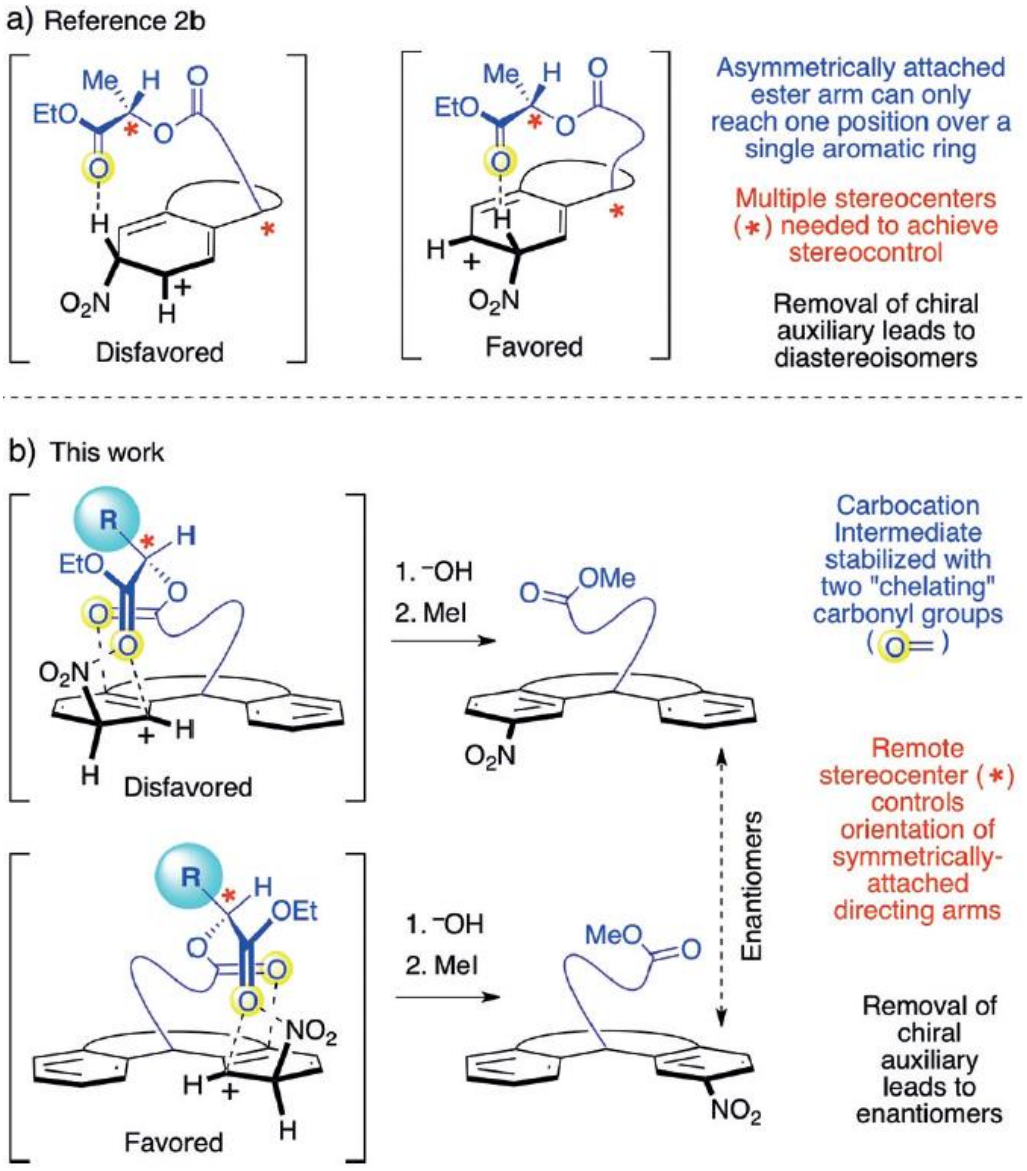

Figure 2.9: Different ways to control selective electrophilic aromatic nitrations through space with carbonyl directing groups.

ester carbonyl groups to the cationic Wheland intermediates positioned underneath these diester directing arms as well as 2) $A_{1,3}$ strain (Figure 2.9 b), which can be controlled by the size of the alkyl substituents attached to the remote chirality centers of the through-space directing groups. This combination of $A_{1,3}$ strain with dicarbonyl-to-arenium

chelation regulates the regiochemistry and axial chirality of the nitrated products simultaneously with a single stereocenter per directing arm and dictates whether each directing arm swings (Figure 2.9 b) to either the left or to the right.

This methodology is distinct from the through-space directed electrophilic aromatic substitution (SEAr) strategies reported by the Lectka group[58-61] and by our group previously. Particularly, in our prior work, the through-space directing groups were attached[28] (Figure 2.9 a) to the substrates in an asymmetric manner, closer to the favored sites of nitration. This arrangement ensured that only the proximal reaction sites could be reached by the directing groups, and therefore to stereoselective nitrations. However, as a direct result of the asymmetric linkage chemistry, our prior nitration strategy was only able to provide diastereoselective product formation after removal (*e.g.* reduction or hydrolysis) of the through-space directing groups, whereas we now enact a more challenging enantioselective aromatic nitration strategy herein.

2.3.1 Synthesis of TBTQ with Chiral Auxiliaries: Lactate Arm

Our research started with the synthesis (Scheme 2.5) of the TBTQ derivative (*S*,*S*,*S*)-15, which contains three symmetrically placed lactate directing arms. To meet this goal, we had to first prepare the tris(methylester) **14**. While a synthesis of **14** exists, [7] no less than four synthetic steps—1) alkylation of the tribromide **9** with allyltrimethylsilane, 2) oxonolysis, 3) oxone oxidation, and 4) esterification—were required to transform the

tribromide **9** into **14** in 37% overall yield. Consequently, to simplify the synthesis of **14**, we first discovered a new reaction (Scheme 2.5), which can directly transform **9** into **14** in a single synthetic step. After reaction optimization, we discovered that this direct transformation of **9** into **14** can be accomplished in 76% yield by simply reacting **9** with an O-silyl-protected ester enolate like the commercial tert-butyl((1-methoxyvinyl)oxy)

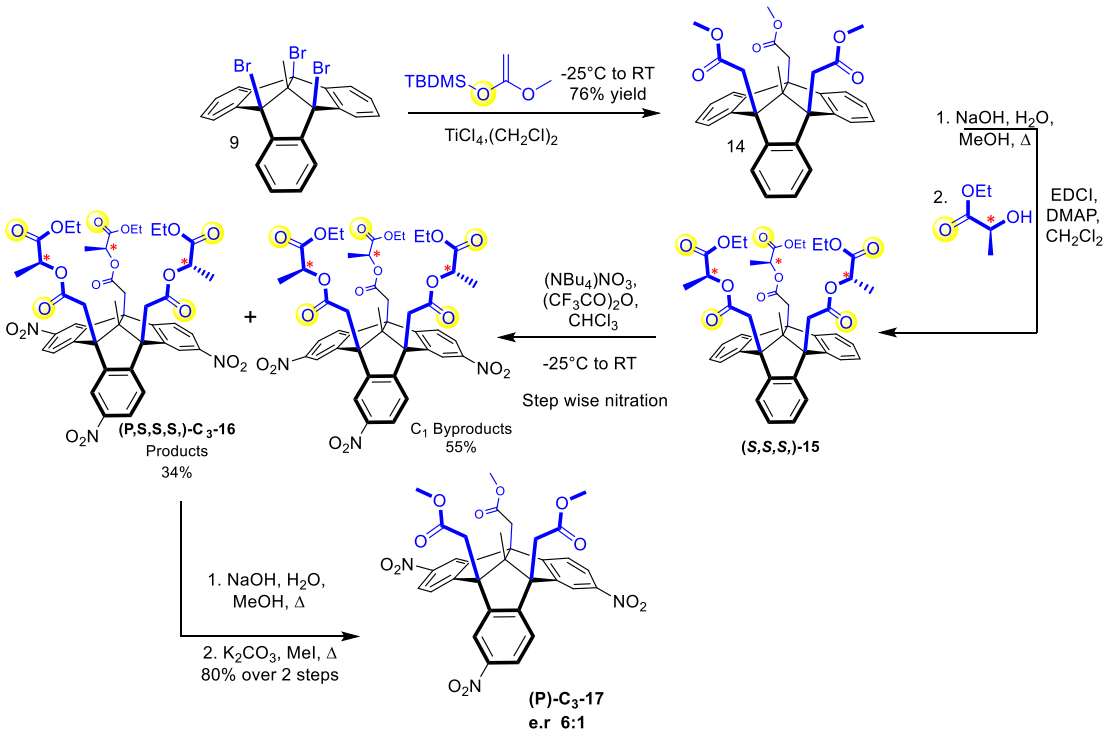

Scheme 2.5: Synthetic scheme in the formation of the first enantioselective electrophilic aromatic nitration to form an axially chiral TBTQ.

dimethylsilane in the presence of a Lewis acid (LA).

With **14** in hand, we proceeded to install our first generation through-space directing group by hydrolysis of the methyl esters, followed by three-fold Steglich esterification with (S)-ethyl lactate to afford the TBTQ derivative (*S*,*S*,*S*)-**15** in good yield.

Next we started to investigate the actual, through-space directed enantioselective nitration strategy with the TBTQ test system (S,S,S)-**15**. We subjected (S,S,S)-**15** to low temperature nitration conditions in anhydrous chloroform, by using a mixture of an organic-soluble nitrate salt $(NBu_4)NO_3$ and trifluoroacetic anhydride (TFAA) as the NO_2^+ source for the electrophilic aromatic substitution reactions. To further enhance the stereoselectivity of the nitration reactions, we removed the trifluoroacetic acid (TFA) by-product formed during TFAA-driven nitration after each nitration step. This goal was accomplished by drying the reaction mixtures under a stream of anhydrous nitrogen.

Our trifold nitration reaction proceeded (Scheme 2.5) in 89% overall yield, affording a mixture of C_3 and C_1-symmetric stereoisomers in a 38:62 ratio. Statistically (i.e. without through-space directing groups) the C_3 isomers required for CAS form in smaller proportions for TBTQ nitrations and typically, C_3 to C_1 product ratio of only about 25:75 are observed[62]. Thus, the through-space directing groups installed in our systems are responsible for the increased fraction of the nitrated C_3-isomers formed, as each of the three through-space directing groups guides nitration to one specific position on its underlying aromatic ring. These favored sites of reactivity are all symmetrically equivalent, so that a C_3 symmetric TBTQ product starts to emerge as a major product, for the first time [62] with direct aromatic nitration reactions.

Moreover, the two possible C_3 symmetric diastereoisomers—(*P*,*S*,*S*,*S*)-C_3-**16** and (*M*,*S*,*S*,*S*)-C_3-**16**—form (Scheme 2.5) in different amounts upon nitration of our TBTQ system. Specifically, a 6:1 ratio in favor of (*P*,*S*,*S*,*S*)-C_3-**16** was observed upon nitration of (*S*,*S*,*S*)-**15**. To determine the exact nitration ratio of *(P,S,S,S)*-**C_3-16** to *(M,S,S,S)*-**C_3-16**, we

first separated all C_1-symmetric side products from the crude reaction mixture by silica gel chromatography. Distinct ^{1}H NMR resonances were observed for the resulting mixtures of the diastereoisomers (*P*,*S*,*S*,*S*)-C_3-**16** and (*M*,*S*,*S*,*S*)-C_3-**16,** and allowed us to analyze the relative amounts of these two diastereoisomers by integration of their corresponding ^{1}H NMR resonances. Finally, to remove the chiral auxiliaries, we subjected (Scheme 2.5) the 6:1 mixture of (*P*,*S*,*S*,*S*)-C_3-**16** and (*M*,*S*,*S*,*S*)- C_3-**16** to standard basic ester hydrolysis, followed by alkylation of the resulting carboxylate functionalities with iodomethane. These transformations afforded enantioenriched (*P*)-C_3-**17** in 80% yield and an approximate 6:1 enantiomeric ratio (e.r.).

2.3.2 Computational Analysis of Lactate Auxiliary

Next, we carried out a detailed computational analysis of our lactate-directed, stereoselective TBTQ nitration system to 1) explain the mechanism of chirality-transfer and 2) help design a more efficient chiral directing arm. All four possible, low-energy Wheland intermediates (Figure 2.10) for the system Me-Model were constructed, the geometries were minimized, and the Gibbs free energies of the structures calculated at the dispersion-corrected B3LYP-MM/cc-pVDZ++//B3LYPMM/LACVP*level[63-67] of density functional theory (DFT). The results of DFT calculations support the notion that our

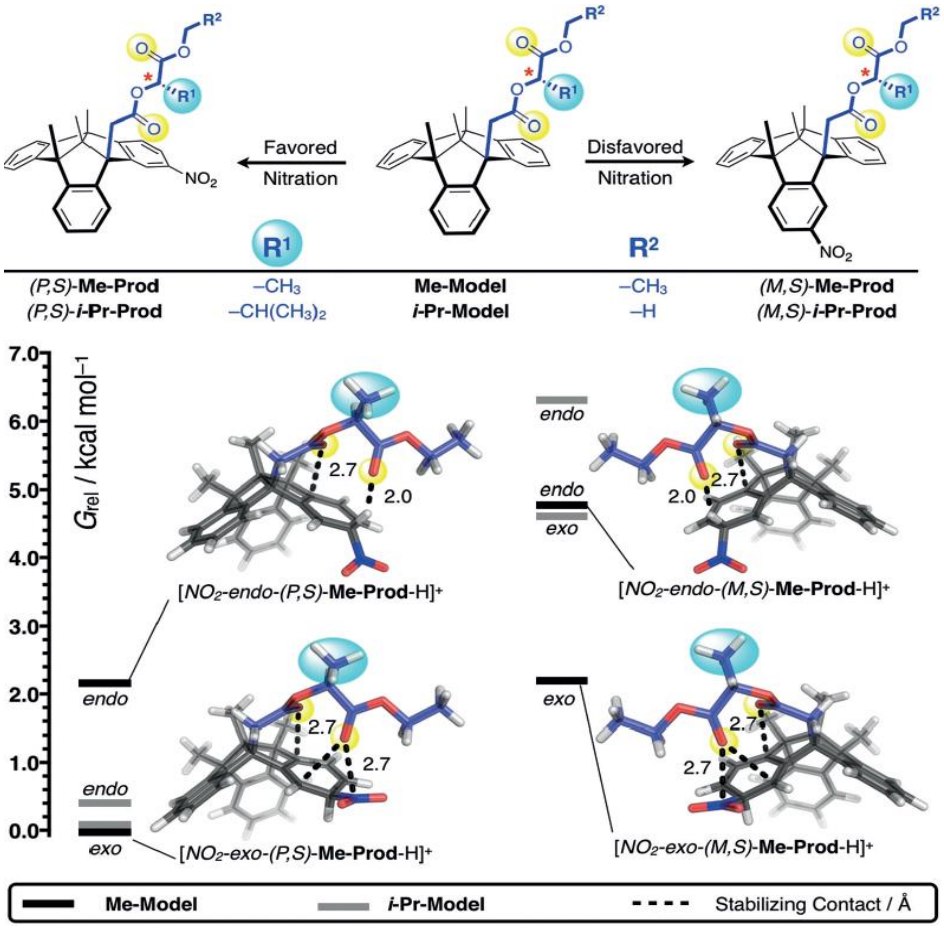

Figure 2.10: DFT-optimized structures (shown for the Me-Model system, see Chapter 5 figure 5.2 for the analogous structures of the i-Pr-Model system) and corresponding Gibbs free-energy plots of the Wheland intermediates for mononitration in the favored and disfavored positions. The DFT calculations were executed on model systems (Me-Model and i-Pr-Model) containing only one chiral ester directing arm. The calculations predict that replacing the methyl substituent -R in Me-Model with an isopropyl substituent will further improve the stereoselectivity of the nitration reaction. All Gibbs free energies (Grel) are reported at the B3LYP-MM/cc-pVDZ+ +//B3LYP MM/LACVP* level of theory relative to the most stable intermediates in units of kcalmol_1. Key stabilizing noncovalent interactions in the intermediates leading to the major products are highlighted with dashed lines. Corresponding distances are provided in _. C=grey/blue, H=white, N=blue, and O=red. Chelating oxygen atoms are highlighted in yellow.

stereoselective TBTQ nitration system follows a mechanism that is clearly distinct from

previously reported stereoselective nitrations of bicyclic compounds. Specifically, the following mechanistic features were revealed by our DFT calculations: 1) The bent nature of the TBTQ backbone seems to favor (Figure 2.10) exo-NO_2^+ attack, while endo-NO_2^+ attack is preferred with triptycene-like starting materials. For instance with our current system, the relative Gibbs free energy of the NO_2-exo Wheland intermediates [NO_2-exo-(P,S)-**Me-Prod**-H]$^+$ and [NO_2-exo-(M,S)-**Me-Prod**-H]$^+$ is 2–3 kcalmol^{-1} lower than the relative Gibbs free energy of the corresponding NO_2-endo Wheland intermediates [NO_2-endo-(P,S)-**Me-Prod**-H]$^+$ and [NO_2-endo-(M,S)-**Me-Prod**-H]$^+$.2) In the previous system, only one carbonyl group of each lactate directing arm can donate electron density into the underlying arenium-ion intermediate. In contrast, two carbonyl oxygen atoms are now fulfilling this role with our TBTQ systems. This dicarbonyl-to-arenium chelation interaction is revealed by the close distances observed (Figure 2.10) between both carbonyl oxygen atoms of the directing arms and several positively polarized atoms of the arenium systems underneath, as well as by noncovalent Interactions (NCI) critical points[68] (Figure 2.11 a) calculated from the electron density.

Overall, the geometry of the electron donating dicarbonyl arms matches the geometric pattern of the delocalized positive charge underneath the arms to selectively stabilize nitration in one specific position. In *Murphy et al*, diastereoselectivity was[69] simply achieved by attaching the directing-arm closer to the desired position of nitration. Here, on the other hand, it is primarily $A_{1,3}$ strain (Figure 2.11 b) between the methyl substituent of the lactate ester and the carbonyl oxygen center proximal to the TBTQ

attachment point that dictates reactivity by controlling whether a directing arm swings to the left or the right.

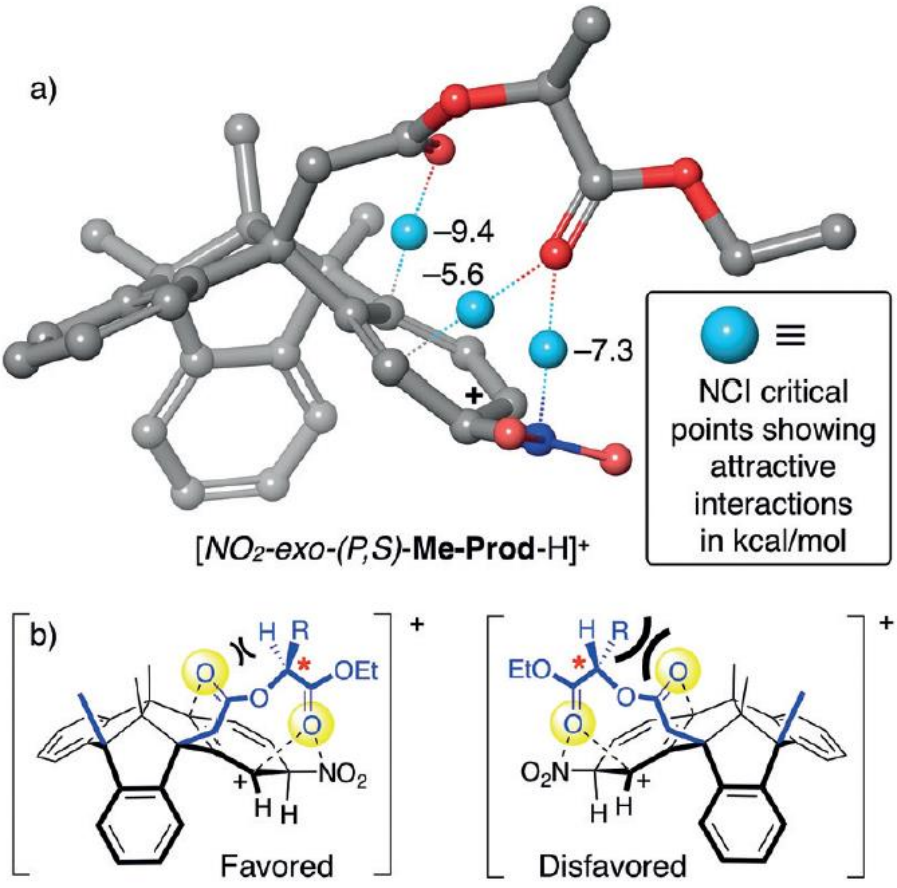

Figure 2.11: a) Noncovalent interaction (NCI) critical points, showing attractive noncovalent interactions in the Wheland intermediate [NO2-exo-(P,S)-Me-Prod-H]+. The NCI critical points illustrate the "chelating" mechanism of stabilizing a carbocation on an aromatic ring from above in multiple positions at the same time. See the Supporting Information for similar NCI plots of the other Wheland intermediates. b) Illustration of how $A_{1,3}$ strain controls the orientation of the symmetrically attached, chiral through-space directing arms.

2.3.3 Modification, Synthesis and Enhanced Selectivity of Chiral Auxiliary

After we discovered that $A_{1,3}$ strain is key to achieving stereoselectivity with our systems, we set out to further enhance the stereoselectivity by replacing the methyl groups

attached to the chirality centers with larger isopropyl substituents. DFT calculations of the isopropyl model system, ***i-Pr*-Model**, confirmed this hypothesis, as the DFT predicted relative Gibbs free-energy gaps between the favored and disfavored Wheland intermediates for nitration increased from about 2 kcal·mol^{-1} with the ***Me-Model*** (Figure 2.10, black energy levels) to greater than 4 kcal·mol^{-1}with the *i-Pr-Model* (Figure 2.10, grey energy levels). According to these computational predictions, we synthesized the TBTQ derivative (*S*,*S*,*S*)-**15** with isopropyl substituents shown in Figure 2.12.

The synthesis of (*S*,*S*,*S*)-**18** is analogous to that of (*S*,*S*,*S*)-**15**, with the exception of the chiral alcohol used in the N-ethyl-N-(3dimethylaminopropyl) carbodiimide hydrochloride (EDCI) coupling. As predicted by the computational models, there was a considerable increase in the amount of stereo control exerted by the through-space directing arms with the isopropyl substituents. Specifically, the C_3 to C_1 product ratio for trinitration increased to 44:56, and the diastereoisomeric ratio (d.r.) of the two C_3 symmetric diastereoisomers (*P*,*S*,*S*,*S*)-C_3-**19** and (*M*,*S*,*S*,*S*)-C_3-**19** increased to 9:1 in favor of (*P*,*S*,*S*,*S*)-C_3-**19.** The additional $A_{1,3}$ strain offered by the isopropyl derivatives therefore orients the dicarbonyl directing arms effectively into one preferred conformation which stabilizes the underlying Wheland arenium intermediates in a selective manner.

This methodology, the first enantioselective SEAr nitration to date, allows the enantioselective synthesis of a trinitrated, C_3 symmetric tribenzotriquinacene, which is obtained in up to 9:1(Figure 2.12 b) enantiomeric excess. DFT modelling shows that through-space chelation of two ester carbonyl groups to the underlying arenium cations, as well as $A_{1,3}$ strain is primarily responsible for the observed central-to-axial chirality

transfer, which is orchestrated by remote stereocenters. Investigations of possible avenues to extend our enantioselective nitration methodology to more general systems, have thus far proven fruitful and will be discussed in Chapter 3. Furthermore, the generalization of this method can have profound impacts in the field of medicine, and specifically within

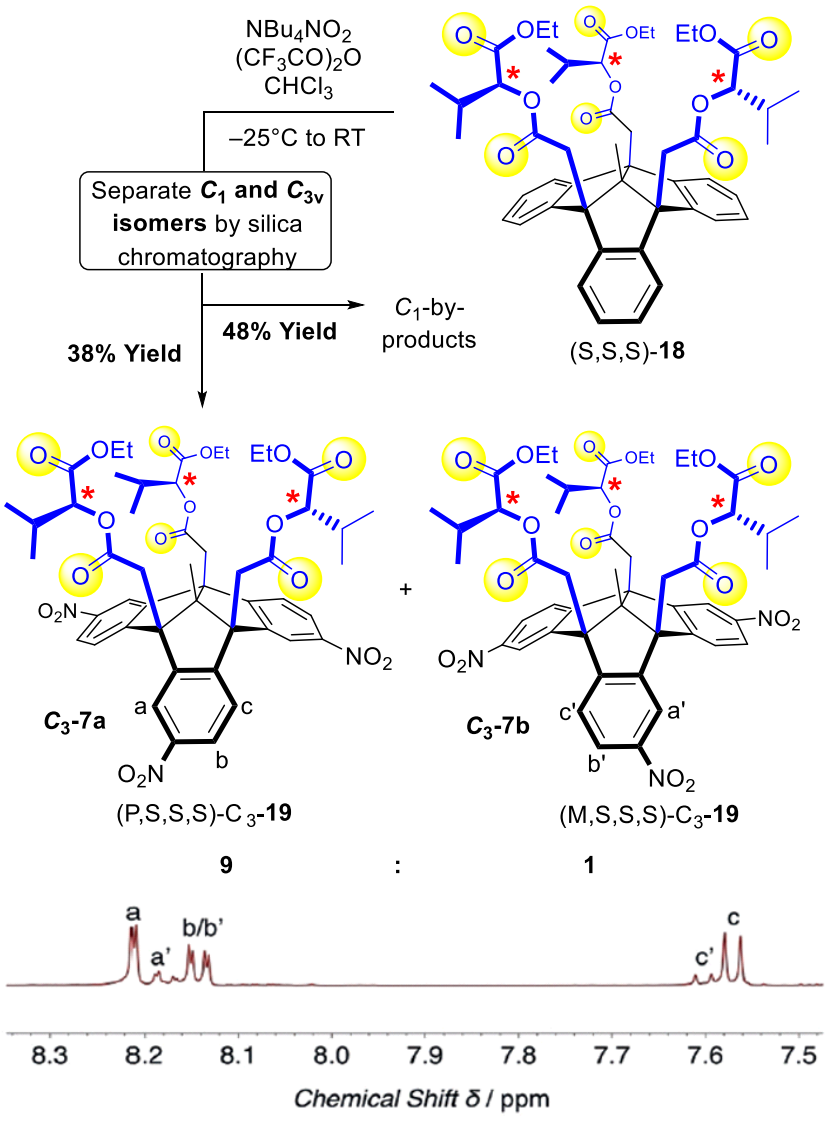

Figure 2.12: Synthesis and determination of d.r in the enhanced selectivity using isopropyl derivative

chirality assisted synthesis. Enantioselective processes will prove to be a powerful tool in the formation of coveted chiral monomers.

2.4 Summary and Future Work

TBTQ systems have been identified as a prominent candidate for the formation of well-defined molecular cubes when used in conjunction with the growing CAS methodology. The unique shape of these compounds along with a vast ability to be modified, are key features in this endeavor as these modifications can play a significant

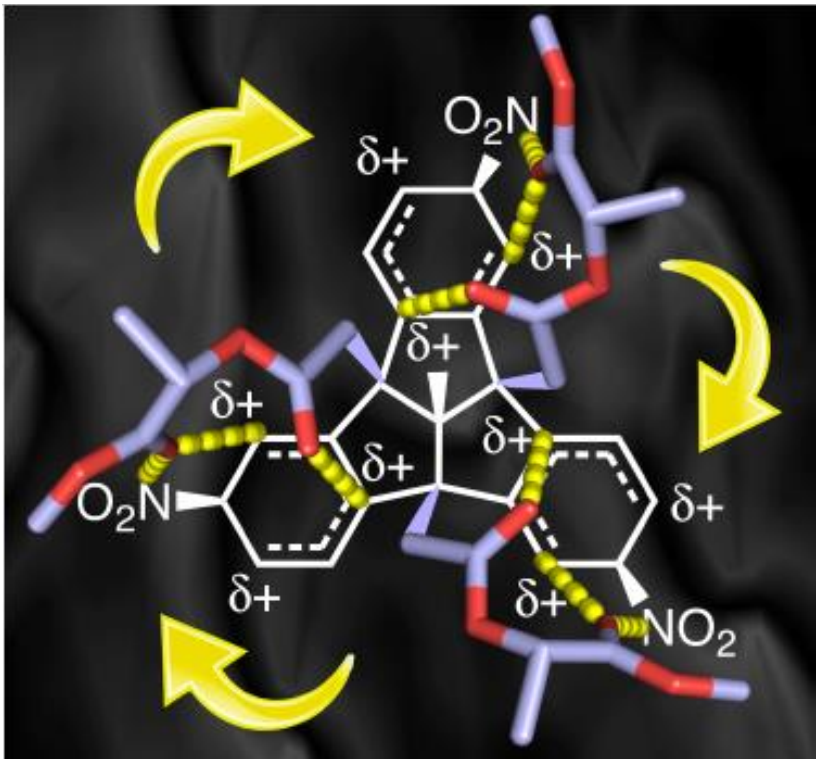

Figure 2.13: Dichelation and swing of chiral auxilary in a single direction to give a selective axially chiral compound

role in the resulting cages. While several difficulties have been encountered when forming the unique monomers, specifically regarding the overall formation of the enantiopure versions of these axially chiral compounds, a new method, developed in our laboratory, demonstrates the first enantioselective, electrophilic aromatic nitration reaction. Computational analysis of these complex TBTQ systems were presented and revealed the ability for these systems to be controlled through $A_{1,3}$ strain dictating which way (left or right, Figure 2.13) the resulting stereogenic arms will swing. With this discovery in mind and the literature precedence supporting a variety of different through space selective processes, further investigations of this method have taken place in order to determine key contributions to this overall synthetic method in an effort to verify this method as a generalized procedure for a larger subclass of substituents outside of TBTQ moieties.

Preliminary findings of the use of this method have been reported with our enantioselective nitration strategy and can be applied to substrates with more flexible arrangements arising with just a single directing arm. For instance, when we 1) esterified 9-fluoreneacetic acid with (S)-ethyl lactate, 2) nitrated the coupled product (S)-**20**, and 3) converted the resulting mono-nitro derivative (*S*,*S*)-**21** into the corresponding methyl ester, we obtained (S)-2-nitro-9-fluorenacetic acid methyl ester ((*S*)-**22)** in 72:28 e.r. (Scheme 2.6). This selectivity is comparable to the average selectivities observed for each single nitration step in the TBTQ systems, which are 64:36 for nitration of (*S*,*S*,*S*)-**15** and 68:32 for nitration of (*S*,*S*,*S*)-**18,** respectively. Furthermore, DFT calculations showed that nitration of this fluorenyl system is controlled by a dicarbonyl to-delocalized-carbocation chelation and $A_{1,3}$ strain, analogous to how the nitrations of the TBTQ systems are directed.

This method could show application as a generalized method for materials, medicinal, and supramolecular chemistry moving forward.

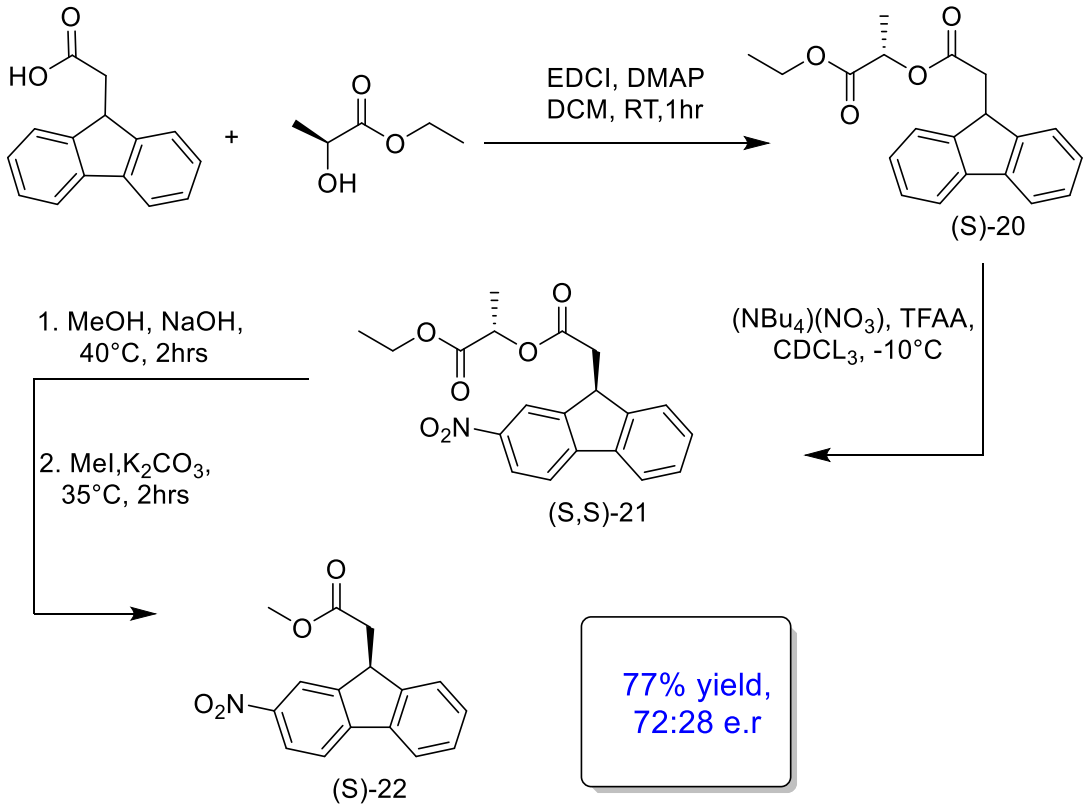

Scheme 2.6: Synthetic pathway from the florenyl carboxcilic acid to the selectively formed chiral methyl ester product. Synthetic steps taken for this system are almost identical to those utilized in the TBTQ system. EDCI coupling was used to install the chiral auxiliary, followed by mild nitration, hydrolysis, and methylation chirality was verified by using CD spectra.

References

1. Beuerle, F.; Dhara, A., Synthetic Strategies for the Regioselective Functionalization of Tribenzotriquinacenes. *Synthesis* **2018,** *50* (15), 2867.
2. Kuck, D.; Lindenthal, T.; Schuster, A., Benzoanellated centropolyquinanes, 11. Synthesis of tribenzotriquinacene and somecentro-substituted derivatives. *Chem. Ber.* **1992,** *125* (6), 1449.
3. Mosher, W. A.; Soeder, R. W., Reactions of some methylene ketones with dimethyl phthalate. New route to 2-substituted 1,3-indandiones. *J. Org. Chem.* **1971,** *36* (11), 1561.
4. Beuerle, F.; Gole, B., Covalent Organic Frameworks and Cage Compounds: Design and Applications of Polymeric and Discrete Organic Scaffolds. *Angew. Chem., Int. Ed.* **2018,** *57* (18), 4850.
5. Kuck, D.; Schuster, A.; Krause, R. A.; Tellenbröker, J.; Exner, C. P.; Penk, M.; Bögge, H.; Müller, A., Multiply bridgehead- and periphery-substituted tribenzotriquinacenes—highly versatile rigid molecular building blocks with C3v or C3 symmetry. *Tetrahedron* **2001,** *57* (17), 3587.
6. Tellenbroker, J.; Kuck, D., Tribenzotriquinacenes bearing three peripheral or bridgehead urea groups stretched into the 3-D space. *Beilstein J. Org. Chem.* **2011,** *7*, 329.
7. Mughal, E. U.; Kuck, D., New C(3v)-symmetrical tribenzotriquinacenes bearing extended and oxy-functionalised alkyl groups at their benzhydrylic bridgeheads. *Org. Biomol. Chem.* **2010,** *8* (23), 5383.
8. Henne, S.; Bredenkoetter, B.; Volkmer, D., Mixed SAMs of backbone-functionalized tribenzotriquinacenes and alkanethiols: Synthesis, preparation and STM-investigations. *Appl. Surf. Sci.* **2015,** *356*, 645.
9. Rommelmann, P.; Greschner, W.; Ihrig, S.; Neumann, B.; Stammler, H.-G.; Gröger, H.; Kuck, D., Combining Stereoselective Enzyme Catalysis with Chirality-Assisted Synthesis in Tribenzotriquinacene Chemistry. *Eur. J. Org. Chem.* **2018,** *2018* (29), 3891.
10. Strube, J.; Neumann, B.; Stammler, H. G.; Kuck, D., Solid-state enantiopure organic nanocubes formed by self organization of a C3-symmetrical tribenzotriquinacene. *Chemistry* **2009,** *15* (10), 2256.
11. Beaudoin, D.; Rominger, F.; Mastalerz, M., Chirality-Assisted Synthesis of a Very Large Octameric Hydrogen-Bonded Capsule. *Angew. Chem., Int. Ed.* **2016,** *55* (50), 15599.
12. Kuck, D.; Lindenthal, T.; Schuster, A., Benzanellated centropolyquinanes. 11. Synthesis of tribenzotriquinacene and some centro-substituted derivatives. *Chem. Ber.* **1992,** *125* (6), 1449.
13. Henne, S.; Bredenkoetter, B.; Alaghemandi, M.; Bureekaew, S.; Schmid, R.; Volkmer, D., Almost Enclosed Buckyball Joints: Synthesis, Complex Formation, and Computational Simulations of Pentypticene-Extended Tribenzotriquinacene. *ChemPhysChem* **2014,** *15* (17), 3855.
14. Henne, S.; Bredenkoetter, B.; Dehghan Baghi, A. A.; Schmid, R.; Volkmer, D., Advanced buckyball joints: synthesis, complex formation and computational simulations of centrohexaindane-extended tribenzotriquinacene receptors for C60 fullerene. *Dalton Trans.* **2012,** *41* (19), 5995.

15. Kuck, D.; Schuster, A.; Krause, R. A.; Tellenbroker, J.; Exner, C. P.; Penk, M.; Bogge, H.; Muller, A., Multiply bridgehead- and periphery-substituted tribenzotriquinacenes - highly versatile rigid molecular building blocks with C3v or C3 symmetry. *Tetrahedron* **2001,** *57* (17), 3587.
16. Harmata, M., Chiral Molecular Tweezers. *Acc. Chem. Res.* **2004,** *37* (11), 862.
17. Klotzbach, S.; Beuerle, F., Shape-Controlled Synthesis and Self-Sorting of Covalent Organic Cage Compounds. *Angew. Chem., Int. Ed.* **2015,** *54* (35), 10356.
18. Linke, J.; Bader, N.; Tellenbroeker, J.; Kuck, D., Sixfold Peripheral Halogenation of Tribenzotriquinacenes: An Alternative Access to Useful TBTQ Building Blocks. *Synthesis* **2018,** *50* (1), 175.
19. Narita, A.; Wang, X.-Y.; Feng, X.; Muellen, K., New advances in nanographene chemistry. *Chem. Soc. Rev.* **2015,** *44* (18), 6616.
20. Wang, T.; Zhang, Y.-F.; Hou, Q.-Q.; Xu, W.-R.; Cao, X.-P.; Chow, H.-F.; Kuck, D., C3-Symmetrical Tribenzotriquinacene Derivatives: Optical Resolution through Cryptophane Synthesis and Supramolecular Self-Assembly into Nanotubes. *J. Org. Chem.* **2013,** *78* (3), 1062.
21. Liu, X.; Weinert, Z. J.; Sharafi, M.; Liao, C.; Li, J.; Schneebeli, S. T., Regulating Molecular Recognition with C-Shaped Strips Attained by Chirality-Assisted Synthesis. *Angew. Chem. Int. Ed.* **2015,** *54* (43), 12772.
22. Hamon, F.; Djedaini-Pilard, F.; Barbot, F.; Len, C., Azobenzenes—synthesis and carbohydrate applications. *Tetrahedron* **2009,** *65* (49), 10105.
23. Mastalerz, M.; Rominger, F.; Beaudoin, D., Synthesis and Chiral Resolution of C3-symmetric Tribenzotriquinacenes. *Eur. J. Org. Chem.* **2016,** *2016* (26), 4470.
24. Esteves, P. M.; De, M. C. J. W.; Cardoso, S. P.; Barbosa, A. G.; Laali, K. K.; Rasul, G.; Prakash, G. K.; Olah, G. A., Unified mechanistic concept of electrophilic aromatic nitration: convergence of computational results and experimental data. *J. Am. Chem. Soc.* **2003,** *125* (16), 4836.
25. Mortier, J., **2015**.
26. Wang, J.; Li, R.; Dong, Z.; Liu, P.; Dong, G., Complementary site-selectivity in arene functionalization enabled by overcoming the ortho constraint in palladium/norbornene catalysis. *Nature Chem.* **2018,** *10* (8), 866.
27. Kochi, J. K., Inner-sphere electron transfer in organic chemistry. Relevance to electrophilic aromatic nitration. *Acc. Chem. Res.* **2002,** *25* (1), 39.
28. Murphy, K. E.; Bocanegra, J. L.; Liu, X.; Chau, H. Y. K.; Lee, P. C.; Li, J.; Schneebeli, S. T., Precise through-space control of an abiotic electrophilic aromatic substitution reaction. *Nature communications* **2017,** *8*, 14840.
29. Sydlik, S. A.; Chen, Z.; Swager, T. M., Triptycene Polyimides: Soluble Polymers with High Thermal Stability and Low Refractive Indices. *Macromolecules* **2011,** *44* (4), 976.
30. Nishita, M.; Park, S.-Y.; Nishio, T.; Kamizaki, K.; Wang, Z.; Tamada, K.; Takumi, T.; Hashimoto, R.; Otani, H.; Pazour, G. J.; Hsu, V. W.; Minami, Y., Ror2 signaling regulates Golgi structure and transport through IFT20 for tumor invasiveness. *Scientific Reports* **2017,** *7* (1), 1.

31. Allemann, O.; Duttwyler, S.; Romanato, P.; Baldridge, K. K.; Siegel, J. S., Proton-catalyzed, silane-fueled Friedel-Crafts coupling of fluoroarenes. *Science* **2011,** *332* (6029), 574.
32. Allemann, C.; Gordillo, R.; Clemente, F. R.; Cheong, P. H.; Houk, K. N., Theory of asymmetric organocatalysis of Aldol and related reactions: rationalizations and predictions. *Acc Chem Res* **2004,** *37* (8), 558.
33. Bandini, M.; Melloni, A.; Umani-Ronchi, A., New catalytic approaches in the stereoselective Friedel-Crafts alkylation reaction. *Angew. Chem. Int. Ed.* **2004,** *43* (5), 550.
34. Jørgensen, K. A., Asymmetric Friedel-CraftsReactions: Catalytic Enantioselective Addition of Aromatic and HeteroaromaticC-H Bonds to Activated Alkenes, Carbonyl Compounds, andImines. *Synthesis* **2003,** *2003* (07), 1117.
35. Mohr, J. T.; Krout, M. R.; Stoltz, B. M., Natural products as inspiration for the development of asymmetric catalysis. *Nature* **2008,** *455*, 323.
36. Paras, N. A.; MacMillan, D. W. C., New Strategies in Organic Catalysis: The First Enantioselective Organocatalytic Friedel−Crafts Alkylation. *J. Am. Chem. Soc.* **2001,** *123* (18), 4370.
37. Kobayashi, S.; Mori, Y.; Fossey, J. S.; Salter, M. M., Catalytic enantioselective formation of C-C bonds by addition to imines and hydrazones: a ten-year update. *Chem. Rev.* **2011,** *111* (4), 2626.
38. Holland, M. C.; Paul, S.; Schweizer, W. B.; Bergander, K.; Muck-Lichtenfeld, C.; Lakhdar, S.; Mayr, H.; Gilmour, R., Noncovalent interactions in organocatalysis: modulating conformational diversity and reactivity in the MacMillan catalyst. *Angew. Chem. Int. Ed.* **2013,** *52* (31), 7967.
39. Li, J. L.; Yue, C. Z.; Chen, P. Q.; Xiao, Y. C.; Chen, Y. C., Remote enantioselective Friedel-Crafts alkylations of furans through HOMO activation. *Angew. Chem. Int. Ed.* **2014,** *53* (21), 5449.
40. Wang, S. G.; You, S. L., Hydrogenative dearomatization of pyridine and an asymmetric aza-Friedel-Crafts alkylation sequence. *Angew. Chem. Int. Ed.* **2014,** *53* (8), 2194.
41. Gustafson, J. L.; Lim, D.; Miller, S. J., Dynamic kinetic resolution of biaryl atropisomers via peptide-catalyzed asymmetric bromination. *Science* **2010,** *328* (5983), 1251.
42. Bencivenni, G., Organocatalytic Strategies for the Synthesis of Axially Chiral Compounds. *Synlett* **2015,** *26* (14), 1915.
43. Wencel-Delord, J.; Panossian, A.; Leroux, F. R.; Colobert, F., Recent advances and new concepts for the synthesis of axially stereoenriched biaryls. *Chem. Soc. Rev.* **2015,** *44* (11), 3418.
44. Wang, J. Z.; Zhou, J.; Xu, C.; Sun, H.; Kurti, L.; Xu, Q. L., Symmetry in Cascade Chirality-Transfer Processes: A Catalytic Atroposelective Direct Arylation Approach to BINOL Derivatives. *J. Am. Chem. Soc.* **2016,** *138* (16), 5202.
45. Hurtley, A. E.; Stone, E. A.; Metrano, A. J.; Miller, S. J., Desymmetrization of Diarylmethylamido Bis(phenols) through Peptide-Catalyzed Bromination: Enantiodivergence as a Consequence of a 2 amu Alteration at an Achiral Residue within the Catalyst. *J. Org. Chem.* **2017,** *82* (21), 11326.

46. Beresis, R. T.; Masse, C. E.; Panek, J. S., Enantioselective Nitration of Chiral (E)-Crotylsilanes: A Concise Asymmetric Synthesis of (E)-Olefin Dipeptide Isosteres. *The Journal of Organic Chemistry* **1995,** *60* (24), 7714.
47. Strube, J.; Neumann, B.; Stammler, H. G.; Kuck, D., Solid-state enantiopure organic nanocubes formed by self organization of a C3-symmetrical tribenzotriquinacene. *Chemistry* **2009,** *15* (10), 2256.
48. Beaudoin, D.; Rominger, F.; Mastalerz, M., Chirality-Assisted Synthesis of a Very Large Octameric Hydrogen-Bonded Capsule. *Angew. Chem. Int. Ed.* **2016,** *55* (50), 15599.
49. Mastalerz, M., Single-Handed Towards Nanosized Organic Molecules. *Angew. Chem. Int. Ed.* **2016,** *55* (1), 45.
50. Markopoulos, G.; Henneicke, L.; Shen, J.; Okamoto, Y.; Jones, P. G.; Hopf, H., Tribenzotriquinacene: a versatile synthesis and C3-chiral platforms. *Angew. Chem. Int. Ed.* **2012,** *51* (51), 12884.
51. Ip, H. W.; Ng, C. F.; Chow, H. F.; Kuck, D., Three-Fold Scholl-Type Cycloheptatriene Ring Formation around a Tribenzotriquinacene Core: Toward Warped Graphenes. *J. Am. Chem. Soc.* **2016,** *138* (42), 13778.
52. Dhara, A.; Beuerle, F., Reversible Assembly of a Supramolecular Cage Linked by Boron-Nitrogen Dative Bonds. *Chemistry* **2015,** *21* (48), 17391.
53. Greschner, W.; Neumann, B.; Stammler, H. G.; Groger, H.; Kuck, D., Enantiomerically Pure Tribenzotriquinacenes through Stereoselective Synthesis. *Angew. Chem. Int. Ed.* **2015,** *54* (46), 13764.
54. Rommelmann, P.; Nachtigall, B.; Guntelmann, T.; Groger, H.; Kuck, D., Stereoselective synthesis of enantiomerically pure bowl-shaped hydroxytribenzotriquinacenes. *Org. Biomol. Chem.* **2018,** *16* (31), 5635.
55. Beaudoin, D.; Rominger, F.; Mastalerz, M., Synthesis and Chiral Resolution ofC3-Symmetric Tribenzotriquinacenes. *Eur. J. Org. Chem.* **2016,** *2016* (26), 4470.
56. Beaudoin, D.; Rominger, F.; Mastalerz, M., Chiral Self-Sorting of [2+3] Salicylimine Cage Compounds. *Angew. Chem. Int. Ed.* **2017,** *56* (5), 1244.
57. Wang, T.; Zhang, Y. F.; Hou, Q. Q.; Xu, W. R.; Cao, X. P.; Chow, H. F.; Kuck, D., C3-symmetrical tribenzotriquinacene derivatives: optical resolution through cryptophane synthesis and supramolecular self-assembly into nanotubes. *J. Org. Chem.* **2013,** *78* (3), 1062.
58. Holl, M. G.; Struble, M. D.; Singal, P.; Siegler, M. A.; Lectka, T., Positioning a Carbon-Fluorine Bond over the pi Cloud of an Aromatic Ring: A Different Type of Arene Activation. *Angew. Chem. Int. Ed.* **2016,** *55* (29), 8266.
59. Bume, D. D.; Pitts, C. R.; Ghorbani, F.; Harry, S. A.; Capilato, J. N.; Siegler, M. A.; Lectka, T., Ketones as directing groups in photocatalytic sp(3) C-H fluorination. *Chem Sci* **2017,** *8* (10), 6918.
60. Guan, L.; Holl, M. G.; Pitts, C. R.; Struble, M. D.; Siegler, M. A.; Lectka, T., Through-Space Activation Can Override Substituent Effects in Electrophilic Aromatic Substitution. *J. Am. Chem. Soc.* **2017,** *139* (42), 14913.
61. Holl, M. G.; Pitts, C. R.; Lectka, T., Fluorine in a C-F Bond as the Key to Cage Formation. *Angew. Chem. Int. Ed.* **2018,** *57* (11), 2758.

62. Wagner, P.; Rominger, F.; Mastalerz, M., Switching the Statistical C3 /C1 Ratio in the Threefold Aromatic Substitution of Tribenzotriquinacenes towards the C3 Isomer. *Angew. Chem. Int. Ed.* **2018,** *57* (35), 11321.
63. Veinot, A. J.; Todd, A. D. K.; Robertson, K. N.; Masuda, J. D., A reinvestigation of mono- and bis-ethynyl phosphonium salts: structural and computational studies and new reactivity. *Can. J. Chem.* **2018,** *96* (1), 8.
64. Lee, C.; Yang, W.; Parr, R. G., Development of the Colle-Salvetti correlation-energy formula into a functional of the electron density. *Physical Review B* **1988,** *37* (2), 785.
65. Becke, A. D., Density-functional thermochemistry. III. The role of exact exchange. *The Journal of Chemical Physics* **1993,** *98* (7), 5648.
66. Stephens, P. J.; Devlin, F. J.; Chabalowski, C. F.; Frisch, M. J., Ab Initio Calculation of Vibrational Absorption and Circular Dichroism Spectra Using Density Functional Force Fields. *The Journal of Physical Chemistry* **1994,** *98* (45), 11623.
67. Schneebeli, S. T.; Bochevarov, A. D.; Friesner, R. A., Parameterization of a B3LYP specific correction for non-covalent interactions and basis set superposition error on a gigantic dataset of CCSD(T) quality non-covalent interaction energies. *J. Chem. Theory Comput.* **2011,** *7* (3), 658.
68. Johnson, E. R.; Keinan, S.; Mori-Sanchez, P.; Contreras-Garcia, J.; Cohen, A. J.; Yang, W., Revealing noncovalent interactions. *J. Am. Chem. Soc.* **2010,** *132* (18), 6498.
69. Murphy, K. E.; Bocanegra, J. L.; Liu, X.; Chau, H. K.; Lee, P. C.; Li, J.; Schneebeli, S. T., Precise through-space control of an abiotic electrophilic aromatic substitution reaction. *Nature Commun.* **2017,** *8*, 14840.

Chapter 3: EXTENDING ENANTIOSELECTIVE ELECTROPHILIC AROMATIC NITRATION

Electrophilic aromatic nitrations are of general interest for organic synthesis[1]. The use of chiral auxiliaries is considered not only one of the most important methods for asymmetric C-C bond formation, but an integral step in the synthesis of natural products and nanomaterials; the marrying of both of these concepts gives way to a synthetic pathway for, asymmetric electrophilic aromatic substitutions (SEAr) reactions to efficiently transfer central symmetry to axial symmetry[2-6]. In addition, we implemented the first through space enantioselective nitrations as discussed in the previous chapter[7]. Ultimately the expansion of this to a generalized method would be a powerful fundamental tool of organic chemistry.

Conventionally, synthetic chemists rely on the installation and well-defined properties of electron withdrawing and donating groups to dictate the positioning of SEAr reactions, *i.e*. ortho, para, and meta directing groups. Concurrently the installation of chiral auxiliary moieties on to planar substituents have proven to add an additional aspect of control to SEAr reactions. Chiral SEAr reactions to this extent have been effective at converging to a singular point of central symmetry but not yet transferring chirality to molecules that will exhibit axial chirality[6, 8, 9] In fact the work done for TBTQ moieties to our knowledge was the first example of an enantioselective electrophilic aromatic nitration undergoing such chemistry.

While synthetic chemists continue to struggle with complex SEAr reactions, nature has already mastered this phenomenon through enzymatic control[10, 11]. Primarily this is done by taking advantage of distinct points both above and below aromatic rings to *i*) align electrophiles to a desired position of attack and *ii*) stabilize reactive intermediates in a "through-space" manner. This approach not only provides efficient reaction selectivity but also allows for evolution to tailor structural enzymatic moieties to form different products from the same starting materials. To date however, there has been recent development regarding abiotic, through space control of SEAr reactions[12-14]and even more in regard to synthetic examples that can not only direct substitution from above/beneath aromatic rings as we have previously shown but then efficiently transfer that control into 3 dimensional axial, chiral analogues such as TBTQ[7, 15]. The remote effects of the chiral center determine whether the arm swings to the left or right, based on $A_{1,3}$ strain, dictating the symmetry of the resulting product, and by extension its final chirality is dictated purely through the fact that the directing group will preferentially stabilize a singular ring to undergo nitration. Herein a comprehensive look at a variety of different reaction conditions, including temperature, chiral auxiliary, solvent and a brief substrate scope (summarized in Scheme

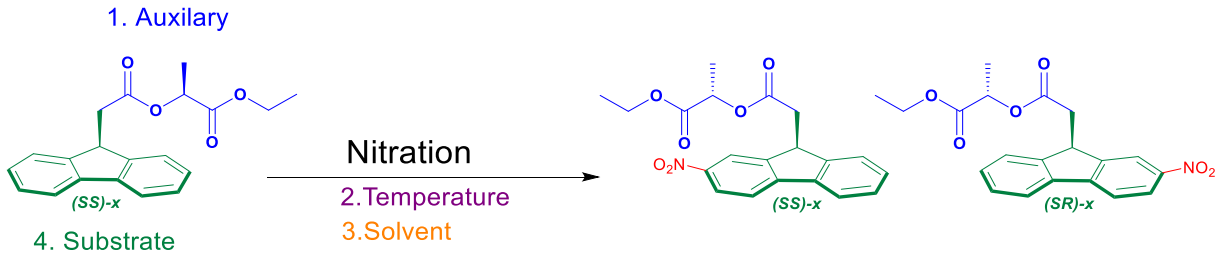

Scheme 3.1 Generalized scheme of reaction variables to be tested to verify as a general enantioselective nitration method.

3.1), are proving that the through space electrophilic aromatic nitrations directed with chiral auxiliaries is in fact a viable and extendable method in the field of electrophilic aromatic substitutions.

3.1 Investigation of Chiral Auxiliaries

The first steps in this investigation were primarily sought out to verify if the same selectivity principles that we observed, were purely due to the chiral auxiliaries $A_{1,3}$ strain in conjunction with the di chelation mechanism previously reported. To this effect the fluorenyl methyl ester was synthesized through EDCI coupling using methanol and the corresponding fluorenyl carboxylic acid, and subsequently mono- nitrated using tetrabutylammonium nitrate. This in conjunction with literature[16-18], verified that the enantioselectivity exhibited is primarily due to the through space nitrating groups. With this knowledge in hand synthetic endeavors turned toward derivatizing the fluorenyl core system with a variety of different chiral auxiliaries all with carbonyl systems; to show

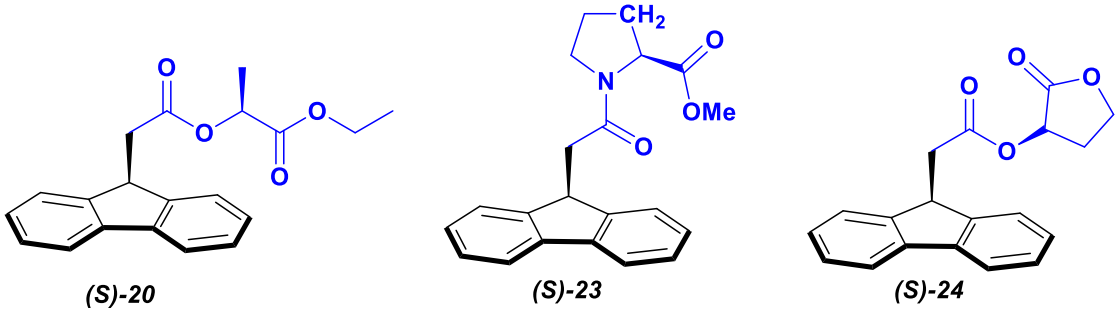

Figure 3.1: Different chiral auxiliaries utilized in study of enantioselective SEAr nitrations.

moderate selectivity, would verify the chiral auxiliary approach. These auxiliaries included the lactate system previously explored in chapter two[7], a lactone system, and a proline derived system all shown in Figure 3.1.

Using our general nitrating approach, all three derivatives were nitrated and analyzed to determine the d.r of the corresponding compounds. Experimentally, we observed an overall trend that the lactate auxiliary *(S,S)*-**21** had the highest selectivity with 2.5:1 d.r followed by the lactone auxiliary *(S,S)*-**25** with 2:1 d.r and finally the proline auxiliary *(S,S)*-**26** at 1.5:1 d.r. Interestingly enough, the lactate arm exhibited the highest selectivities of the tested chiral auxiliaries. This can be attributed to the flexible nature of the lactate arm and its ability to position itself in a manner in which the di-chelation to the aromatic ring below is more prominent and therefore offers more stability to the resulting wheland intermediate. Furthermore, the rigid nature of the cyclic auxiliaries hinders the ability and the strength of the electron donating ability of the overhanging carbonyl groups. The difference in the selectivities exhibited in each of the lactone *(S,S)*-**25**, and proline *(S,S)*-**26,** auxiliaries can be attributed to the degrees of freedom available to them between the nitrogen and the oxygen. Because C–O bonds can rotate more freely, the ability of the dichelation for the lactone is higher than the corresponding lactam. This supports the overall drop off on selectivity as the donating ability in the case of the proline auxiliary is most diminished.

Based on the results of these auxiliaries alone, it can be seen that the overall method of using chiral auxiliaries does give moderate selectivity. Subsequent removal of the auxiliaries leads to the formation of the corresponding enantiomers. This insight lead to the

exploration of different reaction conditions and to the extent that they effect the resulting selectivities.

3.2 Investigation of Temperature

Temperature has proven to be a powerful contributing factor in regard to organic reactions. It has the ability to affect the selectivity of products formed, the rate they are formed[19-21] and in many cases influences not only how diasteromers and enantiomers are formed but their respective ratios[22-24]. For this reason, scale up of compound (*S*)-**20** via a similar EDCI coupling found in Scheme 2.6 was carried out along with experiments to determine the extent of temperature in these reactions.

Compound *(S)*-**20** was dissolved into two separate vials of chloroform, (not deuterated chloroform as in the previous nitrations) used as the solvent and tetrabutyl ammonium nitrate as the nitration reagent. One vial was cooled down to -25°C while the other was kept at room temperature. The reactions were continuously monitored via TLC throughout the process to observe the consumption of starting material. It should be noted that after approximately one hour at room temperature all of the starting material was converted to product. In the case where the reaction was run at -25°C the reaction proceeded very sluggishly and was therefore allowed to warm to room temperature. After

nitration was complete and purification via preparative TLC, d.r. ratios were determined with ^{1}H NMR and summarized in Table 3.1.

Auxilary	Temperature	Solvent	Substrate	Ratio
Lactate	-25°C	$CHCl_3$	***(S)-20***	1.5:1
Lactate	Room Temp	$CHCl_3$	***(S)-20***	1.1:1

Table 3.1: Comparison of d.r. based on temperature for reaction shown in Scheme 3.1

The results of this experiment yielded two valuable points of information. The first, was that the selectivities dropped with the increase in temperature. And the second was that with the change in solvent, $CHCl_3$ vs $CDCl_3$, there was a significant change in the resulting ratios. Up to this point, the nitration involving the fluorenyl substrate, the lactate auxiliary, at lower temperatures, was giving moderate selectivity above 2:1. However with the slight change in solvent a significant decrease in selectivity was observed.

Conclusively however, there is a clear correlation to temperature and the overall observed selectivity in this nitration. Whereas it is not believed that the nitration takes place at temperatures below -20°C it is hypothesized, that due to the difference in the selectivities observed with all other variables held constant, that nitration will take place between -20°C

and room temperature. Furthermore, there is a clear correlation to the elevated selectivities and the reduced temperatures at which these reactions were run.

3.3 Investigation of Solvent Effect

After investigation of the temperature, it was revealed that there was a significant impact of the solvent on the overall selectivities observed within the S_EAr nitrations. This prompted a full investigation of solvent scope to determine the extent in which the solvent

Solvent	Yield	Ratio(d.r)	α^{28}
$CDCl_3$	71%	2.5:1± 0.1	<.20
$CHCl_3$	78%	1.6:1± 0.1	0.20
1,2 $PhCl_2$	76%	1.9:1± 0.1	0.00
1,3 $PhCl_2$	75%	1.8:1± 0.1	0.00
PhCl	71%	1.8:1± 0.1	0.00
THF	Trace	2.0:1± 0.1	0.00
ET_2O	Trace	1.9:1± 0.1	0.00
TFT	70%	2.1:1± 0.1	0.00
DCM	80%	1.7:1± 0.1	0.13

Table 3.2: Comprehensive solvent screening of enantioselective SEAr nitrations.

Reaction conditions: -25°C to r.t, lactate chiral auxiliary, fluorenyl substrate, TFAA, and tetrabutyl ammonium nitrate as the nitrating reagent as summarized in scheme 3.1.

affected the through space nitrations on the fluorenyl system. In these cases, the substrate, temperature, and auxiliary were all held constant. All reagents were dissolved in the same amount of their respective solvents, so the reaction concentrations remained the same. The reactions were run at -25°C and allowed to warm to room temperature until the reactions had reached full conversion. Whereas it was observed that excess acid hindered the selectivities of the TBTQ systems the use of TFAA is highly preferred to the nitration methods using TFA and sodium nitrate[17] to minimize excess TFA in the reaction vessel. The experiments are summarized in Table 3.2 showing the ratios, yields and also a corresponding Kamlett-taft[25-27] hydrogen bond donating capability (α)[28].

The original oddity of the drastic change in selectivity between deuterated chloroform and reagent grade chloroform raised some interesting questions into the mechanism of the reaction and to what extent the role of the solvent could effect selectivity Whereas the basis of our through space method relies heavily on the proximity of the carbonyl directing groups to the underlying rings, any interference of the solvent with these non-traditional interactions could significantly hamper the selectivities. Literature has these nitration reactions proceeding in one of two mechanisms[29, 30].

Both of these mechanisms are based on the generation of two different electrophiles at the start (scheme 3.2). Triflouroacetyl nitrate or the nitronium ion are primarily responsible for the overall nitration. However, in a closer look the conventional pathway for the nitronium ion, according to literature [29, 30] will attack orthogonally to the aromatic ring. After deprotonation and rearomatization the desired nitrated product is left. If the di-chelation effect of our overhanging directing groups can effectively block the top face of

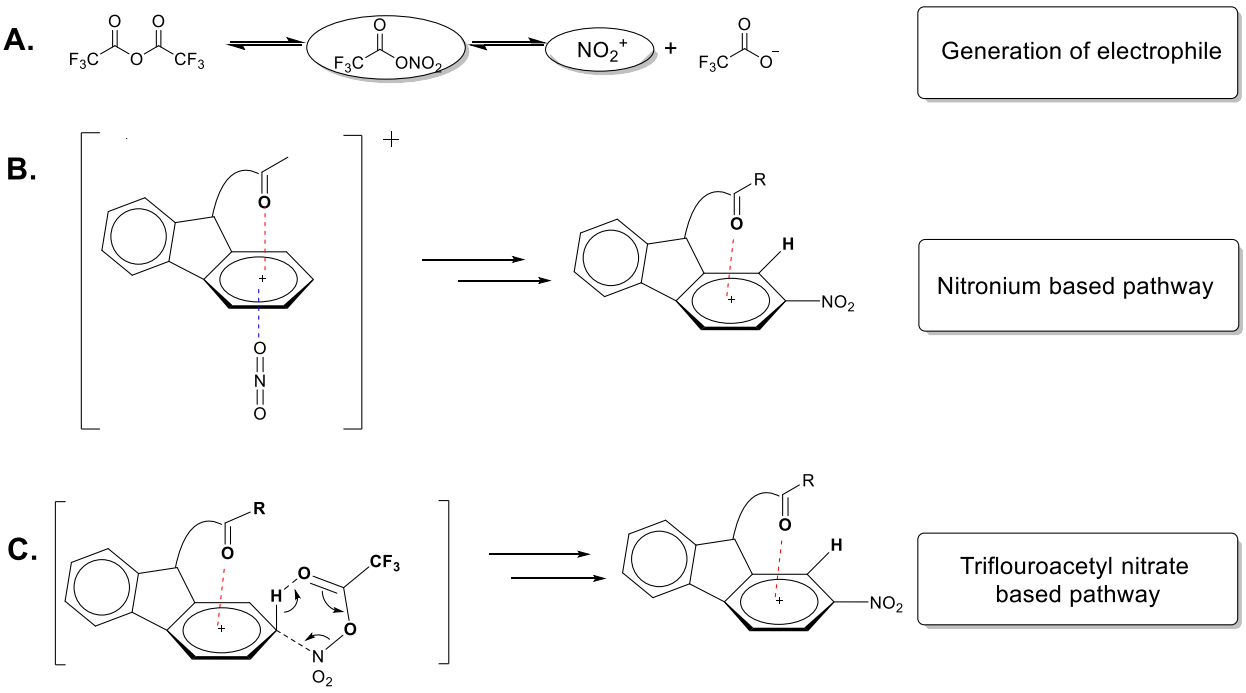

Scheme 3.2: Possible pathways for nitration to occur in through-space directed nitrations.

the aromatic rings the nitration is more likely to proceed via the second path. This steric interaction also supports the higher selectivities exhibited in the TBTQ system. Not only was there substantial steric hindrance from the top face, but additionally the concave nature of the TBTQ system provides noticeable steric hindrance on the bottom face. In the second synthetic pathway, pathway c, after generation of the triflouroacetyl nitrate, a six membered ring transition state is formed prior to deprotonation and re-aromatization. Because this process happens adjacent to the aromatic ring rather than above or below the central delocalized part of the ring, this transition should be more favored sterically as it is not blocked by the auxiliaries. Where it is believed that both mechanisms can occur[31-34] simultaneously it is hypothesized that the selectivity arises out of the stabilized Wheland intermediates reacting faster, as opposed to the pathway in which the nitronium ion nitrates

in a statistical fashion which would result in a racemic mixture[34]. This means that in regard to selectivity there would be a correlation to nitronium and the unfavored isomer, but further investigation is currently being done to expand on this hypothesis.

In reference to solvent effects on selectivity however, this insight to the mechanism was valuable in seeing that additional interactions could interfere with the chelation or the donation of electron density from the carbonyl directing groups to the aromatic rings below. The hydrogen bond donating ability (α) is a parameter commonly observed when looking into the solvent scope of reactions [35-38]. In the case of deuterated chloroform and reagent grade chloroform the substantial difference resides in the projected α values[39, 40]. Here, it seems that the hydrogen bonding capability of the chloroform interferes with the donation from the carbonyl to the aromatic ring. Additionally, when comparing traditional chloroform α=0.20 and DCM α=0.13, the ratios are 1.58:1 and 1.69:1 respectively thus further verifying that the donating ability of the solvent has an inverse relationship on the selectivity. Hydrogen-bond interference also coincides with the observed phenomenon of TFA; while TFA serves as a catalyst to make the reaction proceed faster, it severely disrupts the carbonyl donation into the ring because of its substantial hydrogen bonding capability. Ultimately polar aprotic solvents with α values of zero are ideal for these reactions.

Tetrahydrofuran (THF) and diethylether both have α values of 0.00 and exhibited enhanced selectivity of 2.0:1 and 1.94:1 respectively. Unfortunately, due to the insolubility of the reagents in these trials, only trace amounts of the product were isolated. Aryl solvents also displayed enhanced selectivity. Chlorobenzene, *o*-dichlorobenzene (ODCB) and *m*-dichlorobenzene (MDCB) gave selectivities of 1.78:1, 1.9:1, and 1.82:1 respectively. In

the case of triflourotoluene (TFT) which exhibited a selectivity of 2.1:1, the added selectivity could be attributed to the highly deactivating nature of the trihaloalkyl groups present. Inductive effects in this case could be occurring intermolecularly and by extension facilitating the nitration of the stabilized ring with donating directing groups above it, by effectively further destabilizing the subsequent aromatic ring.

Based on the findings presented herein, there is without a doubt a correlation between solvents and selectivities that are observed. The predominant factor of this phenomena is the hydrogen bonding ability of the solvents that can effectively disrupt the chelation and stabilizing effects of the donating effects of the chiral auxiliary. The final aspects in the exploration of enantioselective SEAr reactions are in the substrates in which the chiral auxiliaries are attached. This will determine the extent in which these reactions can apply to other systems.

3.4 Investigation of Substrates

The final piece in the exploration of this method involves testing the substrate scope. In this case, substrate refers to the base part of the molecule other than the attached chiral auxiliary to see if there is any effect on the selectivities of the molecules. Of these substrates we will look at the effects of ring size, 5 membered ring vs free phenyl groups, the effect of having a heteroatom within the internal ring, and the effect of the CH_2 spacer that is seen in these molecules. A summary of the structural components of the substrates are described (Figure 3.2.) herein where an electronic component screening will be conducted in the near future.

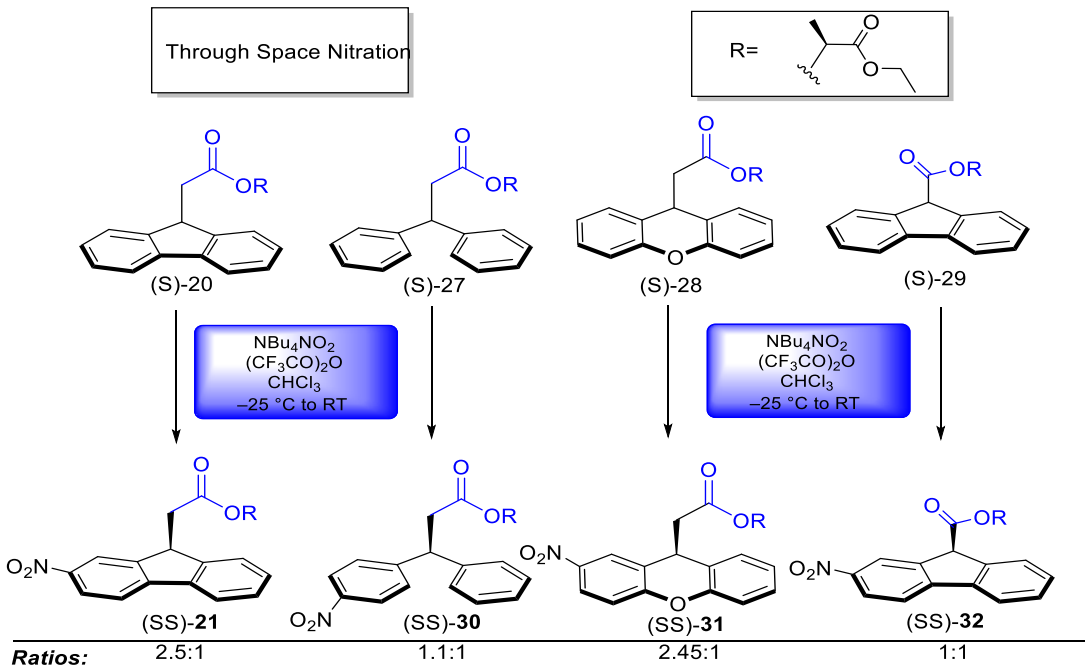

Figure 3.2: Different substrates used in the exploration of chiral nitrations.

(S,S)-**21,** as previously reported[7], has a selectivity of 2.5:1. When looking at the six membered ring with the heteroatom *(S,S)*-**31,** we see comparable selectivities of 2.45:1. In this instance the further donating ability of the oxygen could offer stabilization to the wheland intermediates. In the case where the compound is not conformationally locked at the base and the directing groups are not directly hanging over the aromatic rings, as in the case with compound (*S,S*)-**30** the selectivity is dropped to 1.1 :1. It is important to note that with this occurrence there is a mixture of regioisomers as well. In the case of the removal of the CH_2 spacer *(S,S)*-**32**, resulted in a complex 1H NMR structure in which preliminary results show a selectivity of approximatly 1:1. This can again be explained by the proximity of the through-space directing carbonyls. A brief conformational search revealed that while the first carbonyl is closer to the underhanging aromatic ring the second carbonyl is located

significantly further than the previous analogs, leading to minimal donation and ultimately poor selectivity.

3.5 Summary and Future work

After investigating the various aspects of enantioselective SEAr nitration reactions, solvent, temperature, auxiliaries, and substrates, it appears that using a through space method for SEAr nitrations can further be extended to a more general method. However, there are limitations in which each of these aspects can enhance the selectivities. In this regard, solvents and temperature were more likely to hinder the reaction if there is significant hydrogen bond donating capability or the reaction is run at an elevated temperature. In each case it was observed that selectivities dropped off substantially.

The substrate scope was insightful in the fact that unless the compounds are conformationally locked in a manner that allows for the directing groups to directly hang over the aromatic rings, the chelation and donation into the electron deficient intermediates does not occur as effectively. It is important to note however where the selectivity was severely diminished at 1.1:1 in the case of compound (*SS*)-**30** there was still selectivity present. The auxiliaries for the most part play the most substantial role in the selectivities observed. In order for the reaction to occur in a selective manor the di chelation and predominant shift of the directing arm to swing left and right are imperative. Unless the orientation of the overhanging carbonyl groups for the directing arm are in close enough

proximity to the aryl substituents below then suitable stabilization does not occur to induce selectivity. Ultimately finding a suitable auxiliary for these compounds seems to have the greatest positive impact on enhancing the selectivities.

Future work of this method would greatly benefit from further computational studies to help find other auxiliaries and how they may enhance the selectivities of similar systems. In addition, a more thorough substrate scope including electron donating and electron withdrawing groups on the aromatic rings could change the reactivity of the rings to either enhance or destroy the stabilization of the proposed wheland intermediates. Because of the many nuances within this method there, is a vast variety of exploration still to be done in regard to enantioselective SEAr nitrations.

References

1. Beresis, R. T.; Masse, C. E.; Panek, J. S., Enantioselective Nitration of Chiral (E)-Crotylsilanes: A Concise Asymmetric Synthesis of (E)-Olefin Dipeptide Isosteres. *The Journal of Organic Chemistry* **1995,** *60* (24), 7714.
2. Bandini, M.; Melloni, A.; Umani-Ronchi, A., New catalytic approaches in the stereoselective Friedel-Crafts alkylation reaction. *Angew. Chem. Int. Ed.* **2004,** *43* (5), 550.
3. Holland, M. C.; Paul, S.; Schweizer, W. B.; Bergander, K.; Muck-Lichtenfeld, C.; Lakhdar, S.; Mayr, H.; Gilmour, R., Noncovalent interactions in organocatalysis: modulating conformational diversity and reactivity in the MacMillan catalyst. *Angew. Chem. Int. Ed.* **2013,** *52* (31), 7967.
4. Kobayashi, S.; Mori, Y.; Fossey, J. S.; Salter, M. M., Catalytic enantioselective formation of C-C bonds by addition to imines and hydrazones: a ten-year update. *Chem. Rev.* **2011,** *111* (4), 2626.
5. Li, J. L.; Yue, C. Z.; Chen, P. Q.; Xiao, Y. C.; Chen, Y. C., Remote enantioselective Friedel-Crafts alkylations of furans through HOMO activation. *Angew. Chem. Int. Ed.* **2014,** *53* (21), 5449.
6. Paras, N. A.; MacMillan, D. W. C., New Strategies in Organic Catalysis: The First Enantioselective Organocatalytic Friedel−Crafts Alkylation. *J. Am. Chem. Soc.* **2001,** *123* (18), 4370.
7. Campbell, J. P.; Rajappan, S. C.; Jaynes, T. J.; Sharafi, M.; Ma, Y.-T.; Li, J.; Schneebeli, S. T., Enantioselective Electrophilic Aromatic Nitration: A Chiral Auxiliary Approach. *Angew. Chem., Int. Ed.* **2019,** *58* (4), 1035.
8. Jørgensen, K. A., Asymmetric Friedel-CraftsReactions: Catalytic Enantioselective Addition of Aromatic and HeteroaromaticC-H Bonds to Activated Alkenes, Carbonyl Compounds, andImines. *Synthesis* **2003,** *2003* (07), 1117.
9. Mohr, J. T.; Krout, M. R.; Stoltz, B. M., Natural products as inspiration for the development of asymmetric catalysis. *Nature* **2008,** *455*, 323.
10. Merz, K. In *Role of dynamics in enzymatic electrophilic aromatic substitution*, American Chemical Society: 2017; pp PHYS.
11. Schramma, K. R.; Forneris, C. C.; Caruso, A.; Seyedsayamdost, M. R., Mechanistic investigations of lysine-tryptophan cross-link formation catalyzed by Streptococcal radical S-adenosylmethionine enzymes. *Biochemistry* **2018,** *57* (4), 461.
12. Bume, D. D.; Pitts, C. R.; Ghorbani, F.; Harry, S. A.; Capilato, J. N.; Siegler, M. A.; Lectka, T., Ketones as directing groups in photocatalytic sp(3) C-H fluorination. *Chem Sci* **2017,** *8* (10), 6918.
13. Holl, M. G.; Pitts, C. R.; Lectka, T., Fluorine in a C-F Bond as the Key to Cage Formation. *Angew. Chem. Int. Ed.* **2018,** *57* (11), 2758.
14. Holl, M. G.; Struble, M. D.; Singal, P.; Siegler, M. A.; Lectka, T., Positioning a Carbon-Fluorine Bond over the pi Cloud of an Aromatic Ring: A Different Type of Arene Activation. *Angew. Chem. Int. Ed.* **2016,** *55* (29), 8266.
15. Murphy, K. E.; Bocanegra, J. L.; Liu, X.; Chau, H. K.; Lee, P. C.; Li, J.; Schneebeli, S. T., Precise through-space control of an abiotic electrophilic aromatic substitution reaction. *Nature Commun.* **2017,** *8*, 14840.

16. Beuerle, F.; Dhara, A., Synthetic Strategies for the Regioselective Functionalization of Tribenzotriquinacenes. *Synthesis* **2018,** *50* (15), 2867.
17. Linke, J.; Bader, N.; Tellenbroeker, J.; Kuck, D., Sixfold Peripheral Halogenation of Tribenzotriquinacenes: An Alternative Access to Useful TBTQ Building Blocks. *Synthesis* **2018,** *50* (1), 175.
18. Wang, T.; Zhang, Y.-F.; Hou, Q.-Q.; Xu, W.-R.; Cao, X.-P.; Chow, H.-F.; Kuck, D., C3-Symmetrical Tribenzotriquinacene Derivatives: Optical Resolution through Cryptophane Synthesis and Supramolecular Self-Assembly into Nanotubes. *J. Org. Chem.* **2013,** *78* (3), 1062.
19. Kabir, A.; Endo, S.; Toyooka, N.; Fukuoka, M.; Kuwata, K.; Kamatari, Y. O., Evaluation of compound selectivity of aldo-keto reductases using differential scanning fluorimetry. *J. Biochem.* **2017,** *161* (2), 215.
20. Singh, G.; Virpal; Singh, R. C., Highly sensitive gas sensor based on Er-doped SnO2 nanostructures and its temperature dependent selectivity towards hydrogen and ethanol. *Sens. Actuators, B* **2019,** *282*, 373.
21. Wang, B.; Ma, J.; Lu, L.; Zhu, J.; Wei, D. Method for continuously synthesizing propylene glycol methyl ether acetate by low-temperature high-selectivity catalytic rectification. CN109456190A, 2019.
22. Li, X.-N.; Zhou, H.-Y.; Feng, L.; Duan, K.; Wang, J.-X., Temperature-tuned enantioselectivity in transfer hydrogenation: preparation and catalytic property of amino acid-modified benzimidazole. *Appl. Organomet. Chem.* **2012,** *26* (4), 168.
23. Ljubovic, E.; Majeric-Elenkov, M.; Avdagic, A.; Sunjic, V., Novel biocatalytic methodology: low temperature enhanced enantioselectivity of enzyme catalyzed reactions in organic solvents. *Food Technol. Biotechnol.* **1999,** *37* (3), 215.
24. Watanabe, K.; Koshiba, T.; Yasufuku, Y.; Miyazawa, T.; Ueji, S.-i., Effects of Substituent and Temperature on Enantioselectivity for Lipase-Catalyzed Esterification of 2-(4-Substituted Phenoxy)Propionic Acids in Organic Solvents. *Bioorg. Chem.* **2001,** *29* (2), 65.
25. Abraham, M. H.; Grellier, P. L.; Abboud, J.-L. M.; Doherty, R. M.; Taft, R. W., Solvent effects in organic chemistry-recent developments. *Can. J. Chem.* **1988,** *66* (11), 2673.
26. Fasina, T. M.; Dueke-Eze, C. U.; Familoni, O. B., Synthesis and solvatochromic behaviour of some heterocyclyic isonicotinohydrazide Schiff bases. *Moroccan J. Chem.* **2018,** *6* (3), 504.
27. Marcus, Y., The properties of organic liquids that are relevant to their use as solvating solvents. *Chem. Soc. Rev.* **1993,** *22* (6), 409.
28. http://www.stenutz.eu/chem/solv26.php.
29. Liljenberg, M.; Stenlid, J. H.; Brinck, T., Mechanism and regioselectivity of electrophilic aromatic nitration in solution: the validity of the transition state approach. *J Mol Model* **2017,** *24* (1), 15.
30. Smythe, G. A.; Matanovic, G.; Yi, D.; Duncan, M. W., Trifluoroacetic Anhydride-Catalyzed Nitration of Toluene as an Approach to the Specific Analysis of Nitrate by Gas Chromatography-Mass Spectrometry. *Nitric Oxide* **1999,** *3* (1), 67.

31. Galabov, B.; Koleva, G.; Simova, S.; Hadjieva, B.; Schaefer, H. F., 3rd; Schleyer, P., Arenium ions are not obligatory intermediates in electrophilic aromatic substitution. *Proc. Natl. Acad. Sci. U. S. A.* **2014,** *111* (28), 10067.
32. Proceedings of the Chemical Society, Vol. 6, No. 85. *Proceedings of the Chemical Society (London)* **1890,** *6* (85), 95.
33. Armstrong, H. E., XXVIII.—An explanation of the laws which govern substitution in the case of benzenoid compounds. *J. Chem. Soc., Trans.* **1887,** *51* (0), 258.
34. Galabov, B.; Nalbantova, D.; Schleyer, P.; Schaefer, H. F., 3rd, Electrophilic Aromatic Substitution: New Insights into an Old Class of Reactions. *Acc Chem Res* **2016,** *49* (6), 1191.
35. Baker, S. N.; Baker, G. A.; Bright, F. V., Temperature-dependent microscopic solvent properties of 'dry' and 'wet' 1-butyl-3-methylimidazolium hexafluorophosphate: correlation with ET(30) and Kamlet-Taft polarity scales. *Green Chem.* **2002,** *4* (2), 165.
36. Crowhurst, L.; Mawdsley, P. R.; Perez-Arlandis, J. M.; Salter, P. A.; Welton, T., Solvent-solute interactions in ionic liquids. *Phys. Chem. Chem. Phys.* **2003,** *5* (13), 2790.
37. Jin, P.; Long, J.; Du, Y.; Zheng, X.; Xue, J., Hydrogen bond configuration and protonation of ground and lowest excited triplet states of 4-amino-4'-nitrobiphenyl based on nanosecond transient absorption spectroscopy. *Spectrochim. Acta, Part A* **2019,** *217*, 44.
38. Yuan, Y.; Zheng, M.; Zhao, H.; Kong, L., Solubility Determination and Modeling of p-Nitrobenzamide Dissolved in Twelve Neat Solvents from 283.15 to 328.15 K. *J. Chem. Eng. Data* **2019**, Ahead of Print.
39. Singh, S.; Rao, C. N. R., Deuterium Isotope Effects on Hydrogen Bonding. *Can. J. Chem.* **1966,** *44* (22), 2611.
40. Shi, C.; Zhang, X.; Yu, C. H.; Yao, Y. F.; Zhang, W., Geometric isotope effect of deuteration in a hydrogen-bonded host-guest crystal. *Nature communications* **2018,** *9* (1), 481.

Chapter 4: SIZE CONTROL OF POLYMERS THROUGH A NOVEL ITERATIVE EXPONENTIAL GROWTH METHOD.

Creating defined polymers of specific length and sequence represents one of the oldest vexations for synthetic chemists. Classical polymerization techniques including, step and chain growth polymerizations produce fragmented polymer sequences with various ranges of molecular weights and in some cases shapes. Techniques such as solid-state peptide synthesis allow for the formation of sequence defined oligomers that grow in a sluggish linear rate. This work described herein demonstrates the use of iterative exponential growth (IEG) to grow oligomers of exact sequence and size in an exponential fashion. Utilization of nucleophilic aromatic substitutions, and unique methyl sulfide substituents are used to mask leaving groups which can be then accessed via oxidation.

4.1 Introduction: IEG

It is imperative to gain full control over prominent characteristics, properties and functionalities of synthetic chains in order to realize the full potential of polymers. Fundamental control can only be realized through the strict dictation of molecular weight, sequence and geometric character. Nature in this aspect has accessed the limitless capacity of polymers to procure various biological applications through the manipulation of these properties *i.e*. DNA which are organized in a shape-and sequence-defined fashion[1, 2]. DNA

has four conventional base pairs, or monomers, these four monomers are estimated to store a maximum of 455 billion gigabytes in a single gram of material [3]. With this in mind, enhancement and development of new polymerization techniques is becoming a fundamental challenge to be explored.

Classically, polymers are synthesized in one of two ways, through step growth and chain growth polymerization. Step growth involves the stepwise addition of monomers in a manner that two growing chains can continuously combine. Whereas effective in forming smaller oligomers, larger polymers are difficult to obtain as mono disperse products. Chain growth mechanisms although often more controlled, uses an initiator in which monomers can only add to the growing chains. This method enhances the ability to form large polymers but still poses the drawback of forming a non- specific sized polymer. In fact, to date there are very few methods that allow for specific sized polymers to be formed. Both step and chain polymerizations yield a distribution of molecular weights, which results from the statistical variation observed while synthesizing polymers. This distribution classified by the polydispersity index (PDI) is often higher in polymers that are formed using the standard step and chain growth mechanisms. A combinatorial technique called iterative exponential growth (IEG) in essence allows for the formation of well-defined, mono-disperse polymers to be formed[4].

IEG can be described[5] as a convergent/divergent approach, beginning with a dormant monomer that includes two distinct functionalities, which are orthogonally deprotected, affording two reactive species. These two reactive species are then combined

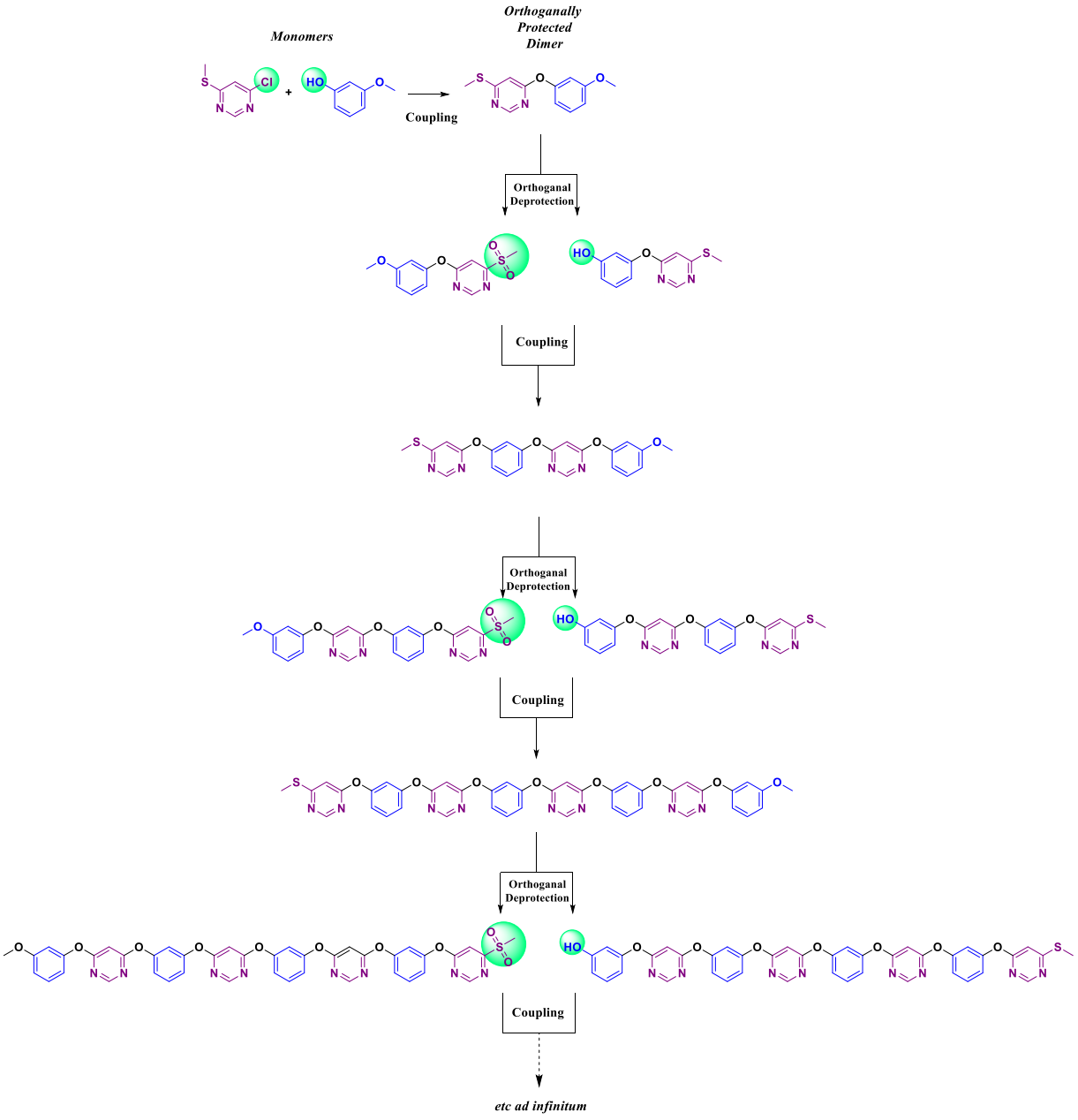

Scheme 4.1: Theoretical scheme of our novel formation of oligoethers using IEG and a unique masking /unmasking of methylsulfone during deprotection.

in a chemoselective manner, resulting in a dormant dimer, which has identical protected functionalities to the dormant monomer. As seen in Scheme 4.1, IEG allows for a well-

controlled growth to a certain length. The ability for the monodispersity lays with in the manner in which these monomers couple. Once the monomer is reacted, it again becomes dormant until a second deprotection and subsequent coupling, which in contrast of conventional "end to end" polymerization gives rise to a more of a "middle out" approach[5].

The potential chain length of the desired polymer can ultimately be dictated exactly to be 2^n where n is the number of cycles the monomers are coupled. Where this method is powerful in terms of size control, use of this technique is limited by synthetic complications of deprotecting a single end revealing different activated ends of the same starting material[6, 7]. Furthermore, to the best of our knowledge, this systematic polymerization technique has yet to be done using nucleophilic aromatic substitutions, and therefore unexplored with reference to sequence. Herein we show the utilization of IEG for the first time using nucleophilic aromatic substitutions but also in the formation of an ABAB sequenced polymers.

4.2 Extending IEG Using Nucleophilic Aromatic Substitution

Whereas CAS directly focuses on shape control, and the shape of polymer folding is directly related to the size of polymers, this IEG method aims to facilitate the formation of specific sized polymers. Outside of work done by Hawker and co-workers[8] use of S_N2 reactions to make IEG oligoethers, polymerizations that are made through nucleophilic aromatic substitutions S_NAr are yet to be reported. S_NAr is characterized by the substitution

of a good leaving group by a nucleophile on an aromatic ring that is activated via an electron withdrawing group (EWG). Mechanistically it proceeds through the addition of a nucleophile to the same carbon that has the leaving group attached. The nucleophile then donates electrons to the π* orbital, breaking aromaticity, and pushing electrons to the EWG group forming a tetrahedral intermediate, also known as a Meisenheimer complex, the rate limiting step in most of these reactions [9-11]. Scheme 4.2 shows a brief mechanism of a general S_NAr reaction.

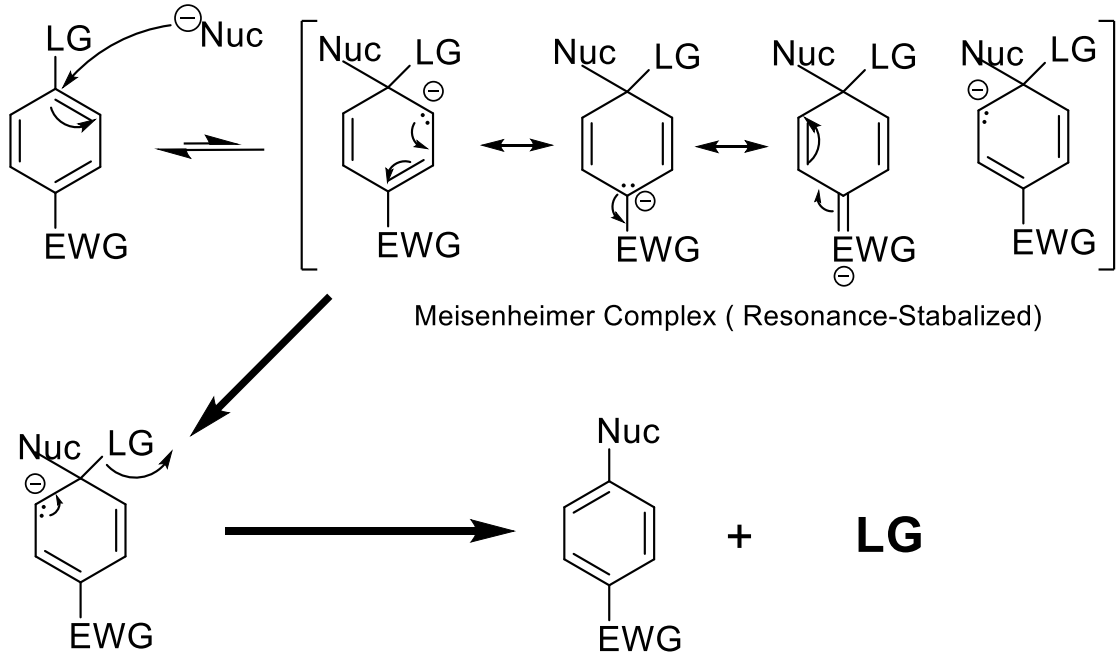

Scheme 4.2: Conventional mechanism of S_NAr reaction through a resonance stabilized Meisenheimer complex

As such, a key aspect in a nucleophilic aromatic substitution is the leaving group. Conventionally halides are used as the leaving groups in S_NAr. However, when we look at the reactivity of the halides in reference to S_NAr reactions compared to S_N2 reactions we see that they are inverse[12].Typically, it is observed that because of the carbon halogen bond

strength, the reactivity order of the halogens in SN2 is I > Br > Cl > F. In contrast when looking at S_NAr reactions we see that it is F >> Cl > Br > I. There is a de-emphasis on the carbon halide strength because the bond breakage does not occur during the Meisenheimer complex and is more of a result of the electronegative nature of the halides and their ability to leave during re-aromatization.

The biggest synthetic challenge using an IEG method in polymerization is that the monomers must have both nucleophilic and electrophilic character built in to the molecule. Furthermore, these same functionalities must be able to be protected and deprotected under different conditions. Our scheme utilizes the methylation of a phenol to easily protect and deprotect the nucleophilic part of the molecule however masking the electrophilic portion poses a bit of creativity as there are very few methods for protecting aryl halides.

This synthetic challenge herein was solved by employing a methyl sulfone as the leaving group in conjunction with a novel masking and unmasking technique to transform from an electron rich methylsulfide. Interestingly enough there is literature precedence for this masking, unmasking technique. Dehaen *et al* showed that methyl sulfones could be effective leaving groups in the functionalization of pyrimidine substituents of macrocycles[13]. Furthermore, Zhao *et al* used methyl sulfides to protect an electrophilic site on hyperbranched poly ethers[14]. Here, this same technique is employed to switch between the dormant form as a methyl sulfide and upon oxidation revealing the prominent leaving group in the methyl sulfone. Research however, in reference to the use of a sulfone as a

leaving group in nucleophilic aromatic substitution to synthesize linear polymers, has yet to be produced and is the foundation for this work.

4.3 Synthesis and Exploration of SNAr and IEG in Polymerizations

Several generations of the monomers were synthesized, predominantly to optimize the yields comparable to yields in materials chemistry [15-19]. To this extent a variety of different protecting groups and methods were explored by Tyler Jaynes in his honors thesis[20]. After issues with degradation, solubility, and fragmentations it was decided as

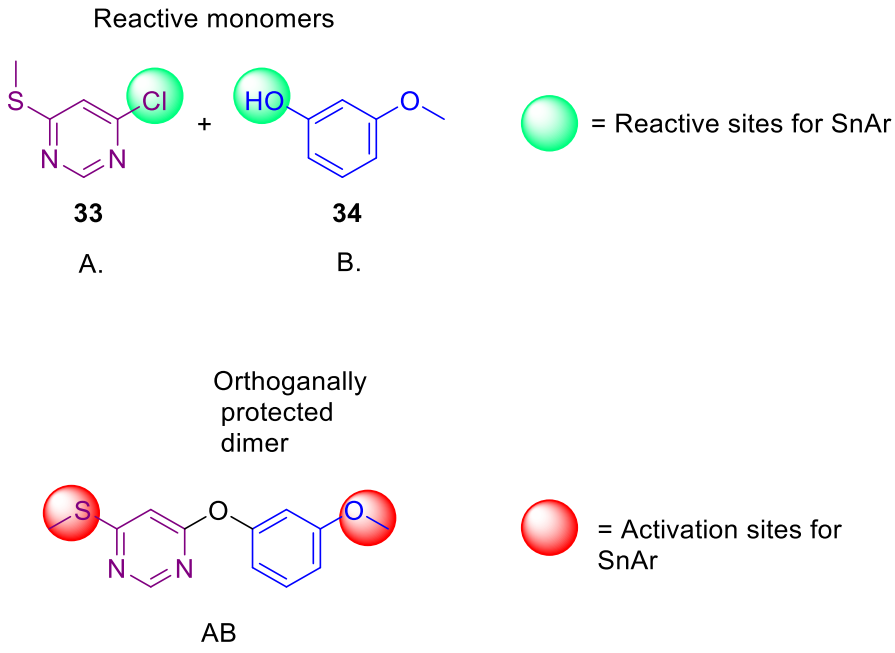

Figure 4.1: Reactive monomers (top) and unreactive dimer with easily activated reactive positions (bottom) used toward sequenced defined oligoethers via SnAr polymerization

shown in Figure 4.1 that the protected nucleophile would be an aryl alcohol group easily de-methylated from the corresponding methoxy group, and the electrophile/ leaving group would be the methylsulfone that could be easily oxidized from its corresponding methylsulfide. The electrophilic core consists of aromatic heterocycles containing nitrogen which have shown precedence to benefit nucleophilic aromatic substitutions. This benefit is due nitrogen's ability to stabilize the anionic intermediate analogous to how electron withdrawing groups do when substituted onto benzene rings[20]

Synthesis of these oligomers started with compounds **33** and **34,** which were bought commercially. They were reacted with a nonnucleophilic base until the coupling was complete to give compound **35** in moderate yields. It is important to note that after the first SnAr coupling that the leaving group was switched to the methylsulfone. This was simply in order to cut down synthetic steps to form the starting material, which was commercially available. When compared to some of the other generations of this attempted scheme it was

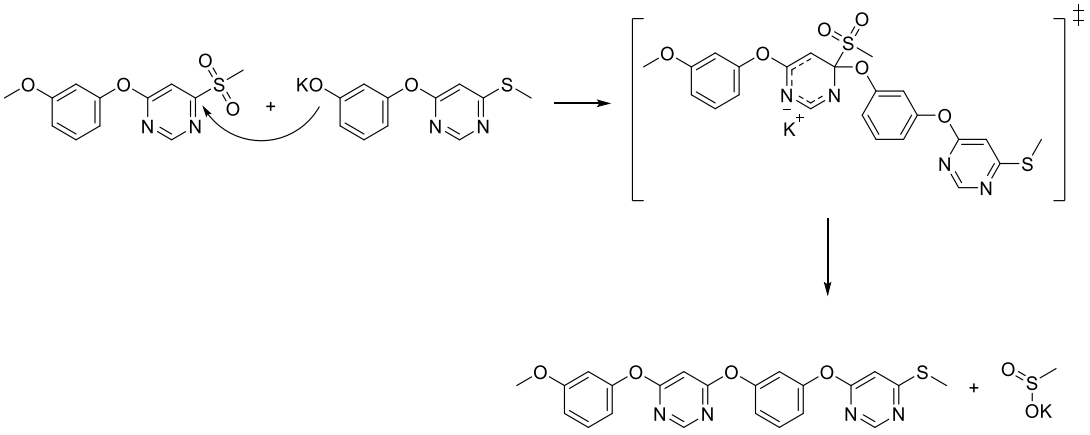

Scheme 4.3: Concerted Mechanism of SnAr with a non-traditional meisenheimer transition-state oy our oligomer according to Jacobsen's proposed mechanism

seen that the SnAr coupling with nitrogen heterocycles occurred in better yields. This was partially attributed to the stabilization of the anion from the pyrimidine ring but also due to the proposed mechanism (Scheme 4.3) of this particular nucleophilic aromatic substitution. Here, the pyrimidine core , in concurrence with Jacobsen and co-workers [21] causes this SnAr to proceed through a concerted mechanism without a typical Meisenheimer complex contrary to the conventional mechanism shown in Scheme 4.2 .

Ultimately, whether or not a SnAr reaction proceeds via a stepwise (Meisenheimer complex) or a concerted mechanism is determined via the starting materials rather than the rate of reaction. To this notion, stepwise mechanisms occur mostly when there is a strongly electron withdrawing group such as a nitro group, and fluorine is used as the nucleophile or the leaving group[21]. Concerted reactions on the other hand give Meisenheimer like transition states and resembles a delocalized but non-aromatic anion produced by heteroatoms present on the incipient aromatic ring resulting into a Meseinheimer like transition state. According to Jacobsen and co-workers [21] the formation of this transition state is produced by concurrent processes *i*) C–O bond formation by donation of the oxygen lone pair from the incoming nucleophile into the C=N π^* orbital) and 2) C–Cl bond cleavage by donation of the incipient nitrogen lone pair into the C–Cl σ^* orbital. Whereas the formation of our product lies on this secondary pathway and goes through a short-lived transition state, leading to a higher yield, the reaction and polymerization of such material garnered high expectations for our IEG method.

Orthogonal demethylation to the corresponding phenol using BBr_3, and oxidation of the thiol to the corresponding methyl sulfone allowed for subsequent iterations and realization of an albeit small but sequenced and size disperse ABAB polymer measuring 16 units long as shown in Figure 4.2.

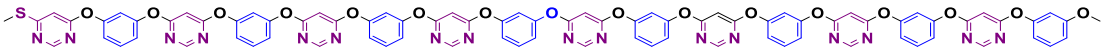

Figure 4.2: ABAB polymer synthesized using IEG with SnAr

4.4 Summary and Future Work

As alluded to in the introduction, overall shape and size control are of paramount importance in the expansion of CAS methodology. Selective methods to form coveted monomers of a tailored size and shape are necessary to realize many CAS proposed structures. In addition to specific size control, sequence defined polymers that could in the future mirror peptide synthesis or artificial enzymes[1, 2, 22, 23] are a powerful synthetic tool and its implications in organic synthesis and materials warrant further exploration of synthetic shape and size.

Iterative exponential growth of novel oligoethers were completed. Use of a unique and unstudied masking and unmasking technique of methylsulfides allowed for the synthetic challenge of our individual monomers to have internal nucleophilic and electrophilic properties that could be tailored and changed to meet synthetic needs. These oligomers are also novel in the fact that they are not only size defined, specifically 2^n, but

this is also the first report of linear polymerizations using nucleophilic aromatic substitutions. Furthermore, we described an effective synthetic path for in the formation of ABAB sequenced defined polymers.

Future work involving these polymers and this method will involve sequential generations with additional substitutions in order to address difficulties such as solubility as the effective length continues to grow. Additionally, expanding on different sequences that could be achieved, such as AABB, *etc*, can add an unexplored nuance to such reactions. Further exploration into the mechanism of the SnAr reactions can offer insight to how effective these reactions can be further utilized. Finally, further exploration of these polymerization products as materials and their intrinsic characteristics could open a new door to methodologies when looking at foldamers and the potential to be able to correlate the folding of longer chains to applicable biomaterials

References

1. Breslow, R., Biomimetic Chemistry and Artificial Enzymes: Catalysis by Design. *Acc. Chem. Res.* **1995,** *28* (3), 146.
2. Hecht, S.; Frechet, J. M. J., Dendritic encapsulation of function: applying nature's site isolation principle from biomimetics to materials science. *Angew. Chem., Int. Ed.* **2001,** *40* (1), 74.
3. Church, G. M.; Gao, Y.; Kosuri, S., Next-generation digital information storage in DNA. *Science* **2012,** *337* (6102), 1628.
4. Odian, G., **2004**.
5. Binauld, S.; Damiron, D.; Connal, L. A.; Hawker, C. J.; Drockenmuller, E., Precise synthesis of molecularly defined oligomers and polymers by orthogonal iterative divergent/convergent approaches. *Macromol. Rapid Commun.* **2011,** *32* (2), 147.
6. Barnes, J. C.; Ehrlich, D. J. C.; Gao, A. X.; Leibfarth, F. A.; Jiang, Y.; Zhou, E.; Jamison, T. F.; Johnson, J. A., Iterative exponential growth of stereo- and sequence-controlled polymers. *Nat. Chem.* **2015,** *7* (10), 810.
7. Hawker, C. J.; Malmstroem, E. E.; Frank, C. W.; Kampf, J. P., Exact Linear Analogs of Dendritic Polyether Macromolecules: Design, Synthesis, and Unique Properties. *J. Am. Chem. Soc.* **1997,** *119* (41), 9903.
8. Markoski, L. J.; Thompson, J. L.; Moore, J. S., Synthesis and Characterization of Linear−Dendritic Aromatic Etherimide Copolymers: Tuning Molecular Architecture To Optimize Properties and Processability. *Macromolecules* **2000,** *33* (15), 5315.
9. Acevedo, O.; Jorgensen, W. L., Solvent Effects and Mechanism for a Nucleophilic Aromatic Substitution from QM/MM Simulations. *Org. Lett.* **2004,** *6* (17), 2881.
10. Kulkarni, M.; Chaudhari, A., Microbial remediation of nitro-aromatic compounds: an overview. *J. Environ. Manage.* **2007,** *85* (2), 496.
11. Terrier, F., Rate and equilibrium studies in Jackson-Meisenheimer complexes. *Chem. Rev.* **1982,** *82* (2), 77.
12. Blaziak, K.; Danikiewicz, W.; Makosza, M., How Does Nucleophilic Aromatic Substitution Really Proceed in Nitroarenes? Computational Prediction and Experimental Verification. *J. Am. Chem. Soc.* **2016,** *138* (23), 7276.
13. Van Rossom, W.; Caers, J.; Robeyns, K.; Van Meervelt, L.; Maes, W.; Dehaen, W., (Thio)ureido anion receptors based on a 1,3-alternate oxacalix[2]arene[2]pyrimidine scaffold. *J. Org. Chem.* **2012,** *77* (6), 2791.
14. Guan, Y.; Wang, C.; Wang, D.; Dang, G.; Chen, C.; Zhou, H.; Zhao, X., Methylsulfone as a leaving group for synthesis of hyperbranched poly(arylene pyrimidine ether)s by nucleophilic aromatic substitution. *RSC Advances* **2015,** *5* (17), 12821.
15. Engler, A. C.; Chan, J. M. W.; Coady, D. J.; O'Brien, J. M.; Sardon, H.; Nelson, A.; Sanders, D. P.; Yang, Y. Y.; Hedrick, J. L., Accessing New Materials through Polymerization and Modification of a Polycarbonate with a Pendant Activated Ester. *Macromolecules (Washington, DC, U. S.)* **2013,** *46* (4), 1283.
16. Kelly, J. V.; O'Neill, F. T.; Sheridan, J. T.; Neipp, C.; Gallego, S.; Ortuno, M., Holographic photopolymer materials: nonlocal polymerization-driven diffusion under nonideal kinetic conditions. *J. Opt. Soc. Am. B* **2005,** *22* (2), 407.

17. Mueller, A.; O'Brien, D. F., Supramolecular Materials via Polymerization of Mesophases of Hydrated Amphiphiles. *Chem. Rev. (Washington, D. C.)* **2002,** *102* (3), 727.
18. Mueller, A.; O'Brien, D. F., Supramolecular materials via polymerization of mesophases of hydrated amphiphiles. *Chem. Rev.* **2002,** *102* (3), 727.
19. Uhlig, D.; Spange, S.; Seifert, A.; Nagel, K.; Anders, S.; Kroll, L.; Stoll, R.; Thielbeer, F.; Mueller, P.; Schreiter, K., Design of nanostructured hybrid materials: twin polymerization of urethane-based twin prepolymers. *RSC Adv.* **2018,** *8* (55), 31673.
20. Jaynes, T. Iterative Exponential Growth through Manipulation of Sulfide Oxidation States. Honors, University of Vermont, 2018.
21. Kwan, E. E.; Zeng, Y.; Besser, H. A.; Jacobsen, E. N., Concerted nucleophilic aromatic substitutions. *Nature Chem.* **2018,** *10* (9), 917.
22. Breslow, R.; Czarnik, A. W., Transaminations by pyridoxamine selectively attached at C-3 in β-cyclodextrin. *J. Am. Chem. Soc.* **1983,** *105* (5), 1390.
23. Cheng, L.; Breslow, R. In *Binding and biomimetic cleavage of the RNA by synthetic deoxypolypeptides/peptoids (DOPPs)*, American Chemical Society: 2016; pp ORGN.

CHAPTER 5: EXPERIMENTAL PROCEDURES

5.1 Methods and Materials

All commercially available starting materials were purchased from Sigma Aldrich, Fisher Scientific, Combi-Blocks or Oakwood Chemical. Removal of solvents was accomplished on a Büchi R-210 rotary evaporator and further concentration was done under a Fisher Scientific Maxima C-Plus vacuum line. Column chromatography was preformed manually with Sorbent grade 60 silica with a mesh size between 230–400 using a forced flow of indicated solvents, or automatically with a Teledyne Combi-Flash chromatography system. High-performance liquid chromatography (HPLC) was accomplished with an Agilent modular 1100 series instrument, equipped with a G1379A Degasser, aG1311A Quarterny pump, and a G1314A VWD detector. Analytical thin layer chromatography (TLC) plates were purchased from Fisher Scientific (EMD Millipore TLC Silica Gel 60 F254). All 1H NMR and 13C NMR spectra were recorded at 298 K on a Bruker ARX 500 (500 MHz) spectrometer. The spectra were referenced to the residual solvent peak (chloroform-d: 7.26 ppm for 1H NMR and 77.16 ppm for 13C NMR. Chemical shift values were recorded in parts per million (ppm). Data are reported as follows: chemical shift, multiplicity (s = singlet, d = doublet, t = triplet, q = quartet, m = multiplet, br = broad peak), coupling constants (Hz), and number of protons. High resolution mass spectrometry data were obtained on Waters XEVO G2-XS QTof in

positive ESI mode. Circular Dichroism spectra were obtained on a Jasco J-815CD spectrometer (scanning range: 400–240 nm, Data pitch:1.0nm, bandwidth:1.0 nm, scan speed:100nm/min, CD detector:PMT). Samples were diluted in chloroform until absorbance was 0.6–1.1 au and normalized by their UV/Vis absorptions at 278.5nm.

5.2 Experimental Procedures for THROUGH SPACE SELECTIVITY: ENANTIOSELECTIVE ELECTROPHILIC AROMATIC NITRATIONS TOWARD WELL DEFINED MACROSTRUCTURES

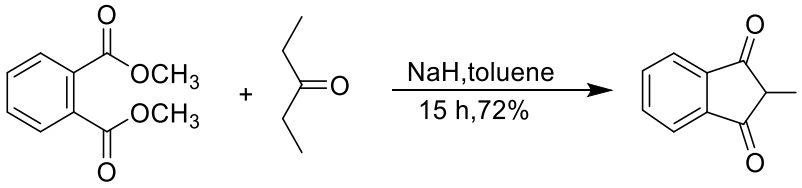

Synthesis of 2-methyl-1H-indene-1,3(2H)-dione (3): Synthesis of x was carried out in a modified procedure as follows: In a flame dried round bottom flask a dispersion of sodium hydride (60% in mineral oil 25g) was made in anhydrous toluene (approximately 600 mL). To this dispersion, commercially available, 3-pentanone **2** and dimethyl phthalate **1** were added slowly and then refluxed for 18 hours. Upon completion the vivid red solid was cooled, and vacuum filtered and allowed to dry. The resulting red powder was dissolved in water (820mL) and slowly acidified using concentrated HCL until the product proceeded to crash out of solution. The solid was collected via vacuum filtration and dried

giving the desired product as a pale yellow solid in 72% yield Spectral Characterization matched literature values [1]

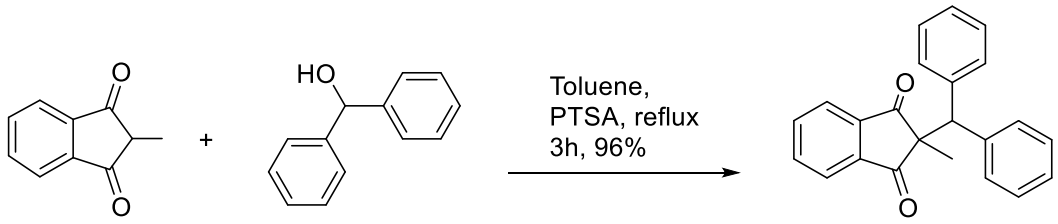

Synthesis of 2-benzhydryl-2-methyl-1H-indene-1,3(2H)-dione (5): Synthesis of 5 was carried out in a modified procedure as follows: A solution 40g (250 mmol) of 2-methyl-1H-indene-1,3(2H)-dione **(3),** 46g of di-phenylmethanol **(4)** (250 mmol) and 4.9g (25 mmol) of p-toluenesulfonic acid (PTSA) in approximately 400 mL of anhydrous toluene was made. The round bottom was equipped with a dean stark apparatus and heated to reflux. The reaction was monitored via the observation of quantitative water formation. Upon completion the solvent was evaporated, the resulting dark orange oil was dissolved in chloroform and washed with 5% Na_2CO_3 and then with water. The organic layer was collected, dried with sodium sulfate and concentrated. Methanol was added to the resulting hot oil in which the diketone **5** was formed as white solid in 90% Spectral Characterization matched literature values [2]

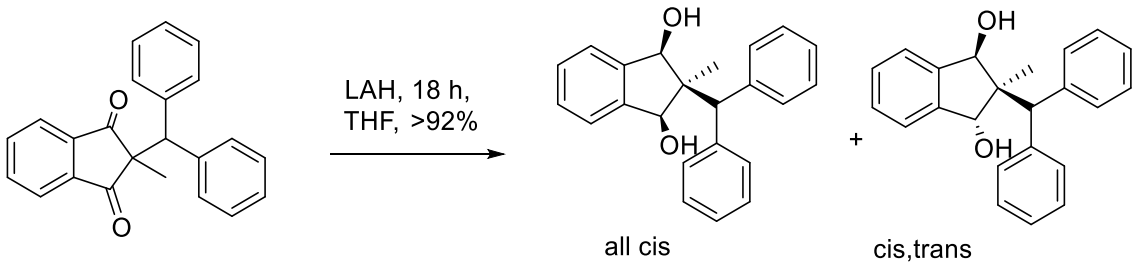

Synthesis of 2-benzhydryl-2-methyl-2,3-dihydro-1H-indene-1,3-diol (6) Synthesis of 6 was carried out in a modified procedure as follows : 6.5 g (20 mmol) of 2-benzhydryl-2-methyl-1H-indene-1,3(2H)-dione (**5**) was dissolved in in 45 mL of anhydrous THF and slowly added to a magnetically stirred suspension of LAH 1.0 g (26.4 mmol) in 150 mL of dry THF, under nitrogen. The reaction mixture was allowed to stir for 20 hours. The solvent was removed, and suspended in diethyl ether , and carefully hydrolyzed using icechips. The solution was filtered and dried using anhydrous sodium sulfate. and concentrated to give a a viscous yellow oil, upon complete removal of the solvent in the high-vac a light pink oil was obtained as the product in >90% yield. Spectral Characterization matched literature values[2]

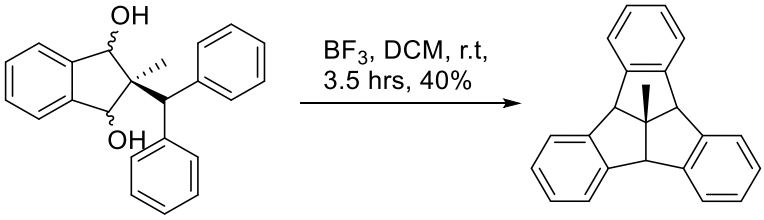

Synthesis of methyl-tribenzotriquinacene (7) Synthesis of 7 was carried out in a modified procedure as follows: 5g (15.2 mmol) of 2-benzhydryl-2-methyl-2,3-dihydro-1H-indene-1,3-diol (**6**) was dissolved in 250 mL of anhydrous DCM in a flame dried round

bottom flask. Upon dissolution, BF3 etherate 2.5 mL (3 equiv) was added drop-wise and the reaction was allowed to stir for 3.5 hours while being monitored via TLC. When the reaction came to completion, it was quenched with the addition of 0.5 M NaOH solution. The solution was then washed with water, and brine, dried with sodium sulfate and concentrated. The yellow solid was then recrystallized with ethyl acetate to give fluffy white crystals. The mother liquor was concentrated again and recrystallized a second time. The crystals were combined to give yields between 38-45 % Spectral Characterization matched literature values [2]

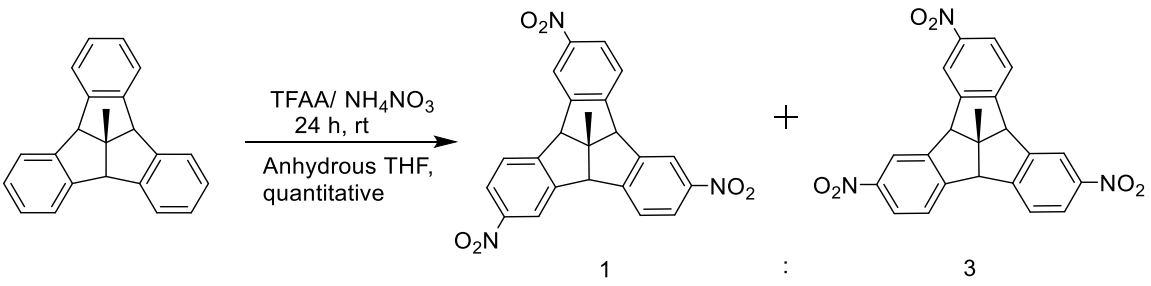

Synthesis of 3x-nitro-TBTQ (8) Synthesis of 8 was carried out in a modified procedure as follows: : methyl tribenzo triquinacene (500mg, 1.7 mmol) was dissolved in chloroform (100mL) 4mL (15 equiv) of trifluoroacetic anhydride (TFAA) was added and allowed to stir for 24 hours. Completion was monitored via TLC. Once complete the reaction was extracted with DCM, washed with water and brine and concentrated. The resulting yellow solid was collected in 86% yield in approximately a 3:1 of C_1 and C_3 regioisomers respectively. Spectral Characterization matched literature values[3].

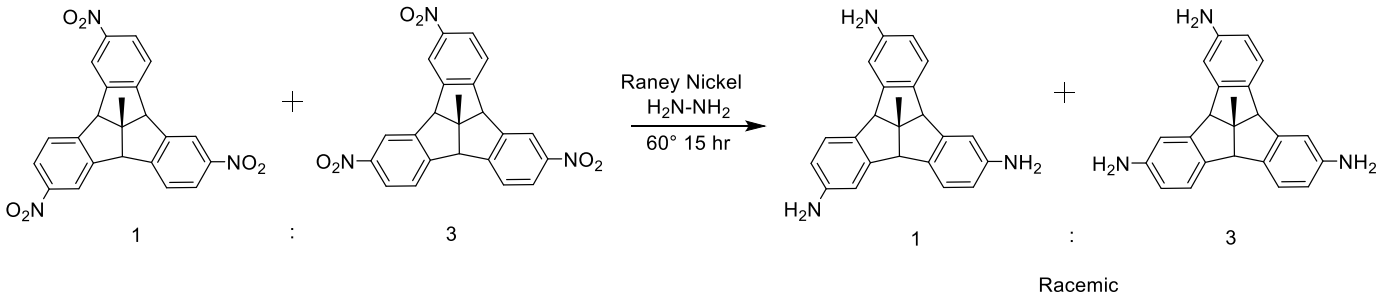

Synthesis of methyl- 3x-amino-TBTQ: methyl-3x-nitro-TBTQ **(8)** was dissolved in THF and "three large clumps of Ranny nickel" (and then a little bit more for good measure) was suspended in the reaction vessel. While stirring vigorously with a magnetic stirrer, a large excess of hydrazine mono-hydrate was added while under dry nitrogen and the reaction was allowed to stir at 50°C overnight. Upon completion the reaction vacuum filtered through a pad of celite and concentrated. The residue was purified using flash column chromatography with ethyl acetate and dichloromethane. Both C_1 and the C_3 products were isolated as a fine white powder in an overall 90% yield. Spectral Characterizations matched literature values [4].

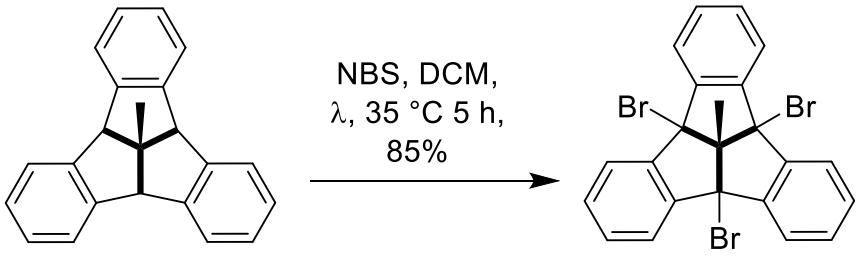

Synthesis of bromo-bridgehead -TBTQ (9) synthesis of 9 was carried out in a modified procedure as follows: 400 Mg of methyltribenzotriquinacene (1.4 mmol) was dissolved in anhydrous DCM (30 ml). a separate solution of NBS was made in DCM concurrently. Addition of the NBS solution was done in a single portion. The reaction mixture was

allowed to stir at 35°C under a lamp overnight. Upon completion the reaction was washed extensively with water, then once with saturated sodium thiosulfate, and brine. The organic layer was separated dried over sodium sulfate, and concentrated. The remaining pale tan product was collected in 85% yield. Spectral Characterizations matched literature values [5].

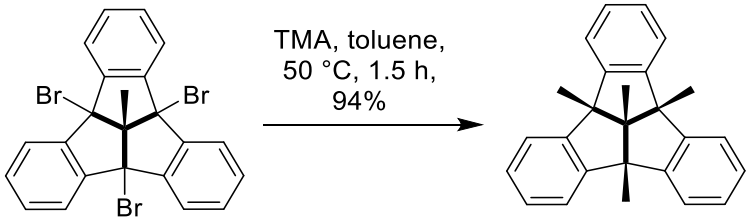

Synthesis of Tetramethyl-TBTQ (10) synthesis of 10 was carried out in a modified procedure as follows: In a small flame dried round bottom flask 300 mg (0.565 mmol) of **bromo-bridgehead -TBTQ (9)** was dissolved in anhydrous toluene (50ml) and stirred with a magnetic stirrer under a nitrogen atmosphere as the solution was heated to 50°C. Once warmed, 2.5 mL of a 1M solution of trimethyl-aluminum in toluene was added dropwise over 10 minutes. The reaction was allowed to proceed for an additional 2 hours. Upon completion, the reaction mixture was cooled, and quenched with water slowly. The reaction was extracted with DCM (3x), washed with water (2x) and dried over magnesium sulfate. Following concentration, a flakey white solid was isolated in 94% yield. Spectral Characterizations matched literature values [5]

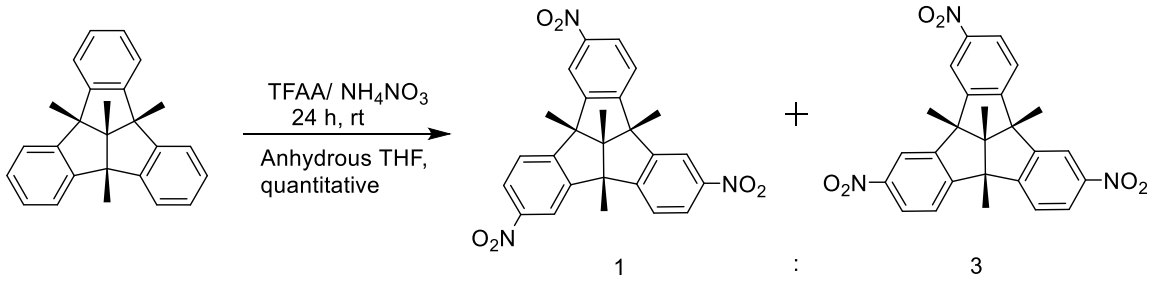

Synthesis of tetramethyl-3x-nitro -TBTQ (11): synthesis was carried out analgous to the procedure of the Synthesis of 3x-nitro-TBTQ **(8)** there was no additional purification needed following workup. Spectral Characterizations matched literature values[6]

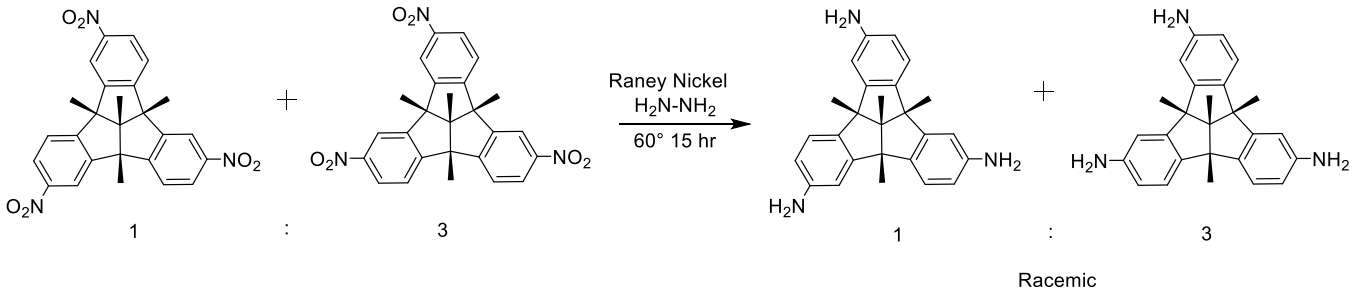

Synthesis of tetramethyl-3x-amino-TBTQ (12): Synthesis was carried oun in a procedure analgous the the procedure for the synthesis of **methyl- 3x-amino-TBTQ**. The residue was purified using flash column chromatography with ethyl acetate and Hexanes(70:30). Both C_1 and the C_3 products were isolated as a fine white powder in an overall 90% yield. Spectral Characterizations matched literature values [6]

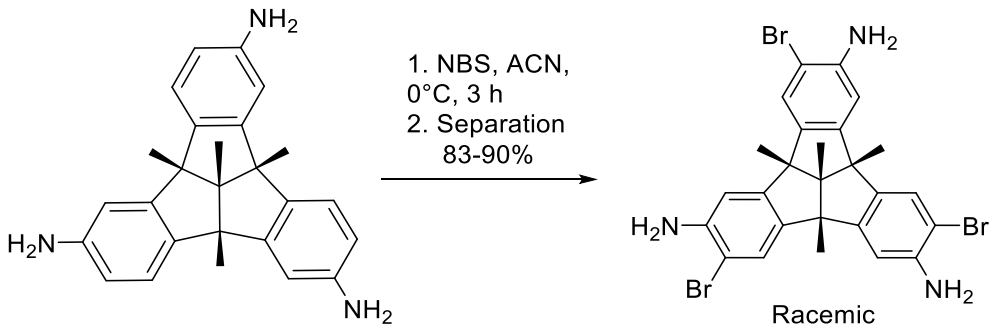

Synthesis of tetramethyl-3x-bromoanaline-TBTQ (13): In a dry 50 mL round bottom 0.100 g (.262 mmol) tetramethyl-3x-amino-TBTQ **(12)** was dissolved in acetonitrile (MeCN) and cooled to 0°C. A solution of NBS was dissolved in acetonitrile and exactly 3 equivalents of NBS (.786 mmol) was added . The solution was kept at 0° C and allowed to stir in the dark for an additional 2.5 hours. Upon completion the reaction was quenched with water and extracted with ethyl acetate (2x). The organic layer was then washed with water, and brine before it was dried over sodium sulfate and concentrated. Purification was done via automatic flash chromatography; Ethyl acetate and DCM, 5:95. Following separation the product was obtained in 74% yield as a tan solid.

Characterization data for **tetramethyl-3x-bromoanaline-TBTQ (11)** ^{1}H NMR (500 MHz, $CDCl_3$): δ = 8.681 (s, J = 2 Hz, 1H), 8.146 (dd, J = 4 Hz, 1H), 7.573 ppm (d, J = 7 Hz, 1H).

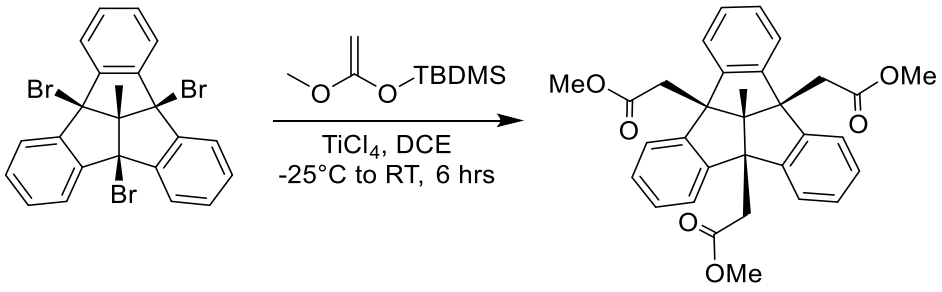

Synthesis of methylester-bridgehead-TBTQ (14). The tribenzotriquinacenederivative **9** (0.500g, 0.941mmol) was added to a flame-dried round-bottom flask and dissolved in 100 mL of anhydrous dichloroethane. Next, the solution was degassed with dry argon for 10 minutes, the argon line was switched to dry nitrogen, and the reaction mixture was cooled to –15 °C with an ice/salt cooling-bath. Subsequently, titanium tetrachloride (2.50mL, 22.7mmol) was added dropwise, the reaction mixture was stirred for 5 mins, and TBDMS-methoxy ethene (2.0mL, 8.5mmol) was added dropwise to the orange-colored solution. The resulting solution was allowed to warm to room temperature and stirred for an additional 6 hours. Upon completion, the reaction mixture was quenched slowly with excess water under vigorous stirring, diluted with more water (50mL), and the crude product was extracted with dichloromethane (3x50 mL). The combined organic layers were washed with water (3x50mL) and brine (1x50mL), dried over anhydrous sodium sulfate, and concentrated under reduced pressure. Ethanol was then added to the resulting thick orange oil, which lead the product to crystallize at –15°C in the freezer and afforded the tribenzotriquinacene derivative 2(0.367g, 0.719mmol) as fine colorless needles in 76% yield. Characterization data for 2 matched with the reported[6] characterization data of the compound, which was previously obtained[6] with a longer synthetic route.

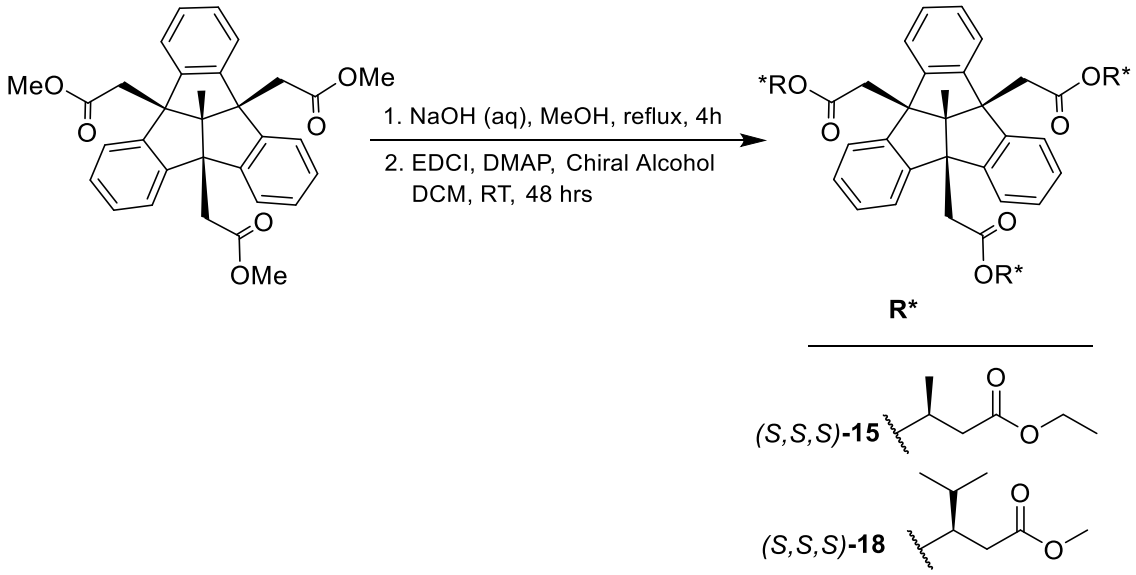

Synthesis of chiral triesters (S,S,S)-**15 and** (S,S,S)-**18.** The tribenzotriquinacene derivative 2(0.259g, 0.507 mmol) was suspended in 10mL of an aqueous 2M sodium hydroxide solution and 12mL of methanol was added. The vessel was sealed and stirred vigorously at 70°C for 20hoursto ensure complete hydrolysis of all three methyl esters. Once completed, the methanol was removed under reduced pressure with a rotary evaporator, the resulting aqueous solution was acidified to pH 1 with conc. HCl and extracted extensively with ethyl acetate. The combined organic layers were washed thoroughly with water, dried over anhydrous sodium sulfate, and concentrated under reduced pressure.

The resulting pale-yellow solid was suspended in 25mL of anhydrous dichloromethane in a flame-dried round bottom flask. DMAP (0.219g,1.7mmol) was added in one portion and the reaction mixture was stirred under a nitrogen atmosphere at room temperature until all components became soluble. EDCI (0.628g, 3.30 mmol) was then added in one portion and the reaction mixture was stirred for 30 minutes. Finally, 4.5 equivalents of a chiral alcohol

—(S)-ethyl-lactate for the synthesis of (*S*,*S*,*S*)-**15** or (S)-methyl-2-hydroxy-3-methylbutanoatefor the synthesis of (*S*,*S*,*S*)-**18**—were introduced into the system and the reaction mixtures were allowed to stir at room temperature for 48 hours. Upon completion, the reaction mixtures were quenched with 30mL of a 1M aqueous HCl solution and extracted with dichloromethane (3x50mL). The combined organic layers were washed with water (50mL) and brine (2x50mL), dried over anhydrous sodium sulfate, and concentrated under reduced pressure. The crude products were purified with flash-column chromatography over silica gel (eluent: 0%-40% ethyl acetate in hexanes). Compound 6was further purified with HPLC (eluent: 80% methanol in water), usingaZorbexC8 reverse phase column

Characterization data for (*S*,*S*,*S*)-**15**:Colorless glassy solid, obtained in 73% yield;^{1}H-NMR (500 MHz, CDCl3) δ= 7.31 (m, 6H), 7.16 –7.11 (m, 6H), 4.89 (q, J=7.1 Hz, 3H), 4.14 (q, J=7.1 Hz, 6H), 3.46 (s, 6H), 1.75 (s, 3H), 1.27 (d, J=7.1 Hz, 9H), 1.23 (t, J=7.1 Hz, 9H). ^{13}C-NMR (126 MHz, CDCl3) δ= 170.98, 170.78, 170.67, 146.73, 136.65, 127.82, 127.74, 122.73, 122.64, 70.95, 68.42, 65.38, 61.24, 41.61, 16.75, 14.08. HRMS (ESI) calcd.for $C_{44}H_{52}NO_{12}$+ $[M^{+}NH_4]^{+}$: m/z= 786.3490; found: 786.3480

Characterization data for (*S*,*S*,*S*)-**18:** Colorless solid, obtained in 61% yield;^{1}H-NMR (500 MHz, $CDCl_3$) δ= 7.37 –7.29 (m, 6H), 7.19 –7.10 (m, 6H), 4.69 (d, J=4.6 Hz, 3H), 3.68 (s, 9H), 3.48 (s, 6H), 2.16 –2.07 (m, 3H), 1.68 (s, 3H), 0.91 (d, J=6.9 Hz, 9H), 0.85 (d, J=6.8 Hz, 9H).^{13}C NMR (126 MHz, $CDCl_3$) δ= 171.60, 170.08, 146.81, 146.60, 127.84,

122.72, 77.27, 77.02, 76.77, 65.41, 51.86, 41.40, 30.04, 18.62, 17.25.HRMS (ESI) calcd. for $C_{47}H_{58}NO_{12}$+$[M^{+}NH_4]^{+}$: m/z= 828.3959; found: 828.3973.

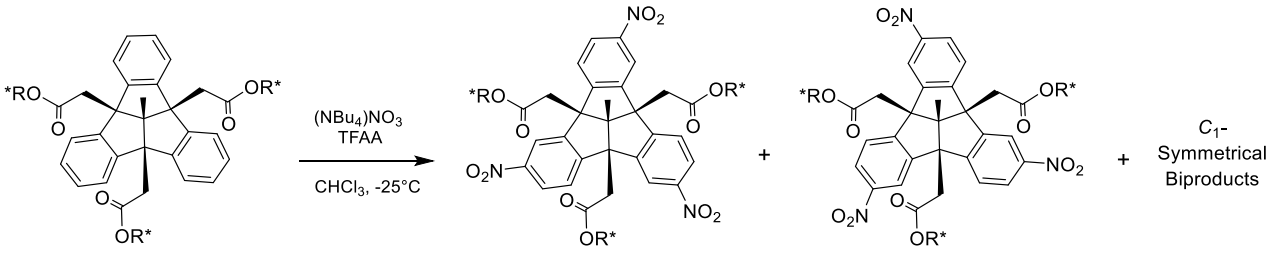

	Major	Minor	R*
(S,S,S)-**15**	*(P,S,S,S,)*-***C3-16***	*(M,S,S,S)*-***C3-16***	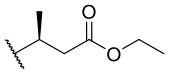
(S,S,S)-**18**	*(P,S,S,S,)*-***C3-19***	*(M,S,S,S,)*-***C3-19***	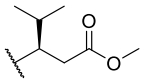

General Procedures for Through space directed nitrations. Compounds (S,S,S)-**15** (0.150g,0.190mmol) or (S,S,S)-**18** (0.020g, 0.025mmol)were dissolved in anhydrous chloroform(25mL for the reaction with (S,S,S)-**15** and 5mL in the case of (S,S,S)-**18**, respectively). The resulting solutions were cooled to -25°C and trifluoroacetic anhydride (TFAA, 9 equiv.) was added, followed by 1.2 equivalents of a saturated tetrabutylammonium nitrate solution in anhydrous chloroform. Afterwards, the reactions were warmed to room temperature and stirred for an additional 6 hours. To remove any trifluoroacetic acid (TFA) formed during the first nitration step, the reaction mixtures were then concentrated under dry nitrogen. Next, fresh anhydrous chloroform was added to the solid residues, the reaction mixtures were again cooled to –25°C, 10 equivalents of TFAA, and 2. 5 equivalents of tetrabutylammonium nitrate were added, and the reaction mixtures

were stirred at room temperature for 24 hours, which resulted in mixtures of mostly di-nitrated products. To proceed to tri-nitrated products, the reaction mixtures were dried once again, dissolved in anhydrous chloroform, cooled to –25°C, reacted with 12 equivalents of TFAA and 6 equivalents tetrabutylammonium nitrate, and stirred at room temperature. Reaction progress was monitored by ^{1}H-NMR spectroscopy. After ~36 hours, when the reactions were complete, they were quenched with a 0.5M aqueous NaOH solution and extracted with dichloromethane (3x30mL). The combined organic extracts were washed with water(1x50mL) and brine(1x25mL), dried over anhydrous sodium sulfate, and purified using preparative thin layer chromatography (eluent: 40% ethyl acetate in hexanes).

Characterization data for (*P*,*S*,*S*,*S*)-**C$_3$-19:**Colorless powder, obtained in 38% yield as a 9:1d.r.mixture of the two diastereoisomers (*P*,*S*,*S*,*S*)-**C$_3$-19** and (*M*,*S*,*S*,*S*)**-C$_3$-19**. The diastereoisomeric ratio (d.r.) was determined by ^{1}H-NMR integration.VCD analysis (vide infra) of the derivative **(***P*)-C$_3$-**17** clearly showed that (*P*,*S*,*S*,*S*)-C$_3$-**19** was formed as the majordiasteroisomer.Major diasteroisomer (*P*,*S*,*S*,*S*)-C$_3$-**19**: 1H-NMR (500 MHz, $CDCl_3$) δ=8.24 (d, J=2.0 Hz, 3H), 8.17 (dd, J=8.5 Hz, 2.1, 3H), 7.59 (d, J=8.6 Hz, 3H), 4.70 (d, J=4.5 Hz, 3H), 3.70 (s, 9H), 3.59 (s, 6H), 2.18 (m, 3H), 1.74 (s, 3H), 0.97 (d, J=6.9 Hz, 9H), 0.92 (d, J=6.8 Hz, 9H).^{13}C-NMR (126 MHz, $CDCl_3$) δ= 170.88, 169.53, 152.81, 148.65, 146.99, 124.46, 123.70, 118.54, 77.54, 77.27, 77.02, 76.77, 72.78, 65.19, 52.03, 40.86, 29.93, 18.59, 17.18.HRMS (ESI) calcd. for $C_{47}H_{55}N_4O_{18}^{+}[M^{+}NH_4]^{+}$: m/z= 963.3511; found: 963.3507. Minor diasteroisomer (*M*,*S*,*S*,*S*)-C$_3$-**19**: ^{1}H-NMR (500 MHz,

$CDCl_3$) δ= 8.21 (d, J=2.0, 3H), 8.18 (dd, J=8.4, 2.1, 3H), 7.63 (d, J=8.5, 3H), 4.74 (d, J=4.4, 3H), 3.71 (s, 9H), 3.61 (s, 6H), 2.18 (m, 3H), 1.73 (s, 3H), 0.96 (d, J=6.7, 9H), 0.91 (d, J=6.5,9H).HRMS (ESI) calcd. for $C_{47}H_{55}N_4O_{18}^+[M^+NH_4]^+$: m/z= 963.3511; found: 963.3507.

Characterization data for (*P*,*S*,*S*,*S*)-C_3-**16:** Colorless powder, obtained in 34% yield as a 6:1 d.r. mixture of the two diastereoisomers **(***P*,*S*,*S*,*S*)-C_3-**16** and (*M*,*S*,*S*,*S*)- C_3-**16**. The diastereoisomeric ratio (d.r.) was determined by 1H-NMR integration. VCD analysis (vide infra) of the derivative (*P*)-C_3-**17** clearly showed that (*P*,*S*,*S*,*S*)-C_3-**16** was formed as the major diasteroisomer. Major diasteroisomer (*P*,*S*,*S*,*S*)-C_3-**16**: ^{1}H-NMR (500 MHz, $CDCl_3$) δ=8.20 (d, J=2.1 Hz, 3H), 8.14 (dd, J=8.5 Hz, 2.1, 3H), 7.56 (d, J=8.5 Hz, 3H), 4.89 (q, J=7.1 Hz, 3H), 4.17 –4.11 (m, 6H), 3.56 (s, 6H), 1.76 (s, 3H), 1.38 (d, J=7.1 Hz, 9H), 1.22 (t, J=7.1 Hz, 9H).^{13}C-NMR (126 MHz, $CDCl_3$) δ= 170.45, 170.20, 152.91, 148.77, 147.21, 124.53, 123.76, 118.71, 72.94, 69.31, 65.30, 61.66, 60.53, 41.13, 21.19, 16.88, 15.20, 14.34, 14.19.HRMS (ESI) calcd. for $C_{44}H_{47}N_4O_{18}^+[M^+NH_4]^+$: m/z= 921.3042 ; found: 921.3038. Minor diasteroisomer (*M*,*S*,*S*,*S*)-C_3-**16**:^{1}H-NMR (500 MHz, CDCl3) δ= 8.18 (d, J=2.0 Hz, 3H), 8.15 (dd, J=8.5 Hz, 2.1, 3H), 7.58 (d, J=8.5 Hz, 3H), 4.91 (q, J=7.1 Hz, 3H),4.17 –4.11 (m, 6H), 3.57 (s, 6H), 1.75 (s, 6H), 1.38 (d, J=7.1 Hz, 9H), 1.23 (t, J=6.8 Hz, 9H). HRMS (ESI) calcd. for $C_{44}H_{47}N_4O_{18}^+[M^+NH_4]^+$: m/z= 921.3042 ; found: 921.3038.

Procedure for Single-step through space-directed nitration of (*S*,*S*,*S*)-15**.** Compound (*S*,*S*,*S*)-15: (0.048g) was dissolved in 5ml of anhydrous chloroform. The resulting solution

was cooled to –25°C and trifluoroacetic anhydride (TFAA, 36 equiv.) was added, followed by 13.5 equivalents of a saturated tetrabutylammonium nitrate solution in anhydrous chloroform. The reaction was then allowed to warm to room temperature over the course of an hour and then stirred at room temperature for 72 hrs. After completion, the reaction mixture was quenched with a 0.5 M aqueous NaOH solution and extracted with dichloromethane (3x15mL). The combined organic extracts were washed with water (1x20mL) and brine (1x20mL), dried over anhydrous sodium sulfate, and purified using preparative thin layer chromatography (eluent: 40% ethyl acetate in hexanes)to afford C3v-4as a colorless powder in 30% yield as a 5:1 d.r .mixture of the two diastereoisomers (*P,S,S,S*)-C_3-**16** and (*M,S,S,S*)-C_3-**16**

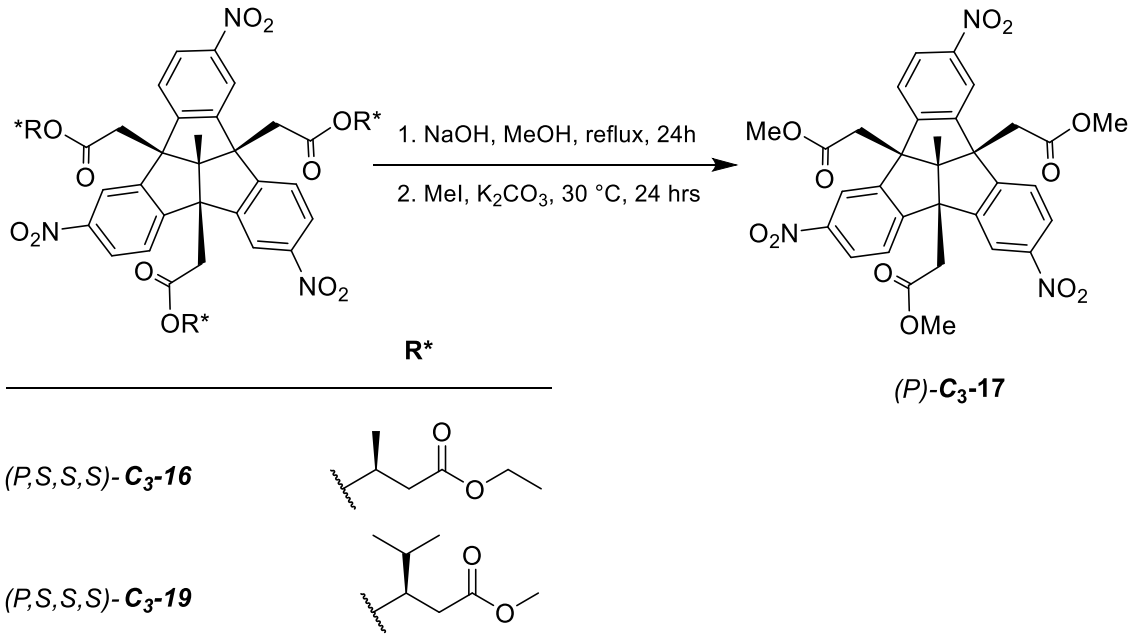

Procedure for Removal of the chiral-auxiliaries.0.038 mmol of the tri-nitrated chiral esters (*P*,*S*,*S*,*S*)-C_3-**19** and (*P*,*S*,*S*,*S*)-C_3-**16** were hydrolyzed in mixtures of a 2M sodium hydroxide solution (6mL) and methanol (5mL). The reaction mixtures were then (i) heated to 70°C for 36 hours to ensure complete hydrolysis of all ester functionalities, (ii) concentrated to remove any remaining methanol, (iii) acidified with a 1M aqueous HCl solution, and (iv) extracted with ethyl acetate (5x20mL).The organic layers were then dried over anhydrous sodium sulfate, filtered, and concentrated under reduced pressure. Next, the crude materials were suspended in iodomethane (10mL), excess potassium carbonate (0.500g) was added, and the reaction mixtures were heated to 40°C for 36 hours. Finally, the reaction mixtures were concentrated, diluted with water, extracted with ethyl acetate (3x35ml) and concentrated under reduced pressure. Following flash chromatography (eluent: 0–30% ethyl acetate in hexanes), 0.020g (0.030mmol) of the pure trimethylester product (*P*)-C_3-**17** was obtained as a white powder in80% yield.

Characterization of the trinitro methyl ester (*P*)-C_3-**17**:^{1}H-NMR (500 MHz, $CDCl_3$) δ= 8.22 –8.15 (m, 6H), 7.57 (d, J=8.4 Hz, 3H), 3.63 (s, 9H), 3.52 (s, 6H), 1.69 (s, 3H).^{13}C-NMR (126 MHz, $CDCl_3$) δ=171.65, 153.00, 148.75, 147.31, 124.69, 123.67, 118.49, 72.85, 65.34, 52.16, 41.14, 15.01, 0.14.HRMS (ESI) calcd. For $C_{32}H_{27}N_3O_{12}^+[M]^+$: m/z= 646.1673; found: 646.1667

5.2.1 Assignment of absolute chiralities of Novel TBTQ

Absolute chiralities were assigned for (*M*)-and (*P*)-C_3-**17** by comparing (Figure 5.1) the vibrational circular dichroism (VCD) spectrum of (*P*)-C_3-**17** to the compound's calculated VCD spectrum, following previously established computational protocols[7]. For the calculation of the VCD spectrum, a conformational search was first performed with MacroModel[8] and the OPLS2005[force field. Then, the Jaguar[9] software package was used

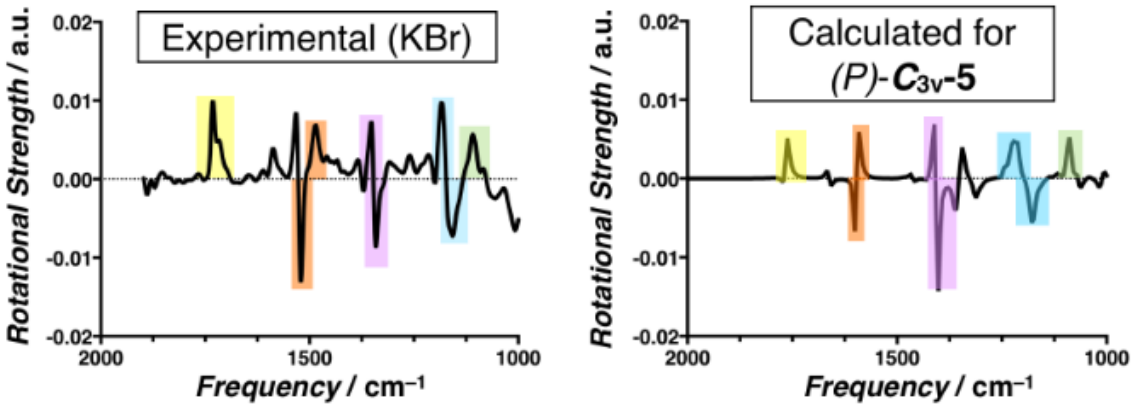

Figure 5.1 Comparison of the experimental and calculated VCD spectrum of (P)-C_3-17. Corresponding regions of the spectra have been color-coded

to reoptimize all representative low energy conformations (within a relative energy window of 0–4kJ/mol) and to calculate the conformationally averaged (Boltzmann weighted by the Jaguar gas phase energy) VCD spectrum at the DFT (M06-2X[10]/6-31G*) level of theory. All DFT calculations were performed in vacuum with extra-fine DFT grids (Jaguar keyword "iacc" =1). Vibrational frequencies were scaled with the previously reported[11] optimal scaling factor for M06-2X/6-31G* of 0.947.

5.2.2 Computational Details and DFT-Optimized Structures

All structures (see below), energies, and vibrational frequencies were computed with the Jaguar[9] software package with default grids andB3LYP-MMdispersion-corrected exchange-correlation functional[12-17] as described in the main text. All energies were converted to Gibbs free energies (at 1 atm and 298 K) by including harmonic zero-point energy, enthalpy, and entropy corrections, obtained from the vibrational frequency calculations critical points[13] of the electron density were calculated with the Jaguar software package at the B3LYP-MM/LACVP* level of theory.

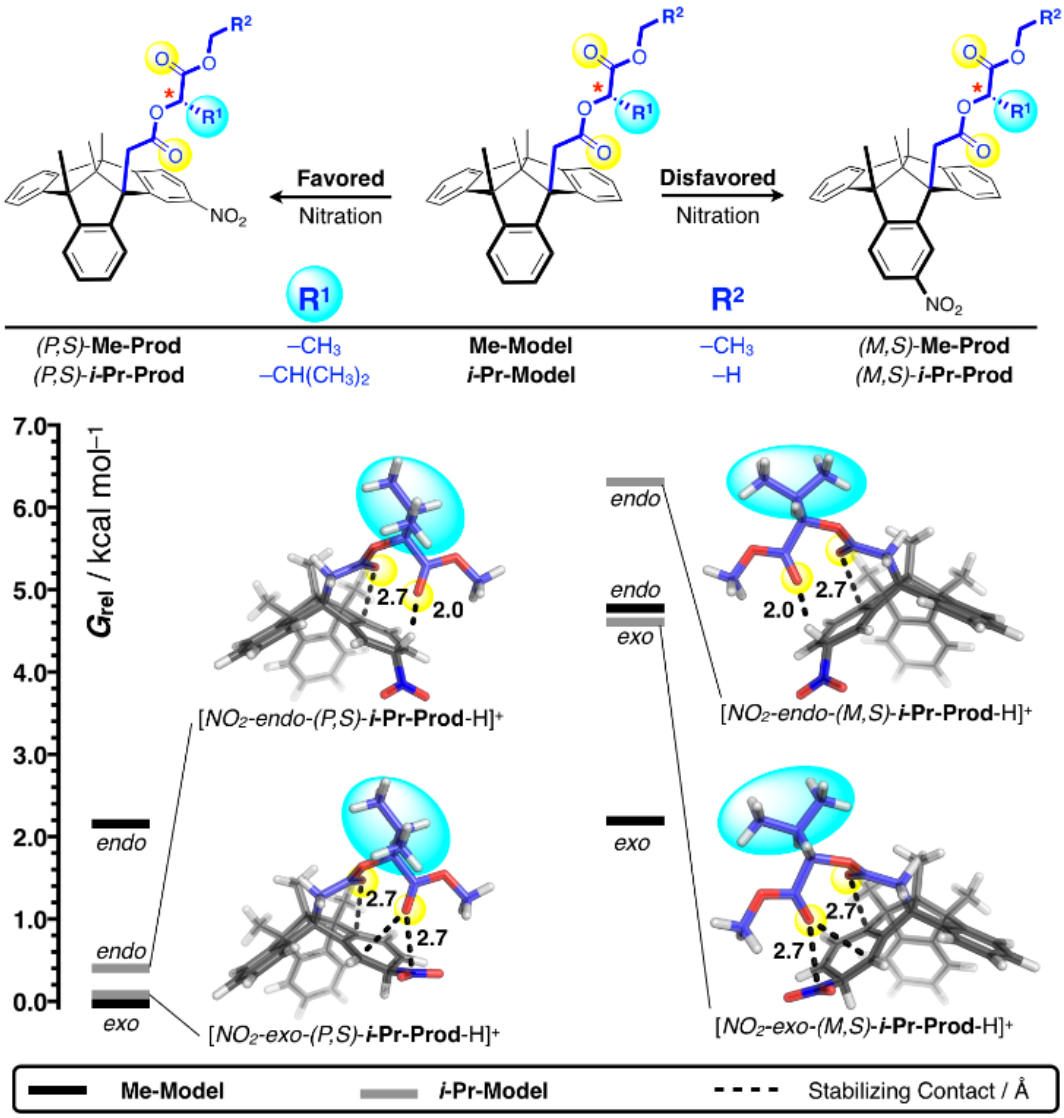

Figure 5.2: DFT-optimized structures (shown for the i-Pr-Model system, see Figure 2.10 for the analogous structures of the Me-Model system) and corresponding Gibbs Free energy plots of the Wheland intermediates for mono-nitration in the favored and disfavored positions. All Gibbs free energies are reported at the B3LYP-MM/cc-pVDZ++//B3LYP-MM/LACVP* level of theory relative to the most stable intermediates in units of kcal mol–1. Key stabilizing noncovalent interactions in the intermediates leading to the major products are highlighted with dashed lines. Corresponding distances are provided in Å. The following color scheme is used: C = grey/blue, H = white, N = blue, and O = red. Chelating oxygen atoms are highlighted in yellow.

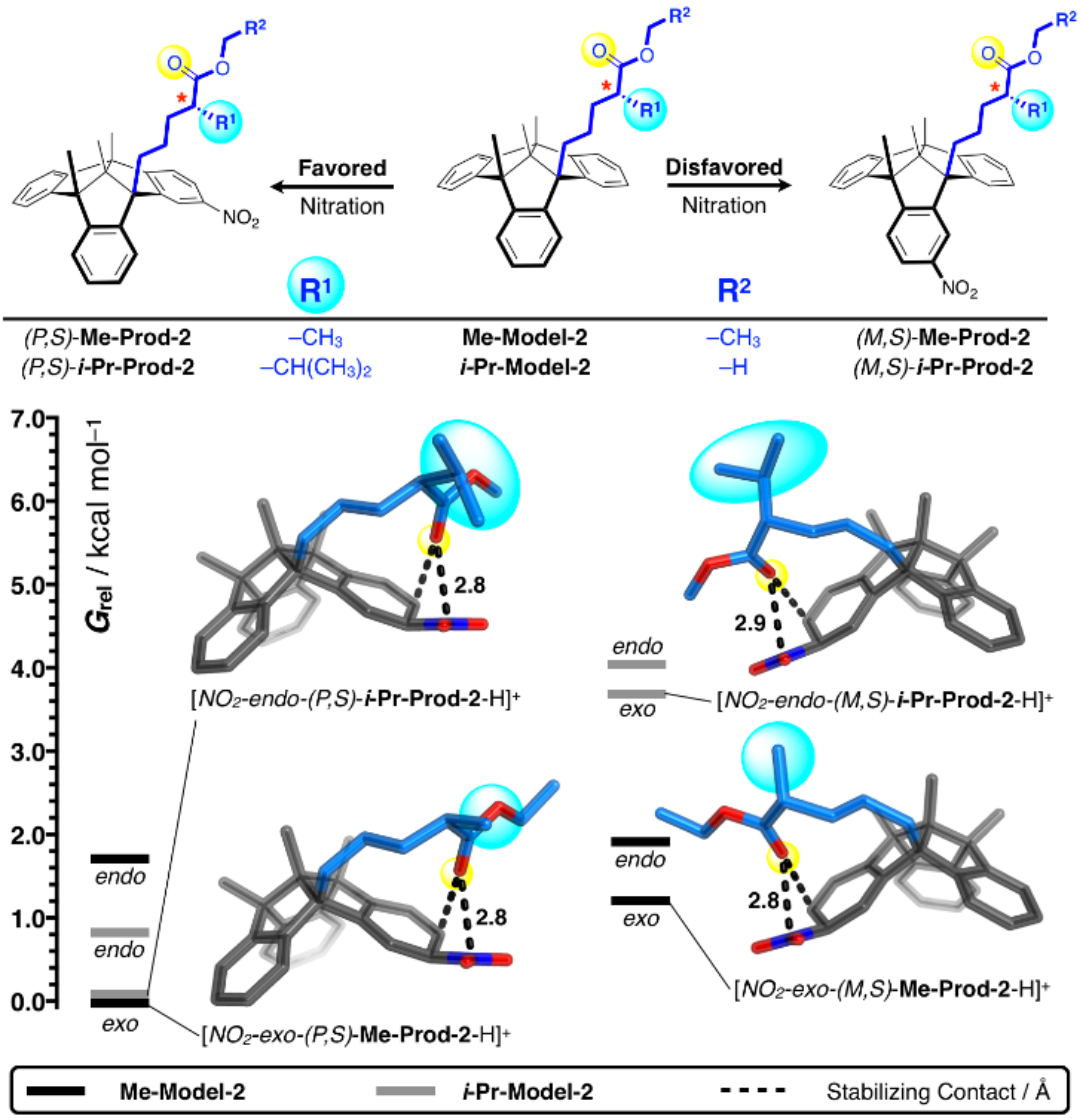

Figure 5.3 : Without the presence of the proximal ester directing group (which enables the dicarbonyl-to-arenium chelation interactions), the selectivity for nitration drops significantly. This fact is demonstrated by DFT-optimized Wheland intermediates of control structures (shown in this figure for the key lowest energy intermediates; optimized coordinates of all structures are provided below), wherein the bridging oxygen and the C=O functionality of the proximal ester-directing groups have been replaced by CH_2 groups. Corresponding Gibbs free energies are plotted at the B3LYP-MM/cc-pVDZ++//B3LYP-MM/LACVP* level of theory relative to the most stable intermediates in units of kcal mol–1. Key stabilizing noncovalent interactions in the intermediates leading to the major products are highlighted with dashed lines. Corresponding distances are provided in Å. The following color scheme is used: C = grey/blue, N = blue, and O = red. Directing oxygen-atoms are highlighted in yellow.

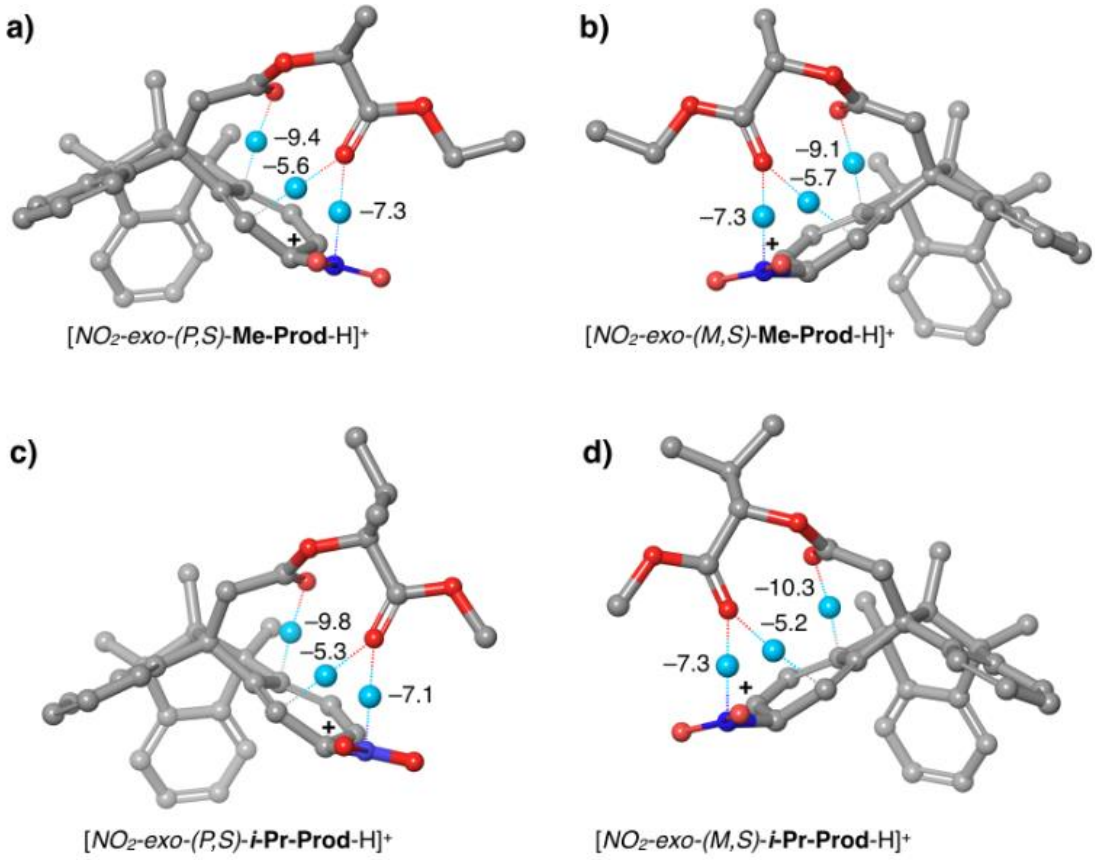

Figure 5.4 :.Plots of the NCI critical points (blue spheres), showing attractive non-covalent interactions in the Wheland intermediates. NCI-interaction strengths are labelled in units of kcal/mol. The NCI critical points illustrate the "chelating" mechanism of stabilizing a carbocation on an aromatic ring from above in multiple positions at the same time.

5.3 Experimental Procedures for EXTENDING ENANTIOSELECTIVE ELECTROPHILIC AROMATIC NITRATIONS

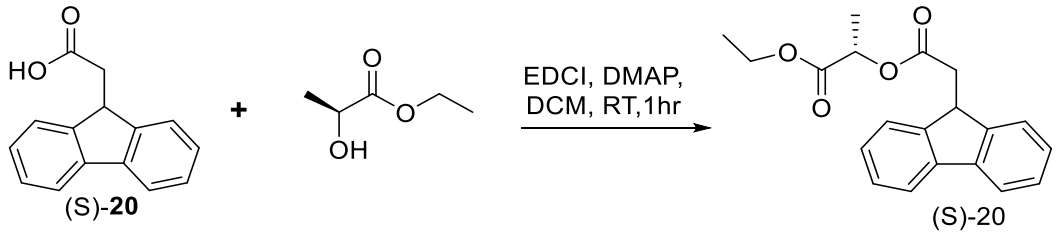

General coupling procedure (S)-**20.** In a flame-dried flask, commercially available fluorene-9-acetic acid (0.100g, 0.446mmol) was dissolved in anhydrous dichloromethane. DMAP (0.669mmol, 1.5equiv.) was added in one portion and the reaction mixture was stirred at room temperature under nitrogen until all the starting materials became soluble. EDCI (0.891 mmol, 2.0 equiv.) was then added in one portion. Afterwards, the solution was stirred for 15 minutes. Next, the chiral alcohol —(S)-ethyl lactate (0.891, 2 equiv.) — was added in one portion to the flask and the reaction mixture was stirred at room temperature for 1 hour. Upon completion, the reaction was quenched with a 1 N aqueous HCl solution. The reaction contents were then extracted with dichloromethane (2 x 20mL), washed with brine (3 x 30 mL), and the combined organic layers were dried over anhydrous sodium sulfate and concentrated under reduced pressure. The crude product was purified with flash column chromatography over silica gel (eluent: 0–15% ethyl acetate in hexanes) to afford 0.1109 g of the product as a clear oil in 76% yield.

Characterization data for (S)-20. ^{1}H-NMR (500 MHz, CDCl3) δ= 7.78 (d, J=7.6 Hz, 2H), 7.58 (d, J=7.5 Hz, 2H), 7.41 (t, J=7.4 Hz, 2H), 7.33 (m, 2H), 5.21 (q, J=7.1 Hz, 1H),

4.47 (t, J=7.1 Hz, 1H), 4.28 (q, J=7.1 Hz, 2H), 2.96 (dd, J=16.5, 6.8, 1H), 2.86 (dd, J=16.5, 7.3, 1H), 1.53 (d, J=7.1 Hz, 3H), 1.33 (t, J=7.1 Hz, 3H).^{13}C-NMR (126 MHz, $CDCl_3$) δ= 171.93, 170.73, 146.18, 140.83, 140.74, 129.70, 128.29, 127.49, 127.24, 127.18, 124.50, 124.47, 119.92, 119.88, 69.07, 61.47, 43.35, 38.28, 16.95, 14.15. HRMS (ESI) calcd. For $C_{20}H_{21}O_4^+[M^+H]^+$: m/z=325.1440; found : 325.1451.

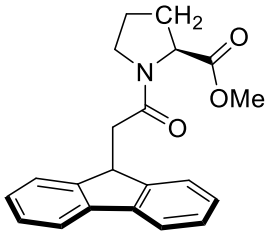

Compound (S)**-23 compound** (S)**-23 was synthesized according to the general procedure for coupling chiral auxiliaries. Rather than a chiral alcohol, proline methylester was used.** The crude product was purified with flash column chromatography over silica gel (eluent: 0–25% ethyl acetate in hexanes) to give the product as a yellow oil in 52% yield.

Characterization data: ^{1}H NMR (500 MHz, $CDCl_3$) δ = 7.78 (d, *J*=7.4 Hz, 2H), 7.66 (d, *J*=7.6 Hz, 1H), 7.58 (d, *J*=7.5 Hz, 1H), 7.40 (m, 2H), 7.36 – 7.30 (m, 2H), 4.73 – 4.61 (m, 2H), 3.85 (s, 3H), 3.54 – 3.49 (m, 1H), 3.34 (m, 1H), 2.89 – 2.64 (m, 2H), 2.30 – 2.12 (m, 2H), 1.99 – 1.88 (m, 2H). ^{13}C NMR (126 MHz, $CDCl_3$) δ = 172.86, 170.52, 147.10, 147.06, 140.83, 140.60, 127.31, 127.28, 127.27, 127.05, 124.85, 124.73, 119.85, 119.77, 58.98, 52.30, 47.16, 43.51, 39.15, 29.30, 24.78.

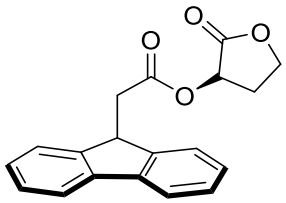

Compound (S)-**24 compound** (S)-**24** was synthesized according to the general procedure for coupling chiral auxiliaries. Rather than ethyl lactate being used lactone was used as a chiral alcohol. The crude product was purified with flash column chromatography over silica gel (eluent: 0–30% ethyl acetate in hexanes product as a white solid in 69% yield.

Characterization data: ^{1}H NMR (500 MHz, $CDCl_3$) δ = 7.78 (d, *J*=7.5 Hz, 2H), 7.60 – 7.54 (m, 2H), 7.42 (t, *J*=7.4 Hz, 2H), 7.34 (m, 2H), 5.56 – 5.52 (m, 1H), 4.48 – 4.43 (m, 2H), 4.32 (m, 1H), 3.03 (dd, *J*=16.3, 6.6, 1H), 2.92 (dd, *J*=16.3 Hz, 7.2 Hz, 1H), 2.68 (dd, *J*=16.3 Hz, 7.1 Hz, 1H), 2.22 (m, 1H). ^{13}C NMR (126 MHz, $CDCl_3$) δ = 172.47, 171.19, 145.76, 145.72, 140.87, 140.76, 127.65, 127.35, 127.25, 124.44, 120.00, 119.96, 67.80, 65.08, 60.40, 43.36, 38.17, 28.73, 21.06, 14.22.

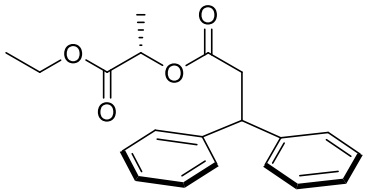

(*S*)-27

Compound (S)-**27.** Compound was synthesized following the general procedure for coupling chiral auxiliaries. 3,3-diphenylpropanoic acid was used as the starting material with ethyl lactate as the chiral alcohol. The crude product was purified with flash column

chromatography over silica gel (eluent: 0–15% ethyl acetate in hexanes) to afford the product as a yellow oil in 64% yield.

Characterization data: ^{1}H NMR (500 MHz, $CDCl_3$) δ = 7.36 – 7.29 (m, 8H), 7.27 – 7.21 (m, 2H), 5.04 (q, *J*=7.0 Hz, 1H), 4.65 (t, *J*=8.0 Hz, 1H), 4.18 (q, *J*=7.1 Hz, 2H), 3.23 (d, *J*=8.0 Hz, 2H), 1.42 (d, *J*=7.1 Hz, 3H), 1.25 (t, *J*=7.1 Hz, 3H). ^{13}C NMR (126 MHz, $CDCl_3$) δ = 171.10, 170.65, 143.48, 143.40, 128.61, 127.81, 127.70, 126.60, 68.75, 61.30, 46.86, 40.37, 16.88, 14.09.

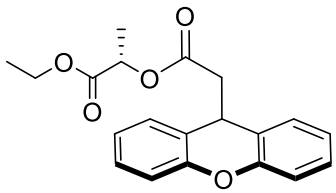

(*S*)-28

Compound (S)-28 : Compound was synthesized following the general procedure for coupling chiral auxiliaries. 2-(9H-xanthen-9-yl) acetic acid was used as the starting material with ethylactate used as the chiral alcohol. The crude product was purified with flash column chromatography over silica gel (eluent: 0–15% ethyl acetate in hexanes) to afford of the product as a clear oil in 79% yield.

Characterization data: ^{1}H NMR (500 MHz, $CDCl_3$) δ = 7.33 (m, 2H), 7.28 – 7.24 (m, 2H), 7.14 – 7.06 (m, 4H), 5.05 (q, *J*=7.1 Hz, 1H), 4.58 (t, *J*=6.8 Hz, 1H), 4.23 – 4.18 (m, 2H), 2.81 (d, *J*=1.8 Hz, 1H), 2.79 (d, *J*=2.7 Hz, 1H), 1.41 (d, *J*=7.1 Hz, 3H), 1.27 (t, *J*=7.1 Hz, 3H). ^{13}C NMR (126 MHz, $CDCl_3$) δ = 170.61, 152.17, 128.64, 128.47, 128.12, 128.10, 124.36, 124.19, 123.48, 123.33, 116.63, 116.61, 68.85, 61.35, 45.18, 35.52, 16.84, 14.08.

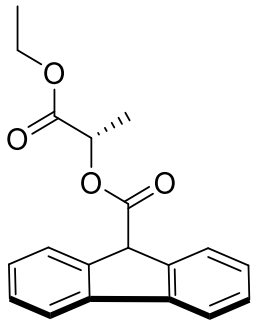

(*S*)-29

Compound (S)-29. Compound was synthesized following the general procedure for coupling chiral auxiliaries. 2-(9H-xanthen-9-yl) acetic acid was used as the starting material with ethylactate used as the chiral alcohol. The crude product was purified with flash column chromatography over silica gel (eluent: 0–10% ethyl acetate in hexanes) to afford a white powder in 44 % yield.

Characterization data: ^{1}H NMR (500 MHz, $CDCl_3$) δ = 7.80 – 7.70 (m, 4H), 7.48 – 7.34 (m, 4H), 5.20 (q, *J*=7.1, 1H), 4.98 (s, 1H), 4.21 (q, *J*=7.1 Hz, 2H), 1.56 (d, *J*=7.1 Hz, 3H), 1.25 (t, *J*=7.1, 3H). ^{13}C NMR (126 MHz, $CDCl_3$) δ = 170.47, 170.28, 141.55, 141.42, 140.34, 140.30, 128.21, 128.19, 127.39, 127.34, 125.85, 125.76, 120.05, 119.99, 69.49, 61.43, 53.00, 16.95, 14.05.

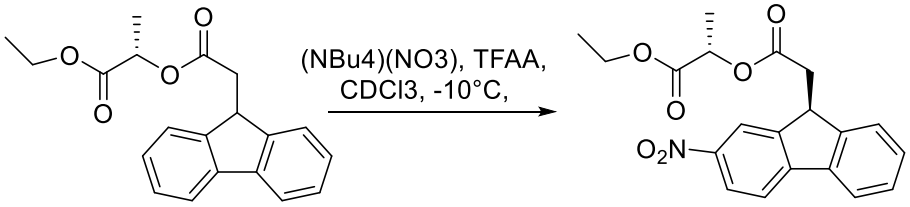

(*S*)-20 (*S,S*)-21

General through space nitration procedure Synthesis of (S,S)-21. **(*S*)-20** (0.194 mmol) was dissolved in $CDCl_3$(15 mL) and the reaction mixture was cooled to –10 °C. Trifluoroacetic anhydride (2 equiv.) was then added, followed by 1 equiv. of a saturated tetrabutylammonium nitrate solution in $CDCl_3$.The mixture was to stirred for 2.5 hours as it was allowed to slowly warm to room temperature. Reaction progress was monitored by TLC and when all the starting material was consumed, the solvent was evaporated under an atmosphere of dry nitrogen, the oily residue was dissolved in a minimal amount of ethyl acetate, and the crude product purified via preparatory thin layer chromatography (30% ethyl acetate in hexanes) to afford 0.055 g of **(*S,S*)-21** in 71% yield and 72:28 d.r.

Characterization data for(S,S)-21: ^{1}H-NMR (500 MHz, $CDCl_3$) δ= 8.04 (d, J=7.1 Hz, 1H), 7.87 (t, J=7.8 Hz, 2H), 7.62 (t, J=6.6 Hz, 1H), 7.50 –7.39 (m, 3H), 5.18 (q, J=7.1 Hz, 1H), 4.52 (t, J=6.7 Hz, 1H), 4.27 (q, J=7.1 Hz, 2H), 3.06 (dd, J=16.6, 6.1, 1H), 2.85 (dd, J=16.6, 7.5, 1H), 1.51 (d, J=7.1 Hz, 3H), 1.33 (t, J=7.1, 3H).^{13}C-NMR (126 MHz, $CDCl_3$) δ= 171.30, 170.56, 149.44, 147.16, 145.30, 136.20, 133.60, 129.25, 128.90, 128.07, 127.25, 124.69, 124.25, 123.52, 69.26, 61.57, 43.09, 38.19, 16.89, 14.15. HRMS (ESI) calcd. For $C_{20}H_{20}NO_6^+[M^+H]^+$: m/z=370.1291; found : 370.1299. **(*S,R*)-21**:1H-NMR (500 MHz, CDCl3) δ= 8.04 (d, J=4.7 Hz, 1H), 7.87 (t, J=7.8 Hz, 2H), 7.62 (t, J=6.6 Hz, 1H), 7.49 –7.39 (m, 3H), 5.18 (q, J=7.1 Hz, 1H), 4.52 (t, J=6.7 Hz, 1H), 4.27 (q, J=7.1 Hz, 2H), 2.98 (dd, J=16.6, 6.5, 1H), 2.93 (dd, J=16.7, 7.2, 1H), 1.50 (d, J=7.0 Hz, 3H), 1.33 (t, J=7.1 Hz, 3H). HRMS (ESI) calcd. For $C_{20}H_{20}NO_6^+[M^+H]^+$: m/z=370.1291; found : 370.1299.

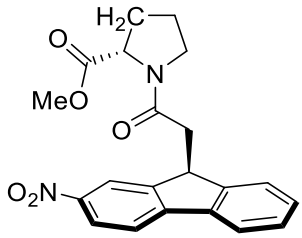

(*SS*)-25

Compound (*SS*)-25 compound SS(x1) was synthesized according to the general procedure for through space nitration the crude product was purified with flash column chromatography over silica gel (eluent: 0–25% ethyl acetate in hexanes) to afford the product as a clear oil in 70% yield.

Characterization data: ^{1}H NMR (500 MHz, $CDCl_3$) δ = 8.04 (dd, *J*=7.8 Hz, 5.5, 1H), 7.89 (m, 2H), 7.71 – 7.58 (m, 1H), 7.49 – 7.37 (m, 3H), 4.79 – 4.71 (m, 1H), 4.67 (m, 1H), 3.85 (s, 3H), 3.56 – 3.34 (m, 2H), 2.95 – 2.60 (m, 2H), 2.31 – 2.20 (m, 1H), 2.13 – 2.07 (m, 1H), 2.06 – 1.92 (m, 2H). ^{13}C NMR (126 MHz, $CDCl_3$) δ = 172.71, 169.87, 150.44, 148.14, 129.53, 129.30, 129.26, 129.04, 127.85, 127.11, 124.65, 124.58, 124.54, 123.30, 59.04, 52.38, 47.17, 43.14, 39.26, 29.25, 24.76.

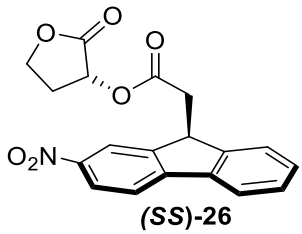

(*SS*)-26

Compound (SS)-26: compound (SS)-26 was synthesized according to the general procedure for through space nitration the crude product was purified with flash column

chromatography over silica gel (eluent: 0–25% ethyl acetate in hexanes) to afford the product as a clear oil in 76% yield.

Characterization data: ^{1}H NMR (500 MHz, $CDCl_3$) δ = 8.06 – 8.02 (m, 1H), 7.86 (m, 2H), 7.61 (dd, *J*=7.7, 6.7, 1H), 7.47 (m, 3H), 5.58 – 5.48 (m, 1H), 4.55 – 4.42 (m, 2H), 4.32 (m, , 1H), 3.15 – 2.89 (m, 2H), 2.71 – 2.62 (m, 1H), 2.28 – 2.21 (m, 1H). ^{13}C NMR (126 MHz, $CDCl_3$) δ = 172.26, 172.21, 129.34, 128.83, 128.23, 127.51, 127.37, 124.78, 124.75, 124.24, 124.18, 123.67, 123.64, 67.96, 65.02, 43.11, 38.01, 30.93, 28.57.

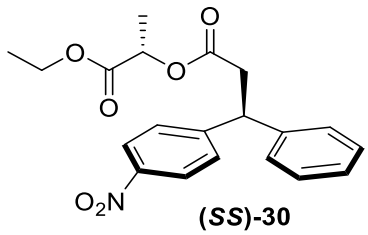

(*SS*)-30

Compound (SS)-30 was synthesized according to the general procedure for through space nitration the crude product was purified with flash column chromatography over silica gel (eluent: 0–25% ethyl acetate in hexanes) to afford the product as a fine white powder in 76% yield.

Characterization: ^{1}H NMR (500 MHz, $CDCl_3$) δ = 8.17 (dd, *J*=8.8, 3.8, 2H), 7.45 (d, *J*=8.7 Hz, 2H), 7.36 – 7.31 (m, 2H), 7.26 – 7.21 (m, 3H), 5.06 – 4.96 (m, 1H), 4.70 (dd, *J*=14.7, 7.1, 1H), 4.16 (m,2H), 3.27 – 3.16 (m, 2H), 1.41 (dd, *J*=7.1 Hz, 2.2, 3H), 1.25 – 1.21 (m, 3H). ^{13}C NMR (126 MHz, $CDCl_3$) δ = 170.52, 170.39, 150.91, 150.77, 141.88, 128.95, 128.72, 128.62, 127.67, 127.56, 127.25, 123.86, 68.95, 68.92, 61.42, 46.56, 39.77, 29.71, 16.84, 14.04.

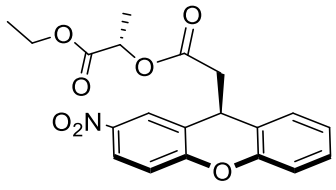

(*SS*)-31

Compound (SS)-31 was synthesized according to the general procedure for through space nitration: The crude product was purified with flash column chromatography over silica gel (eluent: 0–25% ethyl acetate in hexanes) to afford the product as a clear oil in 81% yield.

Characterization data :^{1}H NMR (500 MHz, $CDCl_3$) δ = 7.85 (d, *J*=8.0 Hz, 1H), 7.62 (dd, *J*=8.1 Hz, 1H), 7.37 – 7.30 (m, 2H), 7.19 (m, 3H), 5.07 – 5.01 (q, 1H), 4.65 (t, *J*=6.8 Hz, 1H), 4.21 (q, *J*=14.0, 7.0, 2H), 2.88 – 2.77 (m, 2H), 1.43 (m, 3H), 1.27 (m, 3H). ^{13}C NMR (126 MHz, $CDCl_3$) δ = 170.45, 170.05, 151.13, 145.84, 133.80, 133.55, 128.72, 128.40, 128.20, 127.50, 124.96, 124.81, 124.21, 123.65, 122.58, 117.29, 69.05, 61.47, 44.68, 44.62, 35.43, 35.36, 16.82, 16.76, 14.09.

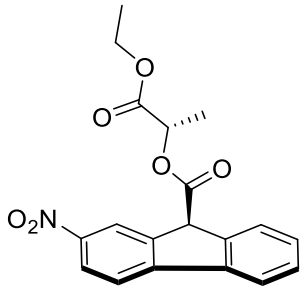

(*SS*)-32

Compound (SS)-32 compound (SS)-32 was synthesized according to the general procedure for through space nitration The crude product was purified with preparative thin layer chromatography on silica (eluent: 40% ethyl acetate in hexanes) to afford the product as a clear oil in 11% yield.

Characterization ^{1}H NMR (500 MHz, $CDCl_3$) δ = 8.07 (m, 1H), 7.98 (m, 2H), 7.85 – 7.74 (m, 1H), 7.55 – 7.44 (m, 3H), 5.19 (m, , 1H), 5.05 (m, 1H), 4.21 (m, 2H), 1.57-1.53 (m,3H), 1.27 – 1.23 (m, 3H).

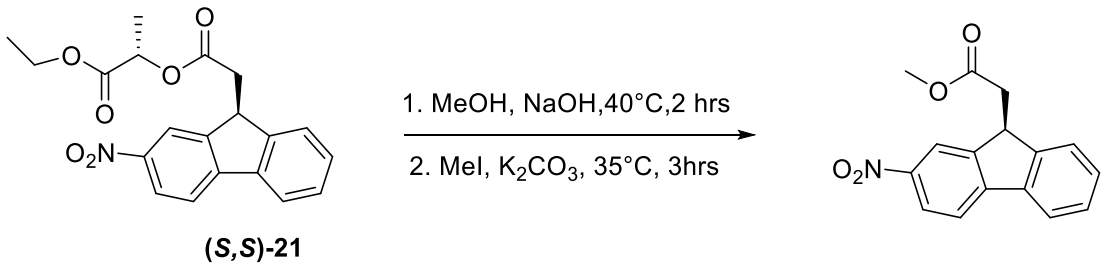

(*S,S*)-21

General procedure for removal of the Chiral Auxiliary. The chiral ester(S,S)-21 (0.043mmol) was hydrolyzed in a mixture of a 2N sodium hydroxide solution (1.5mL) and methanol (3mL). The reaction mixture was then (i) heated to 45°C for 2 hours to ensure complete hydrolysis of all ester functionalities, (ii) concentrated to remove any remaining methanol, (iii) acidified with a 1N aqueous HCl solution, and (iv) extracted with ethyl acetate (5x10mL). The organic layers were then dried over anhydrous sodium sulfate, filtered, and concentrated under reduced pressure. Next, the crude materials were

suspended in iodomethane (4mL) with 2 drops of DMF for solubility purposes. Excess K_2CO_3(0.200g) was added, and the reaction mixture was heated to 40°C for 3 hours. Finally, the reaction mixture was concentrated, diluted with water, extracted with ethyl acetate (3x15mL), and concentrated under reduced pressure. Following flash chromatography (eluent: 0–30% ethyl acetate in hexanes), 9.5mg (0.034mmol) of the pure methylester product was obtained as a white powder in 77% yield.

Characterization data for (S)-22.^{1}H NMR (500MHz, CDCl3) δ= 8.06 –8.03 (m, 1H), 7.87 (d, J=8.0, 1H), 7.78 (d, J=7.5, 1H), 7.56 (dd, J=5.9, 3.0, 1H), 7.42 –7.47 (m, 3H), 4.51 (t, J=7.0, 1H),3.81 (s, 3H),2.91 (dd, J=16.5, 6.6, 1H), 2.81 (dd, J=16.5, 7.4, 1H).^{13}C-NMR (126 MHz, $CDCl_3$) δ= 172.41, 149.57, 147.25, 145.33, 136.21, 133.55, 129.22, 128.68, 128.07, 127.25, 124.76, 124.11, 123.53, 52.07, 43.24, 38.33. HRMS (ESI) calcd. For $C_{16}H_{13}NO_4Na^+$[M^+Na]$^+$: m/z=306.0742; found : 306.0739.

5.3.1 Assignment of Absolute Configurations

The favored and disfavored diastereoisomers formed upon nitration of (S)-8were determined by comparison of experimental and DFT-calculated (B3LYP/6-31G**) chemical shifts for the diastereoisotopic pairs of protons HA and HB, as well as HF and

HG. These proton resonances differ the most between the two diastereoisomers (*S*,*S*)-21 and **(***S*,*R*)-**21**, which is why they are well suited for a reliable, DFT-based prediction of the relative ^{1}H NMR chemical shifts. The five lowest energy conformations for both diastereoisomers —obtained with a conformational search with 10,000 steps and the OPLS2005 force field with MacroModel[8]were optimized at the B3LYP/6-31G** level of theory, before calculation of the isotropic NMR shielding constants with Jaguar[9]As shown in Figure 5.5, the difference in chemical shifts between H_A and H_B of the favored diastereoisomer is significantly larger than the corresponding chemical shift difference between H_F and H_G of the disfavored diastereoisomer, and these relative differences in chemical shift are well reproduced by the Boltzmann-weighted averages of the DFT-calculated chemical shifts for these protons.

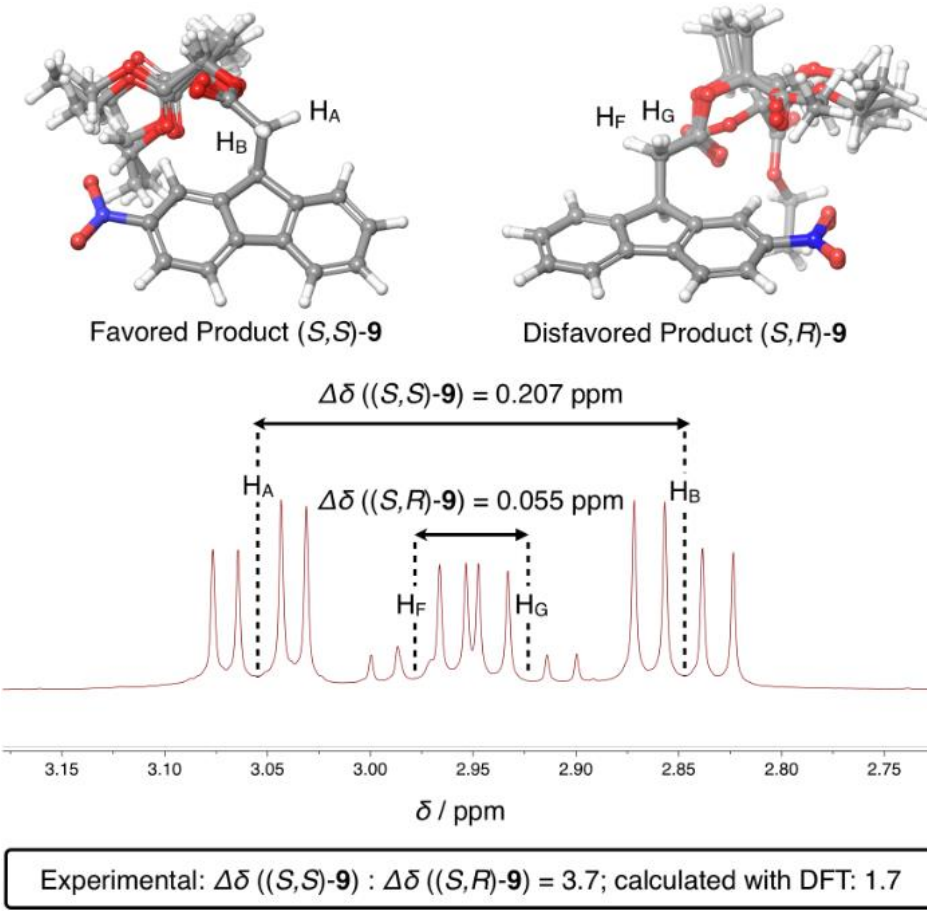

Figure 5.5 Assignment of favored and disfavored diastereoisomers formed upon nitration of (S)-20 by comparison of experimental and DFT-calculated chemical shifts for the diastereoisotopic pairs of protons H_A and H_B, as well as H_F and H_G.

5.3.2 Computational details and DFT- Optimized Structures

All structures (see below), energies, and vibrational frequencies were computed with the Jaguar[9] software package with default grids and B3LYP-MMdispersion-orrected exchange-correlation functional[12-17] as described in chapter 2. All energies were converted to Gibbs free energies (at 1 atm and 298 K) by including harmonic zero-point energy, enthalpy, and entropy corrections, obtained from the vibrational frequency calculations critical points[13] of the electron density were calculated with the Jaguar software package at the B3LYP-MM/LACVP* level of theory.

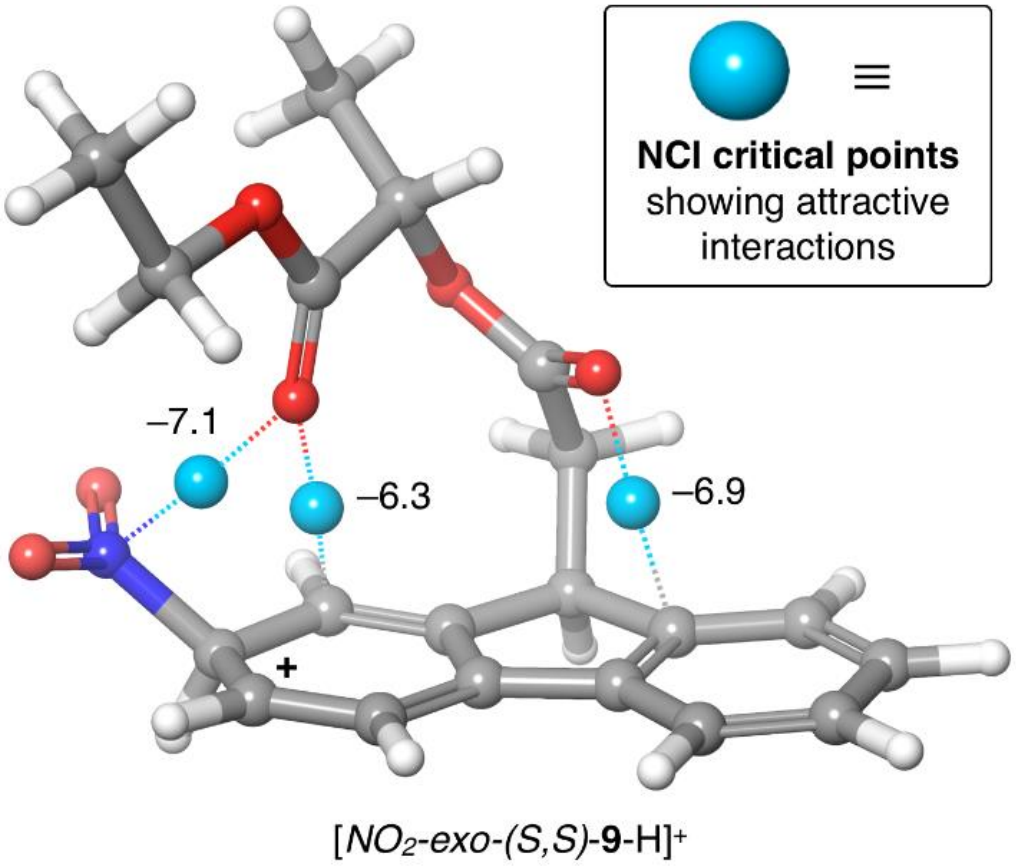

Figure 5.6: Plots of the NCI critical points (blue spheres), showing attractive non-covalent interactions in the most stable Wheland intermediate [NO_2-exo-(S,S)-21-H]$^+$for nitration of (S)-20. NCI-interaction strengths are labelled in units of kcal/mol. The NCI critical points illustrate the "chelating" mechanism of stabilizing a delocalized carbocation on a polyaromatic substrate. Plots of the NCI critical points (blue spheres), showing attractive non-covalent interactions in the most stable Wheland intermediate [NO_2-exo-(S,S)-9-H]$^+$ for nitration of (S)-20. NCI-interaction strengths are labelled in units of kcal/mol. The NCI critical points illustrate the "chelating" mechanism of stabilizing a delocalized carbocation on a polyaromatic substrate from above in multiple positions at the same time. From above in multiple positions at the same time.

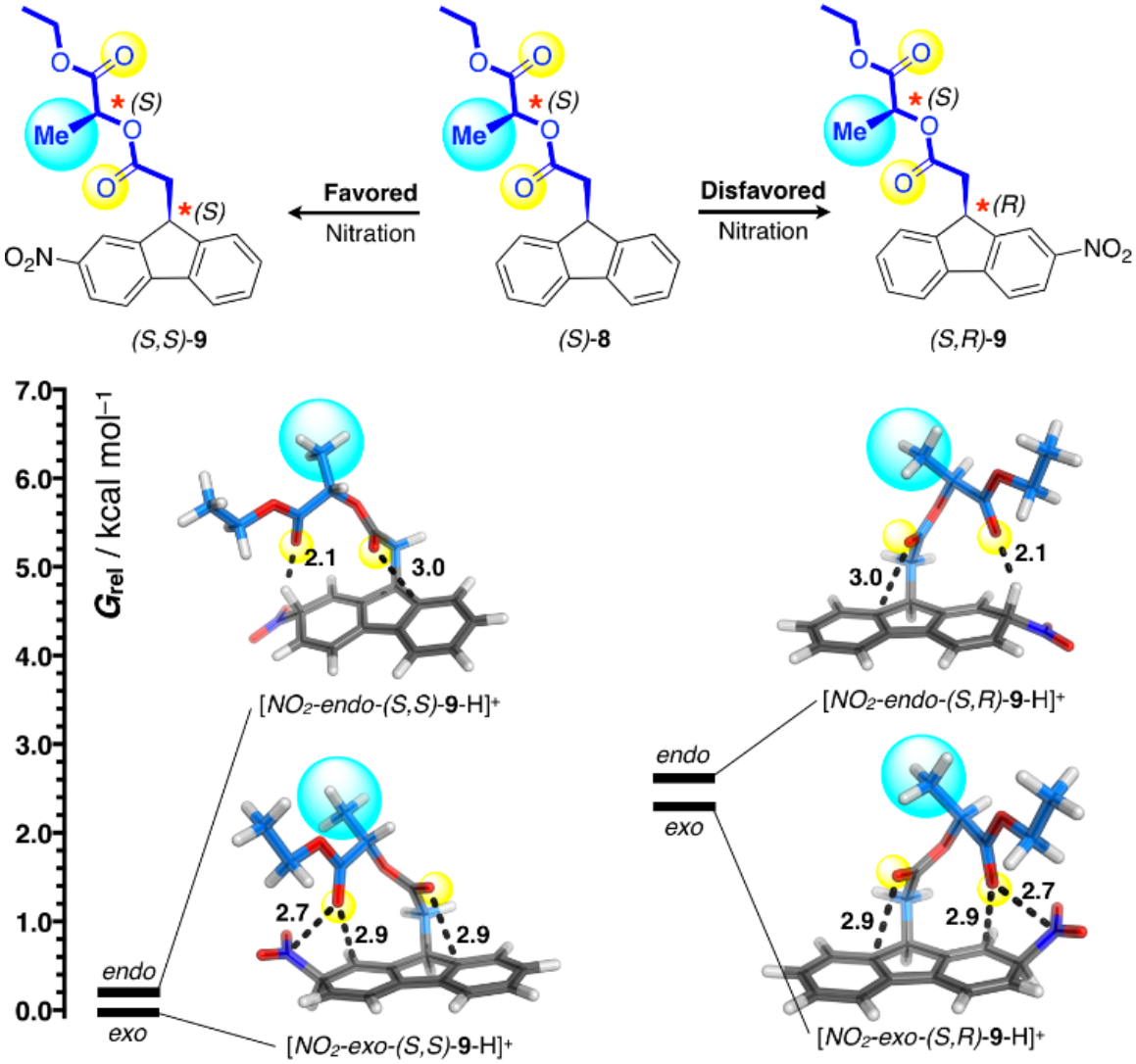

Figure 5.7 .DFT-optimized structures and corresponding Gibbs Free energy plots of the Wheland intermediates for mono-nitration of (S)-21 in the favored and disfavored positions. All Gibbs free energies are reported at the B3LYP-MM/cc-pVDZ++//B3LYP-MM/LACVP* level of theory relative to the most stable intermediates in units of kcal mol–1. Key stabilizing noncovalent interactions in the intermediates leading to the major products are highlighted with dashed lines. Corresponding distances are provided in Å. The following color scheme is used: C = grey/blue, H = white, N = blue, and O = red. Chelating oxygen atoms are highlighted in yellow

5.4 Experimental Procedures for SIZE CONTROL OF POLYMERS THROUGH A NOVEL ITERATIVE EXPONENTIAL GROWTH METHOD.

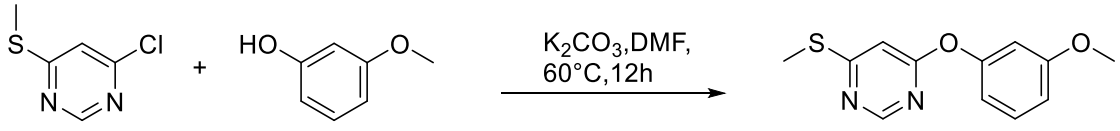

SnAr coupling procedure for IEG growth Synthesis of DIMER (35). and 4-chloro-6-methylthiopyradine **33** and Potassium Carbonate (5.5 g, 25mmol) was added to a dried round-bottom flask and dissolved in 250 mL of anhydrous DMF. Once dissolved, 3-methoxyphenol **34**, (6.2 g, 50 mmol) was added and the solution was allowed to stir at 60 °C for 16 hours. Once complete the reaction mixture was diluted with 0.5M HCl and extracted with ethyl acetate (5 x 100 mL). The solution was then washed with 0.5 M NaOH to ensure all remaining 3-methoxyphenol is removed and dried over sodium sulfate. Following flash chromatography (eluent: 0–15% ethyl acetate in hexanes) to give the product as a fine powder in a 98% yield.

Characterization data Dimer (35): ^{1}H NMR (500 MHz, $CDCl_3$) δ = 8.57 (t, *J*=2.8, 1H), 7.31 (t, *J*=8.2 Hz, 1H), 6.85 – 6.79 (m, 1H), 6.71 (dd, *J*=8.0, 1.5, 1H), 6.68 – 6.65 (m, 2H), 3.79 (s, 3H), 2.53 (s, 3H). ^{13}C NMR (126 MHz, $CDCl_3$) δ = 172.46, 168.54, 160.87, 157.89, 153.36, 130.26, 113.61, 111.57, 107.57, 103.27, 55.43, 12.84.

General procedure for coupling active oligomers: methyl sulfone oligomer, , and Potassium Carbonate (5.5 g, 25mmol) were added to a dried round-bottom flask and dissolved in 250 mL of anhydrous DMF. Once dissolved, phenolic oligomer, (6.2 g, 50 mmol) was added and the solution was allowed to stir at 60 °C for 16 hours. Once complete the reaction mixture was diluted with 0.5M HCl and extracted with ethyl acetate (5 x 100 mL). The solution was then washed with 0.5 M NaOH to ensure all remaining 3-methoxyphenol is removed and dried over sodium sulfate. Following flash chromatography (eluent: 0–15% ethyl acetate in hexanes) to give the product as a fine powder in a 98% yield.

General procedure for Demethylation: Dormant oligomer compound was dissolved in anhydrous DCM (). The mixture was then cooled to –78 °C and placed under N_2. BBr_3 solution was then slowly added via syringe into the stirring solution. Allowed to warm to room temp overnight. After 12hrs, the mixture was cooled to 0°C quenched by adding MeOH until no more fuming occurred. Ice chips were then added until fuming ceased., The mixture was then added to a separatory funnel and the organic layer was removed. The aqueous layer was then extracted DCM (3x) dried over Na_2SO_4 and evaporated under reduced pressure to afford crude product.

General procedure for Oxidation: Dormant Oligomer was added to a rb flask and dissolved in DCM. To this mixture MCPBA was added as a solution. After stirring for 16 hours at room temp, the solution was added to a separatory funnel washed with NaOH followed by brine and dried over sodium sulfate to afford the crude product.

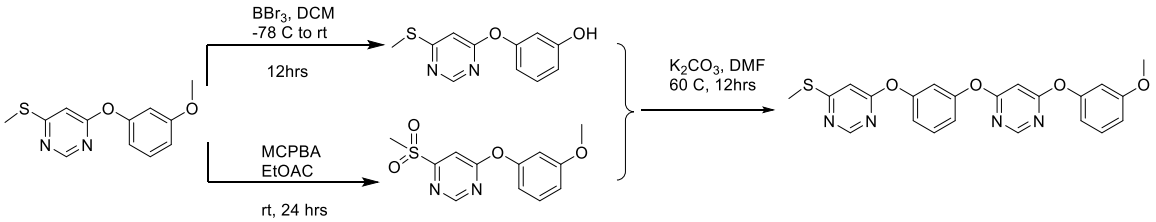

Synthesis of tetramer (38): Dimer (**35**) was subjected the orthogonal deprotection where dimer xx was divided, half the material was subjected to the general procedure for demethylation to the phenol while the other one was oxidized to the methyl sulphone. The two activated crude species were subject to the general procedure for coupling**.** Following flash chromatography (eluent: 0–15% ethyl acetate in hexanes) to give the product as a fine powder in a 98% yield. The product was isolated in 80% yield.

Characterization ^{1}H NMR (500 MHz, $CDCl_3$) δ = 8.58 (d, *J*=1.0, 1H), 8.47 (d, *J*=0.7, 1H), 7.48 (dd, *J*=11.3, 5.1, 1H), 7.34 (t, *J*=8.2 Hz, 1H), 7.10 – 7.05 (m, 2H), 7.00 (t, *J*=2.2, 1H), 6.83 (ddd, *J*=8.4, 2.4, 0.7, 1H), 6.77 – 6.72 (m, 2H), 6.71 (t, *J*=2.3, 1H), 6.36 (d, *J*=0.8, 1H), 3.82 (s, 3H), 2.56 (d, *J*=2.7, 3H). ^{13}C NMR (126 MHz, $CDCl_3$) δ = 173.09, 172.68, 171.64, 171.09, 168.10, 160.88, 158.38, 157.76, 153.40, 153.24, 153.17, 130.46, 130.27, 118.85, 118.78, 115.43, 113.61, 111.72, 107.57, 103.49, 92.47, 60.35, 55.32, 31.57, 22.64, 21.01, 14.19, 14.11, 12.82.

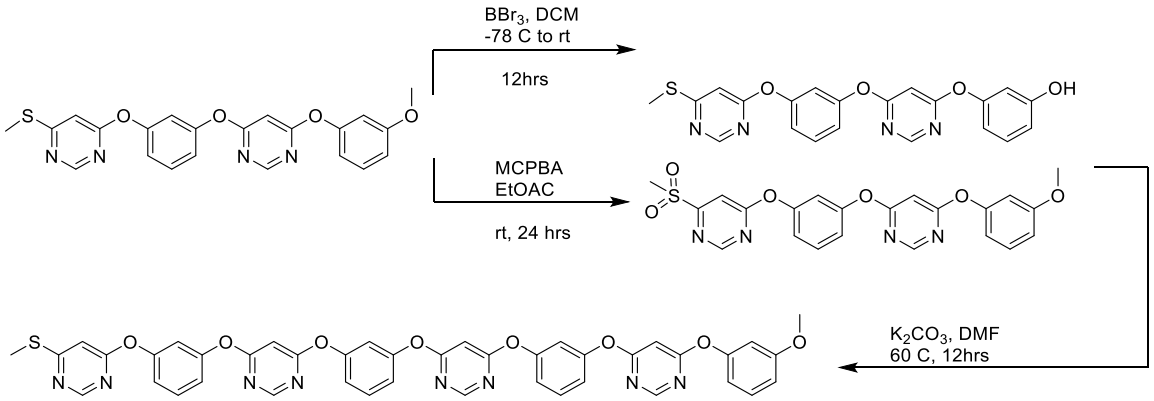

Synthesis of Octomer (39) Tetramer (**38**) was subjected the orthogonal deprotection where tetramer **38** was divided, half the material was subjected to the general procedure for demethylation to the phenol while the other one was oxidized to the methyl sulphone. The two activated species were subject to the general procedure for coupling**.** Following flash chromatography (eluent: 0–15% ethyl acetate in hexanes). The product was isolated in 80% yield.

Characterization ^{1}H NMR (500 MHz, $CDCl_3$) δ = 8.58 (s, 1H), 8.46 (s, *J*=9.9, 3H), 7.48 (td, *J*=8.2, 3.7, 3H), 7.33 (t, *J*=8.2, 1H), 7.13 – 6.98 (m, 9H), 6.83 (dd, *J*=8.3, 2.1, 1H), 6.73 (t, *J*=11.4, 3H), 6.43 (s, 2H), 6.36 (s, *J*=9.9, 1H), 3.81 (s, 3H), 2.56 (s, 3H). ^{13}C NMR (126 MHz, $CDCl_3$) δ = 172.71, 171.67, 171.19, 171.17, 171.08, 168.11, 160.90, 158.42, 158.32, 157.80, 153.40, 153.28, 153.22, 153.20, 153.19, 130.52, 130.49, 130.31, 118.93, 118.84, 118.77, 115.43, 115.42, 113.58, 111.66, 107.59, 103.53, 92.77, 92.75, 92.48, 55.46, 12.86.

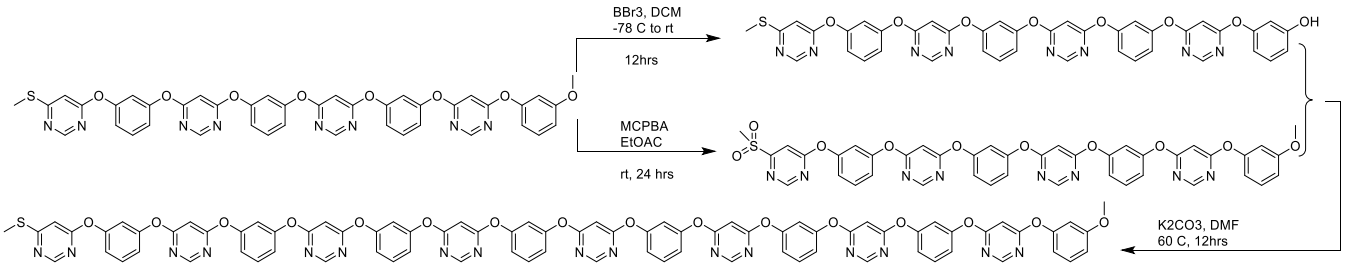

Synthesis of hexadecamer(40) Octomer (**39**) was subjected the orthogonal deprotectin where octomer xx was divided, half the material was subjected to the general procedure for demethylation to the phenol while the other one was oxidized to the methyl sulphone. The two activated species were subject to the general procedure for coupling**.** Following flash chromatography (eluent: 0–15% ethyl acetate in hexanes) to give the product as a fine powder. The product was isolated in 80% yield.

Characterization: ^{1}H NMR (500 MHz, $CDCl_3$) δ = 8.60 (s, 1H), 8.48 (s, 7H), 7.51 (t, *J*=8.2, 3H), 7.36 (t, *J*=8.2, 1H), 7.14 – 7.01 (m, 21H), 6.85 (d, *J*=8.2, 1H), 6.75 (m, 3H), 6.45 (s, 6H), 6.38 (s, 1H), 3.83 (s, 3H), 2.58 (s, 3H). ^{13}C NMR (126 MHz, $CDCl_3$) δ = 172.71, 171.67, 171.08, 171.04, 168.10, 160.90, 158.43, 158.32, 157.80, 153.22, 130.52, 130.30, 118.92, 115.52, 113.58, 111.75, 111.66, 107.59, 103.53, 92.77, 92.48, 55.46, 40.71, 37.60, 29.70, 12.86.

References

1. Mosher, W. A.; Soeder, R. W., Reactions of some methylene ketones with dimethyl phthalate. New route to 2-substituted 1,3-indandiones. *The Journal of Organic Chemistry* **1971,** *36* (11), 1561.
2. Kuck, D.; Lindenthal, T.; Schuster, A., Benzoanellated centropolyquinanes, 11. Synthesis of tribenzotriquinacene and somecentro-substituted derivatives. *Chem. Ber.* **1992,** *125* (6), 1449.
3. Strube, J.; Neumann, B.; Stammler, H. G.; Kuck, D., Solid-state enantiopure organic nanocubes formed by self organization of a C3-symmetrical tribenzotriquinacene. *Chemistry* **2009,** *15* (10), 2256.
4. Beaudoin, D.; Rominger, F.; Mastalerz, M., Synthesis and Chiral Resolution ofC3-Symmetric Tribenzotriquinacenes. *Eur. J. Org. Chem.* **2016,** *2016* (26), 4470.
5. Wang, T.; Zhang, Y. F.; Hou, Q. Q.; Xu, W. R.; Cao, X. P.; Chow, H. F.; Kuck, D., C3-symmetrical tribenzotriquinacene derivatives: optical resolution through cryptophane synthesis and supramolecular self-assembly into nanotubes. *J. Org. Chem.* **2013,** *78* (3), 1062.
6. Mughal, E. U.; Kuck, D., New C(3v)-symmetrical tribenzotriquinacenes bearing extended and oxy-functionalised alkyl groups at their benzhydrylic bridgeheads. *Org. Biomol. Chem.* **2010,** *8* (23), 5383.
7. Freedman, T. B.; Cao, X.; Nafie, L. A.; Solladie-Cavallo, A.; Jierry, L.; Bouerat, L., VCD configuration of enantiopure/-enriched tetrasubstituted alpha-fluoro cyclohexanones and their use for epoxidation of trans-olefins. *Chirality* **2004,** *16* (7), 467.
8. Schrödinger Release 2016-3: MacroModel, S., LLC, New York, NY, 2016.
9. Schrödinger Release 2016-3: Jaguar, S., LLC, New York, NY, 2016.
10. Zhao, Y.; Truhlar, D. G., Density functionals with broad applicability in chemistry. *Acc Chem Res* **2008,** *41* (2), 157.
11. https://cccbdb.nist.gov/vibscalejust.asp.
12. Becke, A. D., Density-functional thermochemistry. III. The role of exact exchange. *The Journal of Chemical Physics* **1993,** *98* (7), 5648.
13. Johnson, E. R.; Keinan, S.; Mori-Sanchez, P.; Contreras-Garcia, J.; Cohen, A. J.; Yang, W., Revealing noncovalent interactions. *J. Am. Chem. Soc.* **2010,** *132* (18), 6498.
14. Lee, C.; Yang, W.; Parr, R. G., Development of the Colle-Salvetti correlation-energy formula into a functional of the electron density. *Physical Review B* **1988,** *37* (2), 785.
15. Schneebeli, S. T.; Bochevarov, A. D.; Friesner, R. A., Parameterization of a B3LYP specific correction for non-covalent interactions and basis set superposition error on a gigantic dataset of CCSD(T) quality non-covalent interaction energies. *J. Chem. Theory Comput.* **2011,** *7* (3), 658.
16. Stephens, P. J.; Devlin, F. J.; Chabalowski, C. F.; Frisch, M. J., Ab Initio Calculation of Vibrational Absorption and Circular Dichroism Spectra Using Density Functional Force Fields. *The Journal of Physical Chemistry* **1994,** *98* (45), 11623.
17. Veinot, A. J.; Todd, A. D. K.; Robertson, K. N.; Masuda, J. D., A reinvestigation of mono- and bis-ethynyl phosphonium salts: structural and computational studies and new reactivity. *Can. J. Chem.* **2018,** *96* (1), 8.

Comprehensive list of references

1. Proceedings of the Chemical Society, Vol. 6, No. 85. *Proceedings of the Chemical Society (London)* **1890,** *6* (85), 95.
2. Abraham, M. H.; Grellier, P. L.; Abboud, J.-L. M.; Doherty, R. M.; Taft, R. W., Solvent effects in organic chemistry-recent developments. *Can. J. Chem.* **1988,** *66* (11), 2673.
3. Acevedo, O.; Jorgensen, W. L., Solvent Effects and Mechanism for a Nucleophilic Aromatic Substitution from QM/MM Simulations. *Org. Lett.* **2004,** *6* (17), 2881.
4. Allemann, C.; Gordillo, R.; Clemente, F. R.; Cheong, P. H.; Houk, K. N., Theory of asymmetric organocatalysis of Aldol and related reactions: rationalizations and predictions. *Acc Chem Res* **2004,** *37* (8), 558.
5. Allemann, O.; Duttwyler, S.; Romanato, P.; Baldridge, K. K.; Siegel, J. S., Proton-catalyzed, silane-fueled Friedel-Crafts coupling of fluoroarenes. *Science* **2011,** *332* (6029), 574.
6. Aoki, Y.; O'Brien, H. M.; Kawasaki, H.; Takaya, H.; Nakamura, M., Ligand-Free Iron-Catalyzed C-F Amination of Diarylamines: A One-Pot Regioselective Synthesis of Diaryl Dihydrophenazines. *Org. Lett.* **2019,** *21* (2), 461.
7. Armstrong, H. E., XXVIII.—An explanation of the laws which govern substitution in the case of benzenoid compounds. *J. Chem. Soc., Trans.* **1887,** *51* (0), 258.
8. Asadi, A.; Ajami, D.; Rebek, J., Covalent capsules: reversible binding in a chiral space. *Chem. Sci.* **2013,** *4* (3), 1212.
9. Ashton, P. R.; Brown, G. R.; Isaacs, N. S.; Giuffrida, D.; Kohnke, F. H.; Mathias, J. P.; Slawin, A. M. Z.; Smith, D. R.; Stoddart, J. F.; Williams, D. J., Molecular LEGO. 1. Substrate-directed synthesis via stereoregular Diels-Alder oligomerizations. *J. Am. Chem. Soc.* **1992,** *114* (16), 6330.
10. Ashwell, G. J.; Hamilton, R.; Wood, B. J.; Gentle, I. R.; Zhou, D., Molecular Lego non-centrosymmetric alignment within interdigitating layers. *J. Mater. Chem.* **2001,** *11* (12), 2966.
11. Baker, S. N.; Baker, G. A.; Bright, F. V., Temperature-dependent microscopic solvent properties of 'dry' and 'wet' 1-butyl-3-methylimidazolium hexafluorophosphate: correlation with ET(30) and Kamlet-Taft polarity scales. *Green Chem.* **2002,** *4* (2), 165.
12. Bandini, M.; Melloni, A.; Umani-Ronchi, A., New catalytic approaches in the stereoselective Friedel-Crafts alkylation reaction. *Angew. Chem. Int. Ed.* **2004,** *43* (5), 550.
13. Barnes, J. C.; Ehrlich, D. J. C.; Gao, A. X.; Leibfarth, F. A.; Jiang, Y.; Zhou, E.; Jamison, T. F.; Johnson, J. A., Iterative exponential growth of stereo- and sequence-controlled polymers. *Nat. Chem.* **2015,** *7* (10), 810.
14. Beaudoin, D.; Rominger, F.; Mastalerz, M., Synthesis and Chiral Resolution ofC3-Symmetric Tribenzotriquinacenes. *Eur. J. Org. Chem.* **2016,** *2016* (26), 4470.
15. Beaudoin, D.; Rominger, F.; Mastalerz, M., Chirality-Assisted Synthesis of a Very Large Octameric Hydrogen-Bonded Capsule. *Angew. Chem. Int. Ed.* **2016,** *55* (50), 15599.
16. Beaudoin, D.; Rominger, F.; Mastalerz, M., Chiral Self-Sorting of [2+3] Salicylimine Cage Compounds. *Angew. Chem. Int. Ed.* **2017,** *56* (5), 1244.

17. Becke, A. D., Density-functional thermochemistry. III. The role of exact exchange. *The Journal of Chemical Physics* **1993,** *98* (7), 5648.
18. Bencivenni, G., Organocatalytic Strategies for the Synthesis of Axially Chiral Compounds. *Synlett* **2015,** *26* (14), 1915.
19. Beresis, R. T.; Masse, C. E.; Panek, J. S., Enantioselective Nitration of Chiral (E)-Crotylsilanes: A Concise Asymmetric Synthesis of (E)-Olefin Dipeptide Isosteres. *The Journal of Organic Chemistry* **1995,** *60* (24), 7714.
20. Bernstein, J.; Davis, R. E.; Shimoni, L.; Chang, N.-L., Patterns in hydrogen bonding: functionality and graph set analysis in crystals. *Angew. Chem., Int. Ed. Engl.* **1995,** *34* (15), 1555.
21. Beuerle, F.; Dhara, A., Synthetic Strategies for the Regioselective Functionalization of Tribenzotriquinacenes. *Synthesis* **2018,** *50* (15), 2867.
22. Beuerle, F.; Gole, B., Covalent Organic Frameworks and Cage Compounds: Design and Applications of Polymeric and Discrete Organic Scaffolds. *Angew. Chem., Int. Ed.* **2018,** *57* (18), 4850.
23. Binauld, S.; Damiron, D.; Connal, L. A.; Hawker, C. J.; Drockenmuller, E., Precise synthesis of molecularly defined oligomers and polymers by orthogonal iterative divergent/convergent approaches. *Macromol. Rapid Commun.* **2011,** *32* (2), 147.
24. Blaziak, K.; Danikiewicz, W.; Makosza, M., How Does Nucleophilic Aromatic Substitution Really Proceed in Nitroarenes? Computational Prediction and Experimental Verification. *J. Am. Chem. Soc.* **2016,** *138* (23), 7276.
25. Bolibrukh, K.; Khoumeri, O.; Polovkovych, S.; Novikov, V.; Terme, T.; Vanelle, P., Novel Synthesis of 5-Substituted 5H-Benzo[b]carbazole-6,11-diones via Double Buchwald-Hartwig Reaction. *Synlett* **2014,** *25* (19), 2765.
26. Breslow, R., Biomimetic Chemistry and Artificial Enzymes: Catalysis by Design. *Acc. Chem. Res.* **1995,** *28* (3), 146.
27. Breslow, R.; Czarnik, A. W., Transaminations by pyridoxamine selectively attached at C-3 in β-cyclodextrin. *J. Am. Chem. Soc.* **1983,** *105* (5), 1390.
28. Bume, D. D.; Pitts, C. R.; Ghorbani, F.; Harry, S. A.; Capilato, J. N.; Siegler, M. A.; Lectka, T., Ketones as directing groups in photocatalytic sp(3) C-H fluorination. *Chem Sci* **2017,** *8* (10), 6918.
29. Campbell, J. P.; Rajappan, S. C.; Jaynes, T. J.; Sharafi, M.; Ma, Y.-T.; Li, J.; Schneebeli, S. T., Enantioselective Electrophilic Aromatic Nitration: A Chiral Auxiliary Approach. *Angew. Chem., Int. Ed.* **2019,** *58* (4), 1035.
30. Cao, J.; Zhu, X.-Z.; Chen, C.-F., Synthesis, Structure, and Binding Property of Pentiptycene-Based Rigid Tweezer-like Molecules. *J. Org. Chem.* **2010,** *75* (21), 7420.
31. Chen, Z.; Swager, T. M., Synthesis and Characterization of Poly(2,6-triptycene). *Macromolecules (Washington, DC, U. S.)* **2008,** *41* (19), 6880.
32. Cheng, L.; Breslow, R. In *Binding and biomimetic cleavage of the RNA by synthetic deoxypolypeptides/peptoids (DOPPs)*, American Chemical Society: 2016; pp ORGN.
33. Chong, J. H.; MacLachlan, M. J., Synthesis and Structural Investigation of New Triptycene-Based Ligands: En Route to Shape-Persistent Dendrimers and Macrocycles with Large Free Volume. *J. Org. Chem.* **2007,** *72* (23), 8683.
34. Chong, J. H.; MacLachlan, M. J., Iptycenes in supramolecular and materials chemistry. *Chem. Soc. Rev.* **2009,** *38* (12), 3301.

35. Church, G. M.; Gao, Y.; Kosuri, S., Next-generation digital information storage in DNA. *Science* **2012,** *337* (6102), 1628.
36. Crane, A. K.; Wong, E. Y. L.; MacLachlan, M. J., Metal-organic frameworks from novel flexible triptycene- and pentiptycene-based ligands. *CrystEngComm* **2013,** *15* (45), 9811.
37. Crowhurst, L.; Mawdsley, P. R.; Perez-Arlandis, J. M.; Salter, P. A.; Welton, T., Solvent-solute interactions in ionic liquids. *Phys. Chem. Chem. Phys.* **2003,** *5* (13), 2790.
38. Dhara, A.; Beuerle, F., Reversible Assembly of a Supramolecular Cage Linked by Boron-Nitrogen Dative Bonds. *Chemistry* **2015,** *21* (48), 17391.
39. Dietrich-Buchecker, C. O.; Sauvage, J. P.; Kern, J. M., Templated synthesis of interlocked macrocyclic ligands: the catenands. *J. Am. Chem. Soc.* **1984,** *106* (10), 3043.
40. Elbert, S. M.; Rominger, F.; Mastalerz, M., Synthesis of a rigid C3v -symmetric tris-salicylaldehyde as a precursor for a highly porous molecular cube. *Chem. Eur. J.* **2014,** *20* (50), 16707.
41. Engler, A. C.; Chan, J. M. W.; Coady, D. J.; O'Brien, J. M.; Sardon, H.; Nelson, A.; Sanders, D. P.; Yang, Y. Y.; Hedrick, J. L., Accessing New Materials through Polymerization and Modification of a Polycarbonate with a Pendant Activated Ester. *Macromolecules (Washington, DC, U. S.)* **2013,** *46* (4), 1283.
42. Esteves, P. M.; De, M. C. J. W.; Cardoso, S. P.; Barbosa, A. G.; Laali, K. K.; Rasul, G.; Prakash, G. K.; Olah, G. A., Unified mechanistic concept of electrophilic aromatic nitration: convergence of computational results and experimental data. *J. Am. Chem. Soc.* **2003,** *125* (16), 4836.
43. Estrella, L. L.; Balanay, M. P.; Kim, D. H., Theoretical Insights into D-D-π-A Sensitizers Employing N-Annulated Perylene for Dye-Sensitized Solar Cells. *J. Phys. Chem. A* **2018,** *122* (30), 6328.
44. Fasina, T. M.; Dueke-Eze, C. U.; Familoni, O. B., Synthesis and solvatochromic behaviour of some heterocyclyic isonicotinohydrazide Schiff bases. *Moroccan J. Chem.* **2018,** *6* (3), 504.
45. Freedman, T. B.; Cao, X.; Nafie, L. A.; Solladie-Cavallo, A.; Jierry, L.; Bouerat, L., VCD configuration of enantiopure/-enriched tetrasubstituted alpha-fluoro cyclohexanones and their use for epoxidation of trans-olefins. *Chirality* **2004,** *16* (7), 467.
46. Galabov, B.; Koleva, G.; Simova, S.; Hadjieva, B.; Schaefer, H. F., 3rd; Schleyer, P., Arenium ions are not obligatory intermediates in electrophilic aromatic substitution. *Proc. Natl. Acad. Sci. U. S. A.* **2014,** *111* (28), 10067.
47. Galabov, B.; Nalbantova, D.; Schleyer, P.; Schaefer, H. F., 3rd, Electrophilic Aromatic Substitution: New Insights into an Old Class of Reactions. *Acc Chem Res* **2016,** *49* (6), 1191.
48. Galan, A.; Escudero-Adan, E. C.; Ballester, P., Template-directed self-assembly of dynamic covalent capsules with polar interiors. *Chem. Sci.* **2017,** *8* (11), 7746.
49. Gao, X.; Lu, Y.; Xing, Y.; Ma, Y.; Lu, J.; Bao, W.; Wang, Y.; Xi, T., A novel anticancer and antifungus phenazine derivative from a marine actinomycete BM-17. *Microbiol Res* **2012,** *167* (10), 616.
50. Gong, X.; Wu, J.; Meng, Y.; Zhang, Y.; Ye, L.-W.; Zhu, C., Ligand-free palladium catalyzed Ullmann biaryl synthesis: 'household' reagents and mild reaction conditions. *Green Chem.* **2019**, Ahead of Print.

51. Greschner, W.; Neumann, B.; Stammler, H.-G.; Groeger, H.; Kuck, D., Enantiomerically Pure Tribenzotriquinacenes through Stereoselective Synthesis. *Angew. Chem., Int. Ed.* **2015,** *54* (46), 13764.
52. Gu, P. Y.; Zhao, Y.; He, J. H.; Zhang, J.; Wang, C.; Xu, Q. F.; Lu, J. M.; Sun, X. W.; Zhang, Q., Synthesis, physical properties, and light-emitting diode performance of phenazine-based derivatives with three, five, and nine fused six-membered rings. *J. Org. Chem.* **2015,** *80* (6), 3030.
53. Guan, L.; Holl, M. G.; Pitts, C. R.; Struble, M. D.; Siegler, M. A.; Lectka, T., Through-Space Activation Can Override Substituent Effects in Electrophilic Aromatic Substitution. *J. Am. Chem. Soc.* **2017,** *139* (42), 14913.
54. Guan, Y.; Wang, C.; Wang, D.; Dang, G.; Chen, C.; Zhou, H.; Zhao, X., Methylsulfone as a leaving group for synthesis of hyperbranched poly(arylene pyrimidine ether)s by nucleophilic aromatic substitution. *RSC Advances* **2015,** *5* (17), 12821.
55. Gustafson, J. L.; Lim, D.; Miller, S. J., Dynamic kinetic resolution of biaryl atropisomers via peptide-catalyzed asymmetric bromination. *Science* **2010,** *328* (5983), 1251.
56. Hahn, S.; Koser, S.; Hodecker, M.; Seete, P.; Rominger, F.; Miljanic, O. S.; Dreuw, A.; Bunz, U. H. F., Phenylene Bridged Cyclic Azaacenes: Dimers and Trimers. *Chem. - Eur. J.* **2018,** *24* (27), 6968.
57. Hamon, F.; Djedaini-Pilard, F.; Barbot, F.; Len, C., Azobenzenes—synthesis and carbohydrate applications. *Tetrahedron* **2009,** *65* (49), 10105.
58. Harmata, M., Chiral Molecular Tweezers. *Acc. Chem. Res.* **2004,** *37* (11), 862.
59. Hassan, S. S. u.; Anjum, K.; Abbas, S. Q.; Akhter, N.; Shagufta, B. I.; Shah, S. A. A.; Tasneem, U., Emerging biopharmaceuticals from marine actinobacteria. *Environ. Toxicol. Pharmacol.* **2017,** *49*, 34.
60. Hawker, C. J.; Malmstroem, E. E.; Frank, C. W.; Kampf, J. P., Exact Linear Analogs of Dendritic Polyether Macromolecules: Design, Synthesis, and Unique Properties. *J. Am. Chem. Soc.* **1997,** *119* (41), 9903.
61. Hecht, S.; Frechet, J. M. J., Dendritic encapsulation of function: applying nature's site isolation principle from biomimetics to materials science. *Angew. Chem., Int. Ed.* **2001,** *40* (1), 74.
62. Henne, S.; Bredenkoetter, B.; Alaghemandi, M.; Bureekaew, S.; Schmid, R.; Volkmer, D., Almost Enclosed Buckyball Joints: Synthesis, Complex Formation, and Computational Simulations of Pentypticene-Extended Tribenzotriquinacene. *ChemPhysChem* **2014,** *15* (17), 3855.
63. Henne, S.; Bredenkoetter, B.; Dehghan Baghi, A. A.; Schmid, R.; Volkmer, D., Advanced buckyball joints: synthesis, complex formation and computational simulations of centrohexaindane-extended tribenzotriquinacene receptors for C60 fullerene. *Dalton Trans.* **2012,** *41* (19), 5995.
64. Henne, S.; Bredenkoetter, B.; Volkmer, D., Mixed SAMs of backbone-functionalized tribenzotriquinacenes and alkanethiols: Synthesis, preparation and STM-investigations. *Appl. Surf. Sci.* **2015,** *356*, 645.
65. Hestand, N. J.; Spano, F. C., Molecular Aggregate Photophysics beyond the Kasha Model: Novel Design Principles for Organic Materials. *Acc. Chem. Res.* **2017,** *50* (2), 341.

66. Hilton, C. L.; Jamison, C. R.; Zane, H. K.; King, B. T., A Triphenylene-Based Triptycene with Large Free Volume Synthesized by Zirconium-Mediated Biphenylation. *J. Org. Chem.* **2009,** *74* (1), 405.
67. Holl, M. G.; Pitts, C. R.; Lectka, T., Fluorine in a C-F Bond as the Key to Cage Formation. *Angew. Chem. Int. Ed.* **2018,** *57* (11), 2758.
68. Holl, M. G.; Struble, M. D.; Singal, P.; Siegler, M. A.; Lectka, T., Positioning a Carbon-Fluorine Bond over the pi Cloud of an Aromatic Ring: A Different Type of Arene Activation. *Angew. Chem. Int. Ed.* **2016,** *55* (29), 8266.
69. Holland, M. C.; Paul, S.; Schweizer, W. B.; Bergander, K.; Muck-Lichtenfeld, C.; Lakhdar, S.; Mayr, H.; Gilmour, R., Noncovalent interactions in organocatalysis: modulating conformational diversity and reactivity in the MacMillan catalyst. *Angew. Chem. Int. Ed.* **2013,** *52* (31), 7967.
70. http://www.stenutz.eu/chem/solv26.php.
71. https://cccbdb.nist.gov/vibscalejust.asp.
72. Hurtley, A. E.; Stone, E. A.; Metrano, A. J.; Miller, S. J., Desymmetrization of Diarylmethylamido Bis(phenols) through Peptide-Catalyzed Bromination: Enantiodivergence as a Consequence of a 2 amu Alteration at an Achiral Residue within the Catalyst. *J. Org. Chem.* **2017,** *82* (21), 11326.
73. Ip, H. W.; Ng, C. F.; Chow, H. F.; Kuck, D., Three-Fold Scholl-Type Cycloheptatriene Ring Formation around a Tribenzotriquinacene Core: Toward Warped Graphenes. *J. Am. Chem. Soc.* **2016,** *138* (42), 13778.
74. Jia, T.; Huang, S.; Bohra, H.; Wang, M., Examining derivatives of quinacridone, diketopyrrolopyrrole and indigo as the visible-light organic photocatalysts for metal-free atom transfer radical polymerization. *Dyes Pigm.* **2019,** *165*, 223.
75. Jiang, Y.; Chen, C.-F., Synthesis and structures of 1,10-phenanthroline-based extended triptycene derivatives. *Synlett* **2010,** (11), 1679.
76. Jin, P.; Long, J.; Du, Y.; Zheng, X.; Xue, J., Hydrogen bond configuration and protonation of ground and lowest excited triplet states of 4-amino-4'-nitrobiphenyl based on nanosecond transient absorption spectroscopy. *Spectrochim. Acta, Part A* **2019,** *217*, 44.
77. Johnson, E. R.; Keinan, S.; Mori-Sanchez, P.; Contreras-Garcia, J.; Cohen, A. J.; Yang, W., Revealing noncovalent interactions. *J. Am. Chem. Soc.* **2010,** *132* (18), 6498.
78. Jørgensen, K. A., Asymmetric Friedel-CraftsReactions: Catalytic Enantioselective Addition of Aromatic and HeteroaromaticC-H Bonds to Activated Alkenes, Carbonyl Compounds, andImines. *Synthesis* **2003,** *2003* (07), 1117.
79. Kabir, A.; Endo, S.; Toyooka, N.; Fukuoka, M.; Kuwata, K.; Kamatari, Y. O., Evaluation of compound selectivity of aldo-keto reductases using differential scanning fluorimetry. *J. Biochem.* **2017,** *161* (2), 215.
80. Kelly, J. V.; O'Neill, F. T.; Sheridan, J. T.; Neipp, C.; Gallego, S.; Ortuno, M., Holographic photopolymer materials: nonlocal polymerization-driven diffusion under nonideal kinetic conditions. *J. Opt. Soc. Am. B* **2005,** *22* (2), 407.
81. Kim, J. Y.; Hwang, T. G.; Kim, S. H.; Namgoong, J. W.; Kim, J. E.; Sakong, C.; Choi, J.; Lee, W.; Kim, J. P., Synthesis of high-soluble and non-fluorescent perylene derivatives and their effect on the contrast ratio of LCD color filters. *Dyes Pigm.* **2017,** *136*, 836.

82. Klotzbach, S.; Beuerle, F., Shape-Controlled Synthesis and Self-Sorting of Covalent Organic Cage Compounds. *Angew. Chem., Int. Ed.* **2015,** *54* (35), 10356.
83. Kobayashi, S.; Mori, Y.; Fossey, J. S.; Salter, M. M., Catalytic enantioselective formation of C-C bonds by addition to imines and hydrazones: a ten-year update. *Chem. Rev.* **2011,** *111* (4), 2626.
84. Kochi, J. K., Inner-sphere electron transfer in organic chemistry. Relevance to electrophilic aromatic nitration. *Acc. Chem. Res.* **2002,** *25* (1), 39.
85. Kuck, D.; Lindenthal, T.; Schuster, A., Benzoanellated centropolyquinanes, 11. Synthesis of tribenzotriquinacene and somecentro-substituted derivatives. *Chem. Ber.* **1992,** *125* (6), 1449.
86. Kuck, D.; Lindenthal, T.; Schuster, A., Benzanellated centropolyquinanes. 11. Synthesis of tribenzotriquinacene and some centro-substituted derivatives. *Chem. Ber.* **1992,** *125* (6), 1449.
87. Kuck, D.; Schuster, A.; Krause, R. A.; Tellenbröker, J.; Exner, C. P.; Penk, M.; Bögge, H.; Müller, A., Multiply bridgehead- and periphery-substituted tribenzotriquinacenes—highly versatile rigid molecular building blocks with C3v or C3 symmetry. *Tetrahedron* **2001,** *57* (17), 3587.
88. Kulkarni, M.; Chaudhari, A., Microbial remediation of nitro-aromatic compounds: an overview. *J. Environ. Manage.* **2007,** *85* (2), 496.
89. Kwan, E. E.; Zeng, Y.; Besser, H. A.; Jacobsen, E. N., Concerted nucleophilic aromatic substitutions. *Nature Chem.* **2018,** *10* (9), 917.
90. Lee, C.; Yang, W.; Parr, R. G., Development of the Colle-Salvetti correlation-energy formula into a functional of the electron density. *Physical Review B* **1988,** *37* (2), 785.
91. Li, J. L.; Yue, C. Z.; Chen, P. Q.; Xiao, Y. C.; Chen, Y. C., Remote enantioselective Friedel-Crafts alkylations of furans through HOMO activation. *Angew. Chem. Int. Ed.* **2014,** *53* (21), 5449.
92. Li, X.-N.; Zhou, H.-Y.; Feng, L.; Duan, K.; Wang, J.-X., Temperature-tuned enantioselectivity in transfer hydrogenation: preparation and catalytic property of amino acid-modified benzimidazole. *Appl. Organomet. Chem.* **2012,** *26* (4), 168.
93. Liang, Q.; Chong, J. H.; White, N. G.; Zhao, Z.; MacLachlan, M. J., Towards a self-assembled honeycomb structure via diaminotriptycene metal complexes. *Dalton Trans.* **2013,** *42* (47), 16474.
94. Liljenberg, M.; Stenlid, J. H.; Brinck, T., Mechanism and regioselectivity of electrophilic aromatic nitration in solution: the validity of the transition state approach. *J Mol Model* **2017,** *24* (1), 15.
95. Lim, C.-H.; Ryan, M. D.; McCarthy, B. G.; Theriot, J. C.; Sartor, S. M.; Damrauer, N. H.; Musgrave, C. B.; Miyake, G. M., Intramolecular Charge Transfer and Ion Pairing in N,N-Diaryl Dihydrophenazine Photoredox Catalysts for Efficient Organocatalyzed Atom Transfer Radical Polymerization. *J. Am. Chem. Soc.* **2017,** *139* (1), 348.
96. Linke, J.; Bader, N.; Tellenbroeker, J.; Kuck, D., Sixfold Peripheral Halogenation of Tribenzotriquinacenes: An Alternative Access to Useful TBTQ Building Blocks. *Synthesis* **2018,** *50* (1), 175.

97. Liu, X.; Weinert, Z. J.; Sharafi, M.; Liao, C.; Li, J.; Schneebeli, S. T., Regulating Molecular Recognition with C-Shaped Strips Attained by Chirality-Assisted Synthesis. *Angew. Chem. Int. Ed.* **2015,** *54* (43), 12772.
98. Ljubovic, E.; Majeric-Elenkov, M.; Avdagic, A.; Sunjic, V., Novel biocatalytic methodology: low temperature enhanced enantioselectivity of enzyme catalyzed reactions in organic solvents. *Food Technol. Biotechnol.* **1999,** *37* (3), 215.
99. Lou, K.; Prior, A. M.; Wiredu, B.; Desper, J.; Hua, D. H., Synthesis of Cyclododeciptycene Quinones. *J. Am. Chem. Soc.* **2010,** *132* (49), 17635.
100. Lu, Y.; Huang, F.; Wang, J.; Xia, J., Affinity-Guided Covalent Conjugation Reactions Based on PDZ-Peptide and SH3-Peptide Interactions. *Bioconjugate Chem.* **2014,** *25* (5), 989.
101. Ma, D.; Glassenberg, R.; Ghosh, S.; Zavalij, P. Y.; Isaacs, L., Acyclic cucurbituril congener binds to local anaesthetics. *Supramol. Chem.* **2012,** *24* (5), 325.
102. MacGillivray, L. R.; Atwood, J. L., A chiral spherical molecular assembly held together by 60 hydrogen bonds. *Nature* **1997,** *389* (6650), 469.
103. Maehara, T.; Sekiya, R.; Harada, K.; Haino, T., Tunable enforced cavities inside self-assembled capsules. *Org. Chem. Front.* **2019**, Ahead of Print.
104. Mano, N.; Kuhn, A., Molecular lego for the assembly of biosensing layers. *Talanta* **2005,** *66* (1), 21.
105. Marcus, Y., The properties of organic liquids that are relevant to their use as solvating solvents. *Chem. Soc. Rev.* **1993,** *22* (6), 409.
106. Markopoulos, G.; Henneicke, L.; Shen, J.; Okamoto, Y.; Jones, P. G.; Hopf, H., Tribenzotriquinacene: a versatile synthesis and C3-chiral platforms. *Angew. Chem. Int. Ed.* **2012,** *51* (51), 12884.
107. Markoski, L. J.; Thompson, J. L.; Moore, J. S., Synthesis and Characterization of Linear−Dendritic Aromatic Etherimide Copolymers: Tuning Molecular Architecture To Optimize Properties and Processability. *Macromolecules* **2000,** *33* (15), 5315.
108. Martin, T.; Obst, U.; Rebek, J., Jr., Molecular assembly and encapsulation directed by hydrogen-bonding preferences and the filling of space. *Science* **1998,** *281* (5384), 1842.
109. Mastalerz, M., Single-Handed Towards Nanosized Organic Molecules. *Angew. Chem. Int. Ed.* **2016,** *55* (1), 45.
110. Mastalerz, M.; Rominger, F.; Beaudoin, D., Synthesis and Chiral Resolution of C3-symmetric Tribenzotriquinacenes. *Eur. J. Org. Chem.* **2016,** *2016* (26), 4470.
111. Mathias, J. P.; Stoddart, J. F., Constructing a molecular LEGO set. *Chem. Soc. Rev.* **1992,** *21* (4), 215.
112. Merz, K. In *Role of dynamics in enzymatic electrophilic aromatic substitution*, American Chemical Society: 2017; pp PHYS.
113. Mino, T.; Yamaguchi, D.; Masuda, C.; Youda, J.; Ebisawa, T.; Yoshida, Y.; Sakamoto, M., Synthesis and application of P,olefin type axially chiral ligands with sec-alkyl groups. *Org. Biomol. Chem.* **2019,** *17* (6), 1455.
114. Miyake, G. In *Organocatalyzed atom transfer radical polymerization driven by visible light*, American Chemical Society: 2017; pp ORGN.
115. Mohr, J. T.; Krout, M. R.; Stoltz, B. M., Natural products as inspiration for the development of asymmetric catalysis. *Nature* **2008,** *455*, 323.
116. Mortier, J., **2015**.

117. Mosher, W. A.; Soeder, R. W., Reactions of some methylene ketones with dimethyl phthalate. New route to 2-substituted 1,3-indandiones. *J. Org. Chem.* **1971,** *36* (11), 1561.
118. Mueller, A.; O'Brien, D. F., Supramolecular materials via polymerization of mesophases of hydrated amphiphiles. *Chem. Rev.* **2002,** *102* (3), 727.
119. Mughal, E. U.; Kuck, D., New C(3v)-symmetrical tribenzotriquinacenes bearing extended and oxy-functionalised alkyl groups at their benzhydrylic bridgeheads. *Org. Biomol. Chem.* **2010,** *8* (23), 5383.
120. Murphy, K. E.; Bocanegra, J. L.; Liu, X.; Chau, H. Y. K.; Lee, P. C.; Li, J.; Schneebeli, S. T., Precise through-space control of an abiotic electrophilic aromatic substitution reaction. *Nature communications* **2017,** *8*, 14840.
121. Muto, Y.; Yokoyama, S., Structural insight into RNA recognition motifs: versatile molecular Lego building blocks for biological systems. *Wiley Interdiscip. Rev.: RNA* **2012,** *3* (2), 229.
122. Narita, A.; Wang, X.-Y.; Feng, X.; Muellen, K., New advances in nanographene chemistry. *Chem. Soc. Rev.* **2015,** *44* (18), 6616.
123. Nishita, M.; Park, S.-Y.; Nishio, T.; Kamizaki, K.; Wang, Z.; Tamada, K.; Takumi, T.; Hashimoto, R.; Otani, H.; Pazour, G. J.; Hsu, V. W.; Minami, Y., Ror2 signaling regulates Golgi structure and transport through IFT20 for tumor invasiveness. *Scientific Reports* **2017,** *7* (1), 1.
124. Niu, W. X.; Wang, T.; Hou, Q. Q.; Li, Z. Y.; Cao, X. P.; Kuck, D., Synthesis and optical resolution of inherently chiral difunctionalized tribenzotriquinacenes. *J. Org. Chem.* **2010,** *75* (19), 6704.
125. Northrup, J. D.; Mancini, G.; Purcell, C. R.; Schafmeister, C. E., Development of spiroligomer-peptoid hybrids. *J. Org. Chem.* **2017,** *82* (24), 13020.
126. Ohlendorf, L.; Velandia, J. E. D.; Konya, K.; Ehlers, P.; Villinger, A.; Langer, P., Synthesis and properties of 5,7-disubstituted 5,7-dihydropyrido[2,3-b:6,5-b']diindoles. *Adv. Synth. Catal.* **2017,** *359* (10), 1758.
127. Oliver, K.; Seddon, A.; Trask, R. S., Morphing in nature and beyond: a review of natural and synthetic shape-changing materials and mechanisms. *J. Mater. Sci.* **2016,** *51* (24), 10663.
128. Paras, N. A.; MacMillan, D. W. C., New Strategies in Organic Catalysis: The First Enantioselective Organocatalytic Friedel−Crafts Alkylation. *J. Am. Chem. Soc.* **2001,** *123* (18), 4370.
129. Pfeiffer, C. T.; Northrup, J. D.; Cheong, J. E.; Pham, M. A.; Parker, M. F. L.; Schafmeister, C. E., Utilization of the p-nitrobenzyloxycarbonyl (pNZ) amine protecting group and pentafluorophenyl (Pfp) esters for the solid phase synthesis of spiroligomers. *Tetrahedron Lett.* **2018,** *59* (30), 2884.
130. Quernheim, M.; Golling, F. E.; Zhang, W.; Wagner, M.; Raeder, H.-J.; Nishiuchi, T.; Muellen, K., The Precise Synthesis of Phenylene-Extended Cyclic Hexa-peri-hexabenzocoronenes from Polyarylated [n]Cycloparaphenylenes by the Scholl Reaction. *Angew. Chem., Int. Ed.* **2015,** *54* (35), 10341.
131. Rahman, F.-U.; Feng, H.-N.; Yu, Y., A new water-soluble cavitand with deeper guest binding properties. *Org. Chem. Front.* **2019**, Ahead of Print.
132. Rommelmann, P.; Greschner, W.; Ihrig, S.; Neumann, B.; Stammler, H.-G.; Gröger, H.; Kuck, D., Combining Stereoselective Enzyme Catalysis with Chirality-

Assisted Synthesis in Tribenzotriquinacene Chemistry. *Eur. J. Org. Chem.* **2018,** *2018* (29), 3891.
133. Rommelmann, P.; Nachtigall, B.; Guntelmann, T.; Groeger, H.; Kuck, D., Stereoselective synthesis of enantiomerically pure bowl-shaped hydroxytribenzotriquinacenes. *Org. Biomol. Chem.* **2018,** *16* (31), 5635.
134. Rowan, S. J.; Cantrill, S. J.; Cousins, G. R. L.; Sanders, J. K. M.; Stoddart, J. F., Dynamic covalent chemistry. *Angew. Chem., Int. Ed.* **2002,** *41* (6), 899.
135. Sadeghi, S. J.; Meharenna, Y. T.; Fantuzzi, A.; Valetti, F.; Gilardi, G., Engineering artificial redox chains by molecular 'Lego'. *Faraday Discuss.* **2000,** *116* (Bioelectrochemistry), 135.
136. Sakata, Y.; Yamamoto, R.; Saito, D.; Tamura, Y.; Maruyama, K.; Ogoshi, T.; Akine, S., Metallonanobelt: A Kinetically Stable Shape-Persistent Molecular Belt Prepared by Reversible Self-Assembly Processes. *Inorg. Chem.* **2018,** *57* (24), 15500.
137. Schafmeister, C. E.; Po, J.; Verdine, G. L., An All-Hydrocarbon Cross-Linking System for Enhancing the Helicity and Metabolic Stability of Peptides. *J. Am. Chem. Soc.* **2000,** *122* (24), 5891.
138. Schneebeli, S.; Li, J.; Sharafi, M.; Weinert, Z.; Cohen, I.; Liao, C.; Ivancic, M., Controlled Self-Assembly inside C-Shaped Polyaromatic Strips. *Synlett* **2016,** *27* (14), 2145.
139. Schneebeli, S. T.; Bochevarov, A. D.; Friesner, R. A., Parameterization of a B3LYP specific correction for non-covalent interactions and basis set superposition error on a gigantic dataset of CCSD(T) quality non-covalent interaction energies. *J. Chem. Theory Comput.* **2011,** *7* (3), 658.
140. Schramma, K. R.; Forneris, C. C.; Caruso, A.; Seyedsayamdost, M. R., Mechanistic investigations of lysine-tryptophan cross-link formation catalyzed by Streptococcal radical S-adenosylmethionine enzymes. *Biochemistry* **2018,** *57* (4), 461.
141. Schrödinger Release 2016-3: Jaguar, S., LLC, New York, NY, 2016.
142. Schrödinger Release 2016-3: MacroModel, S., LLC, New York, NY, 2016.
143. Shaikh, A. M.; Sharma, B. K.; Chacko, S.; Kamble, R. M., Novel electroluminescent donor–acceptors based on dibenzo[a,c]phenazine as hole-transporting materials for organic electronics. *New J. Chem.* **2017,** *41* (2), 628.
144. Sheikh, A. H.; Khalid, A.; Khan, F.; Begum, A., Fluorescent Gadolinium(III)-Oligopeptide Complexes and Carbon Nanotube Composite as Dual Modality Anticancer Agents. *ChemistrySelect* **2019,** *4* (1), 228.
145. Shi, C.; Zhang, X.; Yu, C. H.; Yao, Y. F.; Zhang, W., Geometric isotope effect of deuteration in a hydrogen-bonded host-guest crystal. *Nature communications* **2018,** *9* (1), 481.
146. Sinclair, J. K. L.; Walker, A. S.; Doerner, A. E.; Schepartz, A., Mechanism of Allosteric Coupling into and through the Plasma Membrane by EGFR. *Cell Chem. Biol.* **2018,** *25* (7), 857.
147. Singh, G.; Virpal; Singh, R. C., Highly sensitive gas sensor based on Er-doped SnO2 nanostructures and its temperature dependent selectivity towards hydrogen and ethanol. *Sens. Actuators, B* **2019,** *282*, 373.
148. Singh, S.; Rao, C. N. R., Deuterium Isotope Effects on Hydrogen Bonding. *Can. J. Chem.* **1966,** *44* (22), 2611.

149. Skubi, K. L.; Yoon, T. P., Organic chemistry Shape control in reactions with light. *Nature* **2014,** *515* (7525), 45.
150. Smythe, G. A.; Matanovic, G.; Yi, D.; Duncan, M. W., Trifluoroacetic Anhydride-Catalyzed Nitration of Toluene as an Approach to the Specific Analysis of Nitrate by Gas Chromatography-Mass Spectrometry. *Nitric Oxide* **1999,** *3* (1), 67.
151. Stephens, P. J.; Devlin, F. J.; Chabalowski, C. F.; Frisch, M. J., Ab Initio Calculation of Vibrational Absorption and Circular Dichroism Spectra Using Density Functional Force Fields. *The Journal of Physical Chemistry* **1994,** *98* (45), 11623.
152. Stewart, J. J., Optimization of parameters for semiempirical methods V: modification of NDDO approximations and application to 70 elements. *J Mol Model* **2007,** *13* (12), 1173.
153. Strube, J.; Neumann, B.; Stammler, H. G.; Kuck, D., Solid-state enantiopure organic nanocubes formed by self organization of a C3-symmetrical tribenzotriquinacene. *Chemistry* **2009,** *15* (10), 2256.
154. Sumerin, V.; Schulz, F.; Atsumi, M.; Wang, C.; Nieger, M.; Leskelae, M.; Repo, T.; Pyykkoe, P.; Rieger, B., Molecular Tweezers for Hydrogen: Synthesis, Characterization, and Reactivity. *J. Am. Chem. Soc.* **2008,** *130* (43), 14117.
155. Sydlik, S. A.; Chen, Z.; Swager, T. M., Triptycene Polyimides: Soluble Polymers with High Thermal Stability and Low Refractive Indices. *Macromolecules* **2011,** *44* (4), 976.
156. Takaba, H.; Omachi, H.; Yamamoto, Y.; Bouffard, J.; Itami, K., Selective Synthesis of [12]Cycloparaphenylene. *Angew. Chem., Int. Ed.* **2009,** *48* (33), 6112.
157. Tellenbroker, J.; Kuck, D., Tribenzotriquinacenes bearing three peripheral or bridgehead urea groups stretched into the 3-D space. *Beilstein J. Org. Chem.* **2011,** *7*, 329.
158. Terrier, F., Rate and equilibrium studies in Jackson-Meisenheimer complexes. *Chem. Rev.* **1982,** *82* (2), 77.
159. Tjin, C. C.; Wissner, R. F.; Jamali, H.; Schepartz, A.; Ellman, J. A., Synthesis and Biological Evaluation of an Indazole-Based Selective Protein Arginine Deiminase 4 (PAD4) Inhibitor. *ACS Med. Chem. Lett.* **2018,** *9* (10), 1013.
160. Trabelsi, I.; Oves, D.; Magan, B. G.; Manteca, A.; Genilloud, O.; Nour, M., Isolation, characterization and antimicrobial activities of actinomycetes isolated from a Tunisian Saline Wetland. *J. Microb. Biochem. Technol.* **2016,** *8* (6), 465.
161. Uhlig, D.; Spange, S.; Seifert, A.; Nagel, K.; Anders, S.; Kroll, L.; Stoll, R.; Thielbeer, F.; Mueller, P.; Schreiter, K., Design of nanostructured hybrid materials: twin polymerization of urethane-based twin prepolymers. *RSC Adv.* **2018,** *8* (55), 31673.
162. Van Rossom, W.; Caers, J.; Robeyns, K.; Van Meervelt, L.; Maes, W.; Dehaen, W., (Thio)ureido anion receptors based on a 1,3-alternate oxacalix[2]arene[2]pyrimidine scaffold. *J. Org. Chem.* **2012,** *77* (6), 2791.
163. Vasconcelos, S. N. S.; Reis, J. S.; de Oliveira, I. M.; Balfour, M. N.; Stefani, H. A., Synthesis of symmetrical biaryl compounds by homocoupling reaction. *Tetrahedron* **2019**, Ahead of Print.
164. Veinot, A. J.; Todd, A. D. K.; Robertson, K. N.; Masuda, J. D., A reinvestigation of mono- and bis-ethynyl phosphonium salts: structural and computational studies and new reactivity. *Can. J. Chem.* **2018,** *96* (1), 8.

165. Vergura, S.; Scafato, P.; Belviso, S.; Superchi, S., Absolute Configuration Assignment from Optical Rotation Data by Means of Biphenyl Chiroptical Probes. *Chem. - Eur. J.* **2019**, Ahead of Print.
166. Villalonga-Barber, C.; Micha-Screttas, M.; Steele, B. R.; Georgopoulos, A.; Demetzos, C., Dendrimers as biopharmaceuticals: synthesis and properties. *Curr. Top. Med. Chem.* **2008,** *8* (14), 1294.
167. Wagner, P.; Rominger, F.; Mastalerz, M., Switching the Statistical C3 /C1 Ratio in the Threefold Aromatic Substitution of Tribenzotriquinacenes towards the C3 Isomer. *Angew. Chem. Int. Ed.* **2018,** *57* (35), 11321.
168. Wang, B.; Ma, J.; Lu, L.; Zhu, J.; Wei, D. Method for continuously synthesizing propylene glycol methyl ether acetate by low-temperature high-selectivity catalytic rectification. CN109456190A, 2019.
169. Wang, J.; Li, R.; Dong, Z.; Liu, P.; Dong, G., Complementary site-selectivity in arene functionalization enabled by overcoming the ortho constraint in palladium/norbornene catalysis. *Nature Chem.* **2018,** *10* (8), 866.
170. Wang, J.; Shi, X. In *Novel design and preparation of an triazole-based axial chiral P,N-ligand*, American Chemical Society: 2019; pp ORGN.
171. Wang, J. Z.; Zhou, J.; Xu, C.; Sun, H.; Kurti, L.; Xu, Q. L., Symmetry in Cascade Chirality-Transfer Processes: A Catalytic Atroposelective Direct Arylation Approach to BINOL Derivatives. *J. Am. Chem. Soc.* **2016,** *138* (16), 5202.
172. Wang, S. G.; You, S. L., Hydrogenative dearomatization of pyridine and an asymmetric aza-Friedel-Crafts alkylation sequence. *Angew. Chem. Int. Ed.* **2014,** *53* (8), 2194.
173. Wang, T.; Zhang, Y.-F.; Hou, Q.-Q.; Xu, W.-R.; Cao, X.-P.; Chow, H.-F.; Kuck, D., C3-Symmetrical Tribenzotriquinacene Derivatives: Optical Resolution through Cryptophane Synthesis and Supramolecular Self-Assembly into Nanotubes. *J. Org. Chem.* **2013,** *78* (3), 1062.
174. Watanabe, K.; Koshiba, T.; Yasufuku, Y.; Miyazawa, T.; Ueji, S.-i., Effects of Substituent and Temperature on Enantioselectivity for Lipase-Catalyzed Esterification of 2-(4-Substituted Phenoxy)Propionic Acids in Organic Solvents. *Bioorg. Chem.* **2001,** *29* (2), 65.
175. Wencel-Delord, J.; Panossian, A.; Leroux, F. R.; Colobert, F., Recent advances and new concepts for the synthesis of axially stereoenriched biaryls. *Chem. Soc. Rev.* **2015,** *44* (11), 3418.
176. White, N. G.; MacLachlan, M. J., Soluble Tetraaminotriptycene Precursors. *J. Org. Chem.* **2015,** *80* (16), 8390.
177. Winkler, J. D.; Twenter, B.; Gendrineau, T., Aryl ligation: A new approach to the synthesis of unnatural products. *Heterocycles* **2011,** *84*, 1345.
178. Winkler, J. D.; Twenter, B. M.; Gendrineau, T., Synthesis of substituted phenazines via palladium-catalyzed aryl ligation. *Heterocycles* **2012,** *84* (2), 1345.
179. Wong, W.-S.; Tse, H.-W.; Cheung, E.; Kuck, D.; Chow, H.-F., Enantiopure Aromatic Saddles Bearing the Fenestrindane Core. *J. Org. Chem.* **2019,** *84* (2), 869.
180. Xu, W.-R.; Wang, X.-R.; Chow, H.-F.; Kuck, D., Synthesis and Characterization of Enantiopure Tribenzotriquinacene Dimers Bearing a Platinum-Diacetylene Unit. *Synthesis* **2019**.

181. Xu, X.-N.; Wang, L.; Wang, G.-T.; Lin, J.-B.; Li, G.-Y.; Jiang, X.-K.; Li, Z.-T., Hydrogen-Bonding-Mediated Dynamic Covalent Synthesis of Macrocycles and Capsules: New Receptors for Aliphatic Ammonium Ions and the Formation of Pseudo[3]rotaxanes. *Chem. - Eur. J.* **2009,** *15* (23), 5763.
182. Yadav, D.; Shukla, G.; Ansari, M. A.; Srivastava, A.; Singh, M. S., Chemoselective one-pot access to benzo[e]indole-4,5-diones and naphtho[2,1-b]thiophene-4,5-diones via copper-catalyzed oxidative [3 + 2] annulation of α-oxoketene N,S-acetals/β-ketothioamides with α-/β-naphthols. *Tetrahedron* **2018,** *74* (40), 5920.
183. Young, M. C.; Djernes, K. E.; Payton, J. L.; Liu, D.; Hooley, R. J., Resorcin[4]arenes: A Convenient Scaffold To Study Supramolecular Self-Assembly and Host:Guest Interactions for the Undergraduate Curriculum. *J. Chem. Educ.* **2019**, Ahead of Print.
184. Yuan, Y.; Zheng, M.; Zhao, H.; Kong, L., Solubility Determination and Modeling of p-Nitrobenzamide Dissolved in Twelve Neat Solvents from 283.15 to 328.15 K. *J. Chem. Eng. Data* **2019**, Ahead of Print.
185. Zhang, G.; Mastalerz, M., Organic cage compounds - from shape-persistency to function. *Chem. Soc. Rev.* **2014,** *43* (6), 1934.
186. Zhang, N.-N.; Sa, R.-J.; Sun, S.-S.; Li, M.-D.; Wang, M.-S.; Guo, G.-C., Photoresponsive triazole-based donor-acceptor molecules: color change and heat/air-stable diradicals. *J. Mater. Chem. C* **2019**, Ahead of Print.
187. Zhao, L.; Li, Z.; Wirth, T., Triptycene derivatives: synthesis and applications. *Chem. Lett.* **2010,** *39* (7), 658.
188. Zhao, Y.; Truhlar, D. G., Density functionals with broad applicability in chemistry. *Acc Chem Res* **2008,** *41* (2), 157.

Appendix I

^{1}H NMR, and ^{13}C NMR Spectra

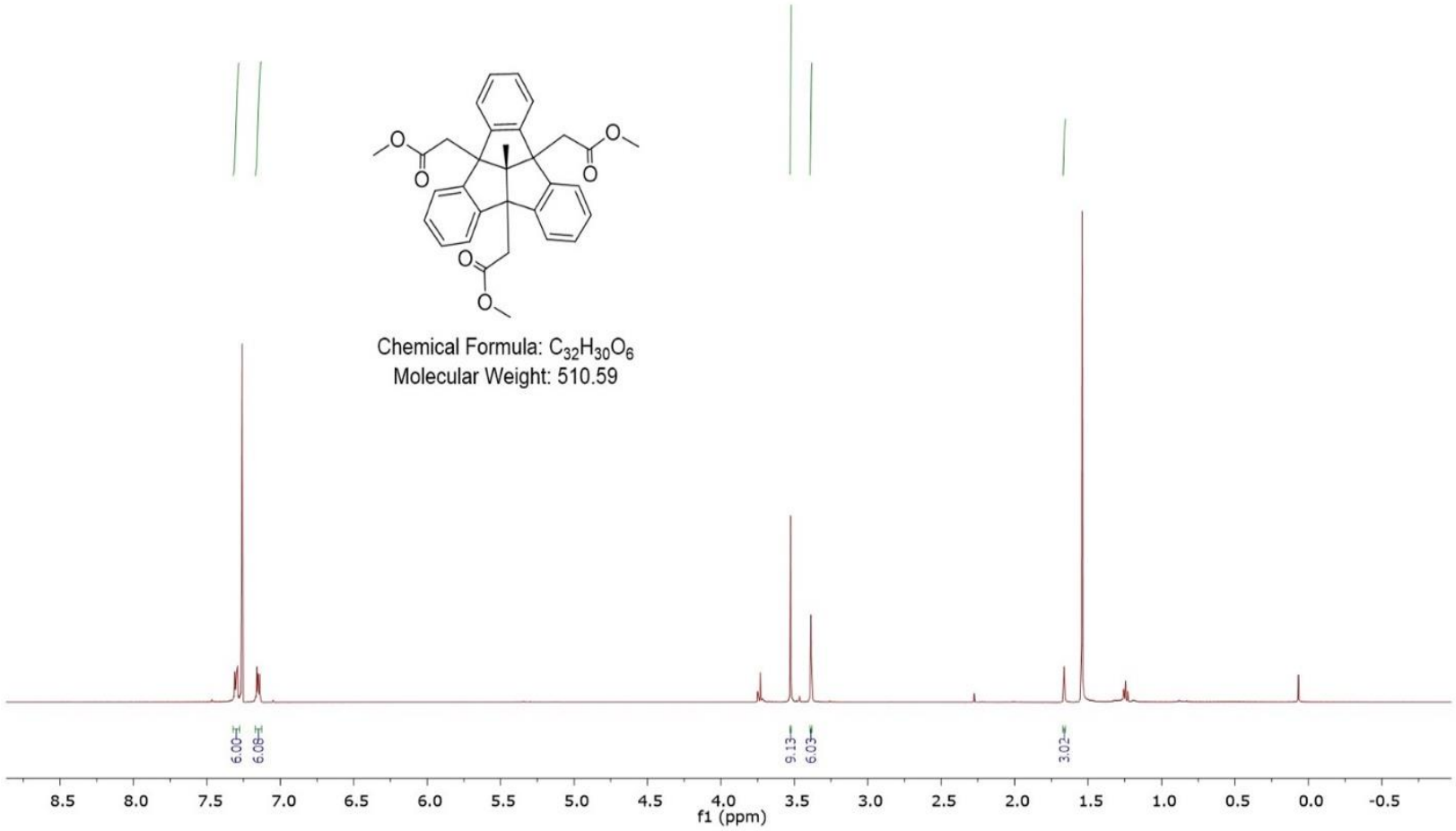
Chemical Formula: $C_{32}H_{30}O_6$
Molecular Weight: 510.59
6.00
6.08
9.13
6.03
3.02
8.5
8.0
7.5
7.0
6.5
6.0
5.5
5.0
4.5
4.0
3.5
3.0
2.5
2.0
1.5
1.0
0.5
0.0
-0.5
f1 (ppm)

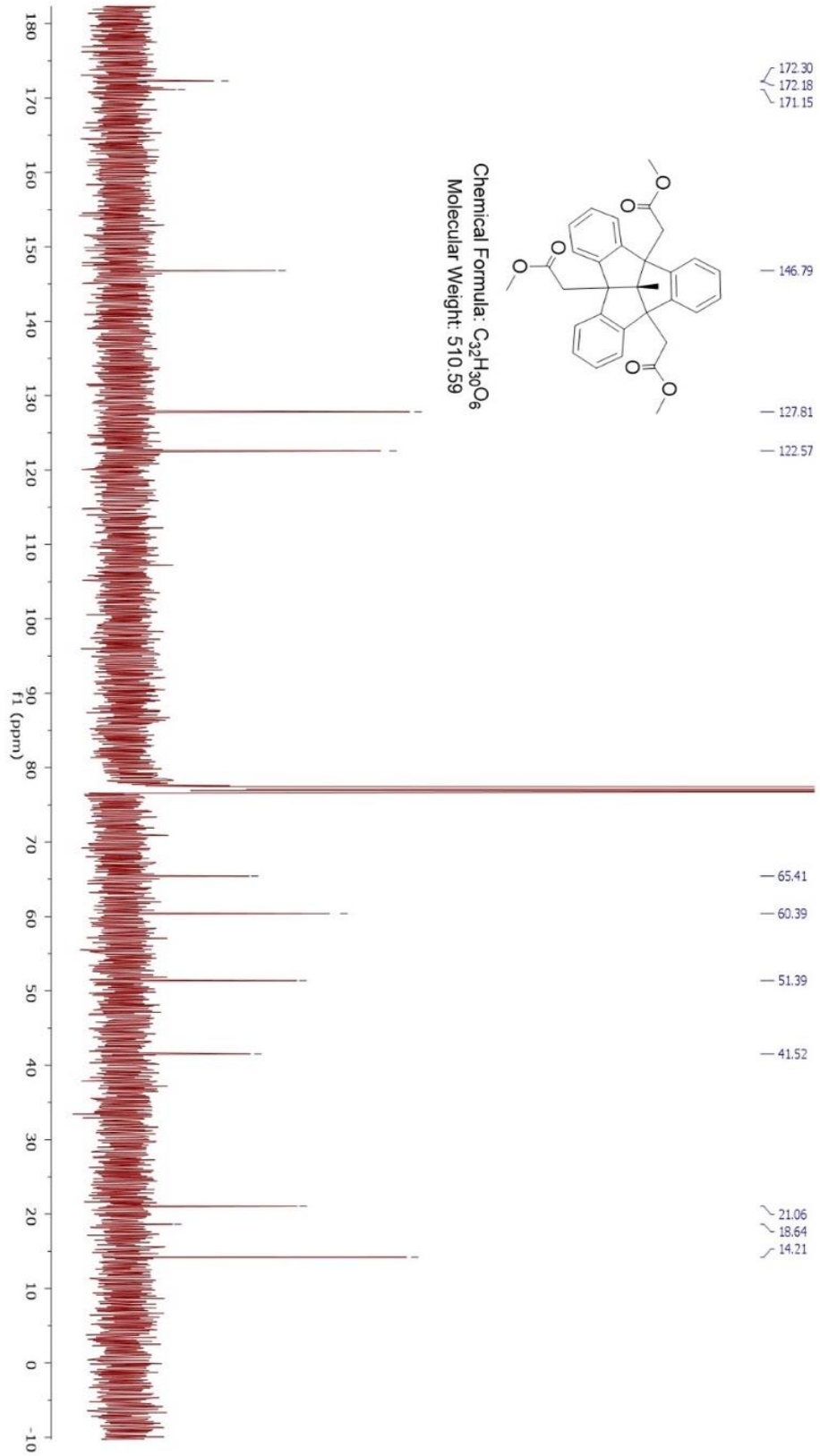
Chemical Formula: C32H30O6
Molecular Weight: 510.59
172.30
172.18
171.15
146.79
127.81
122.57
65.41
60.39
51.39
41.52
21.06
18.64
14.21
f1 (ppm)

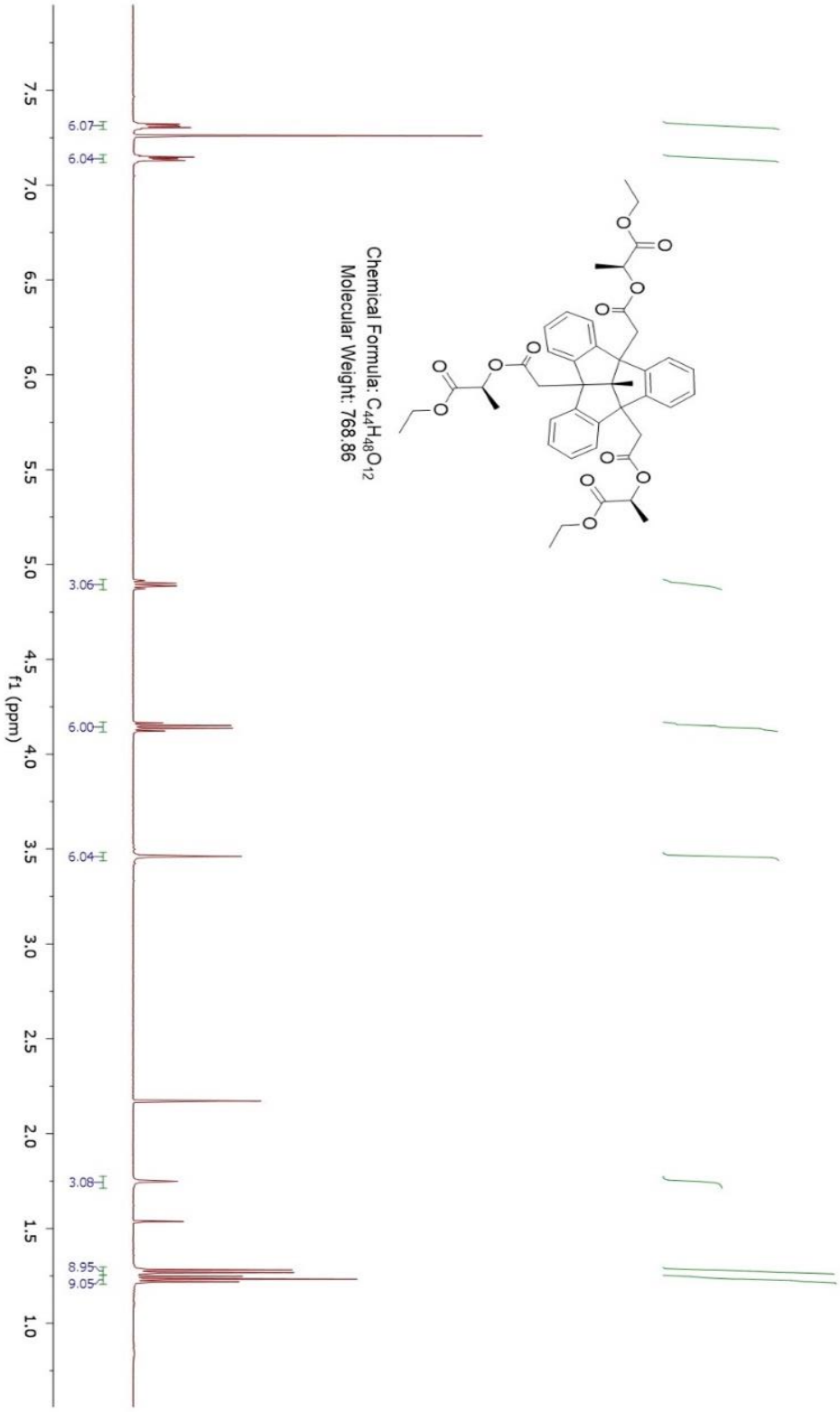
Chemical Formula: C44H48O12
Molecular Weight: 768.86
6.07
6.04
3.06
6.00
6.04
3.08
8.95
9.05
f1 (ppm)

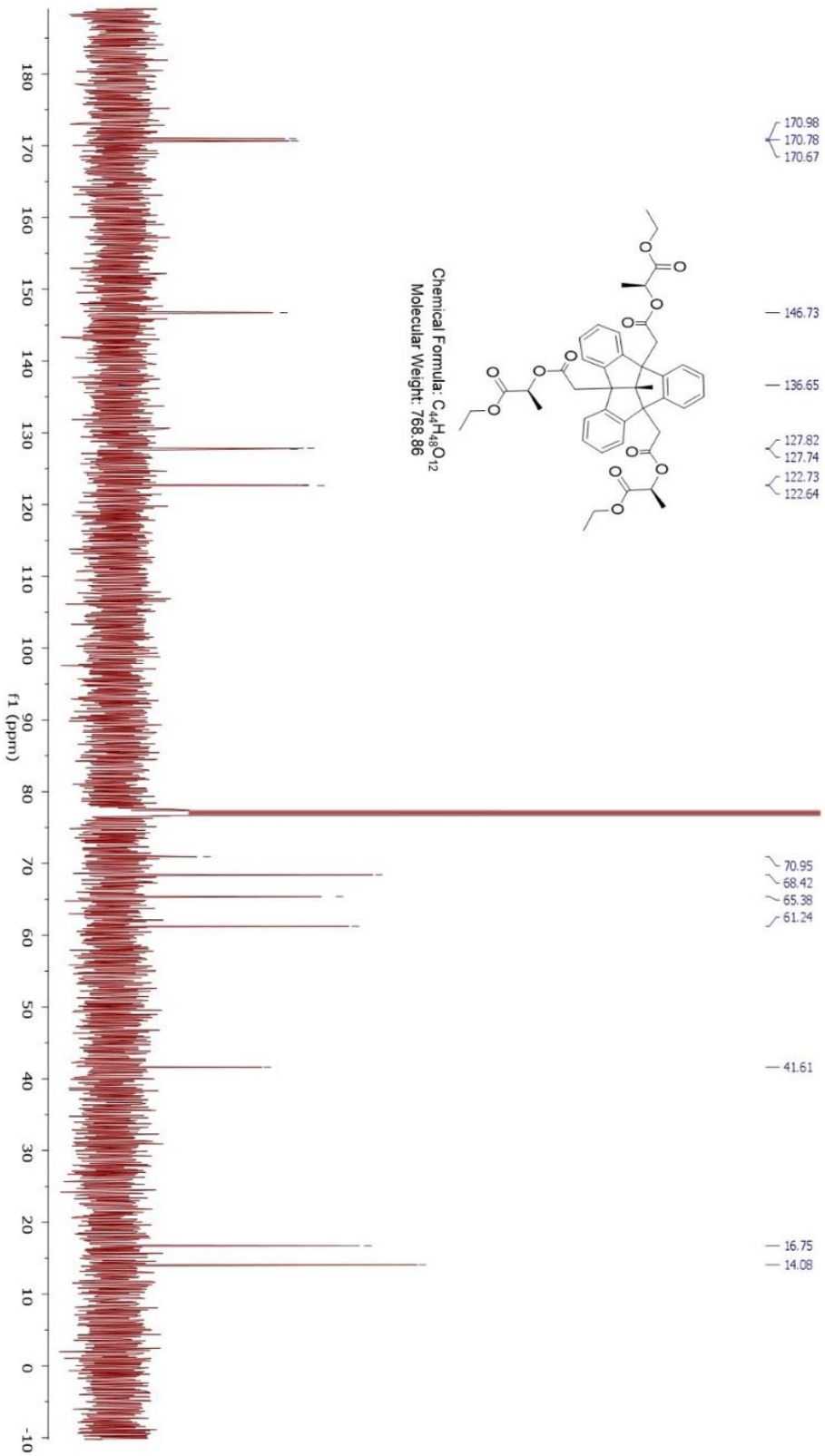
Chemical Formula: $C_{44}H_{48}O_{12}$
Molecular Weight: 768.86
170.98
170.78
170.67
146.73
136.65
127.82
127.74
122.73
122.64
70.95
68.42
65.38
61.24
41.61
16.75
14.08
f1 (ppm)

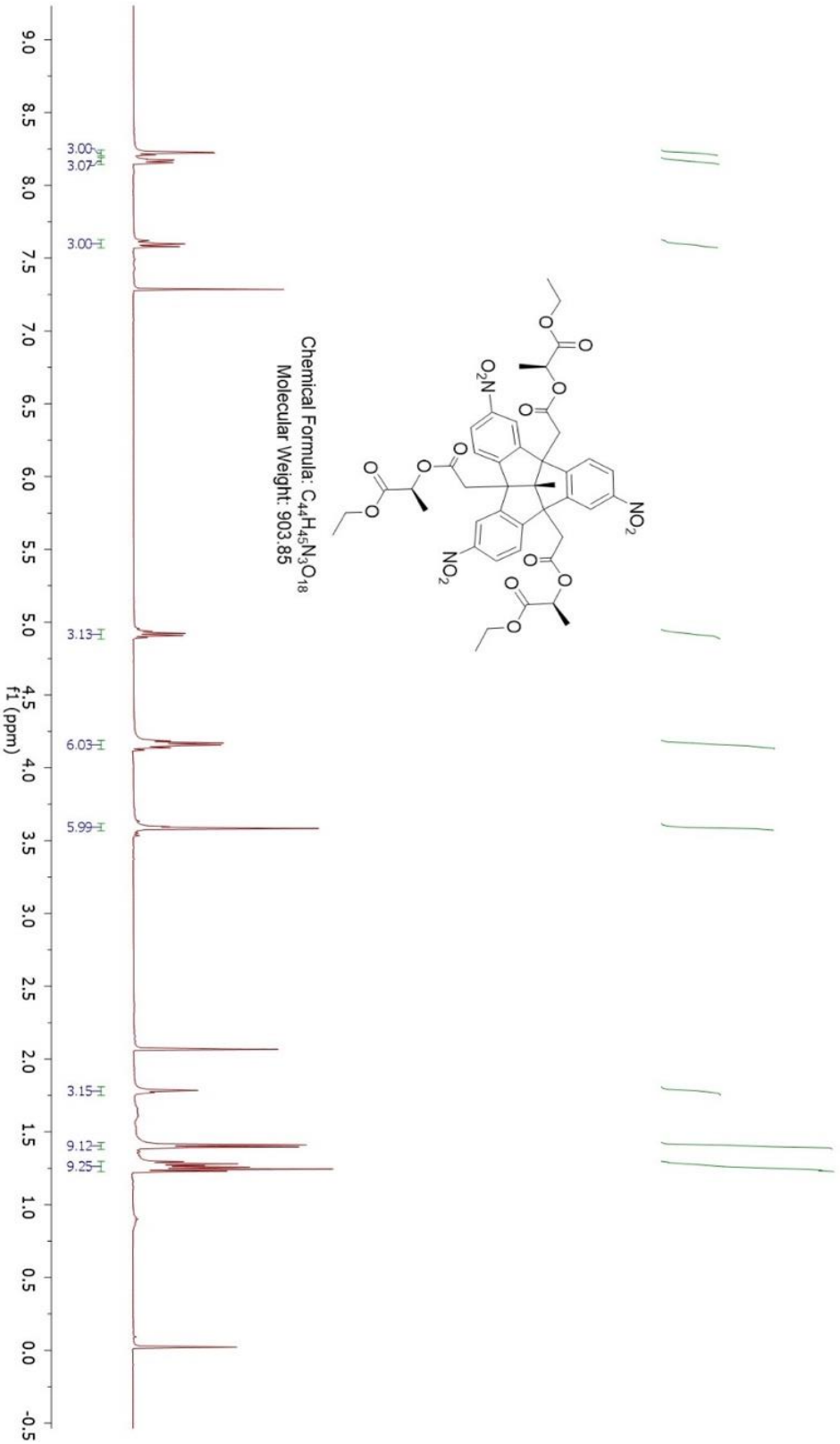
Chemical Formula: $C_{44}H_{45}N_3O_{18}$
Molecular Weight: 903.85
O_2N
NO_2
NO_2
3.00
3.07
3.00
3.13
6.03
5.99
3.15
9.12
9.25
f1 (ppm)

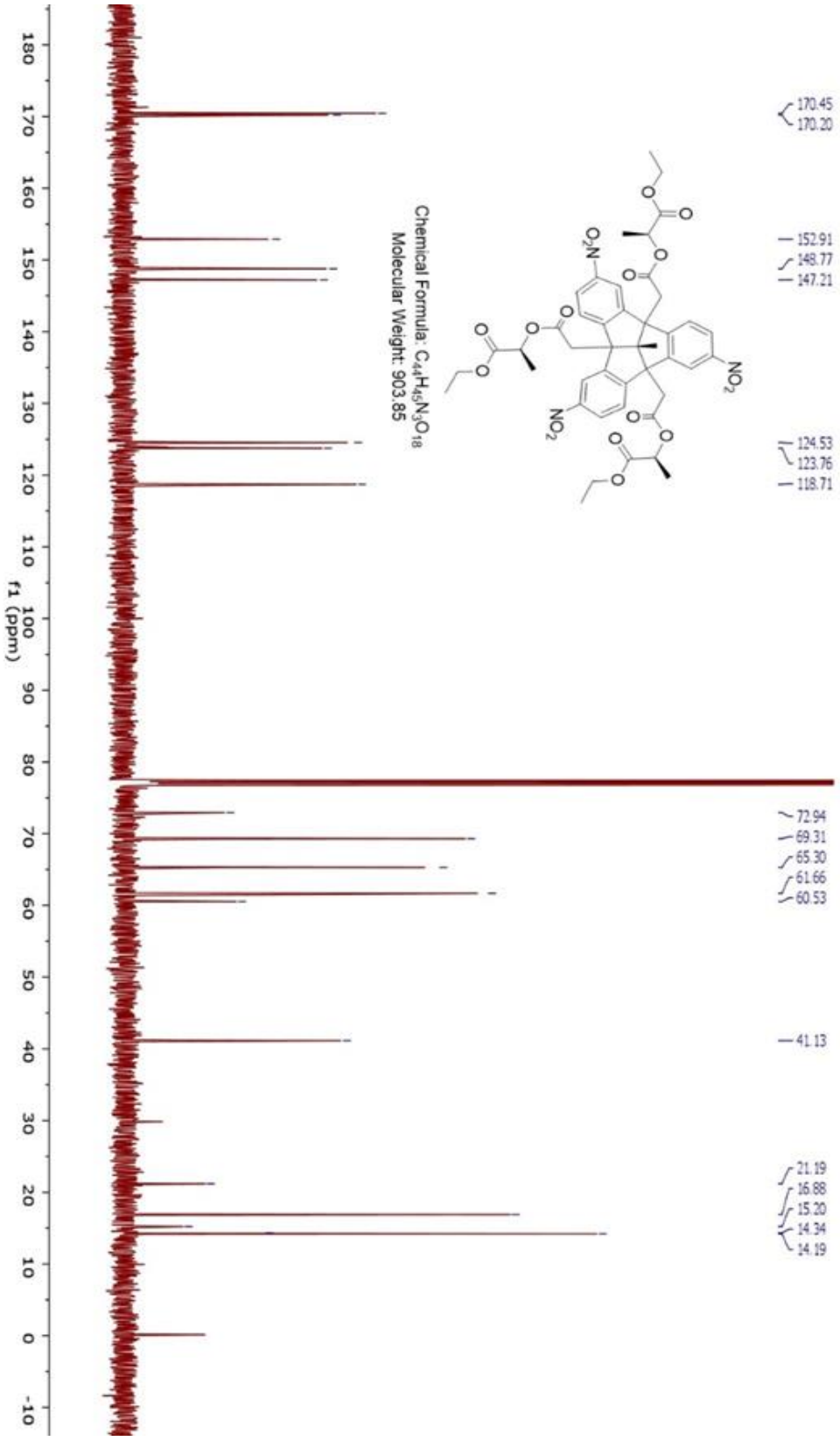
Chemical Formula: C44H45N3O18
Molecular Weight: 903.85
170.45
170.20
152.91
148.77
147.21
124.53
123.76
118.71
72.94
69.31
65.30
61.66
60.53
41.13
21.19
16.88
15.20
14.34
14.19
f1 (ppm)

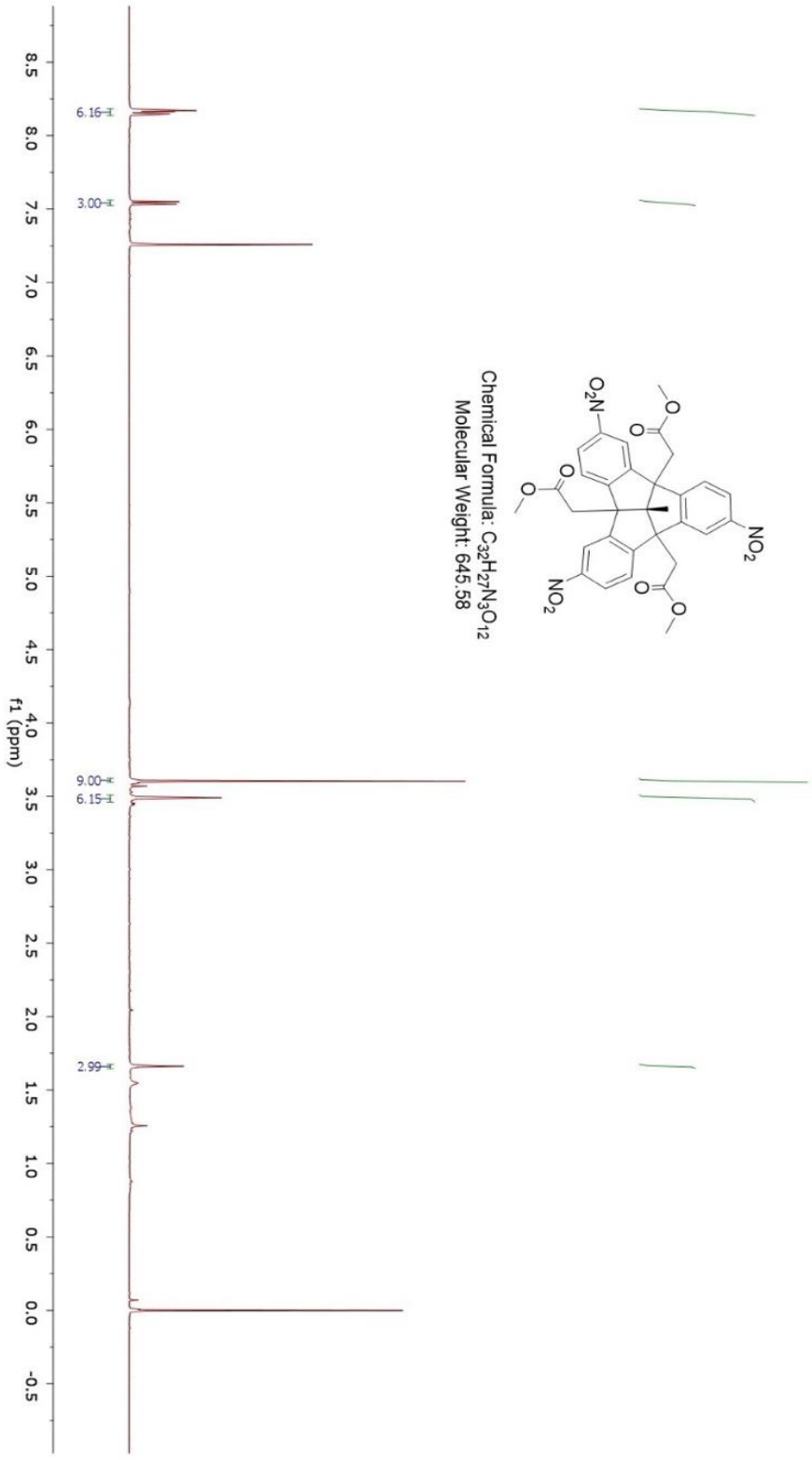
Chemical Formula: $C_{32}H_{27}N_3O_{12}$
Molecular Weight: 645.58
O_2N
NO_2
NO_2
6.16
3.00
9.00
6.15
2.99
f1 (ppm)

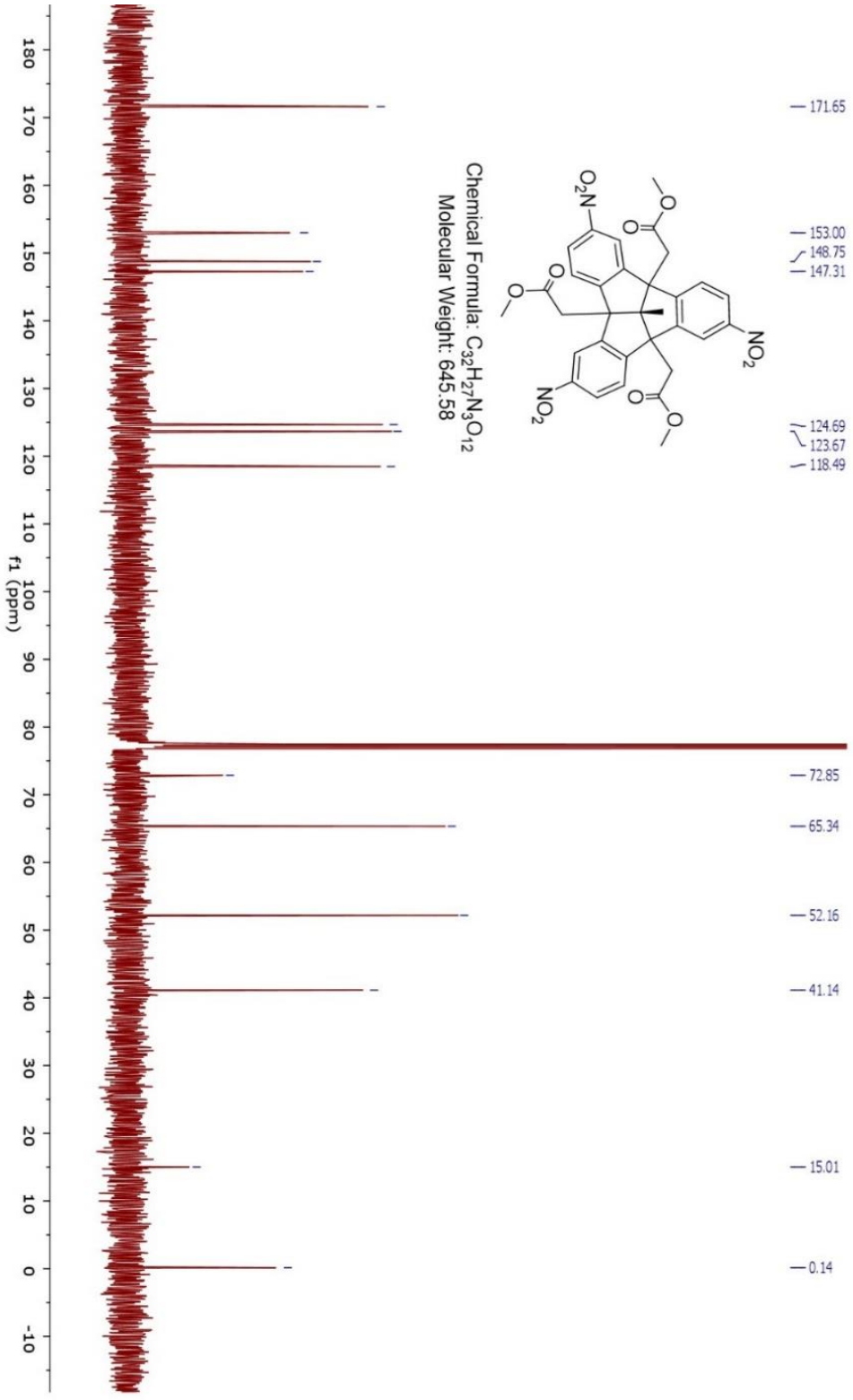
Chemical Formula: $C_{32}H_{27}N_3O_{12}$
Molecular Weight: 645.58
171.65
153.00
148.75
147.31
124.69
123.67
118.49
72.85
65.34
52.16
41.14
15.01
0.14
f1 (ppm)

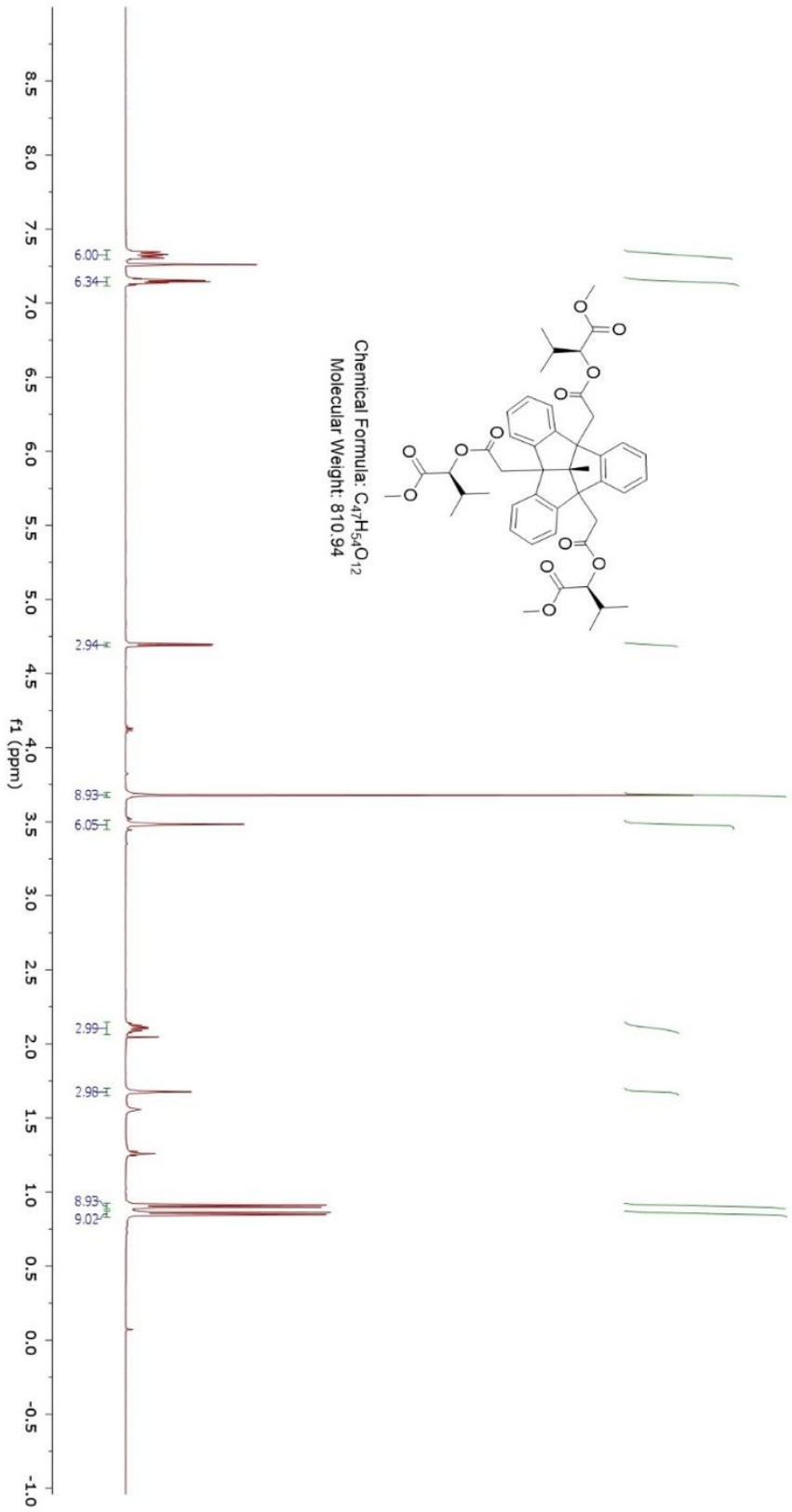
Chemical Formula: C47H54O12
Molecular Weight: 810.94
6.00
6.34
2.94
8.93
6.05
2.99
2.98
8.93
9.02
f1 (ppm)

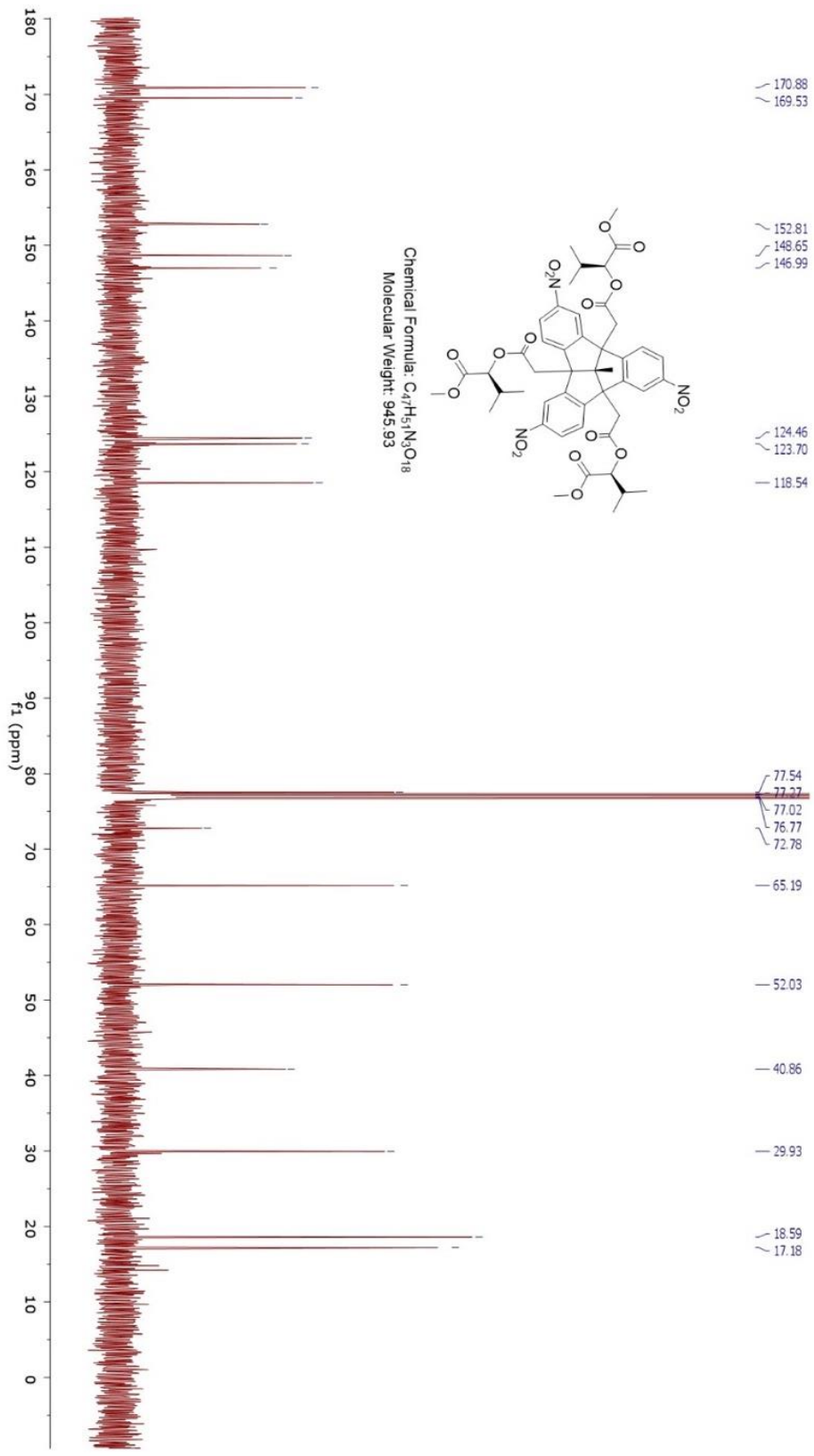
Chemical Formula: C47H51N3O18
Molecular Weight: 945.93
170.88
169.53
152.81
148.65
146.99
124.46
123.70
118.54
77.54
77.27
77.02
76.77
72.78
65.19
52.03
40.86
29.93
18.59
17.18
f1 (ppm)

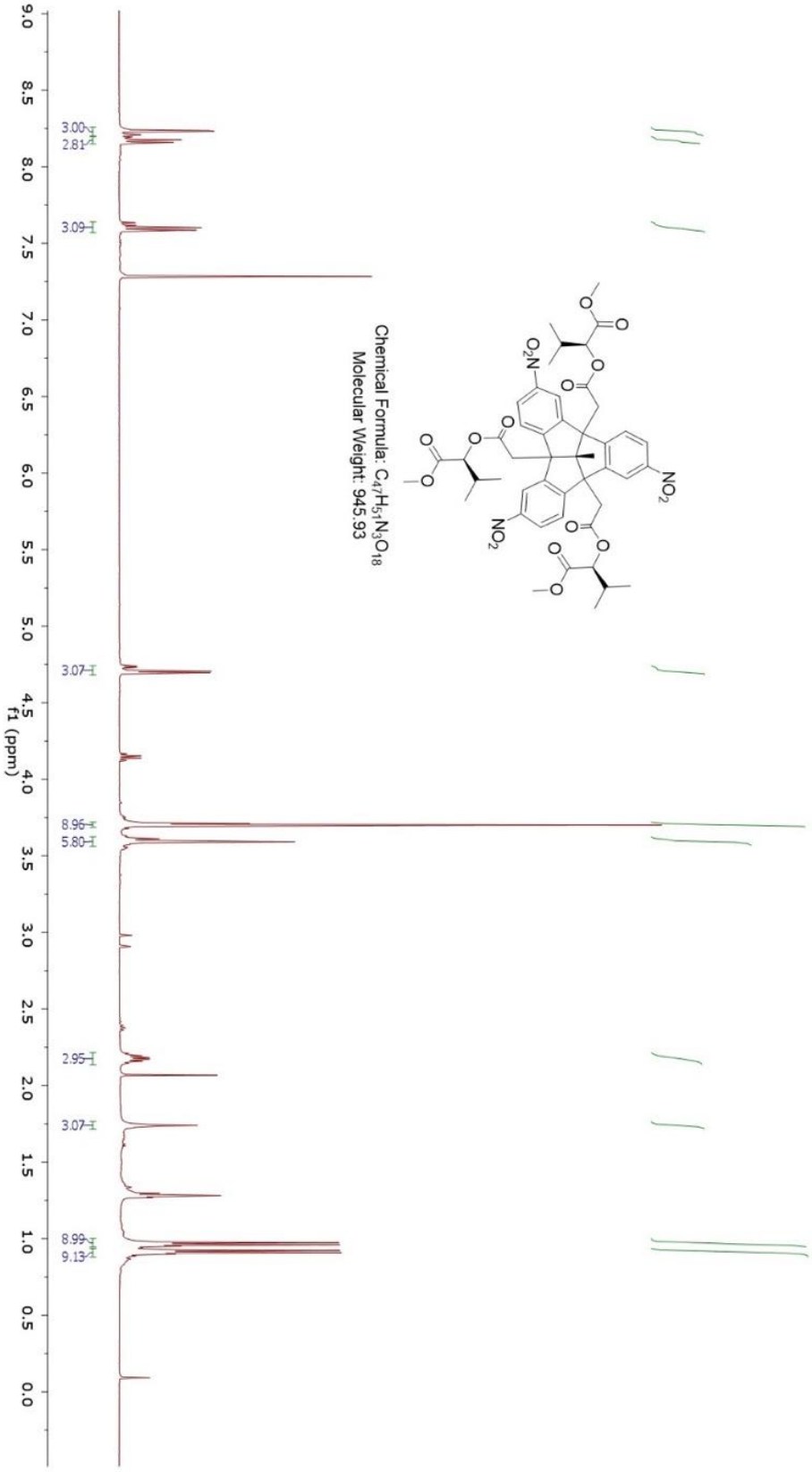
Chemical Formula: $C_{47}H_{51}N_3O_{18}$
Molecular Weight: 945.93
O_2N
NO_2
NO_2
3.00
2.81
3.09
3.07
8.96
5.80
2.95
3.07
8.99
9.13
f1 (ppm)

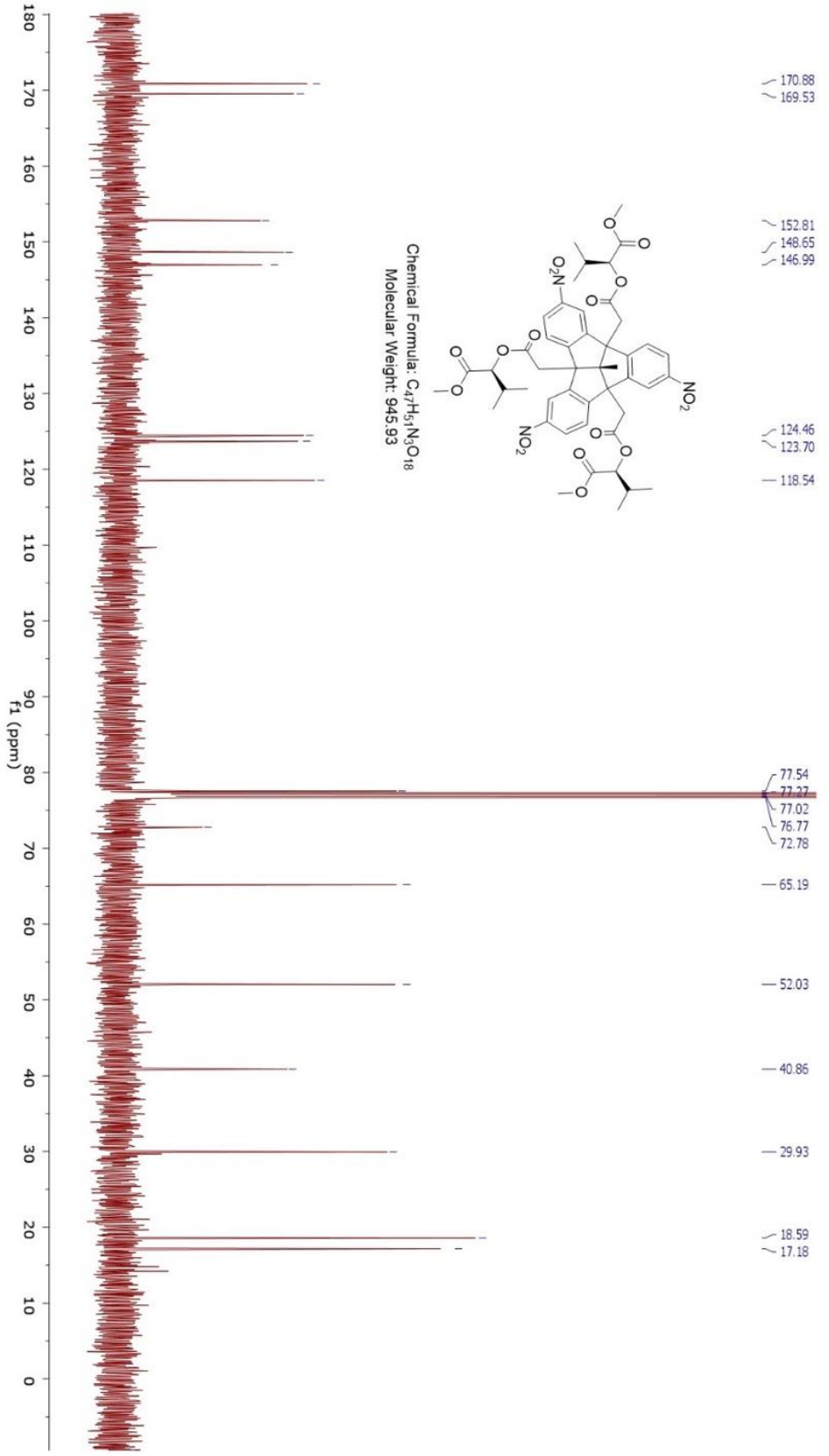
Chemical Formula: $C_{47}H_{51}N_3O_{18}$
Molecular Weight: 945.93
170.88
169.53
152.81
148.65
146.99
124.46
123.70
118.54
77.54
77.27
77.02
76.77
72.78
65.19
52.03
40.86
29.93
18.59
17.18
f1 (ppm)

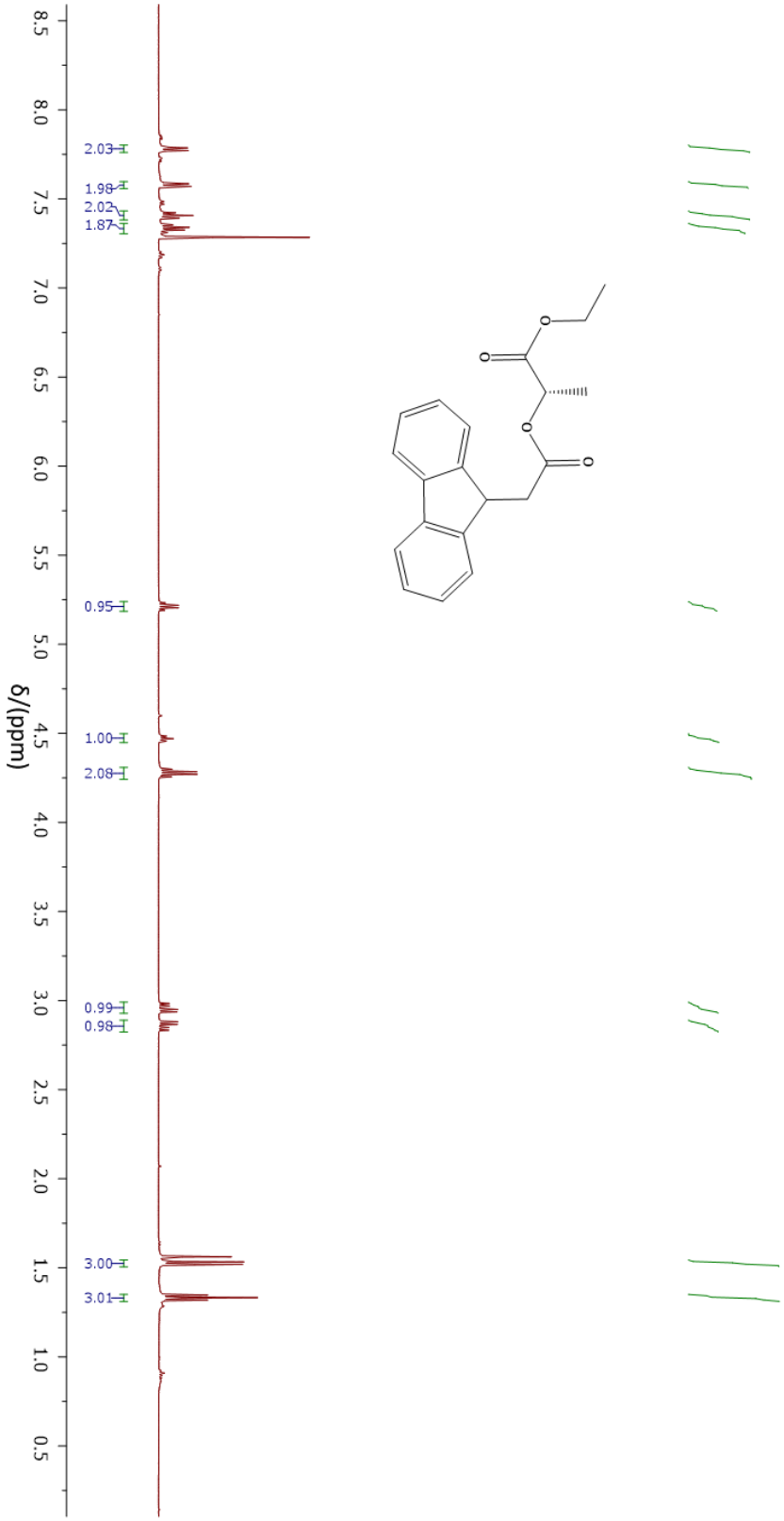
δ/(ppm)
8.5
8.0
7.5
7.0
6.5
6.0
5.5
5.0
4.5
4.0
3.5
3.0
2.5
2.0
1.5
1.0
0.5
2.03
1.98
2.02
1.87
0.95
1.00
2.08
0.99
0.98
3.00
3.01
O
O
O
O

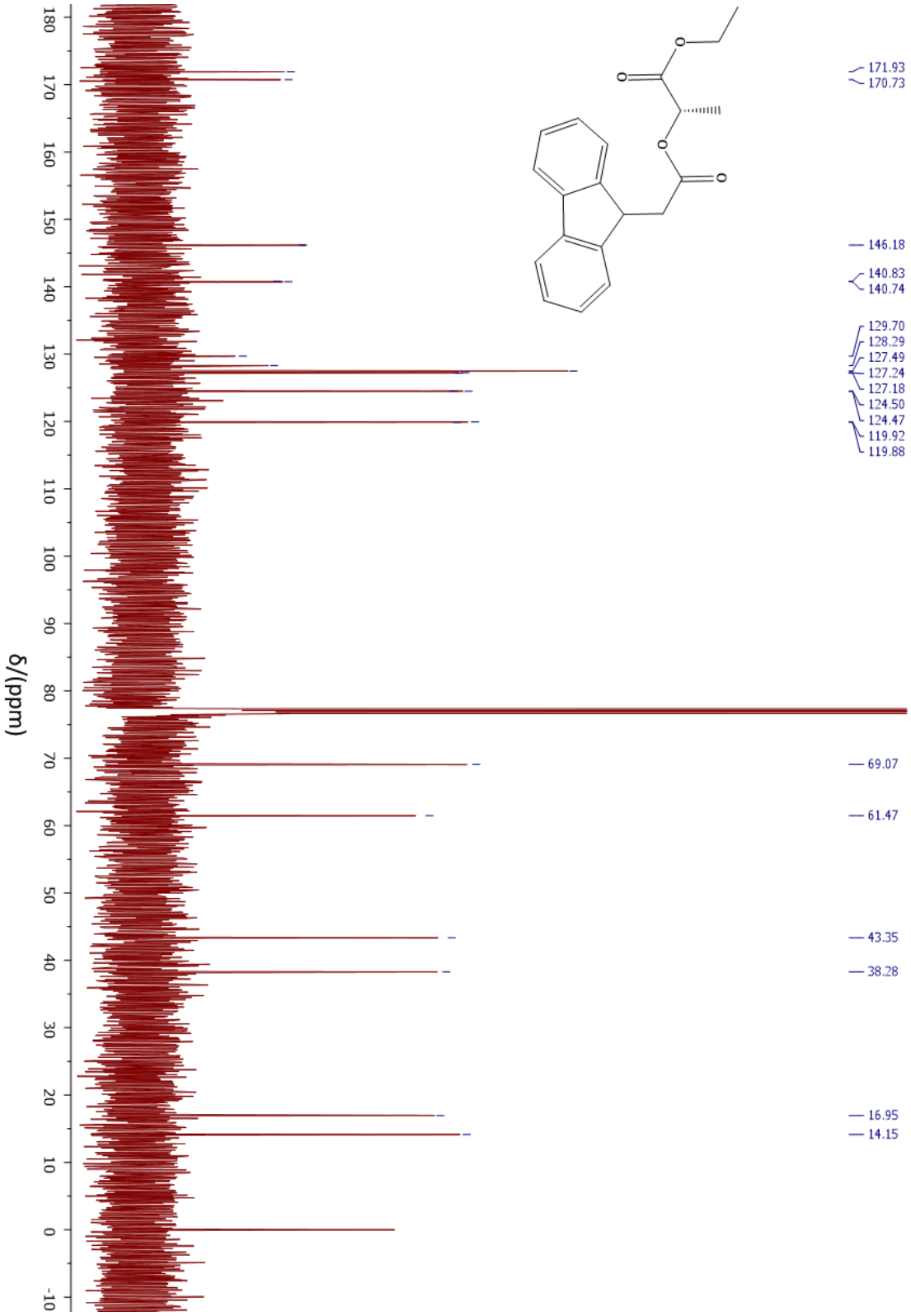
δ/(ppm)
180
170
160
150
140
130
120
110
100
90
80
70
60
50
40
30
20
10
0
-10
171.93
170.73
146.18
140.83
140.74
129.70
128.29
127.49
127.24
127.18
124.50
124.47
119.92
119.88
69.07
61.47
43.35
38.28
16.95
14.15

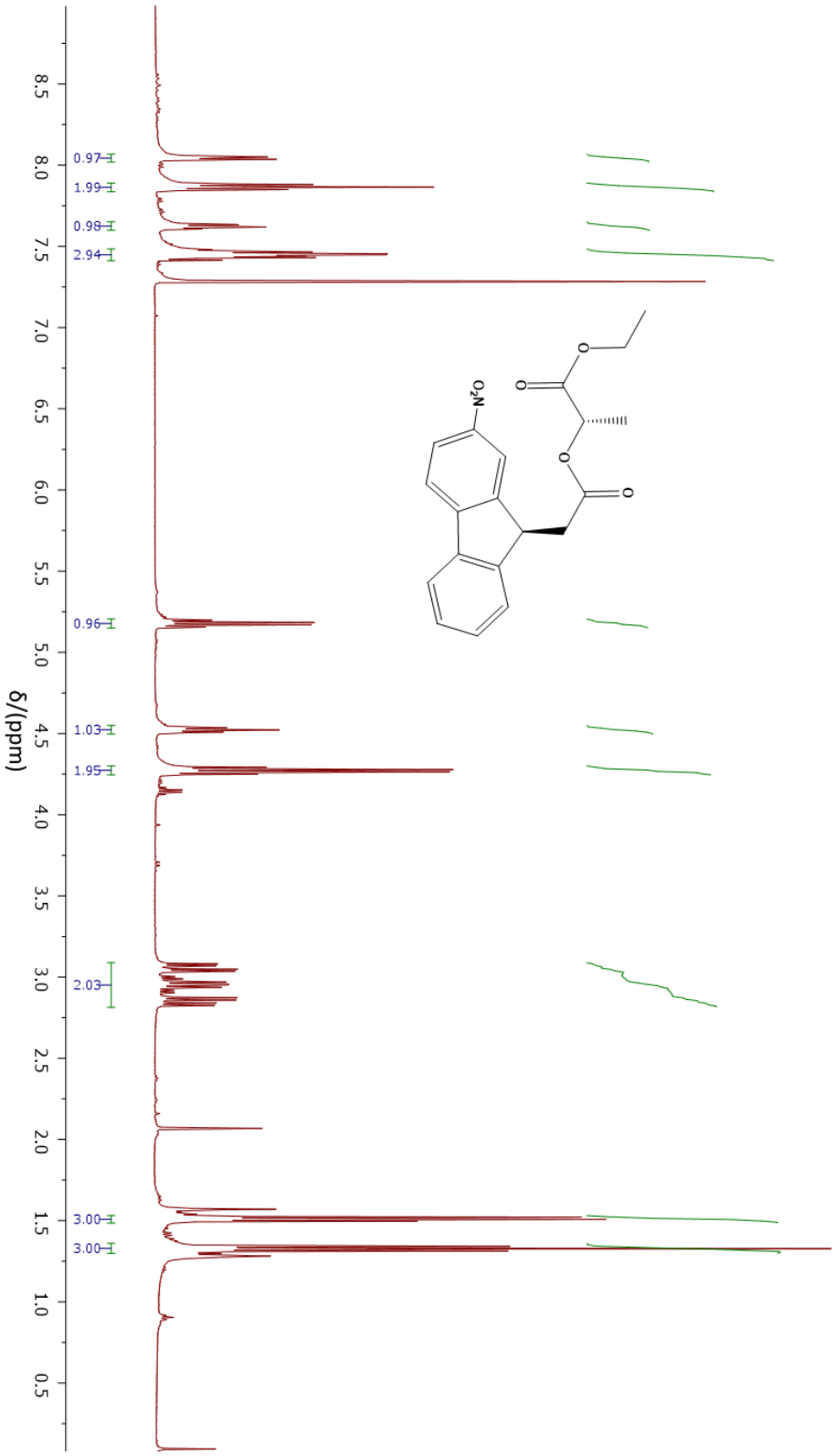
δ/(ppm)
8.5
8.0
7.5
7.0
6.5
6.0
5.5
5.0
4.5
4.0
3.5
3.0
2.5
2.0
1.5
1.0
0.5
0.97
1.99
0.98
2.94
0.96
1.03
1.95
2.03
3.00
3.00
O2N
O
O
O
O

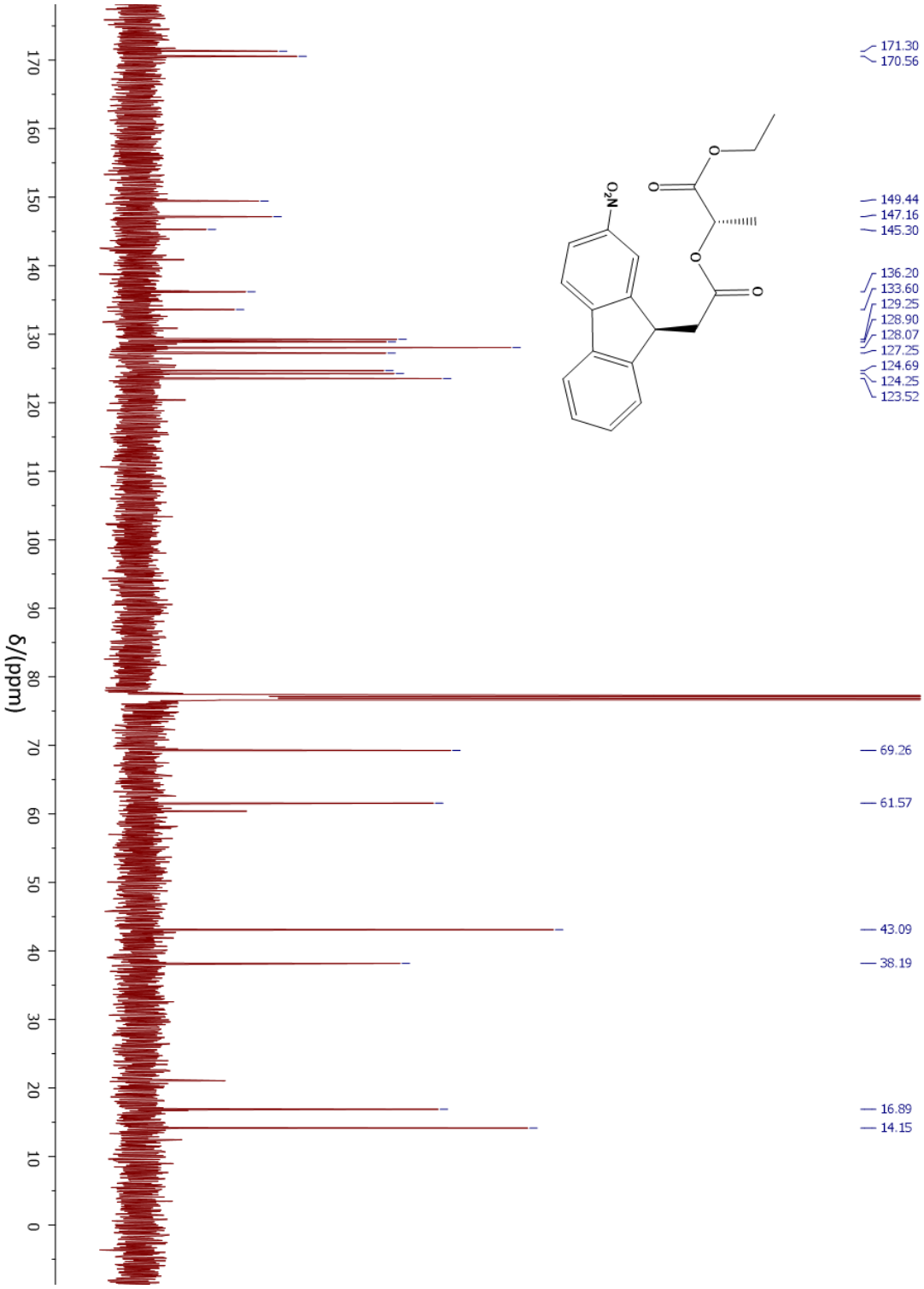
171.30
170.56
149.44
147.16
145.30
136.20
133.60
129.25
128.90
128.07
127.25
124.69
124.25
123.52
69.26
61.57
43.09
38.19
16.89
14.15
δ/(ppm)

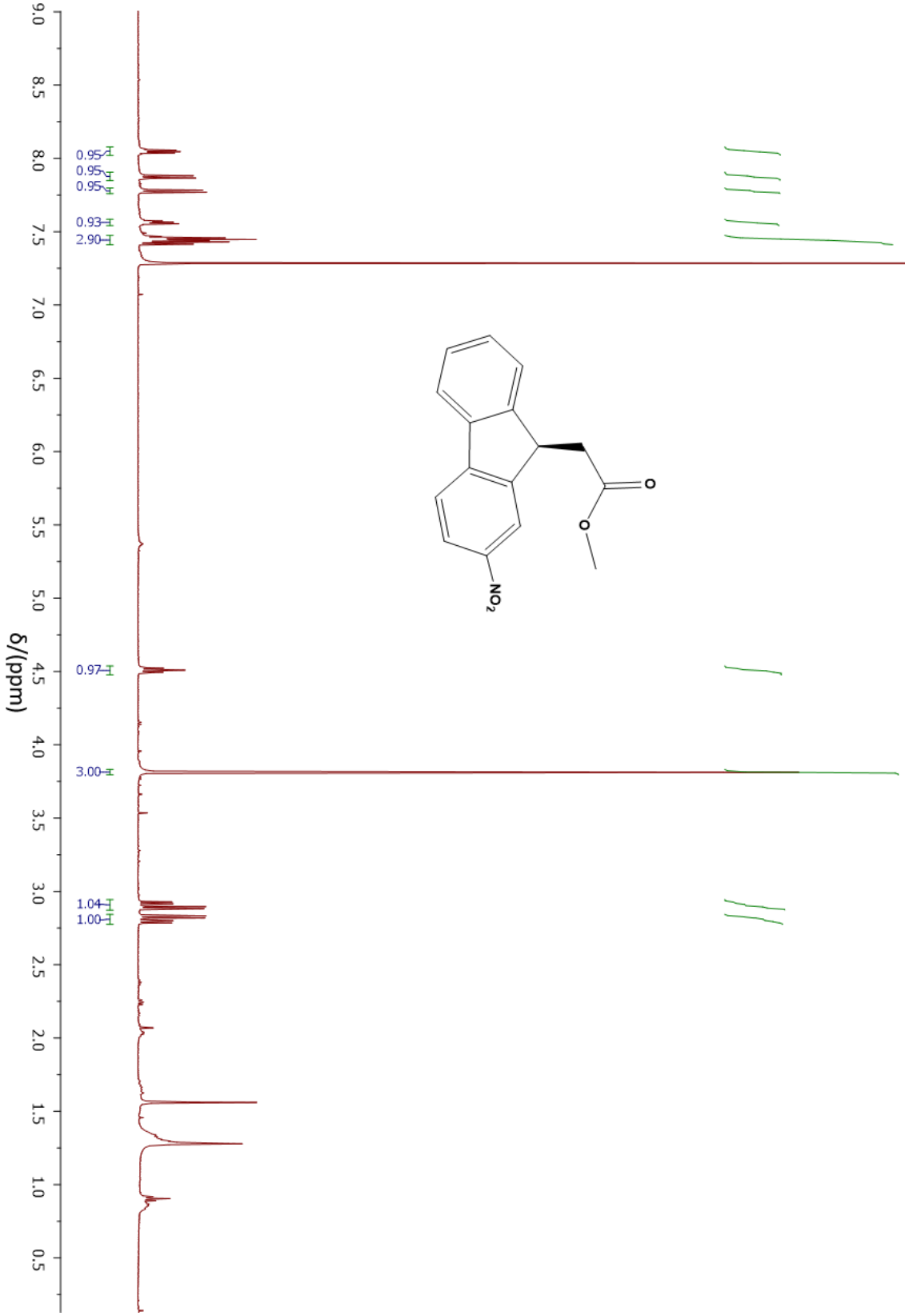
9.0
8.5
8.0
7.5
7.0
6.5
6.0
5.5
5.0
4.5
4.0
3.5
3.0
2.5
2.0
1.5
1.0
0.5
δ/(ppm)
0.95
0.95
0.95
0.93
2.90
0.97
3.00
1.04
1.00
O
O
NO2

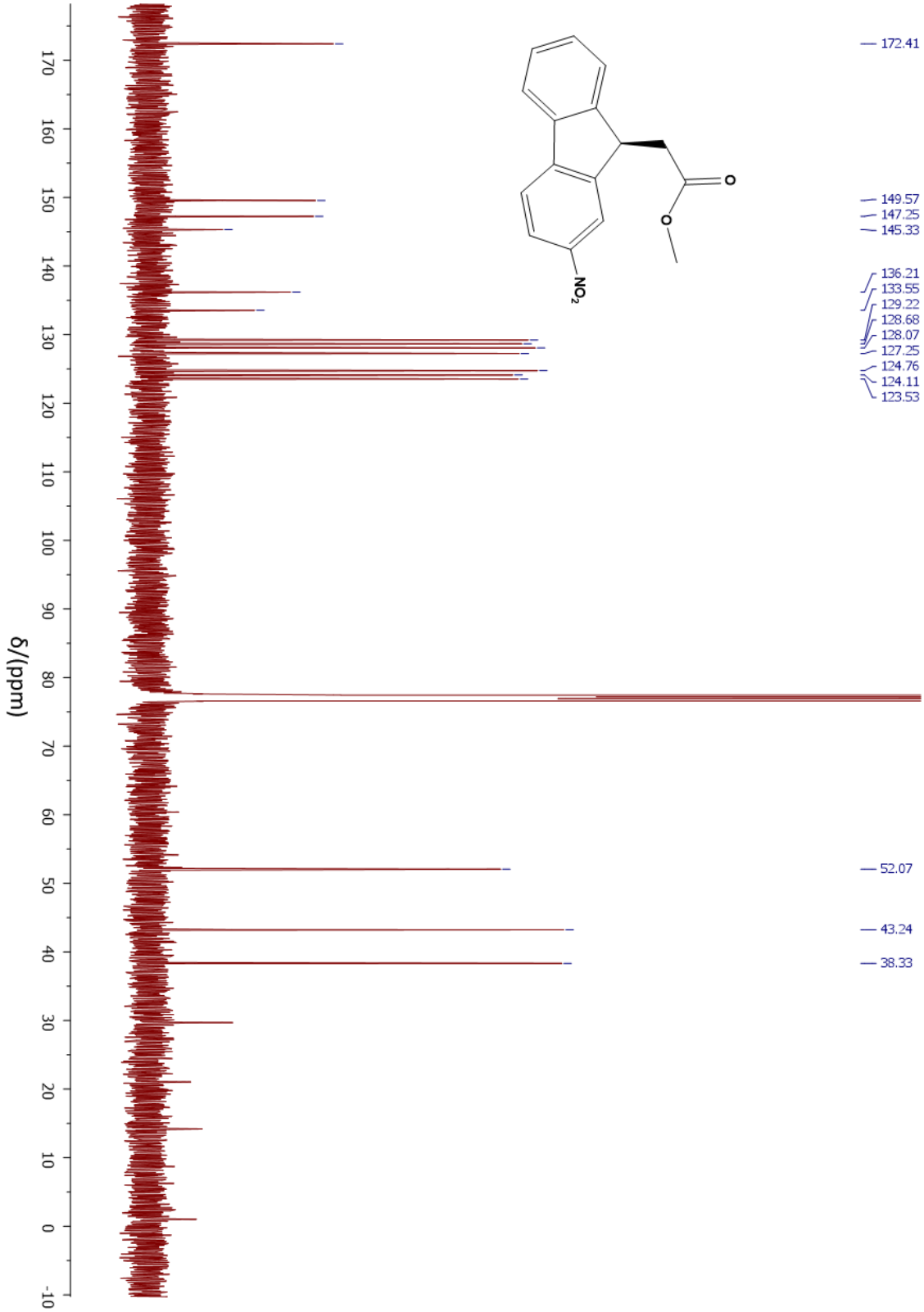
172.41
149.57
147.25
145.33
136.21
133.55
129.22
128.68
128.07
127.25
124.76
124.11
123.53
52.07
43.24
38.33
O
O
NO2
δ/(ppm)
170
160
150
140
130
120
110
100
90
80
70
60
50
40
30
20
10
0
-10

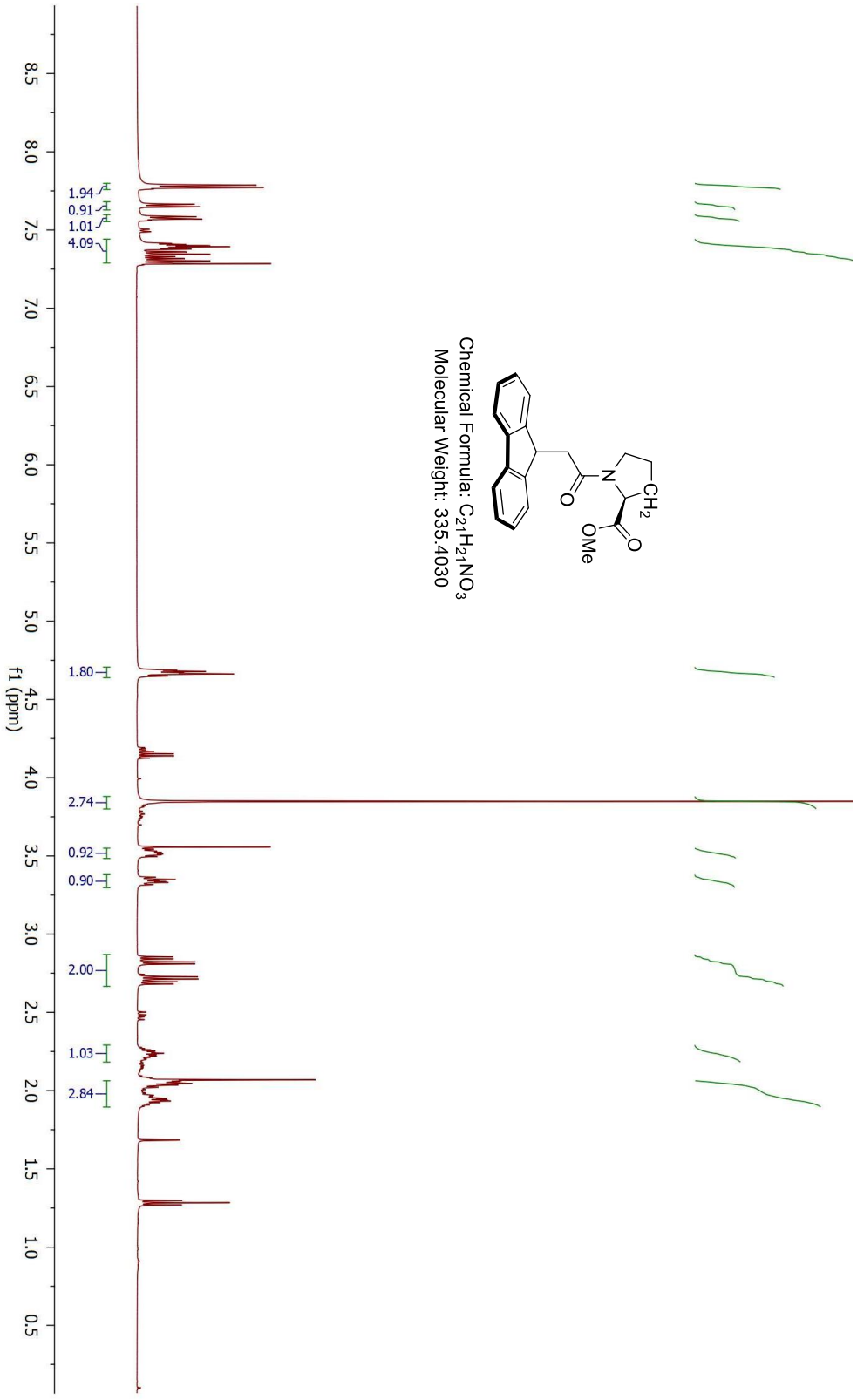
Chemical Formula: C21H21NO3
Molecular Weight: 335.4030
OMe
CH2
1.94
0.91
1.01
4.09
1.80
2.74
0.92
0.90
2.00
1.03
2.84
f1 (ppm)

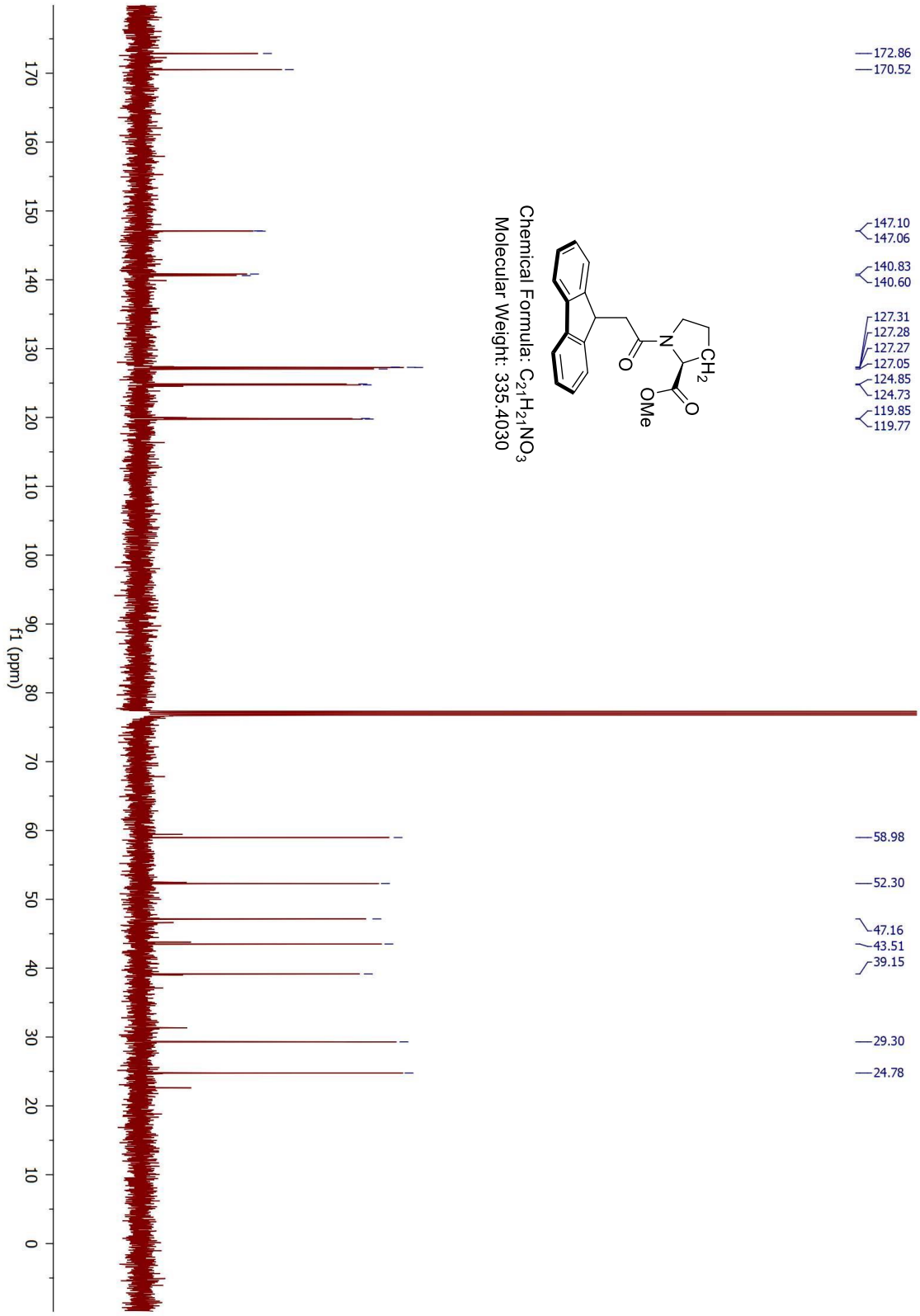
Chemical Formula: C21H21NO3
Molecular Weight: 335.4030
172.86
170.52
147.10
147.06
140.83
140.60
127.31
127.28
127.27
127.05
124.85
124.73
119.85
119.77
58.98
52.30
47.16
43.51
39.15
29.30
24.78
f1 (ppm)

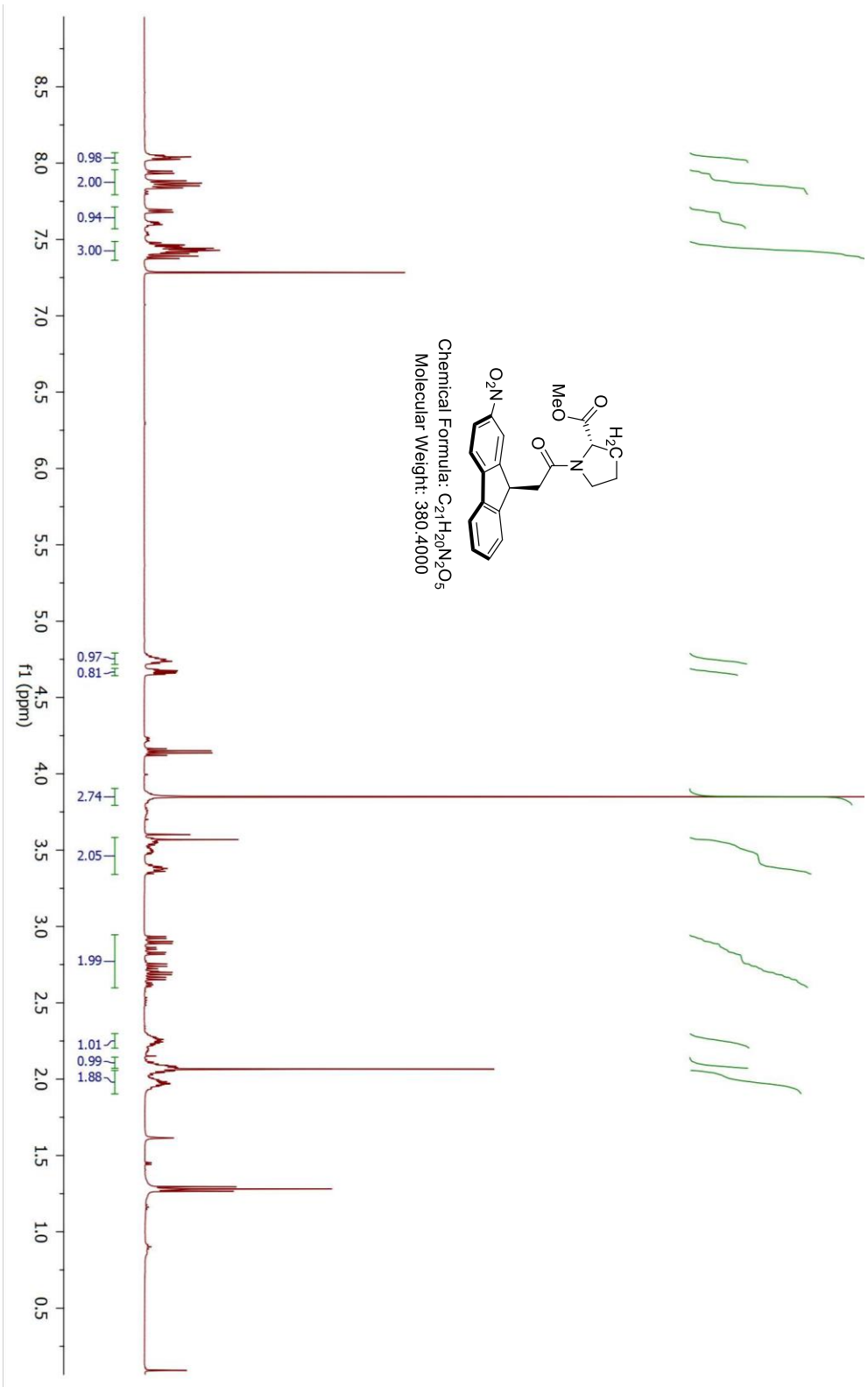
Chemical Formula: C21H20N2O5
Molecular Weight: 380.4000
O2N
MeO
O
H2C
N
f1 (ppm)
0.98
2.00
0.94
3.00
0.97
0.81
2.74
2.05
1.99
1.01
0.99
1.88

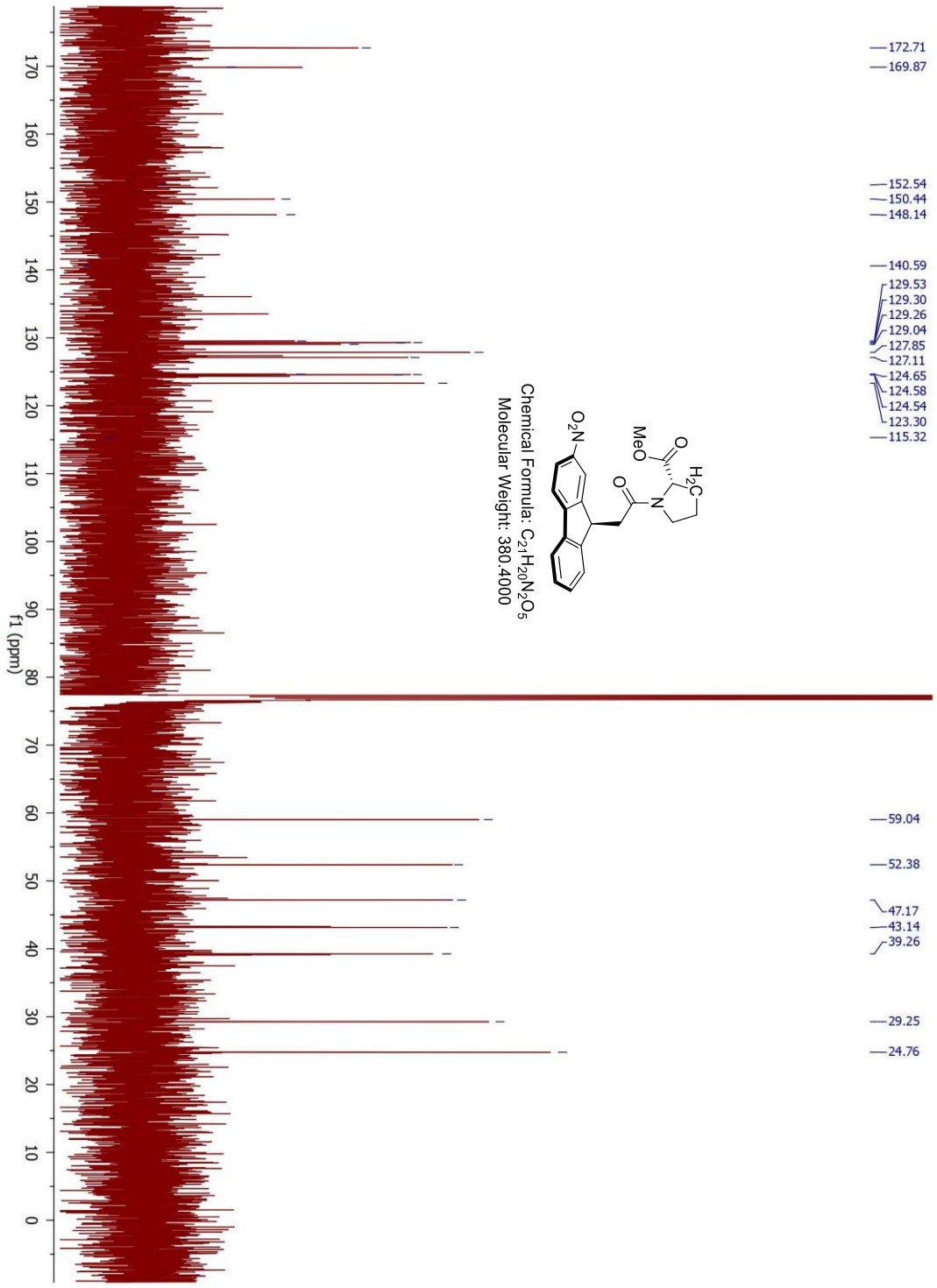
172.71
169.87
152.54
150.44
148.14
140.59
129.53
129.30
129.26
129.04
127.85
127.11
124.65
124.58
124.54
123.30
115.32
59.04
52.38
47.17
43.14
39.26
29.25
24.76
f1 (ppm)
Chemical Formula: C21H20N2O5
Molecular Weight: 380.4000

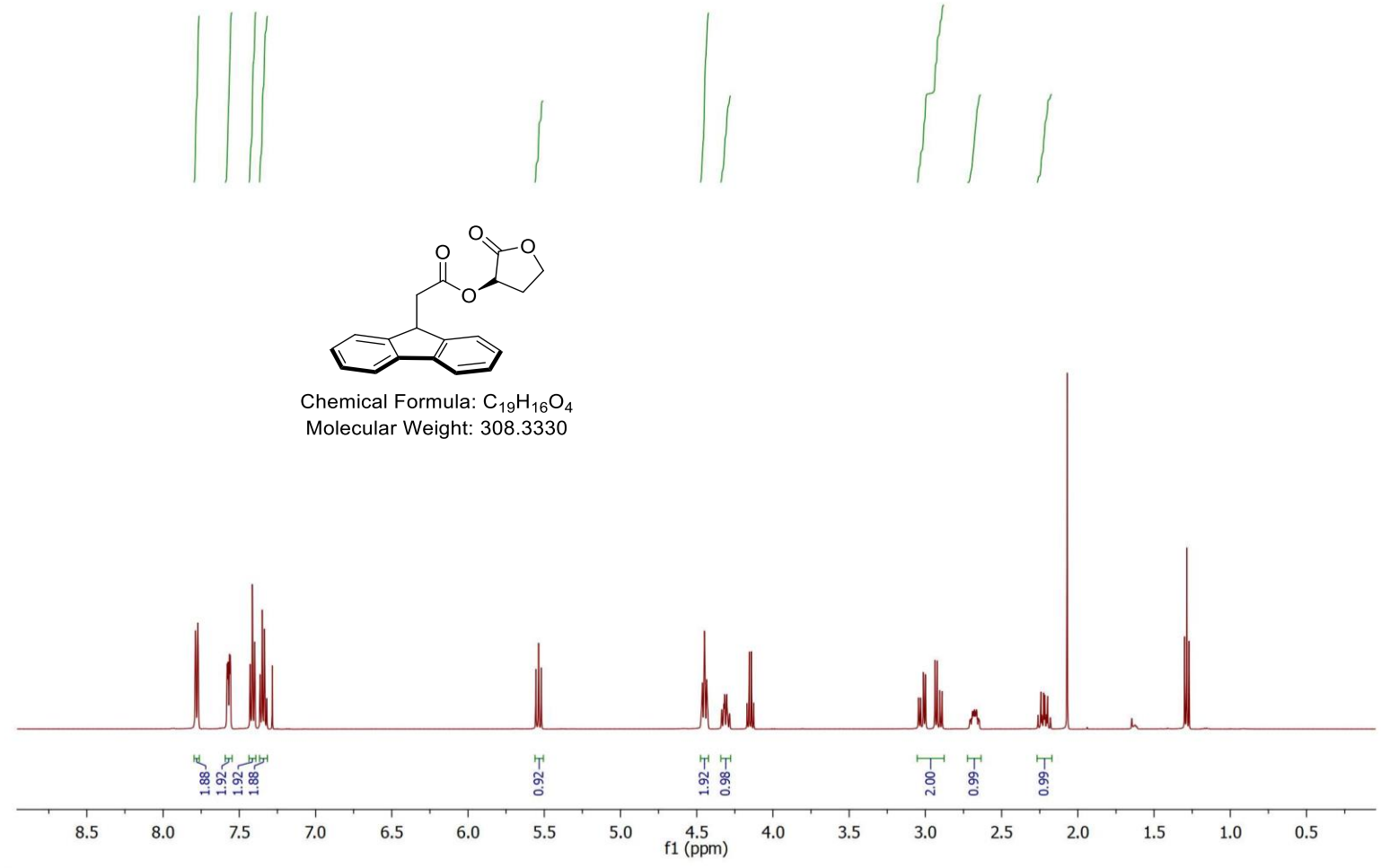
Chemical Formula: $C_{19}H_{16}O_4$
Molecular Weight: 308.3330
1.88
1.92
1.92
1.88
0.92
1.92
0.98
2.00
0.99
0.99
8.5
8.0
7.5
7.0
6.5
6.0
5.5
5.0
4.5
4.0
3.5
3.0
2.5
2.0
1.5
1.0
0.5
f1 (ppm)

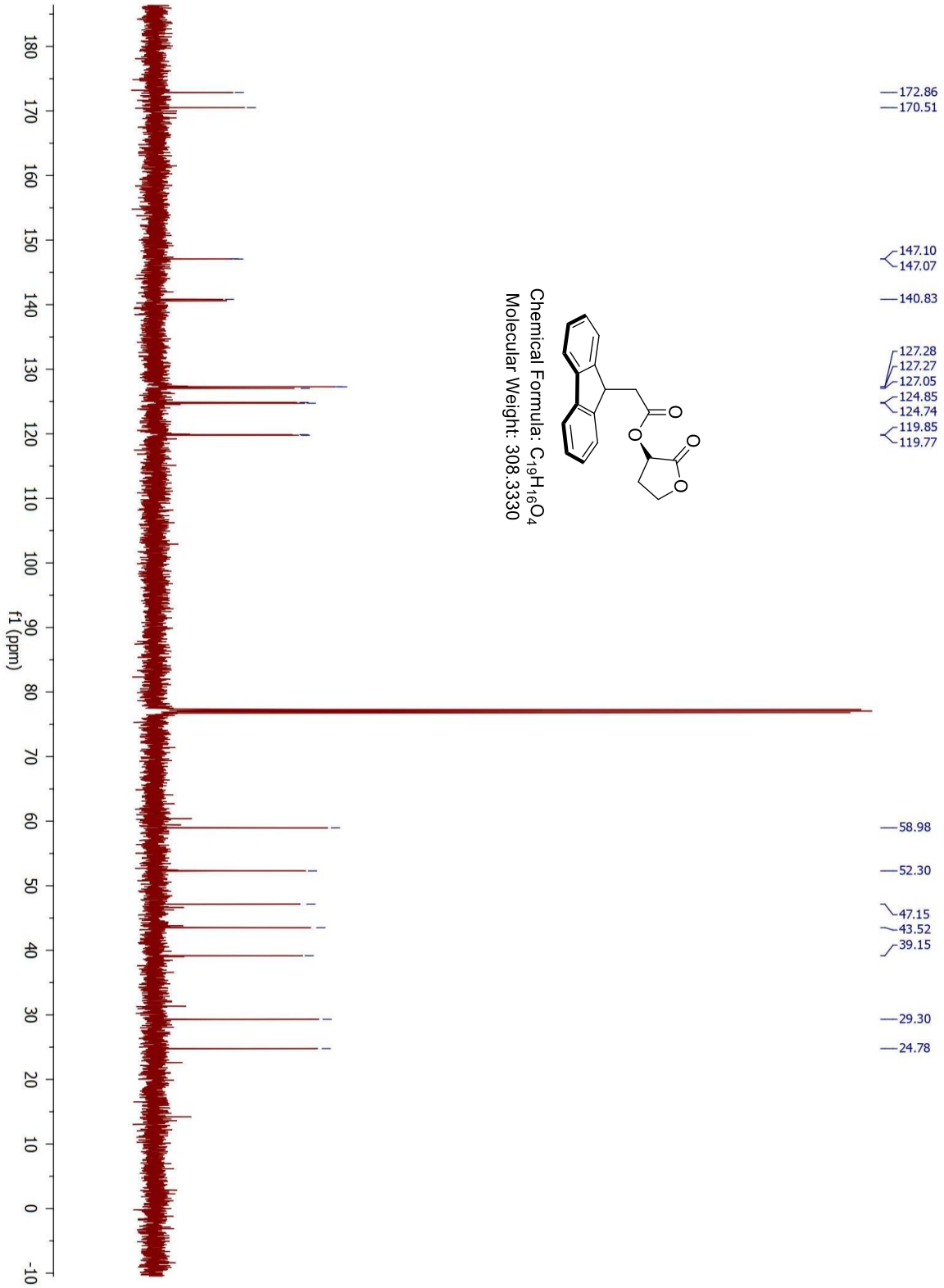
Chemical Formula: $C_{19}H_{16}O_4$
Molecular Weight: 308.3330
172.86
170.51
147.10
147.07
140.83
127.28
127.27
127.05
124.85
124.74
119.85
119.77
58.98
52.30
47.15
43.52
39.15
29.30
24.78
f1 (ppm)

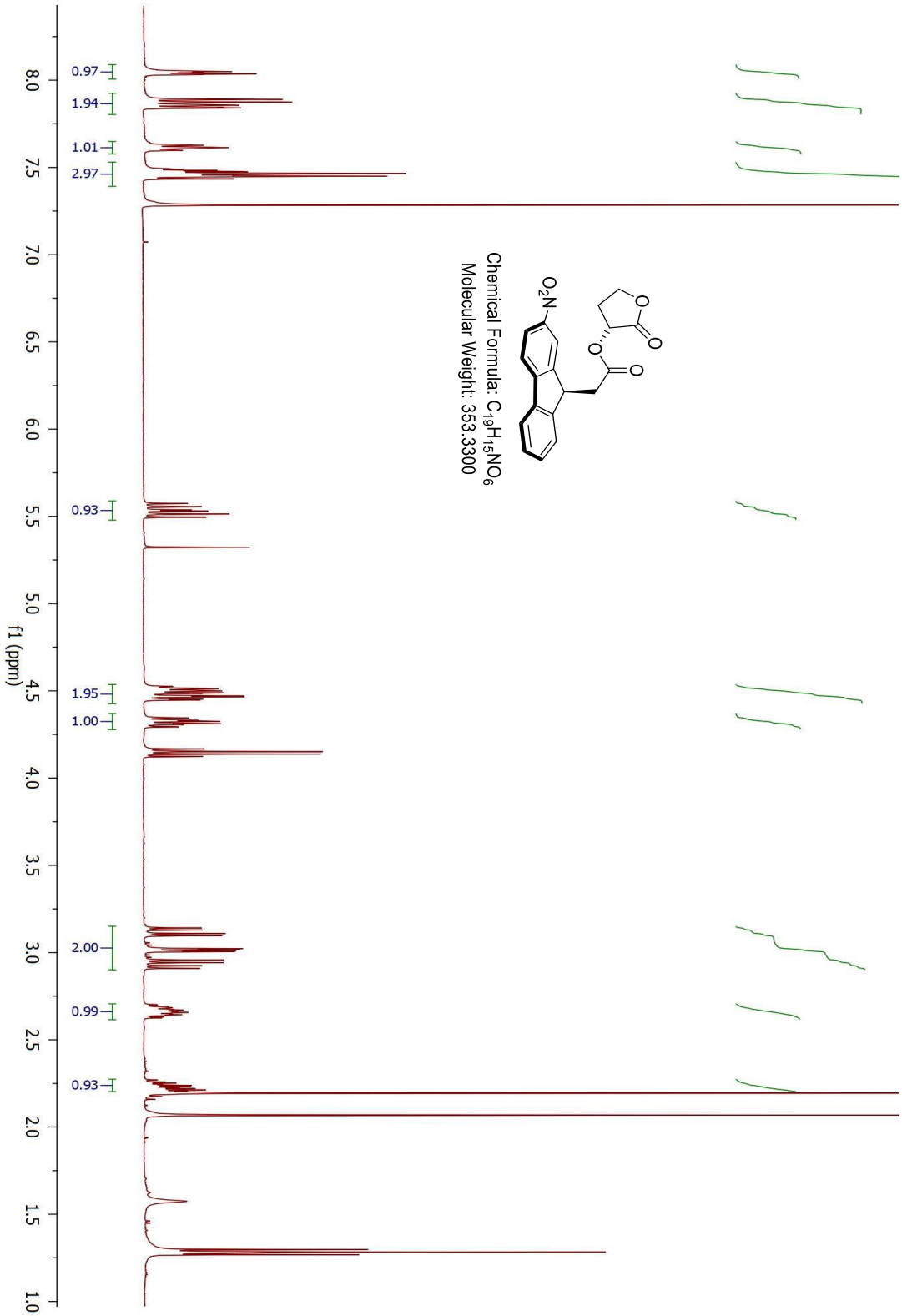
Chemical Formula: C19H15NO6
Molecular Weight: 353.3300
O2N
O
O
O
O
0.97
1.94
1.01
2.97
0.93
1.95
1.00
2.00
0.99
0.93
8.0
7.5
7.0
6.5
6.0
5.5
5.0
4.5
4.0
3.5
3.0
2.5
2.0
1.5
1.0
f1 (ppm)

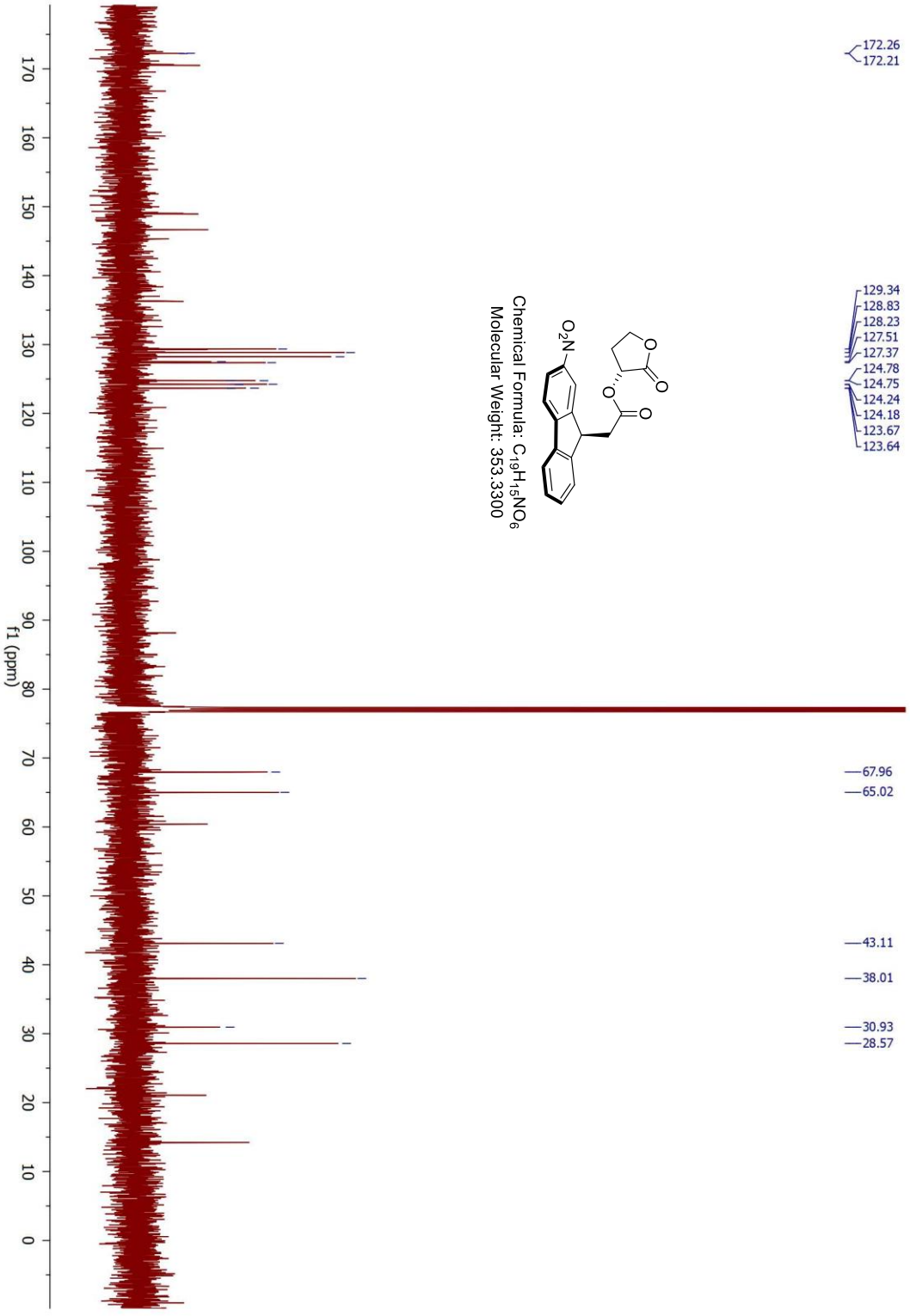
172.26
172.21
129.34
128.83
128.23
127.51
127.37
124.78
124.75
124.24
124.18
123.67
123.64
67.96
65.02
43.11
38.01
30.93
28.57
f1 (ppm)
Chemical Formula: C19H15NO6
Molecular Weight: 353.3300

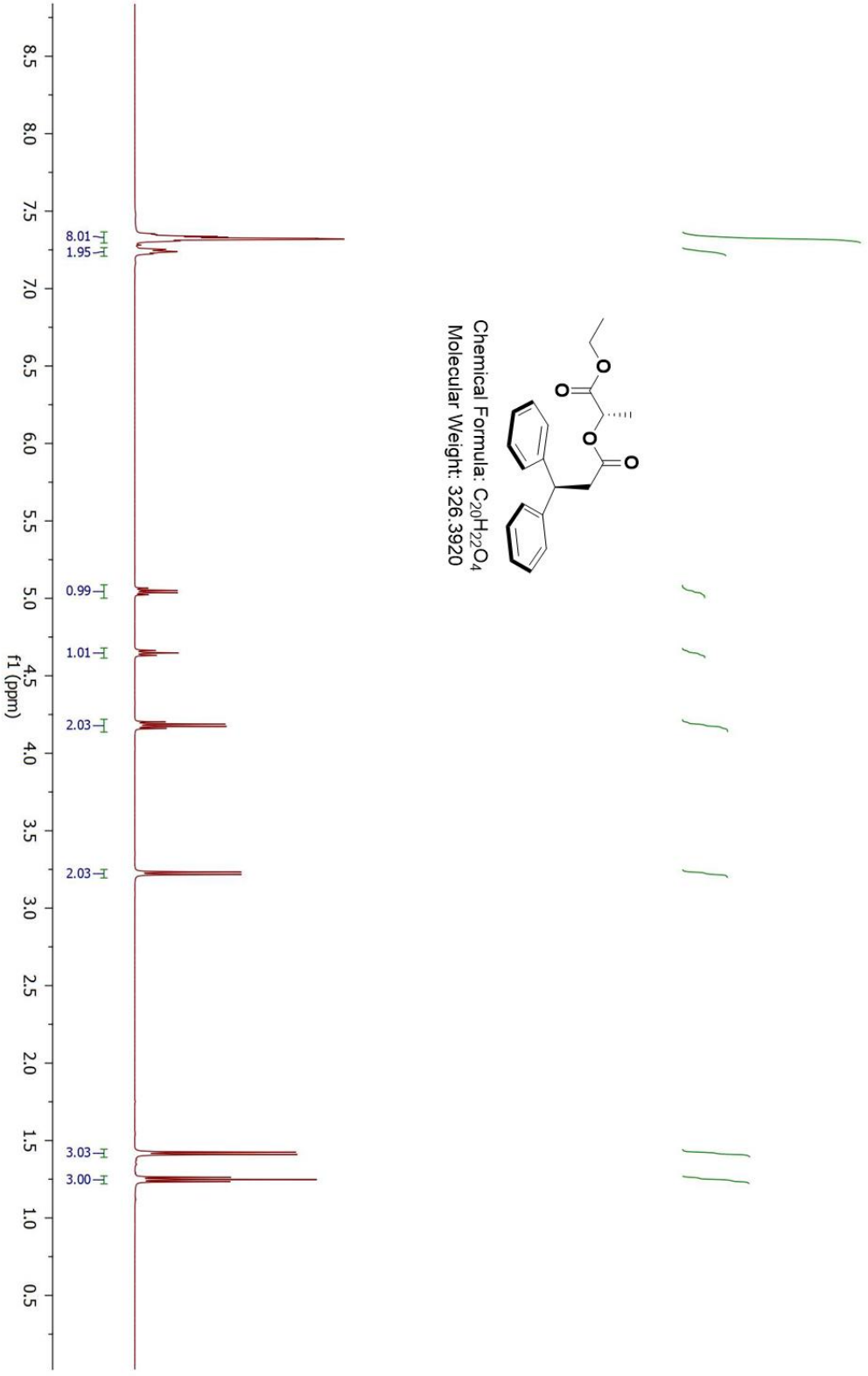
Chemical Formula: C20H22O4
Molecular Weight: 326.3920
8.01
1.95
0.99
1.01
2.03
2.03
3.03
3.00
f1 (ppm)

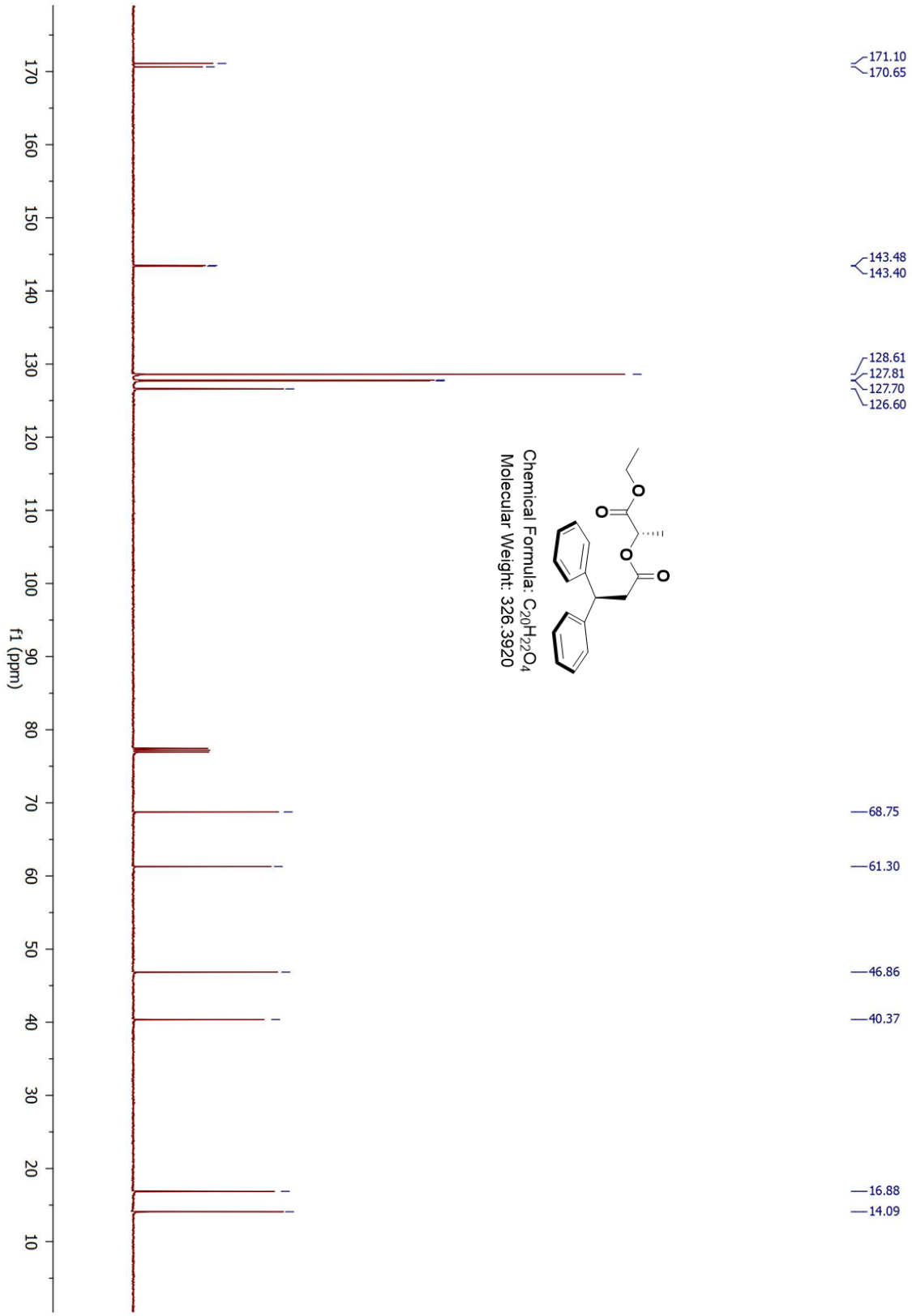
171.10
170.65
143.48
143.40
128.61
127.81
127.70
126.60
68.75
61.30
46.86
40.37
16.88
14.09
f1 (ppm)
Chemical Formula: C20H22O4
Molecular Weight: 326.3920

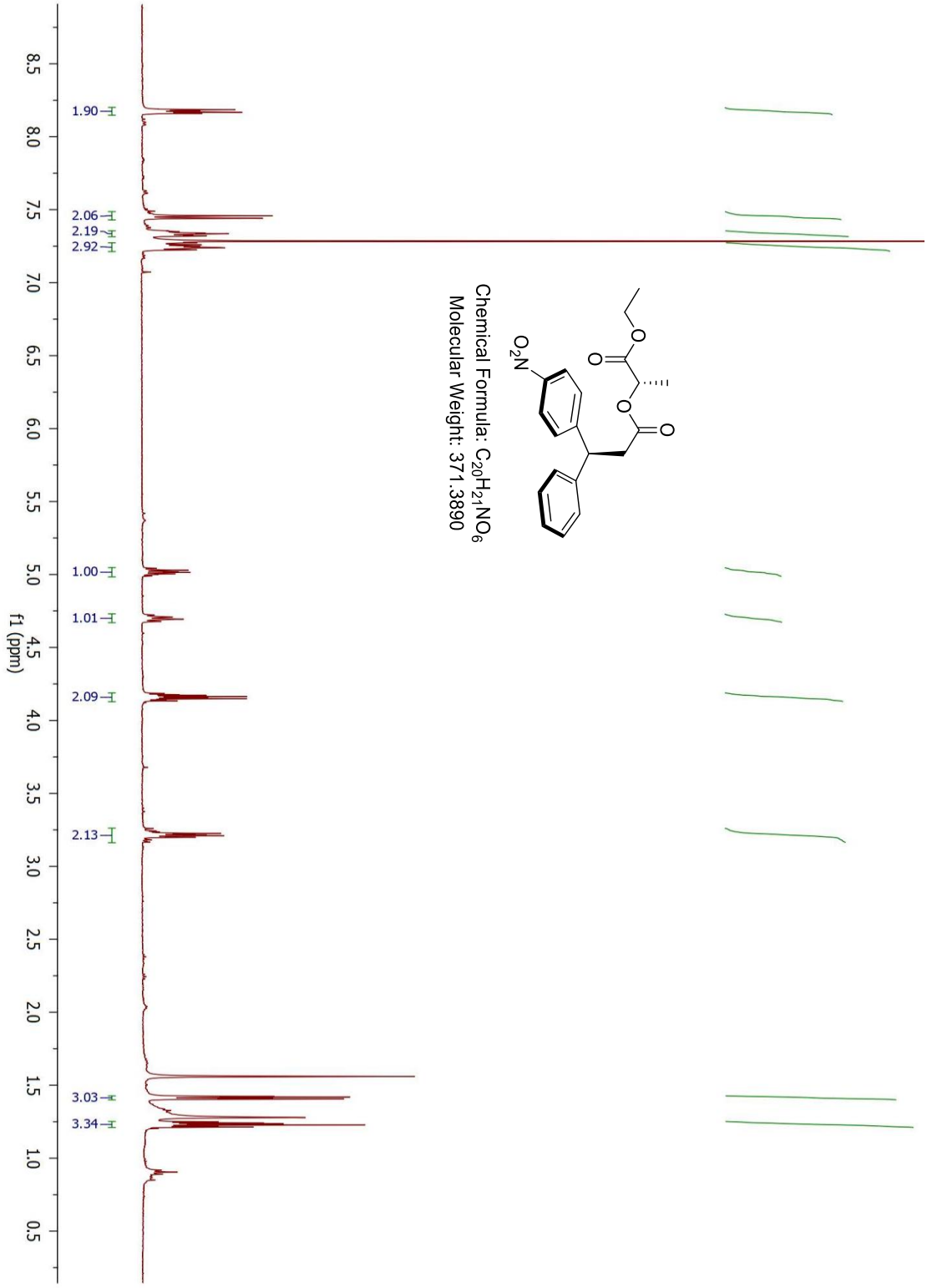
Chemical Formula: C20H21NO6
Molecular Weight: 371.3890
O2N
O
O
O
O
O
1.90
2.06
2.19
2.92
1.00
1.01
2.09
2.13
3.03
3.34
f1 (ppm)

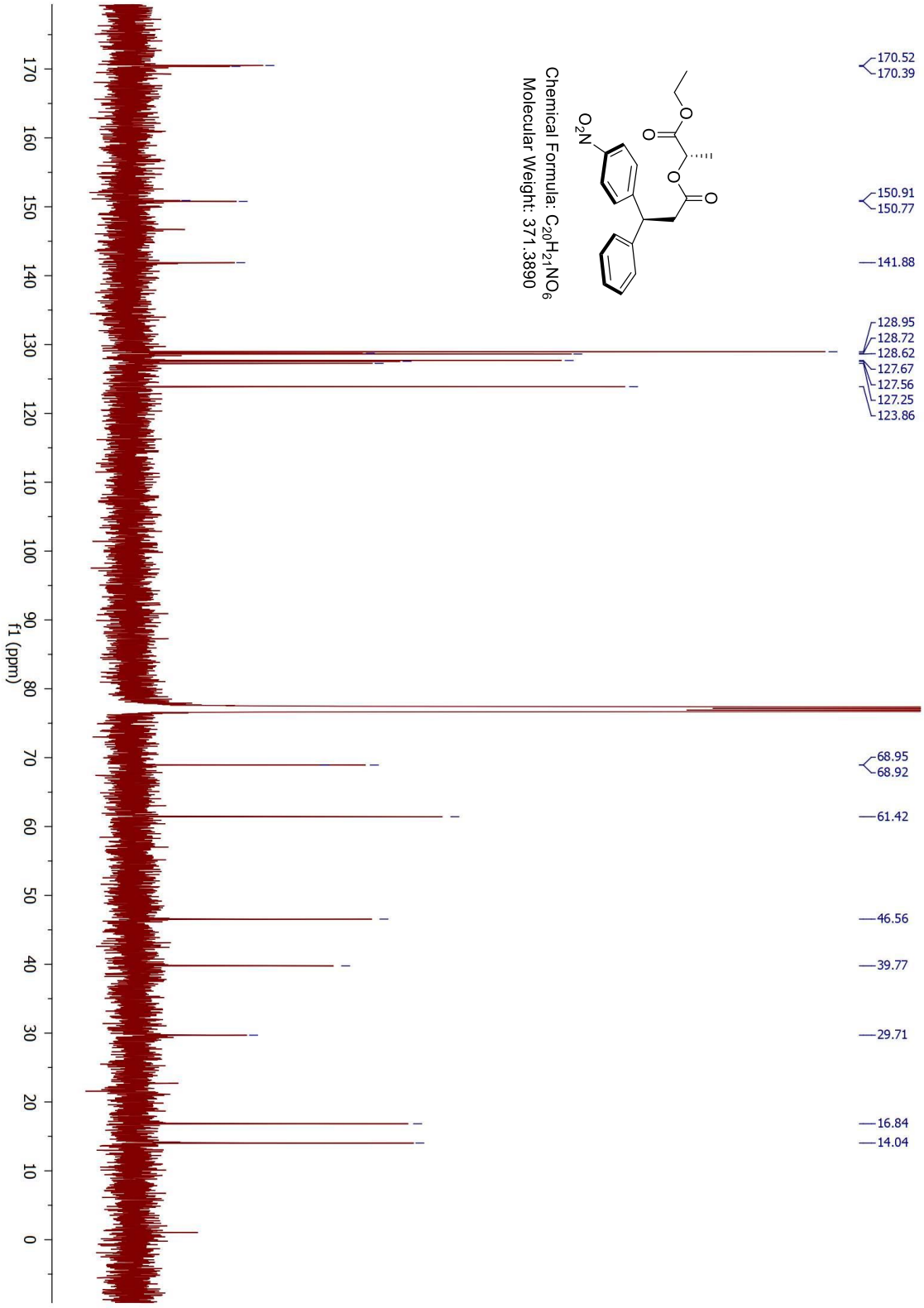
Chemical Formula: $C_{20}H_{21}NO_6$
Molecular Weight: 371.3890
O_2N
O
O
O
O
O
170.52
170.39
150.91
150.77
141.88
128.95
128.72
128.62
127.67
127.56
127.25
123.86
68.95
68.92
61.42
46.56
39.77
29.71
16.84
14.04
f1 (ppm)
170
160
150
140
130
120
110
100
90
80
70
60
50
40
30
20
10
0

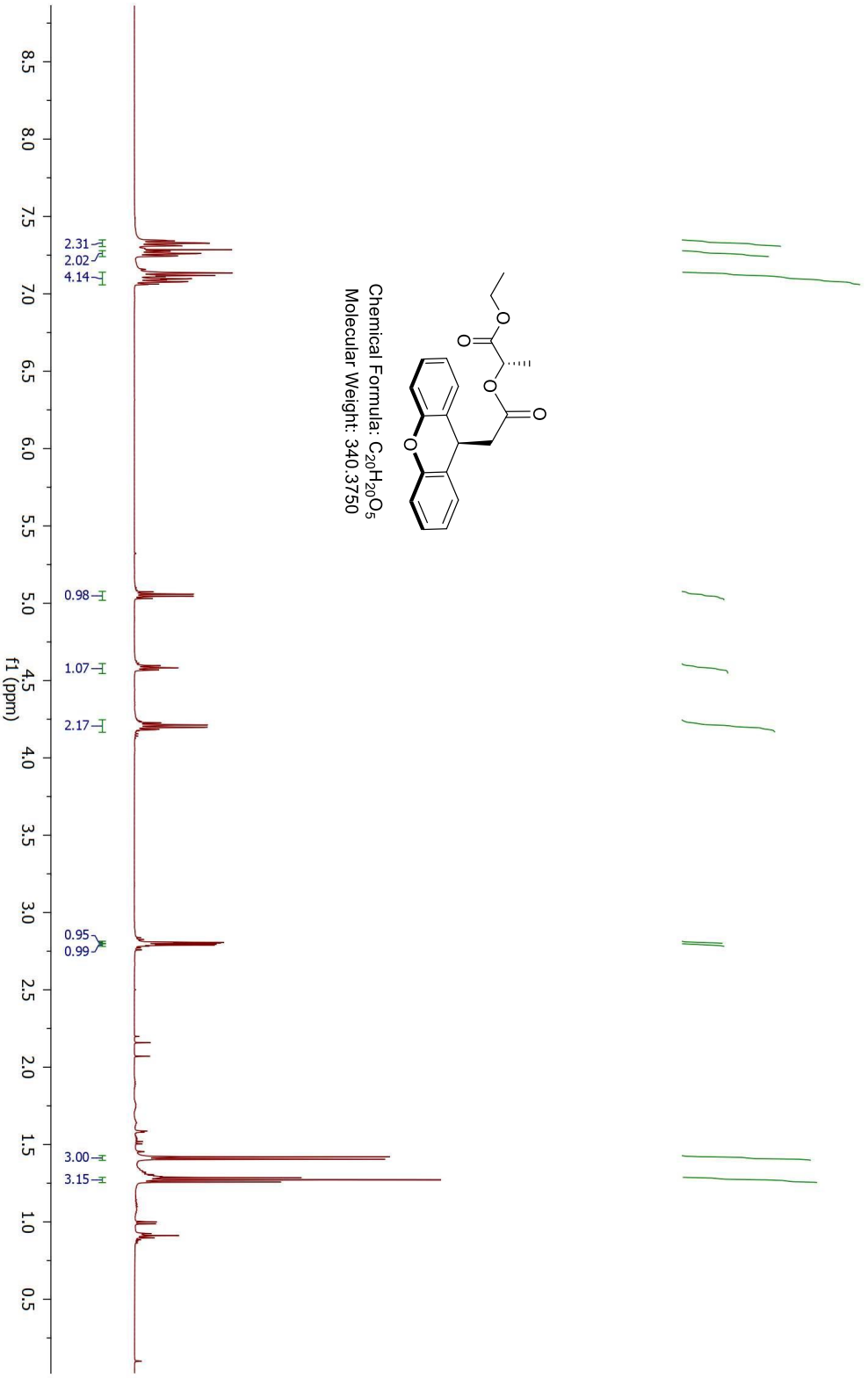
Chemical Formula: C20H20O5
Molecular Weight: 340.3750
2.31
2.02
4.14
0.98
1.07
2.17
0.95
0.99
3.00
3.15
f1 (ppm)

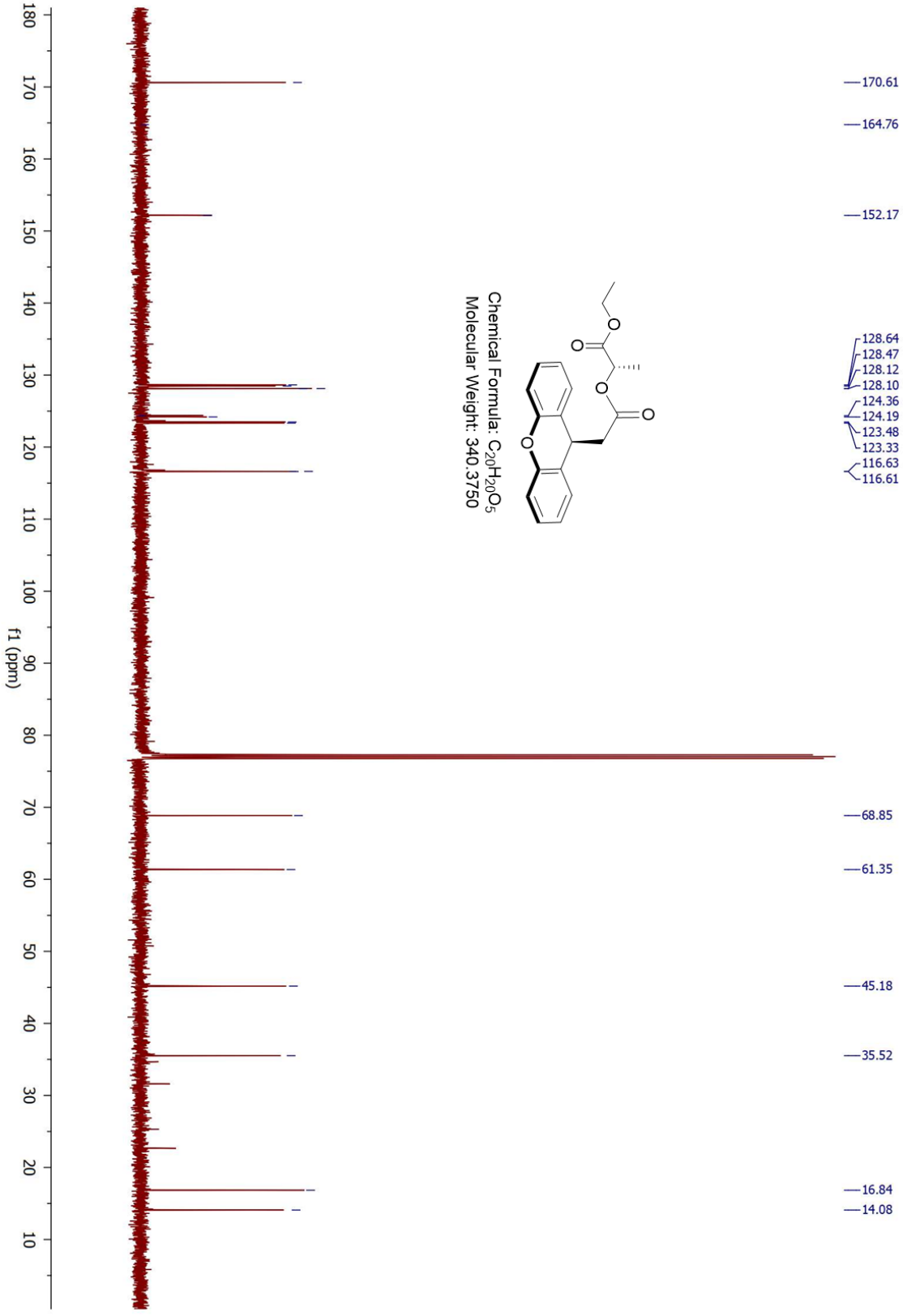
Chemical Formula: C20H20O5
Molecular Weight: 340.3750
170.61
164.76
152.17
128.64
128.47
128.12
128.10
124.36
124.19
123.48
123.33
116.63
116.61
68.85
61.35
45.18
35.52
16.84
14.08
f1 (ppm)

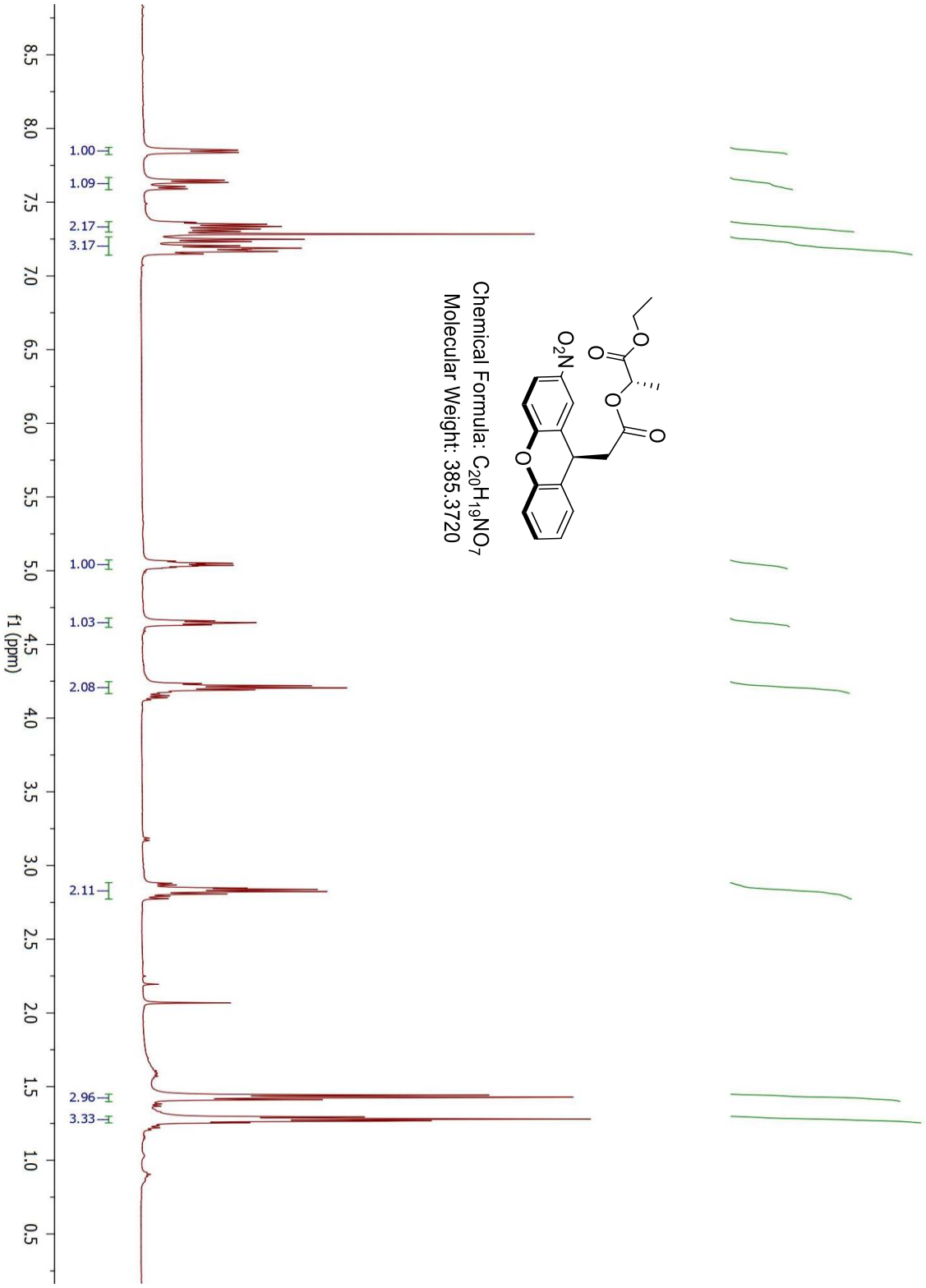
Chemical Formula: $C_{20}H_{19}NO_7$
Molecular Weight: 385.3720
O_2N
O
O
O
O
O
O
1.00
1.09
2.17
3.17
1.00
1.03
2.08
2.11
2.96
3.33
f1 (ppm)
8.5
8.0
7.5
7.0
6.5
6.0
5.5
5.0
4.5
4.0
3.5
3.0
2.5
2.0
1.5
1.0
0.5

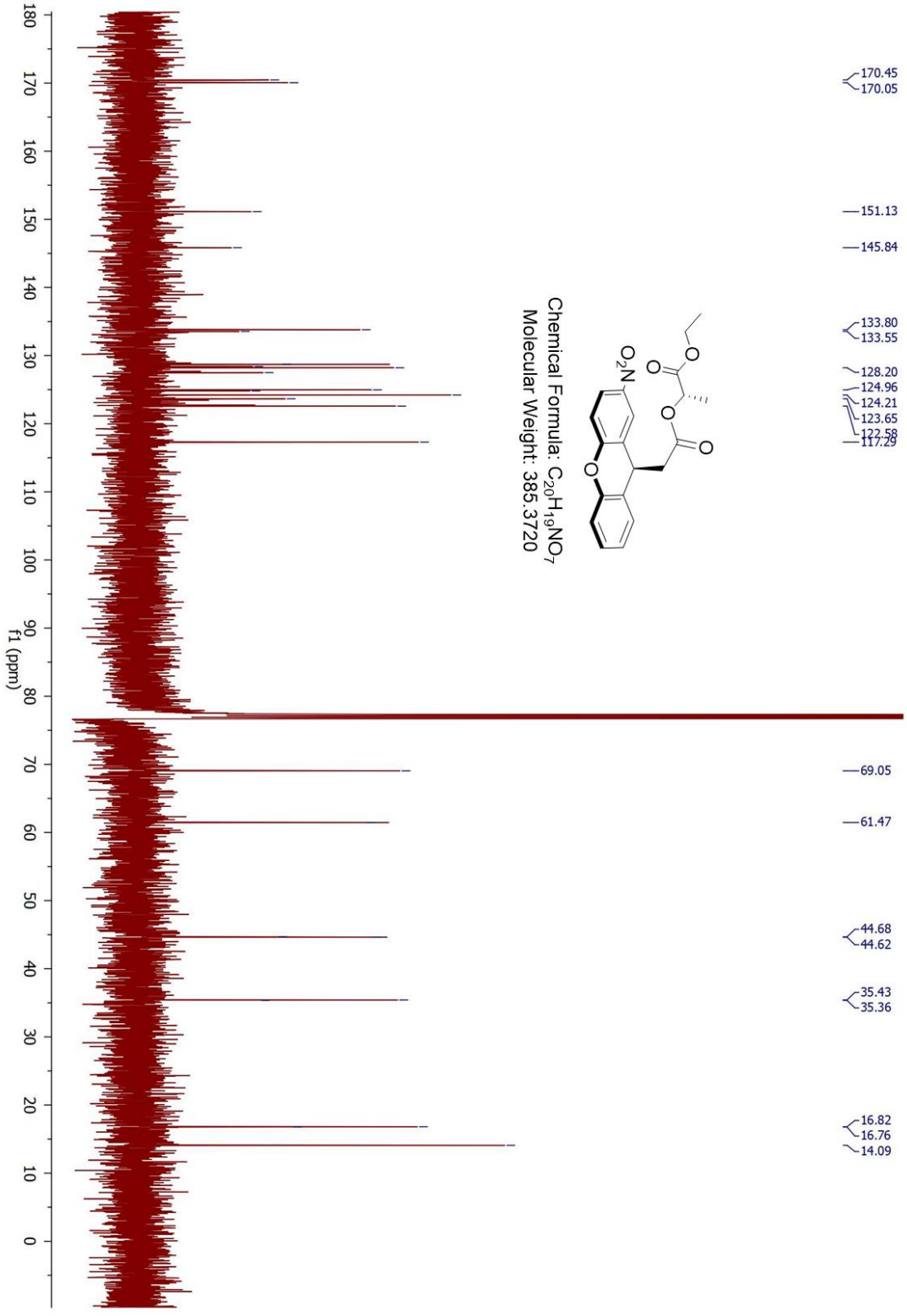
Chemical Formula: $C_{20}H_{19}NO_7$
Molecular Weight: 385.3720
O_2N
O
O
O
O
O
O
170.45
170.05
151.13
145.84
133.80
133.55
128.20
124.96
124.21
123.65
122.58
117.29
69.05
61.47
44.68
44.62
35.43
35.36
16.82
16.76
14.09
f1 (ppm)
180
170
160
150
140
130
120
110
100
90
80
70
60
50
40
30
20
10
0

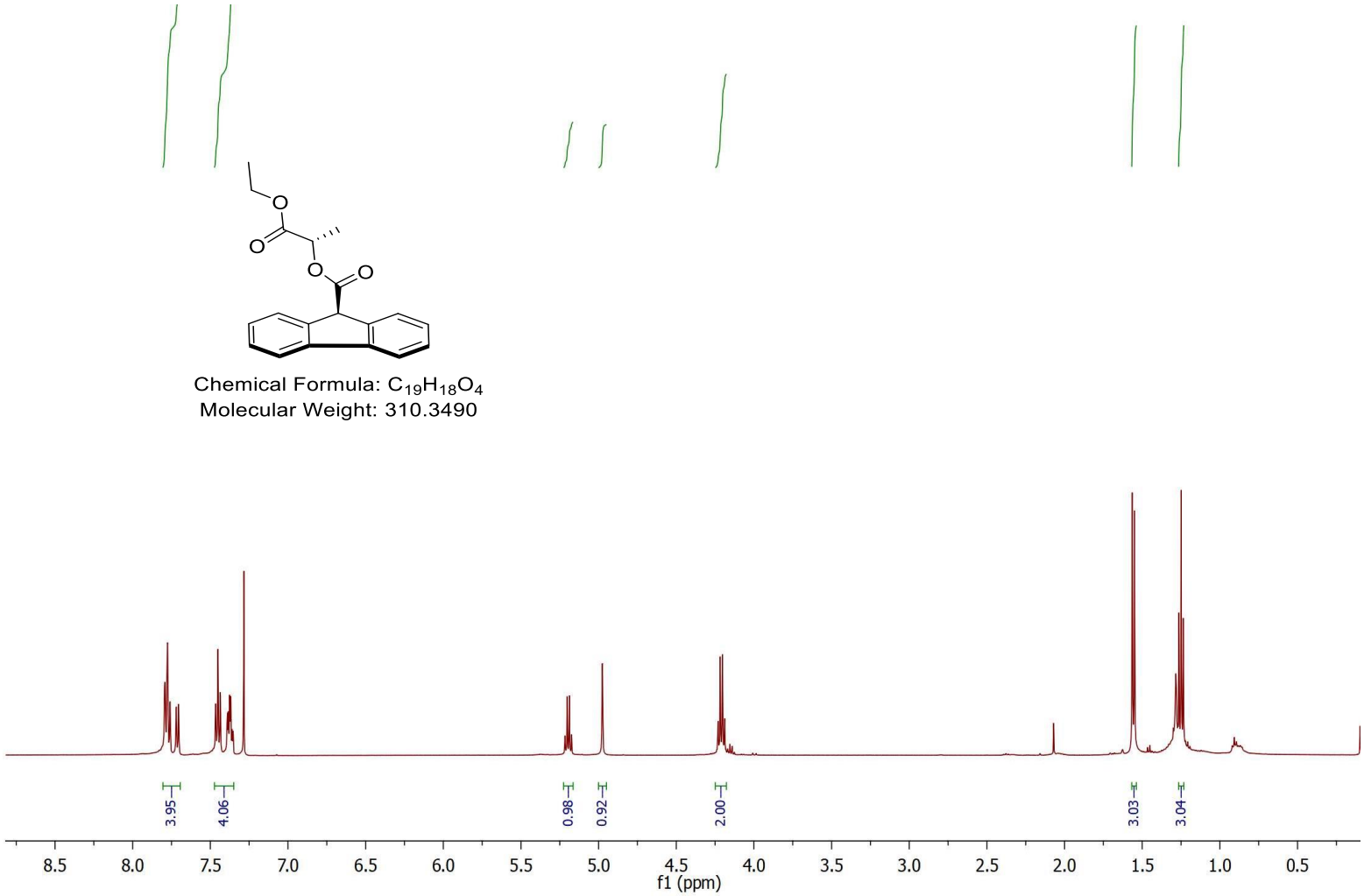
Chemical Formula: $C_{19}H_{18}O_4$
Molecular Weight: 310.3490
3.95
4.06
0.98
0.92
2.00
3.03
3.04
8.5
8.0
7.5
7.0
6.5
6.0
5.5
5.0
4.5
4.0
3.5
3.0
2.5
2.0
1.5
1.0
0.5
f1 (ppm)

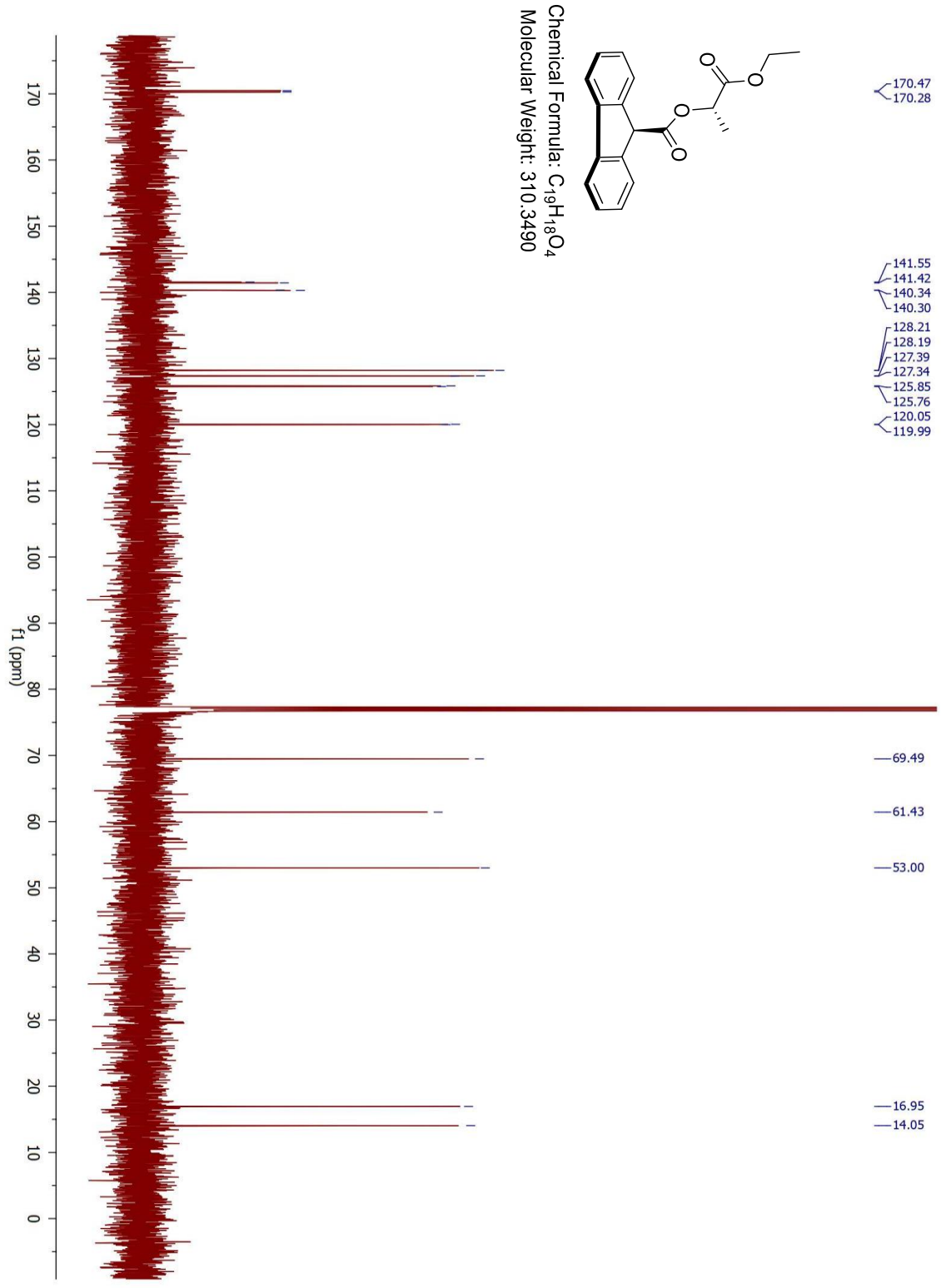
Chemical Formula: $C_{19}H_{18}O_4$
Molecular Weight: 310.3490
170.47
170.28
141.55
141.42
140.34
140.30
128.21
128.19
127.39
127.34
125.85
125.76
120.05
119.99
69.49
61.43
53.00
16.95
14.05
f1 (ppm)

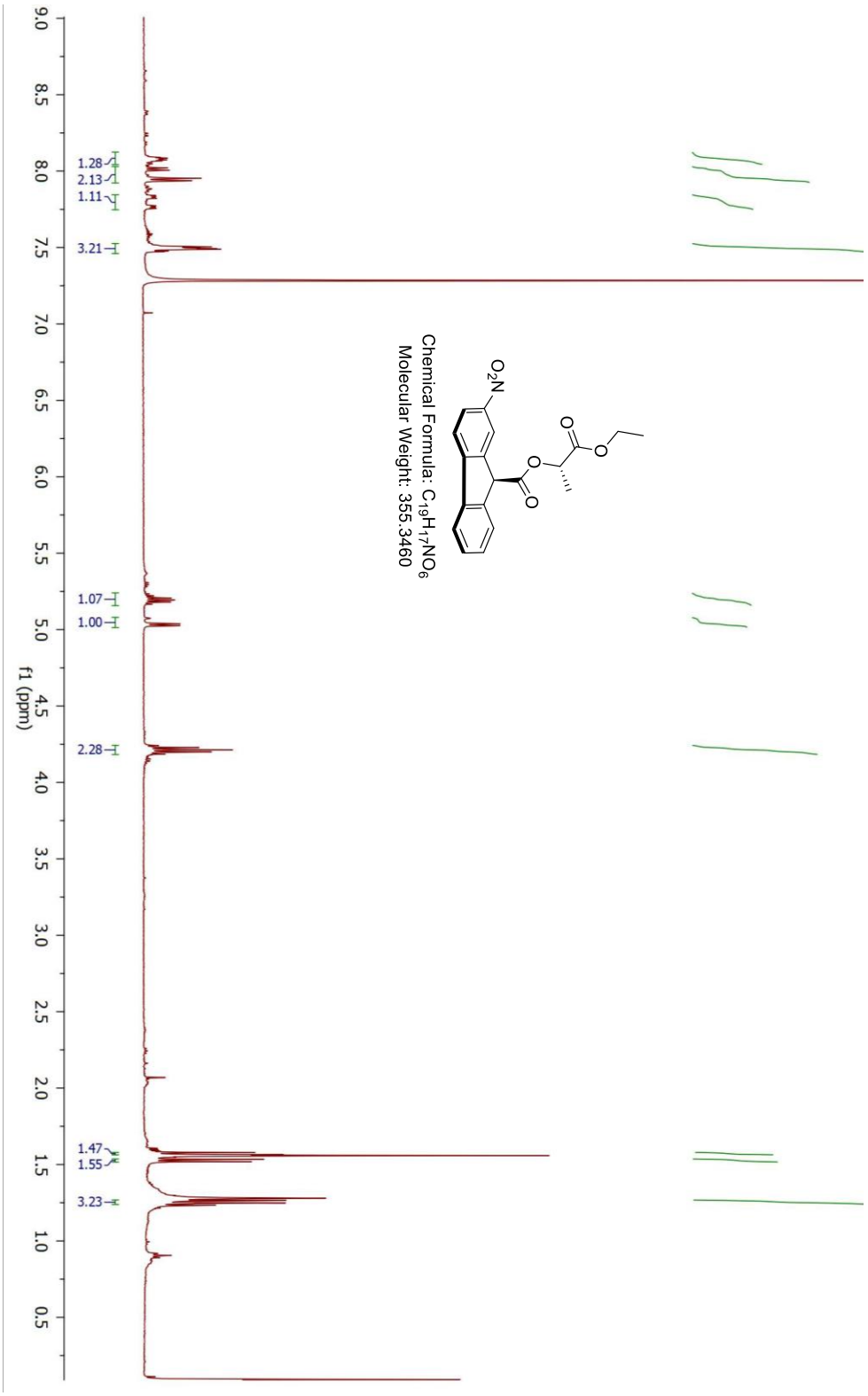
Chemical Formula: C19H17NO6
Molecular Weight: 355.3460
O2N
O
O
O
O
1.28
2.13
1.11
3.21
1.07
1.00
2.28
1.47
1.55
3.23
f1 (ppm)

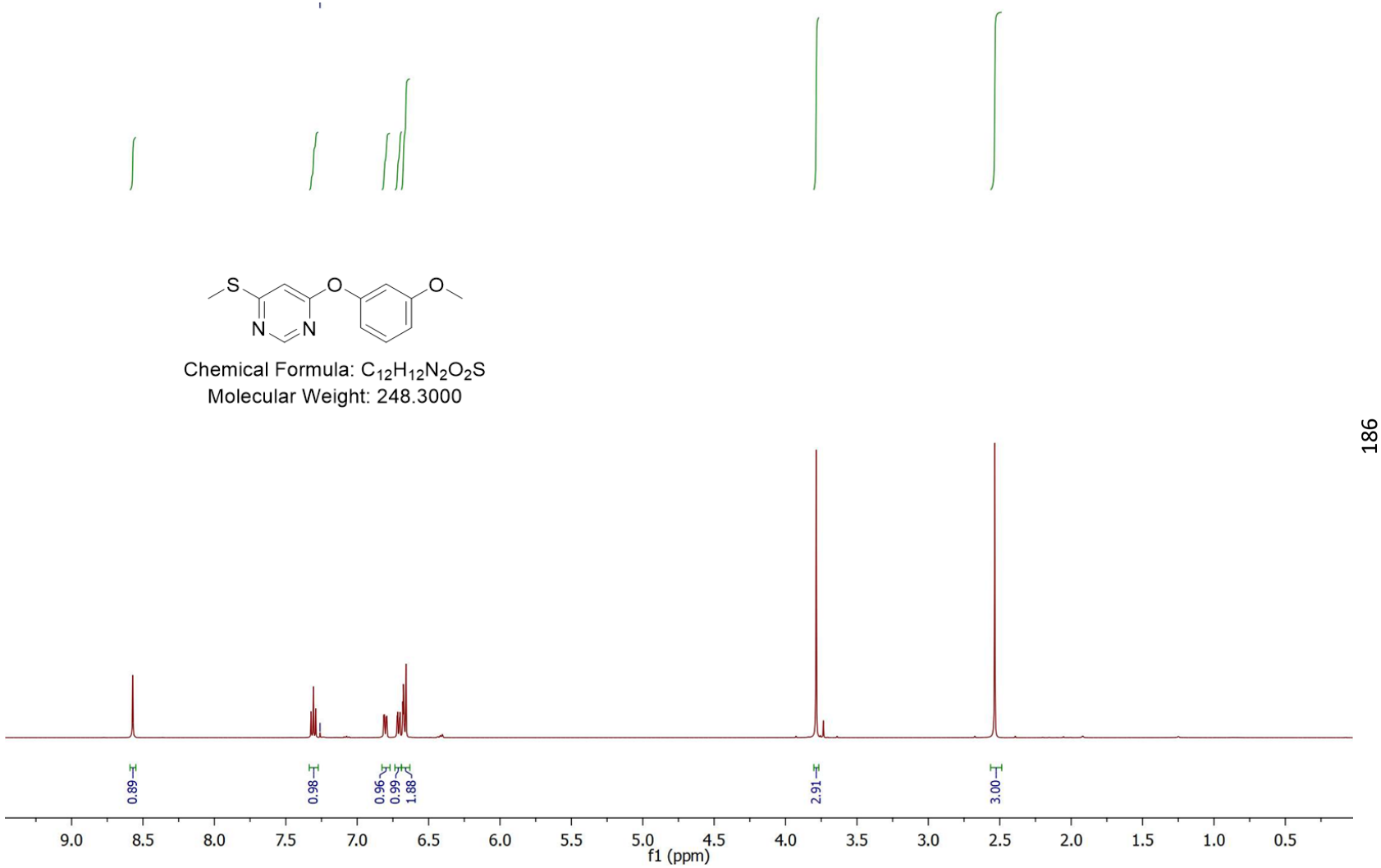
S
O
O
N
N
Chemical Formula: $C_{12}H_{12}N_2O_2S$
Molecular Weight: 248.3000
0.89
0.98
0.96
0.99
1.88
2.91
3.00
9.0
8.5
8.0
7.5
7.0
6.5
6.0
5.5
5.0
4.5
4.0
3.5
3.0
2.5
2.0
1.5
1.0
0.5
f1 (ppm)

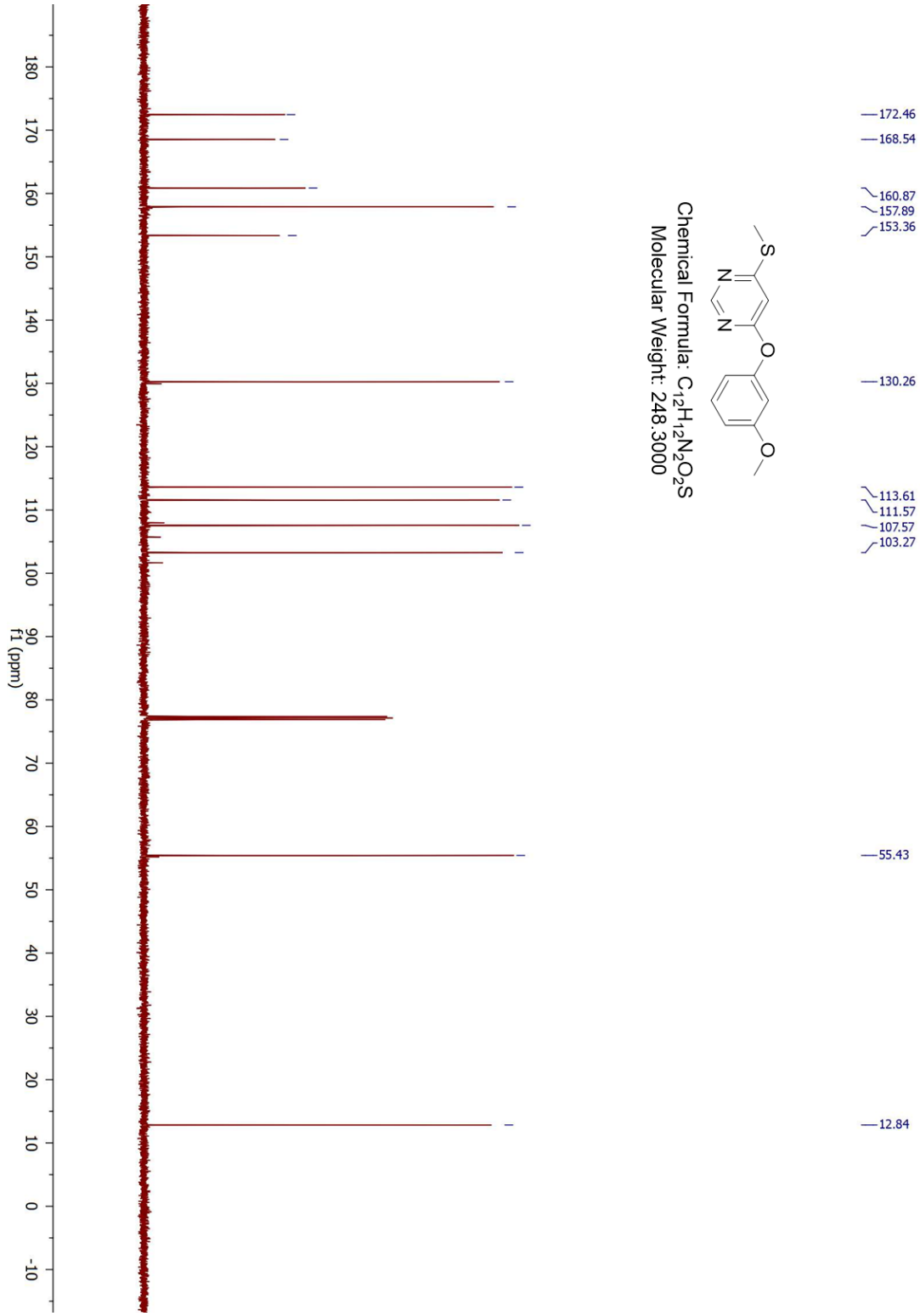
Chemical Formula: $C_{12}H_{12}N_2O_2S$
Molecular Weight: 248.3000
172.46
168.54
160.87
157.89
153.36
130.26
113.61
111.57
107.57
103.27
55.43
12.84
f1 (ppm)

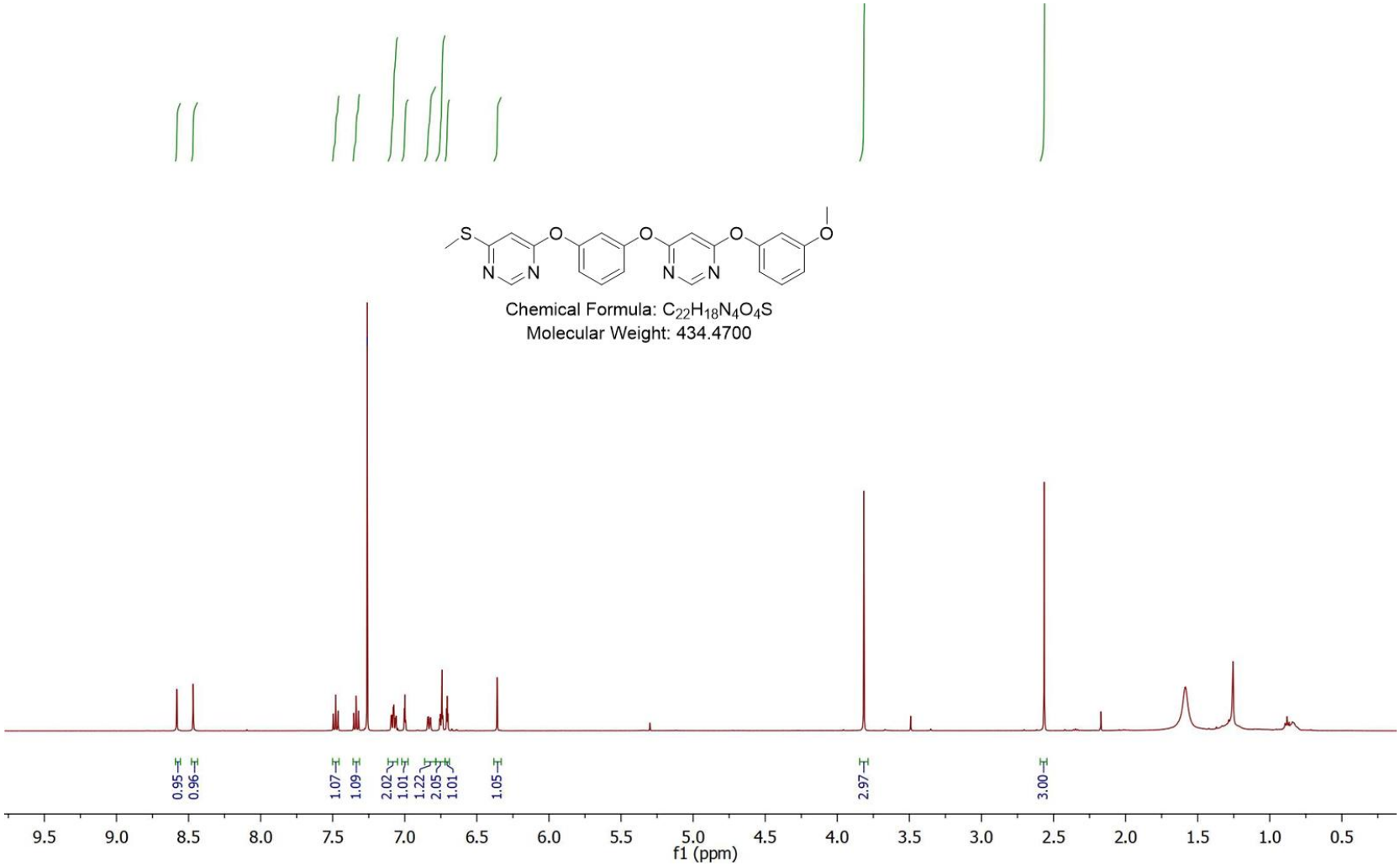
Chemical Formula: $C_{22}H_{18}N_4O_4S$
Molecular Weight: 434.4700
0.95
0.96
1.07
1.09
2.02
1.01
1.22
2.05
1.01
1.05
2.97
3.00
9.5 9.0 8.5 8.0 7.5 7.0 6.5 6.0 5.5 5.0 4.5 4.0 3.5 3.0 2.5 2.0 1.5 1.0 0.5
f1 (ppm)

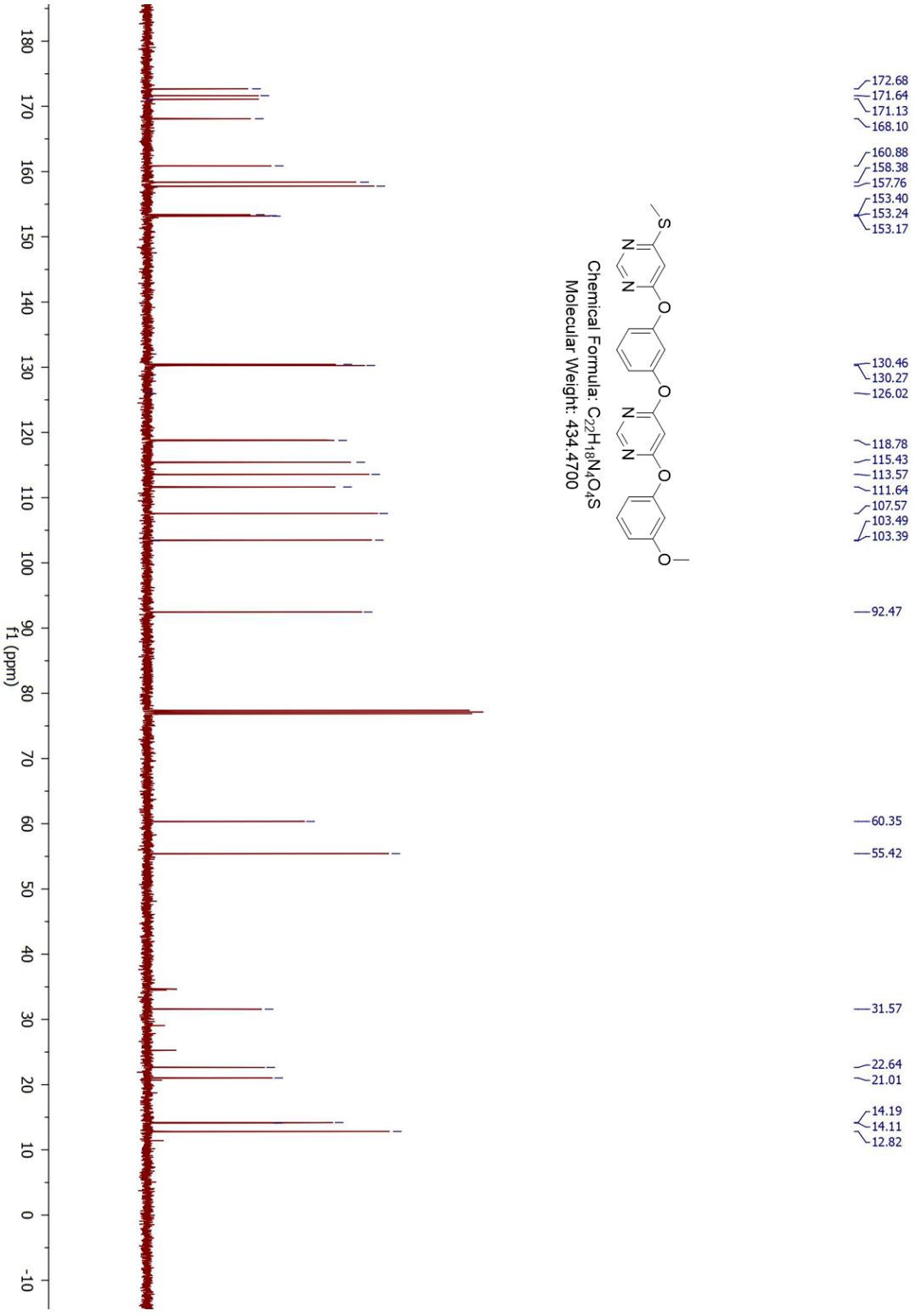
f1 (ppm)
180
170
160
150
140
130
120
110
100
90
80
70
60
50
40
30
20
10
0
-10
Chemical Formula: C22H18N4O4S
Molecular Weight: 434.4700
172.68
171.64
171.13
168.10
160.88
158.38
157.76
153.40
153.24
153.17
130.46
130.27
126.02
118.78
115.43
113.57
111.64
107.57
103.49
103.39
92.47
60.35
55.42
31.57
22.64
21.01
14.19
14.11
12.82

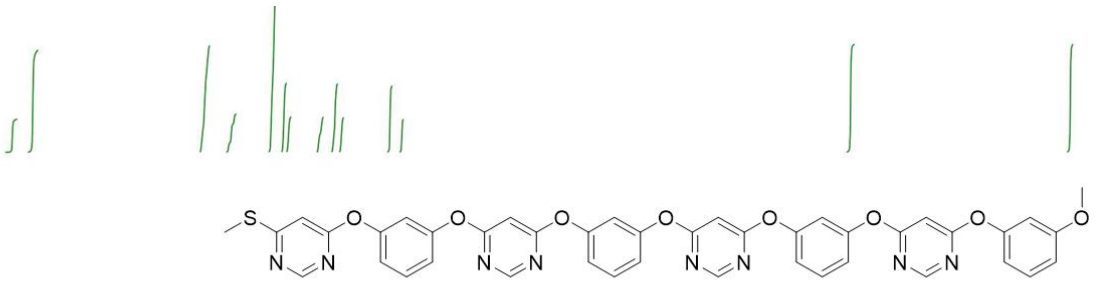

Chemical Formula: $C_{42}H_{30}N_8O_8S$
Molecular Weight: 806.8100

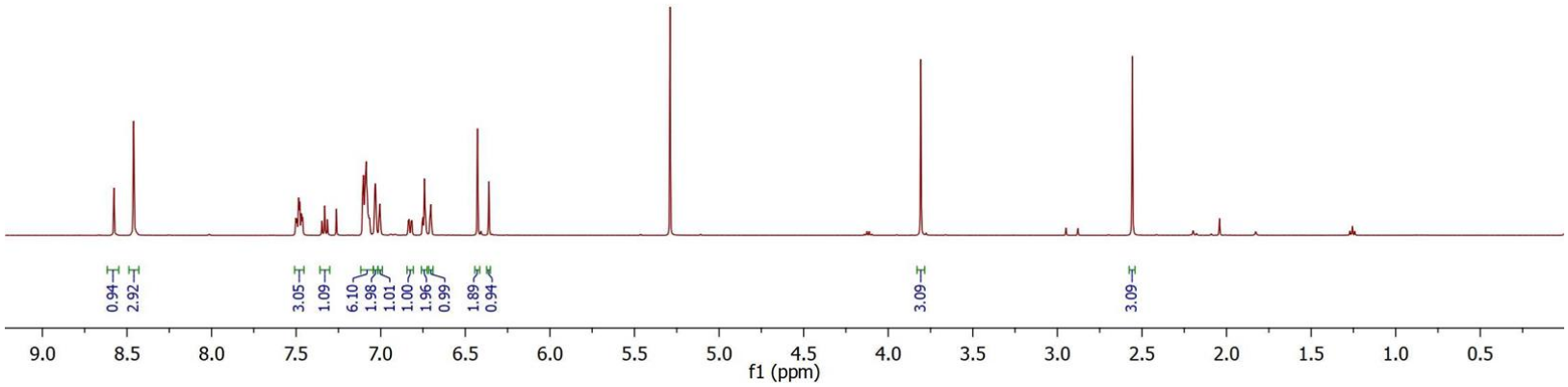

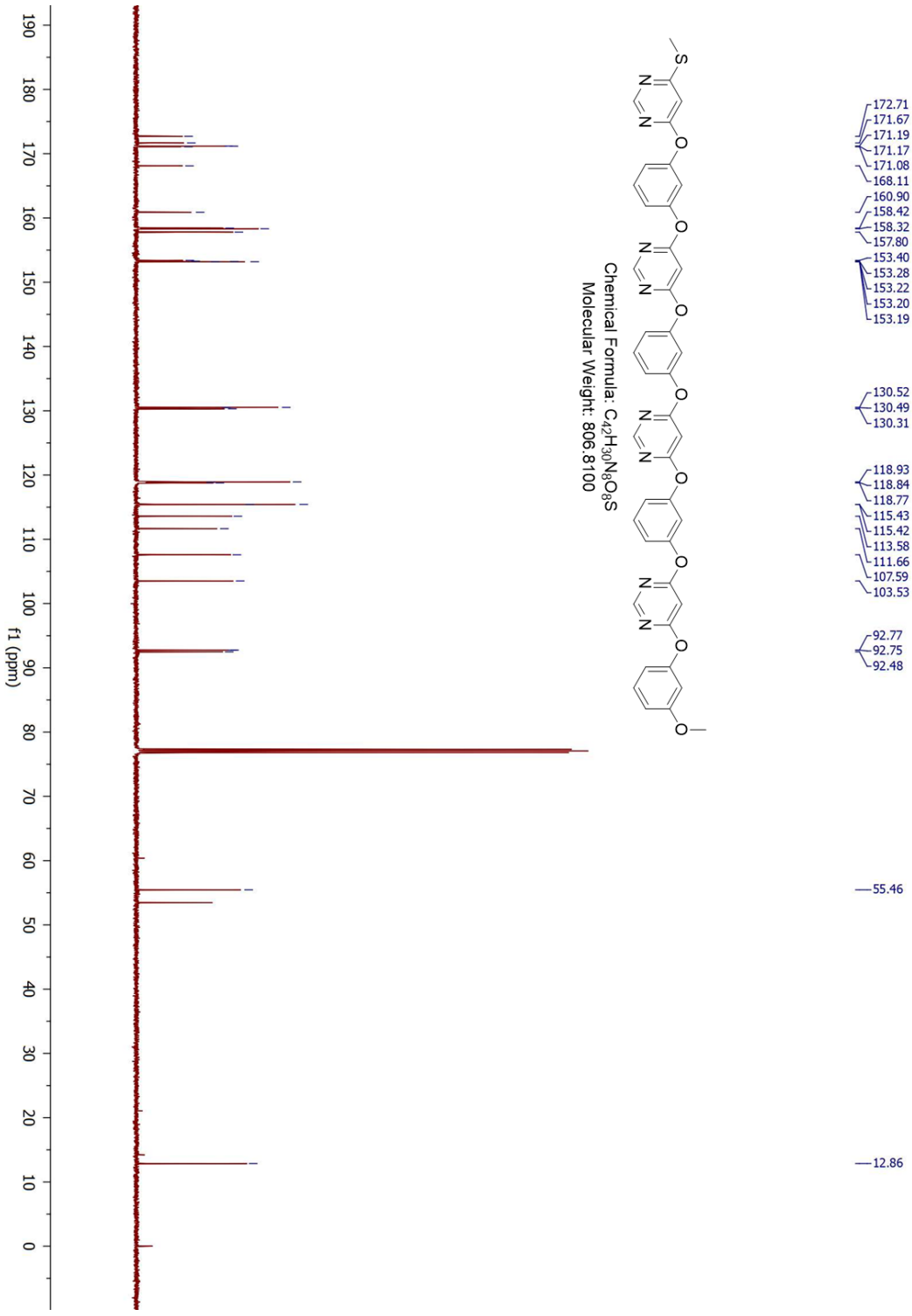
Chemical Formula: C42H30N8O8S
Molecular Weight: 806.8100
172.71
171.67
171.19
171.17
171.08
168.11
160.90
158.42
158.32
157.80
153.40
153.28
153.22
153.20
153.19
130.52
130.49
130.31
118.93
118.84
118.77
115.43
115.42
113.58
111.66
107.59
103.53
92.77
92.75
92.48
55.46
12.86
f1 (ppm)

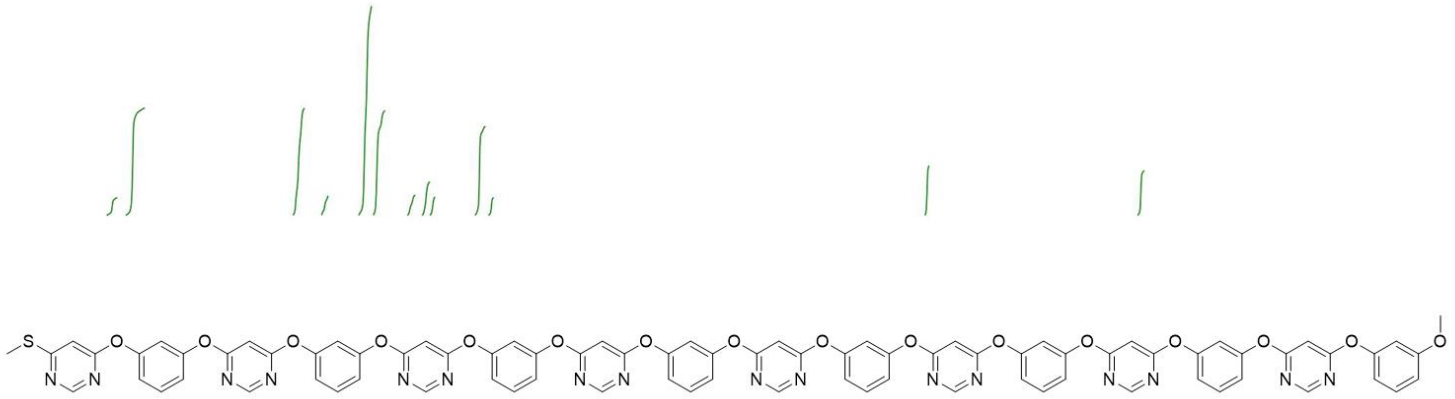

Chemical Formula: $C_{82}H_{54}N_{16}O_{16}S$
Molecular Weight: 1551.4900

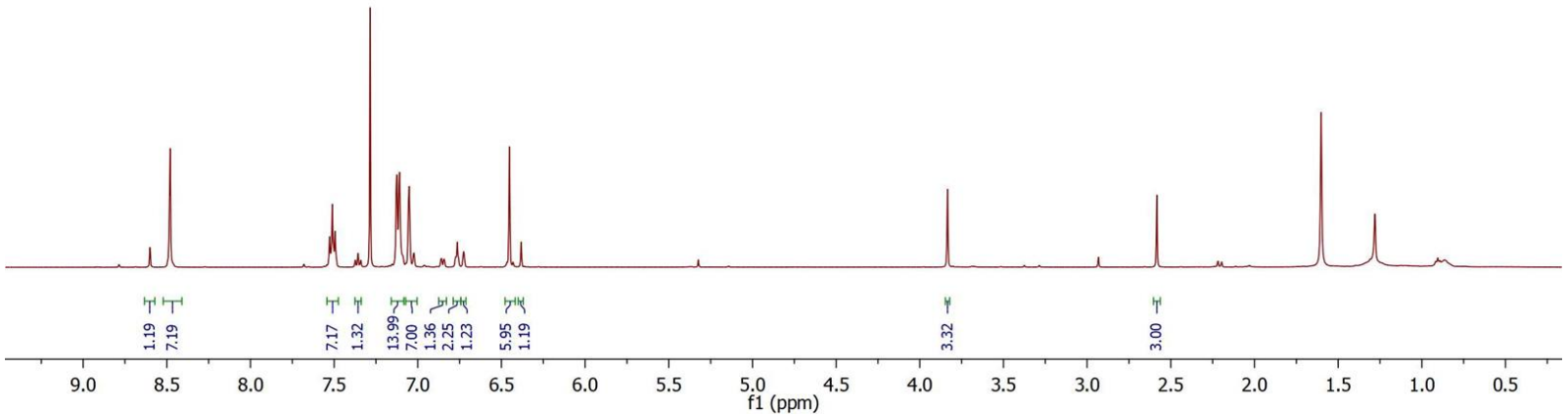

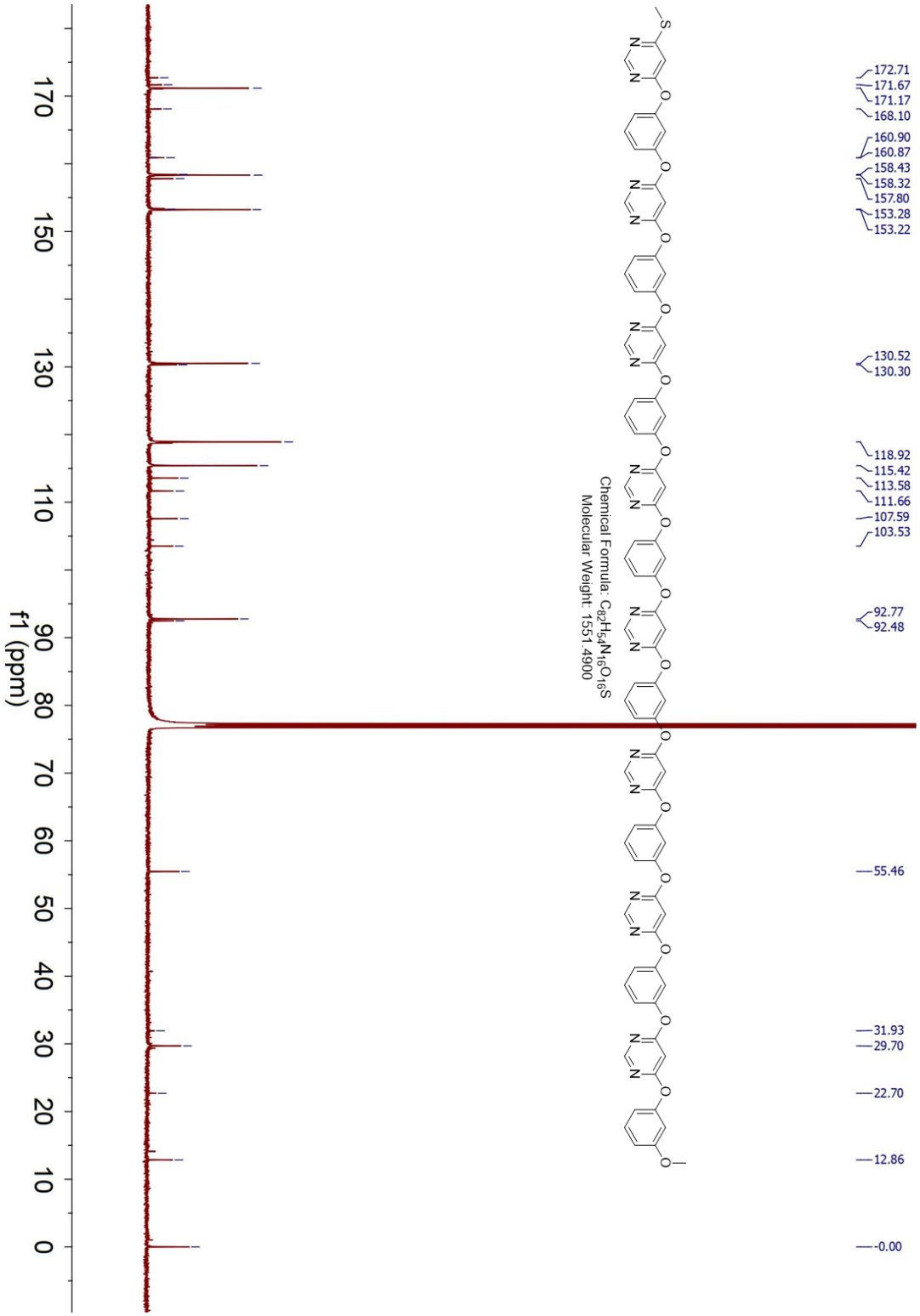
172.71
171.67
171.17
168.10
160.90
160.87
158.43
158.32
157.80
153.28
153.22
130.52
130.30
118.92
115.42
113.58
111.66
107.59
103.53
92.77
92.48
55.46
31.93
29.70
22.70
12.86
-0.00
Chemical Formula: C82H54N16O16S
Molecular Weight: 1551.4900
f1 (ppm)
170
150
130
110
90
80
70
60
50
40
30
20
10
0

Appendix II
Optimized Cartesian Coordinates

Optimized Cartesian Coordinates for [NO_2-*exo-(P,S)*-Me-Prod-H]$^+$ / Å

SCF Energy (B3LYP-MM/cc-pVDZ++//B3LYP-MM/LACVP*) = –1744.670678 hartrees

C	1.77350	9.25200	19.26070
C	1.41150	7.90500	19.19730
C	0.92600	7.36170	18.00560
C	0.80040	8.15680	16.86440
C	1.17230	9.49950	16.92440
C	1.65090	10.04200	18.11740
C	2.34360	10.36410	14.86750
C	2.65480	9.26020	14.07590
C	3.73970	9.32700	13.20000
C	4.50290	10.49630	13.09770
C	4.20050	11.60010	13.88990
C	3.11490	11.52640	14.77190
C	5.91090	11.76080	18.34970
C	4.51260	11.35200	18.64230
C	3.51700	11.72550	17.80650
C	3.78130	12.57580	16.68830
C	5.05600	13.20150	16.53190
C	6.07100	12.86010	17.36300
C	1.15390	10.52220	15.79970
C	2.01680	11.50510	17.95500
C	2.62720	12.61940	15.74700
C	1.42950	11.91650	16.52830
C	0.17100	12.77980	16.62960
C	2.13640	13.73880	19.21710
O	2.48150	14.38990	18.24520
C	2.78960	15.84660	22.10280
C	3.02470	15.37880	20.67100
O	2.25770	14.17440	20.47790
C	4.49470	15.04700	20.38000
O	4.89240	13.95550	20.01780
O	5.26300	16.11170	20.57930

C	6.69590	15.94660	20.35570
C	7.36810	17.24310	20.75700
C	-0.14470	10.44320	14.97060
C	1.53960	12.34620	19.17050
C	2.35890	13.96220	15.06210
H	2.12960	9.66560	20.20130
H	1.49780	7.28080	20.08190
H	0.63530	6.31580	17.96900
H	0.40540	7.72550	15.94880
H	2.06000	8.35340	14.13460
H	3.99000	8.46640	12.58630
H	5.33420	10.54160	12.40040
H	4.79850	12.50260	13.80700
H	4.34930	10.72640	19.51260
H	5.19880	13.95970	15.77030
H	-0.23380	13.00980	15.64150
H	0.37260	13.72740	17.13180
H	-0.61440	12.25460	17.18360
H	1.72620	16.05040	22.25490
H	3.35490	16.76270	22.28920
H	3.10540	15.08230	22.81920
H	2.70000	16.13490	19.95000
H	7.04000	15.09250	20.94460
H	6.84520	15.71100	19.29740
H	8.44800	17.15920	20.59660
H	7.19520	17.46300	21.81500
H	6.99520	18.08170	20.16090
H	-0.21240	9.46710	14.47990
H	-1.03260	10.55990	15.59800
H	0.44700	12.42480	19.17760
H	1.81030	11.83930	20.10020
H	3.24270	14.30710	14.51570
H	2.08650	14.72420	15.79430
H	-0.16560	11.20200	14.18210
H	1.55290	13.85690	14.33100
H	7.05090	13.31860	17.29170
H	6.42720	10.88040	17.91800

N	6.74710	11.98840	19.63740
O	7.71300	12.72630	19.53210
O	6.40890	11.35170	20.61730

Optimized Cartesian Coordinates for [NO_2-*endo*-*(P,S)*-Me-Prod-H]$^+$ / Å

SCF Energy (B3LYP-MM/cc-pVDZ++//B3LYP-MM/LACVP*) = –1744.668942 hartrees

C	1.71620	9.16030	19.35940
C	1.29590	7.83220	19.26790
C	0.75580	7.34580	18.07520
C	0.63380	8.17920	16.96170
C	1.06520	9.50260	17.04870
C	1.59840	9.98860	18.24260
C	2.20120	10.36140	14.97010
C	2.41030	9.26840	14.13050
C	3.46010	9.29910	13.21220
C	4.28710	10.42440	13.11450
C	4.08590	11.51620	13.95420
C	3.03890	11.47600	14.88340
C	5.86390	11.74690	18.67510
C	4.49880	11.19660	18.81220
C	3.52090	11.61970	17.97400
C	3.82760	12.43760	16.84540
C	5.15020	12.92520	16.62530
C	6.14850	12.54730	17.46420
C	1.05920	10.55620	15.95330
C	2.01540	11.44230	18.11620
C	2.66260	12.55690	15.91660
C	1.43490	11.91510	16.70640
C	0.23570	12.85550	16.84130
C	2.21370	13.62620	19.46380
O	2.66790	14.27050	18.53310
C	2.70110	15.68080	22.42190
C	2.98570	15.26190	20.98310
O	2.24730	14.05110	20.73500

C	4.47440	14.97900	20.74870
O	4.94550	13.86590	20.59530
O	5.16800	16.11000	20.76400
C	6.61330	16.01270	20.59800
C	7.17580	17.41620	20.68900
C	-0.27340	10.56490	15.17450
C	1.56960	12.25880	19.35960
C	2.46960	13.94280	15.28870
H	2.11360	9.52940	20.30200
H	1.38010	7.17870	20.13130
H	0.42020	6.31440	18.01640
H	0.19650	7.79210	16.04570
H	1.76300	8.39800	14.18540
H	3.63220	8.44660	12.56140
H	5.08910	10.44540	12.38260
H	4.73160	12.38480	13.86670
H	4.30460	10.54180	19.65450
H	5.36260	13.56370	15.77560
H	-0.16410	13.13180	15.86300
H	0.50190	13.77840	17.35960
H	-0.57730	12.37190	17.39300
H	1.62950	15.85550	22.54980
H	3.23800	16.60460	22.65110
H	3.01540	14.90140	23.12260
H	2.67030	16.03320	20.27580
H	7.00300	15.35290	21.37840
H	6.80970	15.54980	19.62550
H	8.26310	17.38310	20.56450
H	6.95560	17.86400	21.66280
H	6.75830	18.05800	19.90720
H	-0.41160	9.60450	14.66790
H	-1.12990	10.71360	15.83780
H	0.48060	12.37680	19.37500
H	1.81900	11.70940	20.27150
H	3.36440	14.25020	14.73800
H	2.26170	14.69340	16.05350
H	-0.28380	11.33990	14.40190

H	1.64530	13.91800	14.57090
H	7.17780	12.85240	17.30670
H	5.94320	12.47340	19.51810
N	6.98760	10.73520	18.99520
O	8.11640	11.06860	18.67320
O	6.65470	9.72030	19.58200

Optimized Cartesian Coordinates for [NO_2-*exo-(M,S)*-Me-Prod-H]$^+$ / Å

SCF Energy (B3LYP-MM/cc-pVDZ++//B3LYP-MM/LACVP*) = –1744.667814 hartrees

C	1.73510	9.26340	15.93340
C	1.35030	7.92270	15.99230
C	0.86380	7.38200	17.18480
C	0.76040	8.17280	18.33100
C	1.15530	9.50910	18.27560
C	1.63430	10.04910	17.08180
C	2.35010	10.33490	20.33470
C	2.63200	9.22290	21.12590
C	3.72040	9.25930	21.99890
C	4.51710	10.40610	22.09860
C	4.24410	11.51770	21.30680
C	3.15420	11.47450	20.42860
C	5.91350	11.71780	16.77870
C	4.50350	11.33590	16.50810
C	3.53060	11.70230	17.37410
C	3.83120	12.52280	18.50480
C	5.12160	13.11380	18.65890
C	6.11420	12.77920	17.79810
C	1.16180	10.52520	19.40670
C	2.02480	11.50650	17.24800
C	2.68880	12.58370	19.46000
C	1.46490	11.91810	18.68590
C	0.22800	12.81490	18.60760
C	2.16460	13.74010	15.98200
O	2.54470	14.37860	16.94860

C	3.04660	15.34080	14.43320
O	2.26140	14.16090	14.71380
C	4.49440	15.08010	14.87220
O	4.90960	14.00580	15.26380
O	5.23860	16.16730	14.70440
C	6.66200	16.04530	15.00390
C	7.31730	17.35810	14.62780
C	-0.13670	10.46800	20.23860
C	1.53940	12.35880	16.04380
C	2.46110	13.93150	20.15100
H	2.09150	9.67580	14.99230
H	1.41920	7.30180	15.10390
H	0.55490	6.34110	17.21800
H	0.36440	7.74340	19.24700
H	2.01130	8.33350	21.06970
H	3.94710	8.39240	22.61290
H	5.35090	10.42820	22.79390
H	4.86680	12.40330	21.38850
H	4.31220	10.73730	15.62460
H	5.29420	13.84550	19.44000
H	-0.15770	13.04850	19.60250
H	0.44780	13.76010	18.10850
H	-0.57860	12.31470	18.06100
H	7.06070	15.19730	14.44110
H	6.76110	15.82220	16.07090
H	8.38910	17.30670	14.84590
H	7.19470	17.56570	13.56050
H	6.88950	18.18940	15.19660
H	-0.22550	9.48940	20.72080
H	-1.02320	10.61000	19.61460
H	0.44890	12.46100	16.06030
H	1.77710	11.84520	15.10940
H	3.35740	14.25190	20.69170
H	2.20370	14.70210	19.42210
H	-0.13870	11.22000	21.03380
H	1.65760	13.84600	20.88740
H	7.10370	13.21750	17.86360

H	6.42980	10.81650	17.16400
N	6.71950	11.98320	15.47800
O	7.70570	12.69230	15.58890
O	6.33740	11.40130	14.48030
C	2.42960	16.63800	14.95410
H	1.39380	16.70830	14.60880
H	2.98600	17.48790	14.55090
H	2.44800	16.68310	16.04360
H	3.05740	15.36600	13.33850

Optimized Cartesian Coordinates for [NO_2-*endo*-*(M,S)*-Me-Prod-H]$^+$ / Å

SCF Energy (B3LYP-MM/cc-pVDZ++//B3LYP-MM/LACVP*) = –1744.665284 hartrees

C	1.67040	9.16390	16.09700
C	1.23070	7.84290	16.19840
C	0.69680	7.36940	17.39910
C	0.60000	8.20840	18.51080
C	1.05060	9.52460	18.41390
C	1.57800	9.99740	17.21220
C	2.22120	10.36750	20.47880
C	2.41680	9.27360	21.32100
C	3.47780	9.28490	22.22690
C	4.33040	10.39210	22.31050
C	4.14260	11.48470	21.46870
C	3.08410	11.46360	20.55190
C	5.86770	11.68760	16.71970
C	4.49240	11.15840	16.60050
C	3.53300	11.59590	17.45250
C	3.86860	12.40830	18.57700
C	5.20300	12.86930	18.78280
C	6.18360	12.47550	17.93060
C	1.07410	10.58140	19.50630
C	2.02240	11.44460	17.33000
C	2.71770	12.54920	19.52060
C	1.46840	11.93080	18.74630

C	0.28800	12.89630	18.62430
C	2.24330	13.62220	15.97200
O	2.74480	14.24470	16.89390
C	2.99190	15.24070	14.38540
O	2.23840	14.04770	14.70190
C	4.46460	15.00340	14.75430
O	4.95160	13.89680	14.90530
O	5.13790	16.14490	14.80990
C	6.56990	16.06020	15.07070
C	7.11360	17.47400	15.08530
C	-0.25050	10.61700	20.29760
C	1.57530	12.26610	16.09080
C	2.55830	13.93860	20.15030
H	2.06350	9.52340	15.14900
H	1.29500	7.18490	15.33680
H	0.34650	6.34340	17.46570
H	0.16750	7.83110	19.43320
H	1.75090	8.41690	21.27740
H	3.63890	8.43130	22.87890
H	5.14150	10.39830	23.03250
H	4.80790	12.33950	21.54510
H	4.27680	10.50830	15.75970
H	5.43810	13.50010	19.63220
H	-0.09310	13.18360	19.60680
H	0.56750	13.81210	18.10010
H	-0.54220	12.42930	18.08420
H	7.02290	15.44430	14.28840
H	6.70670	15.55280	16.03090
H	8.19060	17.44920	15.28140
H	6.95220	17.96620	14.12150
H	6.63440	18.07100	15.86720
H	-0.40250	9.66000	20.80660
H	-1.11030	10.78200	19.64260
H	0.48860	12.40440	16.08790
H	1.80220	11.70900	15.17750
H	3.46510	14.22880	20.69060
H	2.35610	14.69360	19.38830

H	-0.23790	11.39280	21.06950
H	1.74220	13.92960	20.87770
H	7.22040	12.76030	18.07620
H	5.94240	12.42310	15.88440
N	6.97080	10.66340	16.37070
O	8.10800	10.96920	16.69020
O	6.61480	9.66680	15.76590
C	2.36500	16.51930	14.93510
H	1.31230	16.55840	14.63900
H	2.87480	17.38700	14.50960
H	2.43530	16.56580	16.02240
H	2.95370	15.26200	13.29080

Optimized Cartesian Coordinates for [NO_2-*exo*-*(P,S)*-*i*-Pr-Prod-H]$^+$ / Å

SCF Energy (B3LYP-MM/cc-pVDZ++//B3LYP-MM/LACVP*) = –1783.983833 hartrees

C	1.52260	9.31300	18.31880
C	1.02390	8.03060	18.08150
C	0.36140	7.74270	16.88610
C	0.19250	8.73140	15.91440
C	0.69920	10.00960	16.14670
C	1.35630	10.29690	17.34370
C	1.71050	11.12740	14.12660
C	1.81670	10.16140	13.12790
C	2.79920	10.29450	12.14530
C	3.66350	11.39610	12.14520
C	3.56560	12.36170	13.14290
C	2.58130	12.22130	14.12950
C	5.76530	11.62080	17.33160
C	4.37370	11.27220	17.71850
C	3.33460	11.85800	17.08150
C	3.55620	12.86800	16.09410
C	4.86100	13.41210	15.88670
C	5.92210	12.85710	16.52200
C	0.65530	11.21160	15.21670

C	1.84560	11.73230	17.37780
C	2.31530	13.16270	15.32350
C	1.14730	12.43090	16.12340
C	-0.00070	13.35960	16.52260
C	2.31980	13.70380	18.95270
O	2.62890	14.47240	18.05720
C	3.38080	15.33760	22.03930
C	3.48680	15.01900	20.53710
O	2.59900	13.92260	20.24210
C	4.89050	14.60070	20.08350
O	5.14680	13.56680	19.49620
O	5.78740	15.52840	20.41040
C	7.15890	15.25650	20.04370
C	-0.73090	11.37970	14.56040
C	1.59520	12.38600	18.76370
C	2.10500	14.62000	14.90390
H	2.01760	9.52700	19.26310
H	1.14240	7.25750	18.83510
H	-0.03360	6.74530	16.71520
H	-0.34020	8.49830	14.99670
H	1.14170	9.31070	13.10850
H	2.88980	9.54020	11.36890
H	4.41320	11.49630	11.36600
H	4.24080	13.21250	13.13760
H	4.24550	10.52010	18.48880
H	4.99270	14.27710	15.24650
H	-0.48870	13.78840	15.64440
H	0.34770	14.18710	17.14250
H	-0.76740	12.80930	17.07850
H	3.19010	15.88960	19.94350
H	7.48060	14.29870	20.45670
H	7.25700	15.23430	18.95590
H	-0.94980	10.51270	13.92890
H	-1.52570	11.45290	15.30760
H	0.52310	12.54030	18.92790
H	1.92580	11.71010	19.55660
H	2.95190	14.98410	14.31330

H	1.99130	15.26390	15.77770
H	-0.76700	12.26390	13.91630
H	1.21620	14.70460	14.27270
H	6.92770	13.24570	16.40630
H	6.15120	10.79080	16.70690
N	6.74740	11.56400	18.53290
O	7.75910	12.23910	18.43810
O	6.45610	10.79350	19.42790
C	3.80680	14.15090	22.91650
H	3.15090	13.28780	22.76140
H	3.75290	14.42820	23.97400
H	4.83700	13.83770	22.71060
H	4.08220	16.16440	22.20460
C	1.96510	15.82400	22.38210
H	1.91430	16.12720	23.43260
H	1.22520	15.03160	22.22580
H	1.67600	16.68710	21.77060
H	7.73600	16.07850	20.46470

Optimized Cartesian Coordinates for [NO_2-*endo*-*(P,S)*-*i*-Pr-Prod-H]$^+$ / Å

SCF Energy (B3LYP-MM/cc-pVDZ++//B3LYP-MM/LACVP*) = –1783.982106 hartrees

C	1.80170	9.15100	18.76090
C	1.39400	7.81790	18.68550
C	0.82020	7.32290	17.51220
C	0.65220	8.15250	16.40180
C	1.07100	9.48080	16.47240
C	1.63780	9.97550	17.64710
C	2.12990	10.34510	14.35710
C	2.32200	9.25320	13.51210
C	3.34490	9.29020	12.56410
C	4.16220	10.42030	12.44300
C	3.97750	11.51150	13.28740
C	2.95670	11.46570	14.24500
C	5.88640	11.81460	17.96020

C	4.53740	11.23360	18.13200
C	3.53040	11.63250	17.31740
C	3.79040	12.45330	16.17870
C	5.09680	12.96640	15.92230
C	6.12290	12.61630	16.73910
C	1.01760	10.53150	15.37530
C	2.03270	11.43390	17.50450
C	2.59810	12.54840	15.28270
C	1.40270	11.89600	16.11220
C	0.19900	12.82500	16.28220
C	2.23970	13.62950	18.83490
O	2.66740	14.26890	17.88840
C	2.62100	15.81620	21.73460
C	3.00310	15.29280	20.33630
O	2.28200	14.06990	20.09920
C	4.49870	14.99570	20.18690
O	4.96880	13.89580	19.95850
O	5.21100	16.10790	20.34800
C	6.64730	15.98170	20.26660
C	-0.34010	10.52420	14.64190
C	1.61680	12.24960	18.75860
C	2.36770	13.92640	14.65040
H	2.22610	9.52660	19.68910
H	1.51430	7.16710	19.54650
H	0.49470	6.28770	17.46630
H	0.18960	7.75850	15.50120
H	1.68220	8.37860	13.58550
H	3.50350	8.43870	11.90860
H	4.94340	10.44560	11.68920
H	4.61500	12.38410	13.18170
H	4.37790	10.57970	18.98220
H	5.27430	13.60520	15.06480
H	-0.23480	13.09340	15.31640
H	0.47240	13.75280	16.78790
H	-0.59090	12.33570	16.86180
H	2.73040	16.02590	19.57120
H	7.00570	15.26000	21.00380

H	6.93920	15.66220	19.26310
H	-0.48460	9.56190	14.14060
H	-1.17540	10.66400	15.33350
H	0.52730	12.34860	18.81390
H	1.90920	11.70930	19.66340
H	3.24100	14.24070	14.06990
H	2.17400	14.68060	15.41550
H	-0.38530	11.29850	13.86960
H	1.52210	13.88540	13.95850
H	7.14070	12.94410	16.55510
H	5.97270	12.54110	18.80170
N	7.03960	10.82650	18.25140
O	8.15290	11.18410	17.90210
O	6.74300	9.80450	18.84520
C	3.00400	14.83000	22.84810
H	2.75200	15.25240	23.82590
H	4.07790	14.60930	22.85140
H	2.46380	13.88350	22.74100
C	1.12880	16.17620	21.77740
H	0.87670	16.62300	22.74420
H	0.50330	15.28700	21.64550
H	0.86590	16.89910	20.99610
H	3.20440	16.73610	21.86320
H	7.03690	16.97630	20.47810

Optimized Cartesian Coordinates for [NO_2-*exo*-*(M,S)*-*i*-Pr-Prod-H]$^+$ / Å

SCF Energy (B3LYP-MM/cc-pVDZ++//B3LYP-MM/LACVP*) = –1783.976910 hartrees

C	1.88730	9.24600	16.17200
C	1.53670	7.89490	16.20480
C	1.00500	7.33350	17.36800
C	0.82180	8.11390	18.51160
C	1.18240	9.46060	18.48270
C	1.70690	10.02120	17.31750
C	2.26090	10.31680	20.59300

C	2.55650	9.20820	21.38400
C	3.60660	9.27930	22.30110
C	4.35050	10.45680	22.44400
C	4.06330	11.56540	21.65300
C	3.01220	11.48790	20.73080
C	5.94140	11.85610	17.25630
C	4.56720	11.39900	16.92050
C	3.53320	11.73650	17.72250
C	3.73240	12.58570	18.85700
C	4.98250	13.24230	19.06770
C	6.03380	12.94350	18.26640
C	1.10550	10.46960	19.61750
C	2.04510	11.48760	17.51200
C	2.54300	12.58770	19.75400
C	1.39090	11.87490	18.91590
C	0.12410	12.71940	18.76880
C	2.17980	13.74470	16.29120
O	2.48590	14.36350	17.29570
C	3.05230	15.41150	14.76850
O	2.29150	14.20850	15.04120
C	4.52950	15.05690	14.99190
O	4.92070	14.13350	15.68070
O	5.32830	15.86990	14.30440
C	6.75020	15.62280	14.41350
C	-0.22310	10.36470	20.39440
C	1.60950	12.33690	16.28800
C	2.22040	13.91230	20.45060
H	2.27940	9.67420	15.25250
H	1.66740	7.28140	15.31800
H	0.72320	6.28450	17.38040
H	0.39150	7.66840	19.40430
H	1.97620	8.29450	21.29330
H	3.84450	8.41530	22.91510
H	5.15470	10.50480	23.17220
H	4.64570	12.47430	21.76770
H	4.45030	10.77540	16.04140
H	5.07700	13.99560	19.84150

H	-0.32680	12.93220	19.74080
H	0.33170	13.67550	18.28580
H	-0.62800	12.18790	18.17590
H	6.98340	14.61130	14.07540
H	7.07520	15.74600	15.44870
H	-0.29600	9.38320	20.87370
H	-1.08750	10.47530	19.73410
H	0.51710	12.39620	16.22780
H	1.93300	11.84740	15.36640
H	3.07430	14.26450	21.03830
H	1.96250	14.68210	19.72140
H	-0.28500	11.11560	21.18840
H	1.38780	13.77830	21.14650
H	6.99480	13.43430	18.37280
H	6.49130	10.99150	17.67710
N	6.79090	12.16220	15.99300
O	7.76570	12.87640	16.15990
O	6.45160	11.61260	14.96120
C	2.55060	16.69050	15.49250
H	2.85630	16.63400	16.54070
H	2.90590	15.54860	13.69320
C	3.16330	17.95100	14.85900
H	2.77130	18.83860	15.36650
H	2.89810	18.03150	13.79760
H	4.25250	17.97220	14.93560
C	1.01590	16.75900	15.43270
H	0.67180	17.68820	15.89810
H	0.54010	15.92910	15.96210
H	0.65670	16.75320	14.39620
H	7.21820	16.36630	13.77000

Optimized Cartesian Coordinates for [NO_2-*endo*-*(M,S)*-*i*-Pr-Prod-H]$^+$ / Å

SCF Energy (B3LYP-MM/cc-pVDZ++//B3LYP-MM/LACVP*) = –1783.975622 hartrees

C	1.74800	9.15830	16.41940
C	1.31310	7.83470	16.50850

C	0.74320	7.35970	17.69190
C	0.60550	8.19940	18.79880
C	1.05100	9.51810	18.71450
C	1.61430	9.99260	17.52960
C	2.15360	10.37940	20.81110
C	2.33930	9.28960	21.66040
C	3.37200	9.31810	22.59810
C	4.20530	10.43770	22.70500
C	4.02730	11.52670	21.85630
C	2.99700	11.48900	20.90860
C	5.89930	11.74690	17.17590
C	4.54060	11.18240	17.02340
C	3.54610	11.61230	17.83680
C	3.82740	12.44650	18.96070
C	5.14380	12.94100	19.20180
C	6.15770	12.56240	18.38360
C	1.03170	10.57720	19.80510
C	2.04350	11.44300	17.65980
C	2.64460	12.56900	19.86600
C	1.43250	11.92830	19.05230
C	0.24270	12.87490	18.88200
C	2.28190	13.63080	16.31680
O	2.76880	14.24340	17.25310
C	2.99770	15.29130	14.75620
O	2.25360	14.08960	15.05950
C	4.48550	14.96930	14.98630
O	4.90820	13.85630	15.24330
O	5.25650	16.03870	14.81330
C	6.68240	15.83970	14.92660
C	-0.31540	10.60110	20.55790
C	1.64070	12.25910	16.40300
C	2.44000	13.95500	20.48970
H	2.16930	9.51930	15.48400
H	1.40920	7.17600	15.65050
H	0.39670	6.33170	17.74840
H	0.14520	7.82090	19.70720
H	1.68700	8.42340	21.59830

H	3.52560	8.46820	23.25690
H	4.99410	10.45680	23.45120
H	4.67760	12.39110	21.95080
H	4.36470	10.51820	16.18440
H	5.33780	13.58840	20.04920
H	-0.18070	13.15890	19.84800
H	0.52780	13.79410	18.36690
H	-0.55820	12.39390	18.31090
H	7.01680	15.08630	14.21020
H	6.93790	15.52680	15.94180
H	-0.47200	9.64470	21.06670
H	-1.15770	10.75420	19.87760
H	0.55280	12.37280	16.34290
H	1.92680	11.71030	15.50100
H	3.32230	14.26050	21.06120
H	2.25190	14.70680	19.72100
H	-0.33340	11.38020	21.32640
H	1.59930	13.93200	21.18820
H	7.18220	12.87540	18.55560
H	5.98510	12.46230	16.32550
N	7.03690	10.74070	16.88850
O	8.15780	11.08800	17.22350
O	6.72230	9.71460	16.31080
C	2.45200	16.58430	15.42720
H	2.89520	16.66850	16.42420
H	2.86070	15.38510	13.67280
C	2.83100	17.82600	14.60000
H	2.44600	18.72490	15.09260
H	2.38150	17.78050	13.59980
H	3.91030	17.93920	14.48670
C	0.92270	16.51390	15.57630
H	0.55440	17.46400	15.97720
H	0.60130	15.72380	16.26030
H	0.43280	16.34910	14.60930
H	7.12530	16.80910	14.70350